UNDERSTANDING THE PROMOTION OF AEROBIC OXIDATION OF BENZYL ALCOHOL OVER PT-BASED CATALYSTS

Avela Kunene
MSc (Chemical Engineering), University of Cape Town, South Africa

Thesis presented to the University of Cape Town in
fulfilment of the requirements
for the degree of

Doctor of Philosophy in Engineering

Catalysis institute
Department of Chemical Engineering
University of Cape Town
South Africa
December 2020

Declaration

I, Avela Kunene, certify that this submission is my own, except for the information obtained from literature sources and my prescribed supervisor(s). All sources of information have been adequately acknowledged and referenced.

Signature……Signed by candidate…… Date…17 December 2020……..

Acknowledgements

I would like to give heartfelt gratitude to my Heavenly Father, the Almighty God, for sustaining and strengthening me throughout my academic life. I would also like to thank my Mother, Ntombesithathu Kunene and siblings, especially my Thembsy, for being there for me when I needed her and for the support and encouragement, she offered me. A special mention to my friend Siphosethu Poswa for praying with me and encouraging me throughout my academic journey. You are a friend indeed. Thank you to Dr Thobani Gambu, Marian Flores Granobles and Dr Gerard Leteba for their assistance during my PhD studies. A special gratitude to Cillié Swart and Dr Shepherd Siangwata for assisting me with editing this work, I am truly grateful. Special thank you to my supervisor, Prof Eric van Steen for his assistance, advice and support that contributed beyond measure to this study. Indeed, it takes a village to raise a child. I would also like to acknowledge NRF and MINTEK for financial assistance.

Dedicate this work to my late father, Mcebisi Kunene and grandmother, Nozipho Kunene

Publications and conference contributions

Publications from this work

- Kunene, A., van Heerden, T., Gambu, T.G. and van Steen, E. (2020), Liquid-phase, Aerobic Oxidation of Benzyl Alcohol over the Catalyst System (Pt/TiO_2+H_2O). *ChemCatChem*. doi:10.1002/cctc.202000759
- Kunene, A, Leteba, G and van Steen, E, Liquid-phase oxidation of benzyl alcohol over Pt and Pt-Ni alloy supported on TiO_2: using O_2 or H_2O_2 as oxidant? *Catalysis Letters*. doi:10.1007/s10562-021-03760-z
- Kunene, A and van Steen E, Collaborative influence of H_2O and the oxidic support on aerobic oxidation of benzyl alcohol (***in preparation***)
- Kunene, A, Leteba, G and van Steen, E, Effect of bismuth modified Pt catalyst on alcohol oxidation in an aqueous medium (***in preparation***)

Conference Contributions

Oral presentation

- 28th annual conference of the Catalysis Society of South Africa -2017

The effect of water on benzyl alcohol oxidation reaction over Pt/TiO_2

Kwa Maritane Bush Lodge, Pilanesberg, the North-West Province, South Africa

- 29th annual conference of the Catalysis Society of South Africa -2018

Role of promoters in Pt-catalyzed benzyl alcohol oxidation

Legend Golf & Safari Resort, Limpopo, South Africa

Synopsis

The combination of a metal catalyst with molecular oxygen (which is the cheapest and the most environmental-friendly oxidant) is undoubtedly a more benign alternative to the existing methodologies for the oxidation of alcohol substrates to aldehydes, ketones and/or carboxylic acid products. However, a potential risk is apparent upon the use of volatile and flammable organic solvents, specifically in the presence of molecular oxygen. This makes the liquid-phase oxidation of alcohols a non-trivial chemical reaction that requires safety considerations. As such, designing a new alcohol oxidation procedure should carefully incorporate safety and sustainability principles while maintaining overall reaction efficiency. The solvent system can, thus, be considered carefully to limit the potential risk associated with the oxidation of organic substrates using air/O_2 as an oxidant at elevated temperatures. The use of H_2O (as a non-flammable solvent) would not only present a safety measure in alcohol oxidation (with O_2 as an oxidant) but also has the potential to enhance overall catalytic performance.

In this study, the influence of H_2O on the liquid-phase benzyl alcohol oxidation is explored using a Pt/TiO_2(P25) at 90 °C in a semi-batch reactor. The rate of reaction is significantly enhanced when using H_2O as a solvent (TOF of 677.4 ± 23 hr^{-1} compared to the TOF obtained in the solvent-free system, 27 ± 6 hr^{-1}, in m-xylene as a solvent, 23 ± 1.6 hr^{-1}, or in n-heptane as a solvent, 60 ± 4.9 hr^{-1}). The promotional effect of H_2O is associated with the mole fraction of H_2O in the organic phase rather than the fugacity of H_2O in the system. It is thought that the precise role of H_2O in the organic phase is thought to facilitate the H-transfer reactions. A DFT study suggests that the presence of H_2O facilitates the activation of O_2 over Pt(111) surface.

The promotional effects of H_2O are suppressed significantly upon modifying the active metal by alloying Pt with Ni (forming Pt-skin Ni subsurface alloy). This is ascribed to a weakening of the chemical bond between Pt and adsorbed atomic oxygen due to the suppression of surface states on the Pt surface layer due to the presence of Ni atoms in

the subsurface layer. This further highlight that the promotional effects of H_2O are associated with the adsorption properties of the active metal surface.

In contrast to the effect associated with the presence of Ni in alcohol oxidation, the addition of Bi enhances the rate of benzyl alcohol oxidation. In the oxidation of an aromatic benzyl alcohol substrate, Bi is thought to interact with the benzyl ring of benzyl alcohol substrate through a π-bond, thus weakening the O-H bond of the alcohol. Due to the non-aromaticity of cyclohexyl methanol substrate, catalytic improvement induced by this interaction between the substrate and Bi is improbable. Also, the presence of Bi as a promoter is thought to assist the dissociation of molecular oxygen through the oxygen spillover mechanism. As such, Bi is thought to have a dual promotional effect on alcohol oxidation.

Typically, the active metal in heterogeneous catalysis is immobilized on a metal oxide support. However, it has recently been noted that certain metal oxide support materials may aid the catalysis reaction process. Therefore, an in-depth study of the effect and precise role of metal oxide in alcohol oxidation in the presence of H_2O is investigated in the present study. The Pt-based catalysts were synthesized by incipient wetness impregnation of TiO_2(P25), CeO_2, γ-Fe_2O_3, γ-Al_2O_3 and MoO_3. Upon investigating various metal oxide support materials for influence on benzyl alcohol oxidation as Pt/TiO_2(P25), Pt/CeO_2, Pt/γ-Fe_2O_3, Pt/γ-Al_2O_3 and Pt/MoO_3 catalysts in the presence of H_2O as a solvent, with the exception of Pt/γ-Fe_2O_3, it is apparent that the reducibility of the oxide material and presence of H_2O may influence the rate of benzyl alcohol oxidation congruently. It is thought that H_2O and the reducible support assist the dehydrogenation step of the alcohol substrate through the formation of oxygen vacancy sites, thus forming surface hydroxyl species on the reducible support, which can be eliminated generating an oxygen vacancy on the oxide. This ultimately improves the overall TOF for benzyl alcohol oxidation. Hence, support materials that can generate surface hydroxyl groups, and eliminate them under reaction conditions in the form of water, will enhance benzyl alcohol oxidation.

TABLE OF CONTENTS

List of Tables

Chapter 2: Literature Review

Chapter 3: Experimental procedure

Chapter 4: The influence of water on benzyl alcohol oxidation over Pt/TiO_2(P25)

Chapter 7: Investigating the role of bismuth in Pt-based catalyst for alcohol oxidation

List of Figures

Chapter 2: Literature Review

Chapter 3: Experimental procedure

Chapter 4: The influence of water on benzyl alcohol oxidation over Pt/TiO_2(P25)

Chapter 7: Investigating the role of bismuth in Pt-based catalyst for alcohol oxidation

Figure 8.5: Dissociation of benzyl alcohol assisted by surface oxygen of the support material to form surface benzyl alkoxide and H_2O.

List of Schemes

Chapter 2: Literature Review

Chapter 7: Investigating the role of bismuth in Pt-based catalyst for alcohol oxidation

Abbreviations

BA:	Benzyl alcohol
BE:	Benzyl ether
DFT:	Density Functional Theory
GC:	Gas chromatography
GCxGC-MS:	2-Dimensional gas chromatography coupled with mass spectroscopy
ICP-OES:	Inductively coupled plasma-Optical emission spectroscopy
LLE:	Liquid-liquid Equilibrium
NP:	Nanoparticles
NRTL:	Non-randomly two liquid
OAm:	Oleyl amine
OLEA:	Oleic acid
PTY:	Platinum-time-yield
TOF:	Turnover frequency
TPD:	Temperature-programmed desorption
UNIFAC:	Universal Functional-group Activity Co-efficient

List of symbols

x_i	Mole fraction of component i
G_I	Gibbs-free energy of component i
τ_I	Activity co-efficient
aij	Binary interaction parameter in NRTL
bij	Temperature-dependent binary interaction parameter in NRTL
αij	Non-randomness parameter in NRTL
γ_I	Activity co-efficient of component i
γ	Surface tension of liquid
η	Viscosity of liquid
θ	Liquid contact angle of a solid sample liquid
ρ	Liquid density

CHAPTER 1:

Introduction

1.1. CONTEXT

The oxidation of alcohol is a critical step in the synthesis of high-value commodity chemicals. Specifically, the oxidation of primary and secondary alcohols to the corresponding carbonyl compounds is crucial in organic synthesis due to the comprehensive ranging use of these products as precursors and/or intermediates for numerous drugs, vitamins and fragrances.

Traditional methodologies for alcohol oxidation involve the use of organic solvent and an oxidant such as dichromate and permanganate,[1] which co-produce harmful waste material during alcohol oxidation reactions. Furthermore, the use of flammable organic solvents for alcohol oxidation presents an environmental and safety concern. As such, the pharmaceutical sector has started to limit the use of alcohol oxidation reactions for high-value chemical synthesis due to sustainability reasons.[2] Remarkable efforts are made continually by the scientific community in search of the development of new, sustainable processes for the oxidation of alcohols. The use of molecular oxygen as an oxidant may present an alternative to the existing oxidants promoting green chemistry on a larger industrial scale. However, oxygen in combination with flammable organic substrate and/or organic solvent may pose a potential hazard. It is, therefore, apparent that the design of new processes for the oxidation of organic substrates using the principles of green and sustainable chemistry requires careful considerations and, e.g. water as an alternative solvent will need to be considered.

In homogeneous catalysis, Pd-based organometallic complexes with tertiary phosphine oxides (TPO) and nitrogen-based ligands have shown high activity for primary and secondary alcohols using oxygen under mild reaction conditions.[3] However, for industrial applications, heterogeneous catalysts are typically preferred over

homogeneous catalysts due to product separation limitations from the reaction mixture that is associated with homogeneous catalysts.

In heterogeneous catalysis, typically, liquid-phase oxidation consists of at least 3 phases, i.e. gas phase (oxygen oxidant), a solid phase (heterogeneous catalyst) and a liquid phase (alcohol substrate and solvent system). Depending on the miscibility of the solvent, the liquid phase can be a biphasic system (organic and aqueous phase), leading to up to 4 phases present in the system. Besides the added advantage of easy product separation from the reaction that heterogeneous catalyst offers (compared to homogeneous) but in this case, the efficiency of liquid-phase oxidation may be modified by tailoring each phase in the system.

1.2. METHODS OF IMPROVING LIQUID-PHASE ALCOHOL OXIDATION PROCESS USING NOBLE-METAL-BASED HETEROGENEOUS CATALYST

Metal oxides and noble metals, as heterogeneous catalysts, can drive oxidation reactions successfully while also considering industrial sustainability concerns. Platinum, palladium, and gold are known metals that show catalytic activity for liquid-phase alcohol oxidation.

Often, Au-based catalyst used for oxidation reactions requires a base. Typically NaOH is added into the reaction medium to achieve the activity.[4] This indicates that the active site for oxidation reactions over an Au-based catalyst is the Au-OH site with hydroxide ions (OH^-) in solution regarded to increase the number of active sites.[5,6]

Intuitively, the catalytic activity is then influenced by Au-OH concentration on the catalyst surface ad pH of the reaction medium. Even though Pt and Pd-based catalysts do not necessarily require a base for their activity in oxidation reactions, there are limitations associated with these catalysts as well. Pd-based catalysts are typically the most active catalysts for oxidation reactions compared to Au and Pt-based. However, they are prone to oxidation yielding PdO that diminishes overall catalytic activity. On the other hand the Pt moiety in Pt-based catalyst adsorbs oxygen relatively strongly, thus the removal of the oxygen species may become the rate-determining step.[7] As such, the

saturation of a surface with a strongly adsorbing oxygen species is typically rather difficult due to repulsive lateral interactions, yielding low oxygen coverage.[8] The challenges associated with each catalyst system, Au, Pd and Pt, influences the overall catalytic activity. There are various methods that can modify these catalyst systems, thus addressing the corresponding challenges associated with each system.

Besides the use of a promoter or modifier generally, the specific catalytic properties of the noble metal, such as Pt, Pd and Au nanoparticles, are dependent on their size and dispersion.[9] Highly dispersed noble metal nanoparticles with small size and narrow size distribution show outstanding catalytic performance in heterogeneous catalysis compare to their bulk counterparts. This is attributed to their large surface area, specific electronic structure and high fractions of the coordination of unsaturated metal atoms. Nevertheless, due to high surface energy, nanoparticles are generally not stable and easy to aggregate, resulting in diminished catalytic activity. As such, the active metal nanoparticles are embedded inside porous (high surface) support material to achieve high metal dispersion. Metal oxides such as Al_2O_3, TiO_2 and SiO_2 are typically the support material of choice in heterogeneous catalysis. Carbon is the most often used support material due to the fact that it can be chemically functionalized and/or decorated with metallic nanoparticles relatively easy.[10]

In alcohol oxidation, several metal oxide support materials have also been shown to possess properties that go beyond dispersing the active metal, which can also influence catalytic performance.[11] Reducible metal oxides support such as CeO_2 and TiO_2 are often used as the supports for alcohol oxidation catalysts because of their excellent oxygen spillover capability.[12] This is obtained by switching between Ce^{3+} and Ce^{4+} cations.[12] This characteristic feature of CeO_2 is thought to enhance the catalytic activity during alcohol oxidation over Au-based catalyst.[13] The reducibility of the metal oxide support material can play a role during alcohol oxidation. This offers another alternative to achieve an efficient alcohol oxidation reaction that has promising sustainability considerations.

The catalytic efficiency may also be improved by adding active components that promote important steps, such as adsorption and activation of the reactants, molecular oxygen and the alcohol, which form a bedrock for alcohol oxidation to proceed. In order to further prove this theory, efforts should also be made to produce and understand new catalytic systems that may enhance selective alcohol oxidation. For instance, the adsorption and activation of both molecular oxygen and alcohol substrate may be modified by the incorporation of catalyst additives and/or reaction auxiliaries that still consider sustainability factors.

The most prominent approach to enhance catalytic activity in heterogeneous catalysis is the use of promoters. The promoter element can be incorporated into the lattice structure of the catalytically active metal, Pt, Pd and Au metals, thus forming an alloying or be present as a second metallic phase/particle (though the promoting elements may also be present as an oxide). Known catalytic performance enhancers in alcohol oxidation are Bi, Sn and Pb.[14–16] The role of these promoters is not understood fully. The improved catalytic performances have often been attributed to synergistic effects arising from electronic or geometrical interactions between the alloyed/mixed metals.[17] This may ultimately enhance the overall alcohol oxidation. Not only does the incorporation of a promoter or modifying metal enhance the catalytic activity in alcohol oxidation, but it may also modify the product spectrum. For instance, the addition of a modifier such as Ni as an alloy to Pt-based catalyst suppresses the formation of toluene products during benzyl alcohol oxidation.[18] Moreover, noble metals (which are used in alcohol oxidation) are rather expensive. Therefore, alloyed and/or mixed metal can be regarded as a relatively economical approach for alcohol oxidation.

1.2.1. THE LIQUID COMPONENT OF ALCOHOL OXIDATION

Typically, organic solvents are used in the liquid-phase alcohol oxidation reaction. Alcohols are combustible organic substrates. As such, for alcohol oxidation at relatively high temperatures, an improved safety profile can be achieved by performing the reaction in a non-flammable solvent such as H_2O, particularly when using molecular oxygen/air as the oxidant. The unique properties, low cost and environmentally friendly characteristics

of H_2O make it highly desirable as a solvent in many chemical processes. Furthermore, the use of H_2O has been shown in numerous studies to be more than just a solvent in chemical synthesis.[19–24] This effect of water on the chemical reactivity is not limited to heterogeneously catalyzed systems but is well-known in organic syntheses as well.[25,26] Examples highlighting the promotional effects of H_2O include the preferential oxidation of CO,[6,27] direct hydrogen peroxide synthesis,[28] epoxidation[29,30] and alcohol oxidation.[21,25,39,42,94]

Understanding the precise role of H_2O as a reaction promoter in alcohol oxidation is a non-trivial exercise. There has been a lot of debate in the literature concerning the role of H_2O in alcohol oxidation over a heterogeneous catalyst. It is assumed that water assists in the formation of hydroxyl species on the catalyst surface,[32,34,35], which may facilitate the oxidation of the alcohol substrate.[36] Alternatively, H_2O may act as a base assisting the hydride abstraction step in the alcohol oxidation.[36] In spite of these positive effects attributed to carrying out the reaction in the presence of H_2O, the use of H_2O solvent in alcohol substrate oxidation is rather limited due to the restricted water–solubility of the substrate and products. As such, catalytic liquid-phase oxidation of alcohols to aldehydes in water is challenging, and only a limited number of studies are known in which an efficient catalytic aerobic oxidation of alcohol has been achieved in aqueous media. Miscibility between the organic substrate and water may play a major role in the overall activity of the catalyst. It is apparent, therefore, that an understanding of the precise role of H_2O in alcohol oxidation in light of the liquid-phase separation between H_2O solvent and alcohol substrate forms the core of industrial use of H_2O as a solvent for alcohol oxidation.

1.3. PROBLEM STATEMENT

The aerobic liquid-phase oxidation of alcohols may be carried out in the presence of water, which has shown promoting effects on the oxidation reactions.[37] However, the precise role of H_2O in alcohol oxidation is not very clear. An improved understanding of the influence/effects of H_2O on the alcohol oxidation over various Pt-based catalysts

(which include Pt alloyed systems) may result in improved reaction processes for the heterogeneously catalysed, aerobic oxidation of alcohols using water as a solvent.

1.4. SCOPE OF THE STUDY

The role of water is investigated first by considering the phase equilibrium (LLE) of H_2O, benzaldehyde and benzyl alcohol substrate. Subsequently, the presence of water in the reaction system is probed. The role of water as a contributor to the surface species present on a metal surface is further probed by changing the oxidant from oxygen to hydrogen peroxide. The interaction of water with the catalytically active metal and even the support is not well documented but may hold the key to understanding the effect of water on the catalytic activity.

This thesis is divided into four major chapters (chapter 4, 5, 6 and 7), which explore and gain an understanding of various parameters (i.e., solvent system, support material and promoter effect) in platinum-catalyzed alcohol oxidation. The common theme across these main chapters is that H_2O is employed as a reaction solvent. Chapter 4 specifically interrogates the role of H_2O in benzyl alcohol oxidation, taking into account the miscibility of H_2O with benzyl alcohol substrate. While chapter 5 deals with Pt-Ni bimetallic systems in benzyl alcohol oxidation in the presence of H_2O. In this chapter, the effect of oxidant is probed by alloying Pt with Ni to form Pt-skin Ni subsurface alloy. Chapter 6 further probes the role of the nature of the metal oxide support material in the presence of H_2O in benzyl alcohol oxidation. Finally, Chapter 7 investigates the precise role of Bi in alcohol oxidation.

CHAPTER 2:

Literature review

2.1. SELECTIVE OXIDATION REACTION

Oxidation reactions may be regarded as the heart of chemical synthesis in the pharmaceutical and chemical industry as they can introduce novel functional groups within a substrate. Specifically, the selective oxidation of alcohols is a useful reaction to obtain high-value products, such as aldehydes, ketones and carboxylic acids, from low-cost feedstock, such as carbohydrates and alcohols. These carbonyl products are crucial intermediates, e.g. used in the production of pharmaceuticals, perfumes, and other chemicals.[38]

Methanol can be selectively oxidized, yielding formaldehyde over an iron molybdate catalyst at temperatures of ca. 350 °C and close to atmospheric pressure.[39–41] Owing to its relatively low cost, high purity, and variety of chemical reactions, formaldehyde has become one of the world's most important industrial and research chemicals, finding its use in the production of grocery bags, paper cups and plates, waxed paper, facial tissues, napkins, paper towels, and sanitary napkins.[42] Furthermore, formaldehyde is also used in agriculture for seed treatment and for the production of building materials, cosmetics and fabric softeners.[43] The annual worldwide production of formaldehyde capacity is now over 12.1 metric tons (calculated as 37 % solution).[43] Originally, a silver wire gauze was employed as the catalyst element, which was later replaced with a shallow bed of silver crystals for the production of formaldehyde from methanol oxidation.[44] Further catalyst development resulted in the mixed iron-molybdenum oxide catalyst. However, vanadium-based catalysts supported on metal oxides such SiO_2, Al_2O_3, ZrO_2, and TiO_2 also have been shown to be active for the selective oxidation of methanol to formaldehyde.[45]

Ethanol oxidation forms part of the oxidation of aliphatic alcohol reactions, and it ranks as one of the most promising alternatives for the production of bulk chemicals, such as acetaldehyde and acetic acid. Aerobic fermentation ethanol is still the major process for the production of vinegar. Acetic acid is industrially produced using methanol carbonylation over a homogeneous Rh or Ir-based catalyst.[46] However, selective, catalytic oxidation of acetaldehyde (derived from aerobic fermentation of ethanol) or ethanol may become a commercial process for the synthetic production of acetic acid in the future.[47] Direct oxidation of ethanol over a heterogeneous catalyst, typically Au[48–52], Pd[53] and Pt-based[54] catalyst at 50- 180 °C[51], is one of the promising technologies suitable for industrial production of high-value acetaldehyde and acetic acid. This is mainly due to low ethanol feedstock cost and easy separation of the products from the catalyst employed. Over gold-based catalysts without any additives, aqueous ethanol and oxygen may be converted to acetic acid at temperatures as low as 50 °C.[47,50] This reaction can reach a selectivity to acetic acid of up to 88% in a batch reactor after 20 hours on stream. The reaction process involves two key reaction steps, which are the oxidative dehydrogenation of adsorbed ethanol to acetaldehyde and its subsequent oxidation to acetic acid.[55] The dehydrogenation of ethanol to acetaldehyde is proposed to be the rate-determining step for the formation of the acetic acid from ethanol oxidation reaction over Au-based catalyst.[55] Other methods for the production of acetic acid began in the 1950s and 1960s were established on the oxidation of n-butane or naphtha. The major producers of acetic acid through direct oxidation of hydrocarbons were Celanese, using n-butane[56,57] as a feedstock, and BP[58] with naphtha. However, these reactions also produce substantial amounts of oxidation by-products, such as formic acid and propionic acid. As such, ethanol oxidation is the most preferred method for the production of acetic acid.

2.2. SELECTIVE OXIDATION OF POLYOLS AND CARBOHYDRATES

The selectivity of the oxidation process becomes even more important in the oxidation of highly functionalized molecules such as polyols and carbohydrates. Glycerol, for example, can be oxidized to chemical intermediates and a large number of products,

such as glyceraldehyde, glyceric acid, tartronic acid, hydroxy pyruvic acid, mesoxalic acid and oxalic acid (see Scheme 2.1). This requires a catalytic system that promotes a pathway favouring either dihydroxyacetone or glyceraldehyde product, as these are the desired products for various industrial applications. Dihydroxyacetone (DHA) is typically used in the cosmetic sector as a colour additive in sunless tanning products. DHA was estimated to generate almost $1.011 million in 2017 from the global self-tanning product market.[59] Glyceraldehyde also has various applications in different domains such as organic chemistry, medical and cosmetic industries.[60] This highlights the economic and industrial importance of selective oxidation of glycerol product DHA.

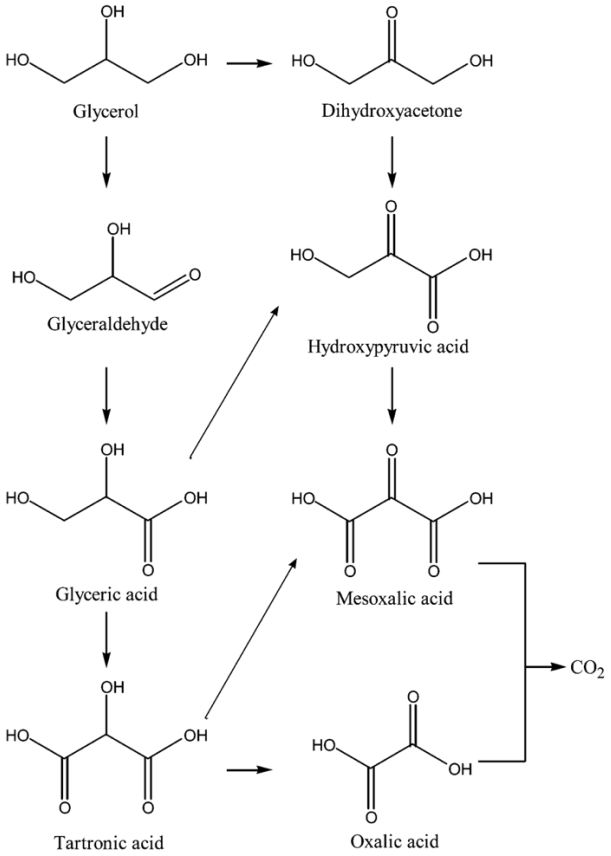

Scheme 2.1: Possible products from glycerol oxidation

Platinum-based catalysts can convert glycerol through a liquid-phase oxidation process either in an acidic or a basic solution; it can be selective for the formation of glyceraldehyde in an acidic solution or base-free solutions.[60] Pd-based catalysts have also been reported to show activity for polyol oxidation.[61]

Oxidation of polyols such as glycerol can proceed at atmospheric conditions.[62] Product selectivity can be controlled by fine-tuning the catalyst, reaction conditions and pH of the reaction medium in the case of liquid-phase oxidation. Kimura et al.,[63] showed that promoting Pt/C with Bi favours the formation of dihydroxyacetone over glyceraldehyde in glycerol oxidation with molecular oxygen. Similar results are obtained by Ning et al.,[17] The oxidation of glycerol over Pt/C resulted in a high selectivity for the formation of glyceraldehyde, but upon the addition of Bi as a promoter, dihydroxyacetone was obtained in excellent yields at similar reaction conditions.[17] This different reaction pathway which results in the different final product upon the promoting Pt with Bi, has been ascribed to the chelating geometry of glycerol substrate during oxidation reaction.[16,17,63,64] Geometric blocking promotional mechanism involves bismuth adatoms acting as site blockers on Pt sites, controlling the orientation of glycerol substrate (chelating through the oxygen atoms of the substrate with the Bi adatoms). This consequently results in high selectivity towards dihydroxyacetone formation, see Figure 2.1.[63]

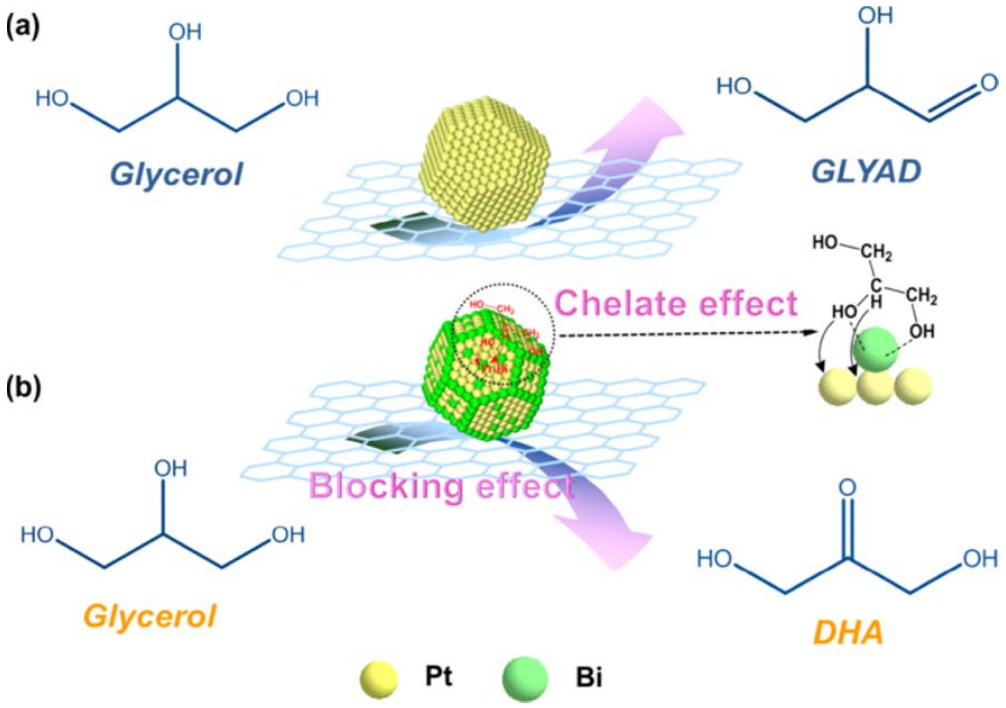

Figure 2.1: Proposed mechanism for the chelating promotional effect of bismuth on glycerol oxidation.[16,17]

Another crucial polyol oxidation is the oxidation of carbohydrates for chemical synthesis. Oxidation of D-glucose to glucuronic acid is one of the prominent examples of carbohydrate oxidation. Glucuronic acid product is a highly valuable chemical, and it is one of the major organic building blocks for hyaluronic acid (whose worldwide market was estimated to be over $1 billion in 2005[65–67]). Glucuronic acid has application in the pharmaceutical and medical industry for the synthesis of modified drugs. It is used as an active compound, predominantly for skin-care product preparation as an antioxidant and as a precursor for the biosynthesis of vitamin C (ascorbic acid).[67] In the food industry, glucuronic acid is utilized as an additive. Pt-based catalysts are typically used for carbohydrate oxidation.

2.3. SELECTIVE OXIDATION OF ALLYLIC ALCOHOLS

A classic example in allylic alcohol reaction is the oxidation of cinnamyl alcohol, an aromatic allylic alcohol. Cinnamyl alcohol and its oxidation product, cinnamyl aldehyde, are used in a wide range of industrial sectors such as the food and perfume industries.[68] Cinnamyl aldehyde is currently synthesized through benzaldehyde condensation using activated methylenes.[69] However, the oxidation of cinnamyl alcohol presents an environmentally more benign alternative for the synthesis of cinnamaldehyde.

The selective oxidation of allylic alcohols proceeds through the oxidative dehydrogenation of the alcohol to the corresponding allylic aldehyde, which may undergo further oxidation to the corresponding acid. However, due to the co-existence of reactive hydroxyl and allylic functional groups in allylic alcohols (e.g., cinnamyl alcohol) complex reaction pathways are possible in the oxidation of this class of alcohols. As such, apart from cinnamaldehyde arising from oxidation of the hydroxyl group of cinnamyl alcohol, 3-phenyl-1-propanol and trans-β-methylstyrene can also be produced through hydrogenation and hydrogenolysis reactions, respectively. These three products could undergo further reaction resulting in the formation of 1-phenylpropane, styrene, 3-phenyl-1-propanal, ethylbenzene and benzaldehyde. As such, due to the competitive reactivity of the hydroxyl and allylic functional groups, a highly selective catalyst is essential for the oxidation of allylic alcohols. Various heterogeneous catalysts that can drive allylic alcohol

oxidation (using air/O_2 as an oxidant) have been developed with palladium and/or gold as the catalyst of choice.[70–72]

Additional to a highly selective catalyst system, reaction conditions such as reaction temperature and the duration of the reaction also influences the reaction route, i.e., hydrogenation of the C=C bond vs reactivity around the C—OH (oxidation and/or hydrogenolysis) bond of the allylic alcohol substrate (e.g., cinnamyl alcohol, see Figure 2.2). Ogliaruso and Wolfe[73] observed that short reaction times have no effect on the allylic functional group in the oxidation of cinnamyl alcohol over Ru-based catalyst, thus yielding high selectivity towards cinnamaldehyde. This suggest that short reaction times favours the oxidation of the C—OH bond route. Ogliaruso and Wolfe[73] further stated that higher temperatures and longer reaction times result in double bond cleavage (allylic group of cinnamyl alcohol), yielding styene, through further reactivity of cinnamaldehyde.[73] Wu et al.,[74] detected *trans*-β-methylstyrene upon increasing temperature from 80 °C to 100 °C in cinnamyl alcohol oxidation over Au-Pd/TiO_2 catalyst. *trans*-β-Methylstyrene is thought to form through hydrogenolysis of the parent alcohol, cinnamyl alcohol. Reaction conditions in the oxidation of allylic alcohol, therefore, form an essential aspect in allylic alcohol oxidation.

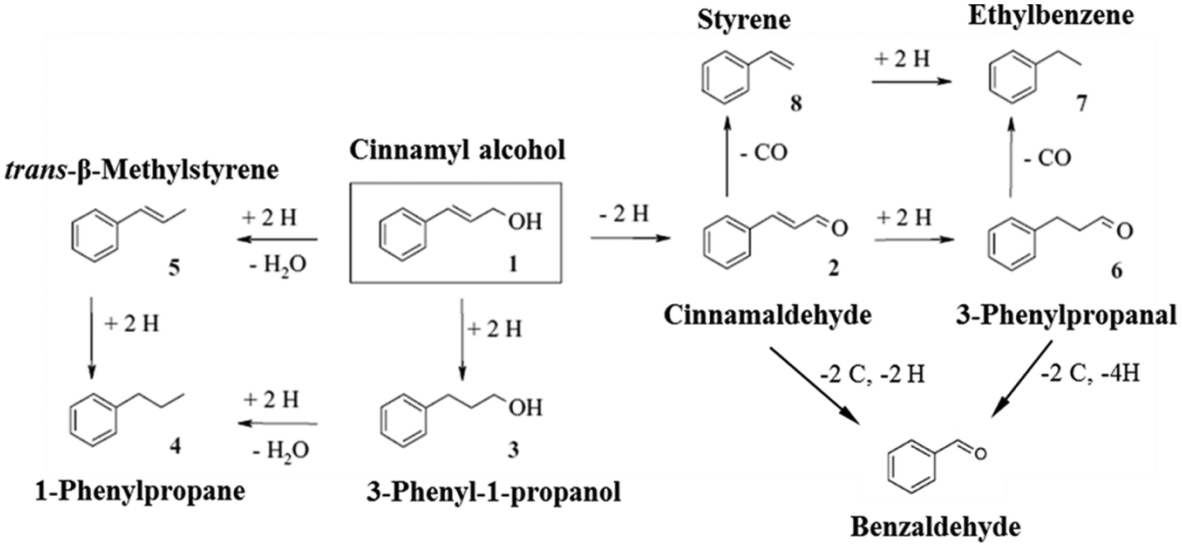

Figure 2.2: Proposed reaction network of cinnamyl alcohol oxidation.[74]

2.4. SELECTIVE OXIDATION OF AROMATIC ALCOHOLS

Benzyl alcohol oxidation is one of the most major alcohol oxidation reactions in the industry due to the demand for benzaldehyde products as an intermediate in the production of fine chemicals, fragrances and flavouring additives.[75,76] Currently, benzaldehyde is commercially produced as a by-product from the oxidation of toluene or through hydrolysis of benzal chloride.[77] Both processes have major drawbacks, with oxidation of toluene having a low benzaldehyde selectivity while the hydrolysis of benzyl chloride leads to unavoidably trace contamination of the product with chlorine,[77] thus making the process not suitable for use in perfumery and pharmaceutical industries. Selective alcohol oxidation is an alternative method for the synthesis of these high-value chemical intermediates. The vapour phase oxidation of benzyl alcohol requires high temperatures of about 320 °C,[78] which result in the co-formation of undesired product, CO_2.[4] Liquid-phase benzyl alcohol oxidation is a possible alternative pathway for the large scale production of high-value benzaldehyde intermediate. Benzyl alcohol oxidation method for benzaldehyde production can present high benzaldehyde selectivity with high purity, thus making it suitable for perfumery and pharmaceutical use.

Alcohol oxidation may proceed to carboxylic acid products through consecutive oxidation of the aldehyde intermediate. It should be noted that in many studies, the formation of the carboxylic acid is regarded as an overoxidation product if the aldehyde is the desired product. Benzaldehyde is more desired in the perfumery industry, while benzoic acid would be the desired product from benzyl alcohol oxidation as antibacterial and antifungal preservatives in the pharmaceutical industry. As such, the formation of benzoic acid from benzyl alcohol oxidation, in that case, would not be regarded as overoxidation.

The traditional method of liquid-phase oxidation of benzyl alcohol included the use of strong oxidants such as chromium (VI) reagents, permanganates,[79] and selenium oxide (SeO_2).[80] The use of these chemicals poses a threat to the ecosystems, public health, and terrestrial, aquatic, and aerial flora and fauna.[33,81,82] On the other hand, an oxidant such as tert-butyl hydroperoxide (TBHP)[83] are toxic or corrosive and unstable under

atmospheric conditions. Thus, they require specialized reactor materials and may produce many undesirable side products, which eventually increases the purification cost. Therefore, using molecular oxygen or air or H_2O_2 as an oxidant for alcohol oxidation is not only economically viable for industrial application of this process but also environmentally benign.

2.5. OXIDATION OF LONG-CHAIN ALIPHATIC ALCOHOLS

Aliphatic alcohols are usually much more demanding substrates for oxidations than aromatic and allylic alcohols. Octanol is the most commonly used as the model substance and the product octanal can be used in the fragrance industry.[84] For instance, long reaction times (ca. 40 hours) was required for the oxidation of 2-octanol in trifluorotoluene solvent in order to obtain relatively high yields (40%) over $Ru/MnO_x/CeO_2$ catalyst in comparison to benzylic and allylic alcohol oxidation (>99 % yield after 1.5 hours).[85] Reactive tendency was determined as follows: benzylic alcohol > allylic alcohol >> aliphatic alcohol.[86] The obvious difference in reactivity of these classes of the substrate induces nucleophilic properties of the molecule, thus causing the substrate to be more reactive. As such, the paraffinic nature of aliphatic alcohols may cause the reactivity of this class during oxidation reaction relatively slow compared to benzylic and allylic alcohols.

A rational design of new catalysts that are environmentally benign for selective liquid oxidation of alcohol requires both an understanding of the mechanisms over existing catalysts and an ability to forecast the behaviour of the modified materials and/or oxidation systems.

2.6. MECHANISM OF ALCOHOL OXIDATION OVER A HETEROGENEOUS CATALYST

Alcohol oxidation can proceed over metal oxide or metal-based heterogeneous catalyst. This then induces different interactions with the different substrates. Hence, depending on the nature of the substrate oxidized and catalyst employed, the mechanism may vary significantly.

2.6.1. MECHANISM OF ALCOHOL OXIDATION OVER METALS

There has been a lot of debate regarding the mechanism for the formation of carbonyl compounds from primary and aromatic alcohol substrates through a selective oxidation process over metal-based catalysts.[36,87] The mechanism of liquid-phase oxidation of primary and/or aromatic alcohol substrates to the corresponding aldehyde over heterogeneous catalyst using oxygen as an oxidant is likely to involve associative adsorption of oxygen, see equation 2.1 (with * denoting metal surface adsorbed species):[75] This is followed by dissociation of molecular oxygen according to equation 2.2.[34]

$$O_2 + * \rightarrow O_2* \qquad 2.1$$

$$O_2* + * \rightarrow 2O* \qquad 2.2$$

While alcohol activation proceeds through the dissociative adsorption of the alcohol substrate over the metal surface, thus forming surface metal alkoxide and interacting through the oxygen lone pair and surface atomic hydrogen.[88] The dissociated hydrogen interacts with the surface atomic oxygen (obtained in equation 2.2) to form surface OH, see equation 2.3:

$$\text{Alcohol} + O* \rightarrow \text{Alkoxy}* + *OH \qquad 2.3$$

Consequently, this gives rise to secondary carbonation alcoholate (otherwise stated, develops a partial positive charge in the transition intermediate, benzyl-$C^{\delta+}$-O-metal), cf. Figure 2.3.[89] This is proceeded by β-hydride (H_β) abstraction from the carbonation alcoholate intermediate while desorbing the aldehyde product.

A β-hydride elimination is generally accepted as the second step of both carbohydrate and primary and/or aromatic alcohol oxidation over metal catalysts, producing an alkoxyl and a metal–hydride surface species.[90]

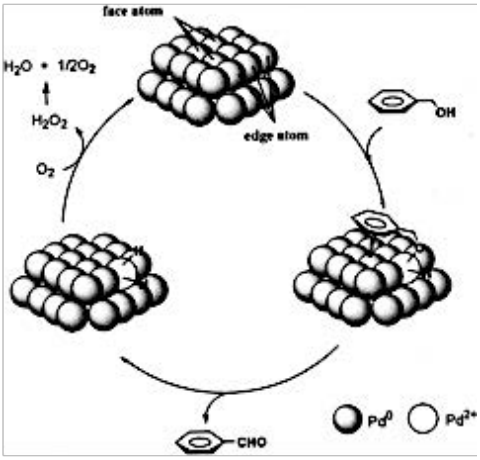

Figure 2.3: Catalytic cycle of benzyl alcohol oxidation to form the corresponding aldehyde over Pd-based catalyst.[91]

The formed alkoxyl and surface OH species (in equation 2.3) interact and desorb as an aldehyde product and H_2O as a co-product. Thus, the active sites are recovered, according to equation 2.4.

$$*\text{Alkoxyl} + *\text{OH} \rightarrow \text{Aldehyde} + H_2O + 2* \qquad 2.4$$

Alternatively, the formed metal alkoxide can lose oxygen to form a metal alkyl species, which may exist in equilibrium with the metal alkoxide, see equation 2.5.

$$\text{Alkoxyl}* + *\text{OH} \rightleftarrows \text{Alkyl}* + 2O* + H* \qquad 2.5$$

Once the alkyl species is formed along with surface hydrogen, the interaction between the two surface species is possible to desorb as toluene, see equation 2.6.

$$\text{Alkyl}* + H* \rightarrow \text{Toluene} + 2* \qquad 2.6$$

Ultimately, the metal surface is regenerated by removal of the surface hydrogen using adsorbed oxygen, yielding surface hydroxyl species. Active site regeneration involves oxidation of the metal hydride by oxygen to form oxygenated hydrogen, such as

OH, OOH, H_2O_2 and H_2O, while recovering the initial metallic site. It is possible that the oxidation of the metal hydride can proceed in different pathways, thus forming various species, see equation 2.7 -2.13.

$$O^*+H^* \rightarrow OH^* \quad 2.7$$

$$OH^* + H^* \rightarrow H_2O \quad 2.8$$

$$OH^*+OH^* \rightarrow H_2O + O^* \quad 2.9$$

The metal hydride may interact with molecular oxygen, according to equation 2.10, which could thus yield a surface hydroperoxyl species. The formed hydroperoxyl may further dissociate to form atomic oxygen and hydroxyl species on the catalyst surface, see equation 2.11.[34,90]

$$O_2^* + H^* \rightarrow OOH^* \quad 2.10$$

$$OOH^* \rightarrow O^* + OH^* \quad 2.11$$

However, the formed OOH on the surface may also react with an adsorbed hydrogen, thus forming hydrogen peroxide, according to equation 2.12. The HO-OH bond of the possible formed H_2O_2 species can cleave forming OH species (see equation 2.13) on the surface of the catalyst.[34]

$$OOH^*+ H^* \rightarrow HOOH^* \quad 2.12$$

$$HOOH^* \rightarrow 2OH^* \quad 2.13$$

Surface hydroxyl species can further interact with adsorbed alcohol species resulting in the formation of the alcoholate species and water, thus facilitating the overall oxidation process.

Regeneration of the active site is essential for the catalyst lifespan. This may be dependent on the adsorption strength of the different adsorbates. The product of the

benzyl alcohol oxidation over Pt catalyst, benzaldehyde, has adsorption energy of -1.14 eV while O_2, OH, OOH, and H_2O_2 adsorption energy (on the bridge site over Pt(111) surface) of -072 eV[92], -1.82 eV[93], -0.96 eV[93] and -0.64 eV[94], relative to O_2 in the gas phase respectively. This indicates that OH and OOH are relatively weakly adsorbed on Pt(111) surface compared to molecular oxygen. This suggests that the regeneration of the sites occupied by OH and OOH is relatively facile compared to O species and perhaps even the aldehyde product. Thus, the removal of hydride species in the form of surface OH and OOH species is fast in comparison to the formation of the carbonyl species. This may, then, be subject to the active metal composition used.

Likewise, carbohydrate oxidation over metal is characterized by the coordination of the carbohydrate substrate with the (platinum) metal through the oxygen lone pairs of hydroxyl groups in a chelating fashion.[91] C_1 of the substrate forms a carbonyl carbon while undergoing dehydrogenation, subsequently forming a metal hydride and aldehyde product, as shown in Figure 2.4.

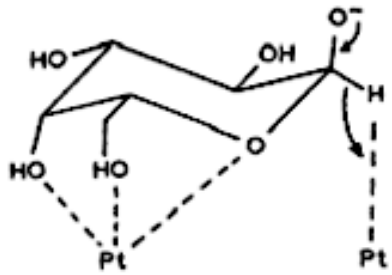

Figure 2.4: Mechanism of galactose oxidation to form the corresponding aldehyde over Pt-based catalyst.[91]

The recovering of the active site from metal hydride may follow a similar pathway as in the oxidation of primary alcohols.

2.6.2. MECHANISM OF ALCOHOL OXIDATION OVER A METAL OXIDE CATALYST

Abad et al.,[89] proposed that oxidation of alcohol over metal oxide catalysts advances through hydride abstraction of the H_β, as illustrated in Figure 2.5. Two distinct FTIR bands associated cerium alkoxide and growing band attributed to cerium hydride

during anaerobic oxidation of 2-propanol on Au/CeO_2 monitored *in situ* by IR spectroscopy were observed.[89] As such, similar to oxidation of alcohol over metal oxide has been postulated to proceeds through the formation of the β-hydride species.

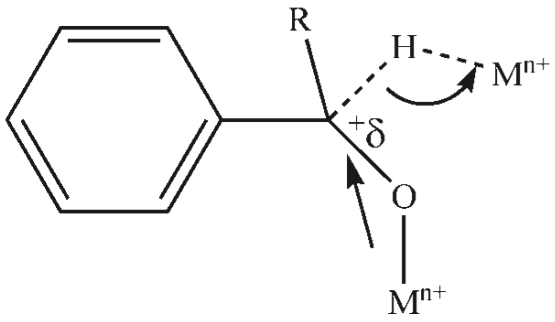

Figure 2.5: The proposed transition state in the aerobic oxidation of alcohols (benzyl alcohol) over a metal oxide heterogeneous catalyst.[89]

Figure 2.6 illustrate a closed catalyst cycle for the oxidation of a primary or aromatic alcohol yielding an aldehyde over a metal oxide heterogeneous catalyst using oxygen as an oxidant.

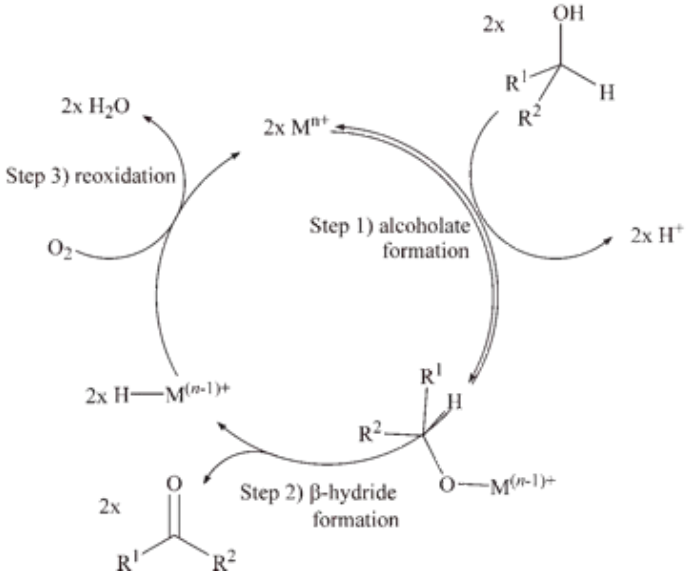

Figure 2.6: Proposed closed catalytic cycle mechanism for the oxidation of primary/aromatic substrate.[89]

2.7. CATALYSTS FOR SELECTIVE ALCOHOL OXIDATION: CATALYTICALLY ACTIVE MATERIAL

Gold (Au), platinum (Pt) and palladium (Pd) deposited on support material[25,91,95–100] are well-known as catalytically active metals that can drive the selective oxidation of alcohols. Though, the alcohol oxidation reaction can also proceed over metal oxides such as CeO_2[101] and heteropoly acids, HPA, a catalyst such as $H_3PW_{12}O_{40}$.[102]

The use of supported platinum/palladium nanoparticles in catalysis is well established for selective alcohol oxidation reactions.[7,44–48,50–53] Generally, Pd-based catalysts are more active compared to Pt and Au catalysts in alcohol oxidation. However, they are prone to oxidation forming inactive PdO surface species, thus lowering catalytic activity. Wu et al.,[105] observed a reciprocal correlation between the surface PdO on the catalyst and the catalytic activity: a larger amount of surface PdO species results in a decrease of the catalytic activity. As such, a major impediment in alcohol and carbohydrate oxidation over supported Pd catalysts is the rapid deactivation over a wide range of reaction conditions. The deactivation could be ascribed to oxidation of the Pd metal.[106]

The use of the gold catalyst for oxidation reactions has attracted much attention.[107] It has been specifically shown that supported gold nanoparticles can be very effective catalysts for the oxidation of alcohols, including diols.[4,108,109] Bianchi and coworkers[110] have shown that supported gold catalysts can also be effective for glycerol oxidation, affording *ca*. 100% selectivity towards glyceric acid. Despite these promising observations, Au-based catalysts are known to dissociate O_2 poorly[111], and thus NaOH is typically added as an auxiliary base in order for the reaction to proceed.[76,112] The active sites are, therefore, identified to be Au-OH with hydroxide ions (OH^-) in solution regarded to increase the number of active sites.[5,6] The OH moiety in the reaction medium may thus facilitate the cleavage of the O-O bond in molecular oxygen, thus assisting in molecular activation. This may proceed via the formation of a hydrogen bond between adsorbed O_2 and the OH on the gold surface, weakening the O-O bond, which may result in O_2 dissociation. As such aqueous oxidation of alcohol or carbohydrates typically proceeds in a weakly acidic or alkaline medium (pH 6–11).[113,114]

Aerobic oxidation of glucose to gluconic acid (with industrial application in food additives and beverage bottle detergents) over Pt-based heterogeneous catalyst has been investigated for decades.[115,116] This opened up research on oxidation of oxygen-bearing organic compounds, such as carbohydrate and alcohols, over Pt-based heterogeneous catalysts for industrial application.[117–122] However, platinum adsorbs oxygen strongly, and as such, the removal of the oxygen species may become the rate-determining step.[7] Furthermore, the saturation of a surface with a strongly adsorbing oxygen species is typically rather difficult due to repulsive lateral interactions.[8] These lateral interactions reduce the saturation coverage of oxygen significantly. It can be estimated that on Pt(111), only 30-50% of the surface is covered with either molecular or atomic oxygen due to lateral interactions.[8] The result of lateral interaction does not only yield low oxygen coverage over Pt catalyst surface but may also limit the adsorption of the alcohol substrate into the metal surface, even though the adsorption of the substrate may be relatively weaker.

Each metal that has been shown to have some catalytic activity for alcohol oxidation has limitations, with Au requiring an auxiliary base in order to activate molecular oxygen, thus observing the catalytic activity. On the other hand, Pd is prone to oxidation, thus losing the active site for the oxidation reaction. Oxygen coverage for Pt-based catalysts may be diminished due to repulsive lateral interaction resulting in a more stable catalyst. Typically, researchers address these catalytic limitations that the oxidation active metals are prone to by introducing a secondary element (whether as an alloy and/or mixed metal (oxide), changing the fluid components of the reaction and reaction conditions, such as temperatures.

2.7.1. Effect of catalyst promoters on alcohol/polyol oxidation

In heterogeneous catalysis, the performance of the catalytically active material can be fine-tuned by using appropriated promoter in order to address various limitations associated with the known active metal (Au, Pd and Pt) or to tailor the product selectivity profile. Extensive research has therefore investigated the promotion and alloying of Pt and Pd catalysts to improve their resistance to deactivation in alcohol oxidation reactions.

It has been suggested that the addition of a second metal may prevent oxidation of the Pd metal and inhibiting the corrosion of metal catalysts, thus improving the catalyst activity and life span.[17]

Pt or Pd-based catalysts have been modified using combinations of Bi[17,64,106,123–126], Sn[127,128] or Pb[15,126] species yielding substantial enhancement of catalytic performance for liquid-phase alcohol oxidation using O_2 as an oxidant.[14,97,106,129–131] Various studies discussed the enhanced activity obtained with promoted platinum-group metal catalysts in the oxidation of alcohols based on the so-called third-body effect.[64] This involves the promoting species (e.g. Bi) blocking the formation of poisonous species during the oxidation of small organic molecules.[17] EXAFS analysis showed that the primary effect of Bi in the oxidation of 1-phenylethanol and cinnamyl alcohol on Pd/Al_2O_3 was to protect Pd from oxidation and to act as a geometric promoter (see Figure 2.1 *vide supra*) on the Pd particles.[130] It has also been argued that the presence of a promoter on the surface of platinum decreased the size of the active site ensemble,[17] which may suppress the rate of poisoning by oxidation of the active metal. Pd oxidation inhibition seems to be a primary promotional effect brought by Bi addition. A similar conclusion was drawn by Mondelli et al.,[106,131] using liquid-phase ATR-IR coupled with XAS analysis in the liquid-phase oxidation of benzyl alcohol over Bi promoted Pd and Pt. Besson et al.,[97] explained the promoting effect of bismuth on a platinum-based catalyst in the oxidation of alcohols to the adsorption of oxygen on bismuth adatoms forming Pt-Bi-OH ad-species on the surface, which may act as new active sites for the alcohol oxidation. It is thought that these species are involved in the regeneration of the active sites through the oxidation of the metal hydride to form H_2O. Therefore, oxygen as the oxidant interacts with Bi adatoms to form bismuth oxide species, which may react with hydrogen on the metal surface resulting in the formation of H_2O, thereby regenerating the active metal site (see Figure 2.7).

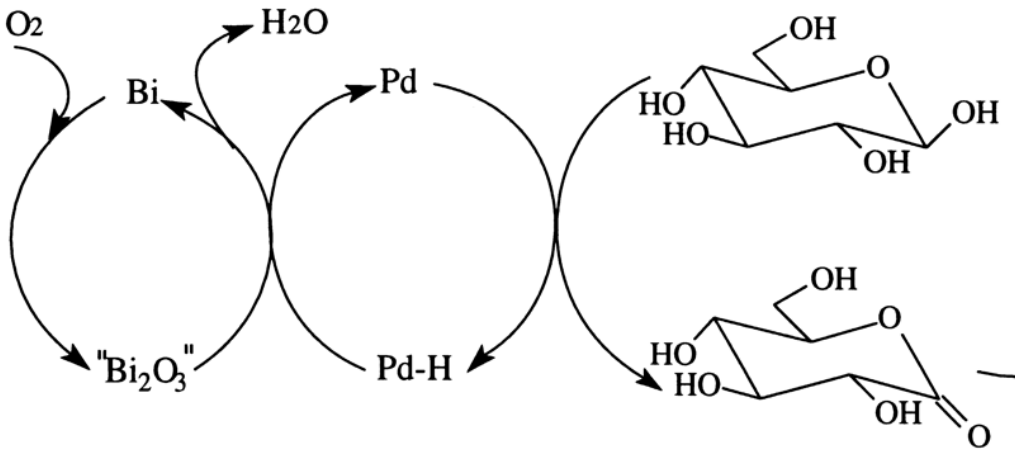

Figure 2.7: Proposed mechanism for bismuth as a promoter in the oxidation of carbohydrates over Pd-based catalysts.[97,125]

The affinity of bismuth for oxygen does not only accelerate the oxidation of hydrogen on the metal surface but may also protect metallic palladium/platinum from oxidation, thereby preventing catalyst deactivation thus prolonging the catalyst life span.[97]

The rate of oxidation of carbohydrates is also enhanced by the presence of Bi, Sn[17,97,128] and Pb.[35,93] Besson et al.,[132] also proposed that bismuth adatoms prevent poisoning of the catalytically active palladium surface with oxygen in oxidative dehydrogenation of alcohol and carbohydrates. It is believed that carbohydrates may interact with this type of promoters (Bi and Sn) in a chelating fashion,[97] thus prompting coordination of the substrate to the promoting adatom see Figure 2.8.

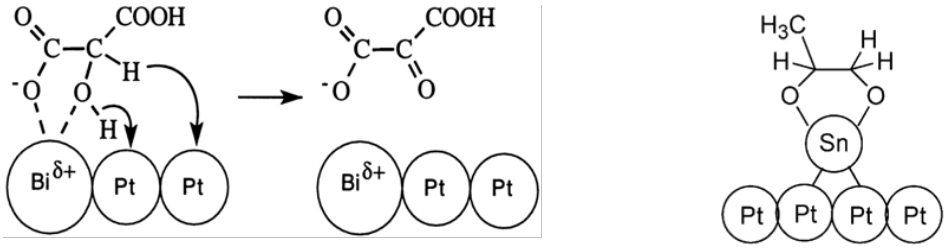

Figure 2.8: Proposed chelating promoting mechanism in the selectivity catalytic oxidation of carbohydrates.[17,97,128]

Intuitively, the promoting effect of Bi and Sn on selectivity for electron-rich substrates such as aromatic ring bearing molecules, e.g., benzyl alcohol, may be due to the interaction of the substrates by the π-adsorption of the ring on the promoter atoms deposited on the platinum surface. Besson et al.,[132] also observed an enhanced catalytic activity upon using bismuth as a promoter on benzyl alcohol oxidation over Pt/C catalyst.

2.7.2. PROMOTIONAL EFFECTS OF THE ALLOYED CATALYST SYSTEM IN ALCOHOL OXIDATION

Gold has also been shown to have promotional effects[61,105,121,133,134] in alcohol oxidation for Pd and Pt catalyst, even though it can be used as a catalyst in its own right. Wu et al.,[105] observed an improvement in the rate of benzyl alcohol oxidation upon Pd alloying with Au with a TOF of 57300 hr^{-1} compared to 12500 hr^{-1} obtained over monometallic Pd catalyst system at 110 °C. This is ascribed to a prevention of the oxidation of surface Pd and the formation of PdO species due to the presence of Au.[105] This, then, improves the catalytic activity for the alcohol oxidation reaction. On the contrary, Dimitratos et al.,[135] obtained a decrease in TOF in the oxidation of cinnamyl alcohol over Pt-Au ally compared to Pt catalyst with TOF decreasing from 38 hr^{-1} to 12 hr^{-1} over 0.4wt.-%Pt/AC and 0.6wt.-%Au0.4wt.-%Pt/AC catalyst, respectively at 60 °C. The reaction was carried out in base-free condition, which would imply that Au sites are inactive for this oxidation reaction. Hence, the TOF may have been reduced due to a decrease in the number of Pt-sites available on the surface that are blocked by an inactive Au component of the catalyst.

Table 2.1 shows examples of bimetallic catalyst systems investigated for oxidation reactions of the various organic substrate using oxygen as the oxidant. Zhang et al.,[136] showed that Pb-Pt alloy had a higher reaction rate for the oxidation of glycerol using O_2 as an oxidant at 90 °C with a TOF 101 hr^{-1} compared to monometallic Pt, which measured a TOF of 77 hr^{-1} . Similarly, Tang et al.,[137] observed in the oxidation of benzyl alcohol that alloying Pd with Pb enhances the activity, doubling the turnover frequency from $8.4 \cdot 10^4$ hr^{-1} to $19.1 \cdot 10^4$ hr^{-1} over Pd/TiO_2(P25) and Pd_3Pb/TiO_2(P25), respectively at 130 °C. Mallat et al.,[138] showed that promoting Pd supported on carbon or alumina with bismuth improves conversion of 1-methoxy-2-propanol and selectivity of 1-methoxy-2-propanone.

Similarly, a remarkably improved catalyst performance was obtained over PtBi/ NCNT in the selective oxidation of glycerol to dihydroxyacetone compared to the performance over Pt/NCNT at 60 °C.[17]

Alloying Pt/Pd catalyst system is not limited to improved activity but may also suppress the formation of undesired products during oxidation reaction. Besides modifying the active metal's adsorption properties, Ni's addition to the Pd catalyst system for the oxidation of benzyl alcohol has also been shown to enhance the productivity and selectivity of benzaldehyde by effectively suppressing the formation of toluene in benzyl alcohol oxidation.[18] The promotional effect of Ni in Pd-based system on benzyl alcohol oxidation has been ascribed to weakening of the dissociative adsorption of benzyl alcohol and prevent C-O bond cleavage owing to the synergistic effect between Pd and Ni.[18] Moreover, the presence of nickel in Pd-based catalysts is thought to enhance the removal of hydrogen by the oxygen species on the Ni surface, inhibiting the C-H bond formation. Alloying Pt/Pd with Ni may modify the interaction between oxygen and the metal, thus influencing product selectivity. Contrary to Pd-based catalyst, alloying Pt with Ni to form Pt-skin alloy weakens the adsorption of oxygen thus, retarding molecular oxygen dissociation over Pt-skin Ni-subsurface alloy.[139]

Table 2.1: Bimetallic system effect on the catalytic performance of on oxidation reaction compared to a monometallic system using oxygen as an oxidant.

Catalyst	**Substrate**	**X (%)**	**TOF (hr^{-1})**	**Selectivity (%) (Product)**
$Pd_{100}/MCF\text{-}H_2$	Benzyl alcohol[a, 105]	16	12500	66 (Benzaldehyde)
$Au_8Pd_{92}/MCF\text{-}H_2$		83	57300	71 (Benzaldehyde)
Pd NCs/TiO_2(P25)	Benzyl alcohol[c, 137]	99	$8.4 \cdot 10^4$	31 (Benzaldehyde)
Pd_3Pb NCs/TiO_2(P25)		91	$19.1 \cdot 10^4$	91 (Benzaldehyde)
5wt.-%Pt/AC	Glycerol[b, 136]	36	77	68 (Lactic acid)
1wt.-%Pb-5wt.-%Pt/AC		48	101	62 (Lactic acid)
0.4wt.-%Pt/AC	Cinnamyl alcohol[d, 135]	22	60	100 (cinnamaldehyde)
0.6wt.-%Au-0.4wt.-%Pt/AC		18	45	100 (cinnamaldehyde)

[r]**eaction conditions**: 50 mg of catalysts, 10.8 g of benzyl alcohol, T = 110 °C, pO_2 = 0.8 MPa and t = 1 h. Calculation of TOF (h^{-1}) value was done after 1h of reaction based on the total exposed metal sites.

[b]**Reaction conditions**: 0.25 g of catalyst, T = 90 °C, p = 1 atm, F_{O2} = 100 mL/min, $n_{LiOH}/n_{glycerol}$ = 1.5, stirring rate = 800 r/min. TOF was calculated based on the loading of Pt (Pb mainly served as a promoter), and conversion after 2 h.

[c]**Reaction condition**: Benzyl alcohol = 5 ml; catalyst weight = 12.5 mg; T = 130 °C; p = 10 bar; oxidant = O_2; TOF was calculated using conversion at reaction of 30 min.

[d]**Reaction condition**: Cinnamyl alcohol 0.3 M, cinnamyl alcohol/metal 1/500 (mol/mol), T = 60 ◦C, pO_2 = 1.5 atm; time of reaction = 2 h, stirring rate 1250 rpm.

Metal oxides can also be considered as a promoter for alcohol oxidation reaction as well. Redina et al.[49] suggested that the high activity for Au-CuO/SiO_2 catalyst in ethanol oxidation compared to the monometallic catalyst, Au/SiO_2 and Cu/SiO_2. This can be attributed to the interaction between metallic Au and Cu^{2+} ions. Similarly, Bauer et al.,[48] implies that close contact between the metal core and oxide shell of the Au-CuO_x catalyst generates the active sites for benzyl alcohol oxidation. This results in enhanced catalytic activity.

Bimetallic/alloyed metal nanoparticles are more beneficial in activity and selectivity than their monometallic equivalent. These improved performances can be attributed to synergistic effects arising from electronic and/or geometrical interactions between the two metals. However, it should be noted that the promotional effect of the known alcohol oxidation promoters can be multi-faceted; the role of a promoter may vary from reaction system to reaction system.

2.8. EFFECT OF SUPPORT MATERIAL ON THE ALCOHOL OXIDATION REACTION

Heterogeneous catalysis is a surface phenomenon. Thus, typically the intrinsic catalytic activity per unit mass of the active metal will decrease with increasing crystallite size of metal due to reduced exposure of the reactants to the catalytically active metal.[140] The required high dispersion of the active metal[141,142] and the required mechanical strength of the catalyst[143] require the use of support materials such as refractory oxides or carbon to deposit the catalytic active material. It has been observed that support material may play a role beyond dispersing the active metal in oxidation reactions by inducing a synergy between the active metal and the support material.[144] The effect of support material on oxidation reactions has been observed over Pt, Pd and Au-based catalysts. Qi et al.,[144] compared the effect of Mn_3O_4, CeO_2, Fe_2O_3 as support on solvent-

free, liquid-phase, palladium-catalyzed benzyl alcohol oxidation (at 1wt.-% Pd metal loading). Different levels of benzyl alcohol conversion were obtained with Pd/Mn_3O_4, Pd/CeO_2, Pd/Fe_2O_3 yielding 66 %, 43 % and 49 %, respectively. Though the reason for the observed variation in activity is not stated, however, it may be influenced by metal dispersion arising from the varying surface area of the support material. Though the surface area of the support may affect the dispersion of the active metal, the chemical nature of the support material may have a stronger influence on dispersion. Thus, resulting in different conversion levels.

Liu et al.,[82] investigated the effect of an oxide support material on the platinum-catalyzed benzyl alcohol oxidation at comparable metal dispersion. Interestingly, the TOF for benzyl alcohol oxidation within 10 hours on stream varied significantly with 6.2 hr^{-1}, 1.4 hr^{-1}, 9.5 hr^{-1}, 13.0 hr^{-1} and 0 hr^{-1} corresponding to Pt/Al_2O_3, Pt/MgO, Pt/TiO_2, Pt/ZnO and Pt/SiO_2 catalyst, respectively as summarized in Table 2.2. This gives an indication that the catalytic activity is closely linked to the metal oxide support employed. Otherwise stated, the oxide support material may influence the performance of the catalyst under oxidation reaction (of benzyl alcohol). It was noted that the high TOF obtained from Pt/ZnO may be attributed to the synergistic effect between the Pt and ZnO support. At the same time, the inactivity of the Pt/SiO_2 system is not clear. Similarly, under comparable reaction conditions, Pt/TiO_2 anatase showed a better catalytic performance for the benzyl alcohol oxidation than platinum supported on Ca(Mg)-ZSM-5 resulting in a turnover frequency of 7.3 hr^{-1} and 3.7 hr^{-1}, respectively.[145] This is ascribed to the more facile activation of molecular oxygen on TiO_2, implying a role of the support.

Table 2.2: The catalytic performance effect of an oxide support material on benzyl alcohol oxidation reaction at comparable reaction conditions[a] over Pt-based catalyst.[82]

Catalyst	Pt-loading (wt-%)	d_{Pt} [b] (nm)	D_{Pt}[c] (%)	Surface area (m^2/g)	Conversion (%)	TOF[d] (hr^{-1})
Pt/ZnO	0.80	3.2 ± 0.3	35	5	94.1	13
Pt/Al_2O_3	0.81	3.4 ± 0.4	33	150	43.0	6.2
Pt/MgO	0.83	2.5 ± 0.3	45	26	13.3	1.4
Pt/SiO_2	0.83	2.9 ± 0.3	39	423	0	0
Pt/TiO_2	0.81	3.5 ± 0.5	32	51	63.4	9.5

[a]0.1 g of a catalyst, 0.2 mmol of benzyl alcohol, and 10.0 mL of H_2O in a flask in the open air at room temperature (26 °C) in the dark for 10 hours
[b]The average particle size of Pt determined using TEM.
[c]Platinum dispersion based on particle size (D_{Pt} (%) = $113/d_{Pt}$)
[d]Defined as the amount of benzyl alcohol reacted per hour per surface Pt site.

Various factors may affect the catalytic activity, including the average particle size of the active metal at constant loadings. Chen et al.,[146] probed the influence of support material on average particle size (subsequently catalytic activity) by varying the SiO_2:Al_2O_3 ratio on silica-alumina supported Pd catalyst in the benzyl alcohol oxidation. It was stated that decreasing the SiO_2:Al_2O_3 ratio resulted in a decrease in the size of the Pd nanoparticles. This was attributed to the relative strength of interactions of the Pd precursor with the support. The decrease in particle size resulted in an increase in the TOF for benzyl alcohol oxidation. Furthermore, the particle size of Pd metal in Pd/Al_2O_3 and Pd/SiO_2 was 2.6 nm and 5.7 nm, respectively. The subsequent initial rate of reaction was over 0.52 wt.-% Pd/Al_2O_3 (1.78 mol/g/s) is thus higher than that obtained over 0.55 wt.-% Pt/SiO_2 catalyst obtaining 0.26 mol/g/s with corresponding TOF of 2988 hr^{-1} and 936 hr^{-1}, respectively evaluated from the average particle size of the Pd active metal. It was then concluded that the variation in activity cannot be correlated to Pd nano-particle size since the TOF would have to be comparable for all the samples. Therefore, the observed difference in TOF must be attributed to other factors that are unclear.

2.8.1. SYNERGISTIC EFFECT OF SUPPORT MATERIAL AND THE ACTIVE METAL ON CATALYST PERFORMANCE

It has been argued that the promoting effect of the support material is not only attributed to a physical promotion (dispersion of the active metal) but also ascribed to electronic contributions through a synergistic effect. This can be best evaluated using the turnover frequency: a change in the turnover frequency obtained with metals supported on different supports would indicate a role of the support beyond dispersing the catalytically active material. Abad et al.,[13] observed in the oxidation of 3-octanol reaction under solvent-free conditions that supporting Au over different carriers, CeO_2, TiO_2, Fe_2O_3 and C, yielded different performances, as measured by TOF (ca. 430 hr^{-1}, 215 hr^{-1}, 96 hr^{-1} and 15 hr^{-1}, respectively). This suggests that the activity of the catalyst can also be influenced by the type of support material employed for the oxidation reaction of alcohols. Corma et al.,[89] also reported a synergic effect between the noble metal (gold) and the support (ceria as nano-cubic particles) in 3-octanol oxidation. Strikingly, Corma et al.,[89] showed that ceria as nano-cubic particles exhibit an improved activity compared to ceria in a less-defined shape. This was ascribed to the presence of edge sites nano-cubic ceria, which changes in the presence of oxygen from metal ion terminated edge sites to oxygen terminated sites. Zhao et al.,[147] showed using scanning tunnelling microscopy (STM) in conjunction with Density Functional Theory calculations that benzyl alcohol adsorbs preferentially at the oxygen-terminated FeO/Pt (with FeO islands immobilized on a Pt(111) surface). The interaction between the oxygen at the edge of the FeO/Pt interface and the hydrogen of the hydroxyl group of the substrate increases the strength of adsorption of benzyl alcohol. At the same time effectively weaken the O-H bond of the substrate.[147] This will result in a decrease in the activation energy for O-H bond cleavage in the substrate when performed in the presence of boundary oxygen.[147]

It has also been suspected that some support materials may form part of the active sites during the oxidation reaction, acting as oxygen/hydroxide reservoir sites.[48,83,147] A comparison between, e.g. $Ru(OH)/Fe_3O_4$ and Ru/Al_2O_3 catalyst for the oxidation of benzyl alcohol shows that $Ru(OH)/Fe_3O_4$ showed better performance than Ru/Fe_3O_4 catalyst at comparable Ru loading and reaction conditions.[90] It is hypothesized that the formation of

Ru-alkoxide in the benzyl alcohol oxidation in the presence of $Ru(OH)/Fe_3O_4$ occurs through ligand exchange between Ru(OH) and alcohol substrate, forming water molecules as co-product. However, the metal alkoxide formation on Ru/Al_2O_3 proceeds via the activation of the O-H bond (through O-H bond breaking) in benzyl alcohol on the metal surface.[89,98,146,148] The presence of surface-bound hydroxyl (intermediate) may facilitate the O-H bond activation of the substrate through hydrogen transfer.

Puigdoller et al.,[11] and Helali et al.,[149] also argued that the reducibility of the support also affects the overall catalytic performance in alcohol oxidation reactions. Reducible oxidic support may facilitate the oxidation reaction by donating oxygen to an adsorbed species with a consequent change in the surface composition, from M_nO_m to M_nO_{m-x} thus forming oxygen vacancy sites.[11] Due to the oxygen vacancy formation, the reduced oxide may yield an enhanced reactivity compared to the stoichiometric oxide. The organic substrates may interact with these specific oxygen sites in the metal oxide surface, e.g., oxygen atoms located at low-coordinated sites (MO_{x-1}). Furthermore, the formed surface atomic oxygen derived from oxygen vacancy formation is added as a reactant, thus forming carbonyl compounds leaving behind oxygen vacant sites.[11] It is also possible that the reducible metal oxide support material may have labile oxygen species on the surface that can participate in the oxidation reactions.

The alcohol oxidation is a typical consecutive reaction, with often the formation of the carbonyl compound followed by further oxidation reactions yielding products such as carboxylic acids. In this type of reaction, the selectivity can be a strong function of the conversion level. The effect of the support material on the product selectivity thus becomes a non-trivial exercise since the selectivity over different catalyst systems must only be at comparable conversion levels.

2.9. ALCOHOL OXIDATION IN THE LIQUID-PHASE

The heterogeneously catalyzed, liquid-phase oxidation of organic substrates occurs at the liquid−solid interfaces. As such, the composition of the liquid phase near the solid surface may determine the catalytic performance, depending on the nature of

the solvent used. Toluene is often used as a solvent for benzyl alcohol oxidation,[135,150]; however, it is also one of the possible products from benzyl alcohol oxidation.[18] Narayanan et al.,[77] investigated the effect of solvent on benzyl alcohol oxidation over nanocrystalline hierarchical zeolite, NH-ZSM-5, catalyst using a variety of polar and non-polar solvents. In the study, the use of acetonitrile in benzyl alcohol oxidation exhibited the highest benzyl alcohol conversion of 97% compared to DMSO (aprotic polar solvent), hexane (non-polar) and H_2O (polar), which yielded benzyl alcohol conversion of 76%, 71% and 57%, respectively. In the presence of aprotic and non-polar solvent benzyl aldehyde selectivity is achieved in excellent yields of >96% while polar solvent H_2O resulted in low benzaldehyde selectivity of 77%. This example illustrates that the nature of the solvent in oxidation reaction of alcohols may influence the catalyst performance. Villa et al.,[151] also observed that the use of different solvents for benzyl alcohol oxidation varying catalyst performance over 1 wt.-% Pd/activated carbon (AC) and1wt.-% Pd/carbon nanotube (CNT) catalysts. In the study it is observed that various amount of a specific solvent result in very different catalytic performance. Increasing H_2O content resulted in a diminished catalyst performance. Upon substituting H_2O solvent with cyclohexane again the catalytic activity differed significantly, as summarized in Table 2.3. Also, increasing cyclohexane initial concentration, decreases the TOF for benzyl alcohol oxidation over Pd-based catalyst.

Table 2.3: Benzyl alcohol oxidation over 1wt.-%Pd-based catalyst at comparable reaction conditions[a].[151]

Solvent	TOF[b] (hr^{-1})		Toluene selectivity[c] (%)		Benzaldehyde Selectivity[c] (%)	
	Pd/AC	Pd/CNT	Pd/AC	Pd/CNT	Pd/AC	Pd/CNT
Neat	2980	1412	33	17	61	78
25 vol-% H_2O	1485	730	25	25	71	73
50 vol-% H_2O	1227	506	30	41	67	57
75 vol-% H_2O	840	554	36	37	62	59
20 vol-% Cyclohexane	2846	1462	29	24	67	74
50 vol-% Cyclohexane	1482	1340	23	3	74	92
80 vol-% Cyclohexane	490	493	8	8	88	88

[a]Reaction condition: alcohol/metal 3000/1 (mol/mol), 80 °C, pO_2 =2 atm, 1250 rpm.

[b]TOF calculated after 15 min of reaction.
[c]Selectivity at 90% conversion.

The solvent used in the alcohol oxidation also affects the product selectivity. The benzyl alcohol oxidation over Pd/(AC) in an organic solvent, cyclohexane, favours the formation of benzaldehyde at high cyclohexane initial mole contents, i.e., 80% cyclohexane. On the contrary, increasing H_2O initial moles decreases the selectivity towards benzaldehyde compared to the solvent-free system and the system using cyclohexane as a solvent at comparable conversion levels. Not only did the study reinforce that various support materials influence the catalyst performance, but also various initial moles of different solvents employed (in this case, H_2O and cyclohexane) has an influence on alcohol oxidation reaction. Furthermore, due to the formation of toluene as opposed to benzoic acid, it is evident that a parallel reaction is more probably than a consecutive reaction over Pd-based. This may indicate that Pd-based catalyst promotes carbonyl scission in benzyl alcohol oxidation, thus forming toluene as a product. As such, in a case where toluene is not desired (as it is in this current study), Pt-based catalyst can be considered for benzyl alcohol oxidation. Alternatively, Ni can be incorporated on a Pd-based catalyst to inhibit the formation of toluene, as previously discussed.[18]

In the oxidation of 1-octanol over Pt/C[25,88] the conversion of 1-octanol increased with increasing water content in the water/dioxane solvent. This has also been observed in the oxidation of 2-octanol over Pt/C catalyst[25] and 2-propanol over Pt/MCF-17[24]. The turnover frequency was 4 times higher when the liquid phase contained 80 mol-% water compared to a non-aqueous liquid phase. Donze et al.,[152] also showed that adding water to the benzyl alcohol oxidation over Pt/C increased the conversion. The role of water is still much debated. It has been proposed that water acts as a weak base, thereby facilitating the dehydrogenation step of alcohol oxidation.[25]

Alcohol oxidation is a consecutive reaction. This means that the aldehyde product that forms from alcohol oxidation can be further oxidized to carboxylic acid through its hydrate.[152] The hydrate is then oxidized to the corresponding carboxylic acid, cf. Scheme 2.3.

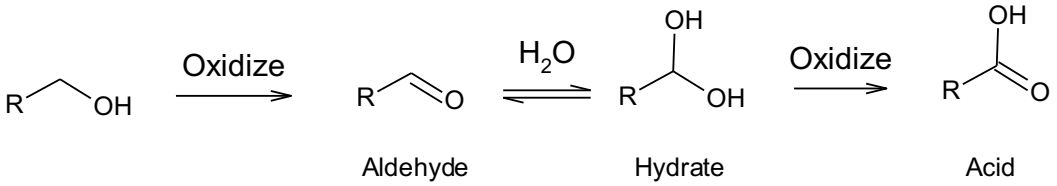

Scheme 2.3*:* Hydration of the aldehyde product, thereby forming carboxylic acid in the presence of H_2O**.**

The formed aldehyde may react further in the presence of water to generate hydration, thereby forming carboxylic acid. Donze et al.,[152] observed that the presence of water enhances benzyl alcohol conversion over Pt/C and at the same time, the increasing water content favoured further oxidation, *i.e*. the formation of benzoic acid formation through aldehyde intermediate hydration.[152]

CHAPTER 3:

Experimental procedure

Chemicals used

Chloroplatinic acid, $H_2PtCl_6 \cdot 6H_2O$, platinum(II) acetylacetonate, $Pt(O_2C_5H_7)_2$, bismuth(III) chloride, $Bi(Cl)_3$, nickel(II) acetate, $Ni(CH_3CO_2)_2 \cdot 4H_2O$, and molybdenum pentacarbonyl, $Mo(CO)_6$ (all from Sigma Aldrich) were used as precursors for the catalytically active material. The synthesis of the catalyst was performed using solvents, chloroform ($CHCl_3$, Sigma Aldrich) and benzyl ether ($(C_6H_5CH_2)_2O$, Sigma Aldrich) in the presence of surfactants, oleylamine ($C_{18}H_{37}N$, Sigma Aldrich) and oleic acid ($C_{18}H_{34}O_2$, Sigma Aldrich). Furthermore, formic acid (CH_2O_2, Sigma Aldrich), sodium hydroxide (NaOH, Kimix), iron(III)chloride ($FeCl_3$, Sigma Aldrich), Chloroform ($CHCl_3$, Sigma Aldrich), Absolute ethanol (C_2H_5OH, 99.9% Merck) given purity), and acetone (C_3H_6O, ≥99.9%, Sigma Aldrich) were used.

The catalytically active material was supported on TiO_2 (Degussa P25, Evonik, S_{BET} = 46.4 m^2/g), TiO_2 (rutile, Sigma Aldrich, S_{BET} = 44.5 m^2/g), γ-Al_2O_3 (Puralox SCCa 5-150, Sasol Technology, S_{BET} = 140.5 m^2/g), MoO_3 (Sigma Aldrich, S_{BET} = 3.0 m^2/g) and CeO_2 (Sigma Aldrich, S_{BET} = 1.7 m^2/g) were used as supports.

The reactants benzyl alcohol (C_7H_8O) and cyclohexyl methanol ($C_7H_{14}O$) were obtained from Sigma Aldrich. The solvents used in the oxidation of alcohols are deionized water (0.8 μS/cm), *m*-xylene ($C_7H_{14}O$, Kimix) and *n*-heptane (C_7H_{16}, Sigma Aldrich). The oxidation was typically performed using synthetic air (Afrox, 20% O_2 in N_2) or hydrogen peroxide (30 vol-% solution, Merck). Hydroquinone ($C_6H_6O_2$, Sigma Aldrich) was in some experiments added as a scavenger.

3.1 SYNTHESIS OF PLATINUM-BASED CATALYST BY SLURRY IMPREGNATIONS

A series of supported platinum catalysts (ca. 4 wt.-% Pt) were prepared by slurry impregnation of an aqueous chloroplatinic acid solution (0.52 M) on various support materials, which include TiO_2 (P25), γ-Al_2O_3, γ-Fe_2O_3, MoO_3 and CeO_2.

The γ-Fe_2O_3 support was synthesized by precipitation of $FeCl_3$ in an aqueous solution of NaOH at 40 °C with $FeCl_3$ and NaOH in equimolar amounts. The resulting precipitate was then washed in copious amounts of distilled H_2O three times. The resulting suspension is recovered by filtration and dried in an oven overnight at 120 °C.

The support materials were calcined in the air in a static oven at 350 °C for 2 hours before use to remove any adsorbing species, e.g., organics while in storage. The temperature was chosen to avoid any possible phase change of the support material, which may occur at higher temperatures, while being sufficiently high to desorb/decompose any adsorbing organics. The pre-treated support material was slurried in an aqueous solution of chloroplatinic acid (0.52 M). After sonication for 15 mins, the sample was placed in a crucible. The solvent water was removed by heating the sample in an oven at 120 °C for 2 hours at atmospheric pressure. The catalyst was subsequently calcined in a static oven at 350 °C for 6 hours.

3.2 SYNTHESIS OF CATALYSTS USING COLLOIDAL IMPREGNATION OF NANOPARTICLES

Various platinum-based nanoparticles were synthesized in the presence of a surfactant to obtain nano-sized particles with a narrow size distribution. The synthesis method is based on the tungsten carbonyl facilitated reductive precipitation[153–155] in the presence of surfactants. Tungsten acts as the reductant for the (noble) metal ions. In this study, a modified process using molybdenum carbonyl as the reductant for bimetallic nanoparticle synthesis was used instead of tungsten carbonyl.[156]

3.2.1 Synthesis of Pt nanostructures:

In a typical synthesis of platinum nanoparticles (NP), platinum acetylacetonate ($Pt(acac)_2$) (0.16 g, 0.41 mmol) was dissolved in benzyl ether (25 mL) and oleylamine

(OAm, 40 mL), with the latter acting as a surfactant also. The resulting metal salt-surfactant-solvent reaction mixture was heated to 150 °C and kept at that temperature for 5–10 minutes under vigorous magnetic stirring in a round bottom flask. Upon addition of the reducing agent, molybdenum hexacarbonyl ($Mo(CO)_6$) (0.1 g, 0.38 mmol), the resultant pale-yellow homogeneous solution turned dark purple with evolving cloudy smoke suggesting the evolution of gaseous CO. The synthesis mixture was then heated to 240 °C using a heating rate of 10 °C/min, upon which the mixture turned dark brown. After that, the colloidal medium was removed from the heat source and rapidly quenched to room temperature by flowing tap water over the round bottom flask to ensure minimal structural transformations/changes. Subsequently, the as-synthesized NPs were extracted from the bulk organic synthesis medium through flocculation by adding an excess amount of absolute ethanol and chloroform at equal volume. After settling (typically 1–2 days), the excess organic solvent was decanted. The particles were further cleaned by re-suspending in 20 mL absolute ethanol. This colloidal refining process was performed 3 times. The black product was finally re-dispersed in chloroform, yielding a dark brown colloidal suspension.

3.2.2 Synthesis of Pt-Ni nanoparticles

$Pt(acac)_2$ (0.16 g, 0.41 mmol) and nickel(II) acetate tetrahydrate ($Ni(CH_3CO_2)_2{\cdot}4H_2O$) (0.034 g, 0.14 mmol) were dissolved in a mixture of benzyl ether (25 ml) and oleyl amine (40 mL). The resulting metal salt-surfactant-solvent reaction mixture was heated to 150 °C and kept at that temperature for 5–10 minutes under vigorous magnetic stirring in a round bottom flask. The reduction was initiated by the addition of the reducing agent, molybdenum hexacarbonyl ($Mo(CO)_6$, 0.1 g, 0.38 mmol). The synthesis mixture was then heated to 240 °C using a heating rate of 10 °C/min. Thereafter, the colloidal medium was removed from the heat source and rapidly quenched to room temperature. Subsequently, the as-synthesized NPs were extracted from the bulk organic synthesis medium through flocculation by adding excess amounts of absolute ethanol and chloroform at equal volume. After settling (typically 1–2 days), the excess organic solvents were decanted, and the particles were further cleaned by re-suspending in 20 mL absolute ethanol. This colloidal refining process was performed 3 times. The

black product was finally re-dispersed in chloroform, yielding a dark brown colloidal suspension.

3.2.3 Synthesis of Pt-Bi nanoparticles

Chloroplatinic acid, $H_2PtCl_6 \cdot xH_2O$ (Pt content = 37-40%, 0.2 g, 0.38 mmol) and $BiCl_3$ (0.04 g, 0.13 mmol) were dissolved under vigorous stirring at 150 °C in benzyl ether (20 mL), a solvent with a high boiling point, in the presence of a mixture of surfactants oleylamine (OAm, 15 mL) and oleic acid (OLEA, 5 mL). Oleylamine also acts as a reducing agent. The resultant pale-yellow homogeneous solution was heated up to 200 °C with a heating rate of ca. 10 °C/min, subsequently obtaining a dark brown suspension. The resultant bulk organic synthesis media was maintained at 200 °C for 5-10 mins, removed from the heat source and allowed to cool down to room temperature. Subsequently, the as-synthesized material was extracted from the bulk organic synthesis medium through flocculation by adding excess amounts of absolute ethanol and chloroform. After settling (typically 1–2 days), the excess organic solvent was decanted, and the material was further cleaned by re-suspending in absolute ethanol. This colloidal refining process was performed 3 times. The black product was finally re-dispersed in chloroform, yielding a dark brown colloidal suspension.

3.2.4 Deposition of platinum-based catalyst on TiO_2 (Rutile)

The as-prepared nanoparticles were deposited on titanium(IV)dioxide (TiO_2) rutile (nano-powder, particle size <100 nm) via colloidal impregnation. On the basis of calculated Pt mass (0.075 g), 1 wt.-% loading of Pt in Pt/TiO_2, Pt_3Ni/TiO_2, $PtNi/TiO_2$ and $Pt\text{-}Bi/TiO_2$ was prepared by adding TiO_2 (7.4 g, assuming 100% recovery of the Pt-nanoparticles during the flocculation/purification process) to the 20 mL colloidal suspension, followed by vigorous sonication at room temperature for 20 mins. The resulting catalyst-support mixture was dried in a fume hood at room temperature overnight. The surfactants attached to the surface of the nanoparticles were removed by the addition of 20 mL formic acid (CH_2O_2) to the dried sample and further sonication for 15-20 mins. The product, catalyst-support, was again washed six times using an excess

mixture of ethanol and acetone in an equimolar ratio to remove CH_2O_2 and some surfactants. Finally, the as-impregnated materials were dried overnight at 70 ℃ in an oven.

3.3 CATALYST CHARACTERIZATION

A variety of characterization methods have been employed to elucidate the composition, morphology of the catalyst.

3.3.1 Inductively coupled plasma-optical emission spectroscopy (ICP-OES)

The elemental composition of the catalysts was determined by inductively coupled plasma-optical emission spectroscopy (*ICP-OES*) using a Varian ICP 730-ES spectrophotometer. The samples were digested in a MARS-5 Microwave digester. The calcined and uncalcined samples of the catalysts (ca. 50 mg) were placed in Xpress Teflon tubes. A mixture of 6 mL concentrated HCl-solution, 2 mL concentrated HF-solution, and 2 mL concentrated HNO_3-solution was used to digest each sample.

3.3.2 Transmission electron microscope (TEM)

The morphology of the unsupported nano-sized particles and nanoparticles on the supports were imaged using a transmission electron microscope (TEM) using a TECHNIA 200II operating at 200 kV. The samples were sonicated in methanol for ca. 10 minutes. Subsequently, the suspension was loaded on a carbon copper-coated grid for analysis. The particle size distribution and the average particle size of the nano-sized particles representing the noble metal were determined by measuring between 70 and 200 nanoparticles using ImageJ®.

3.3.3 X-ray diffraction analysis (XRD)

The phase composition of the catalyst samples was analyzed using XRD on a Bruker D8 ADVANCE diffractometer (Co-K_α radiation, 35 kV, 40 mA). The scan was taken from 2θ =20° to 100°, and the obtained diffraction patterns were compared to the one reported for standard compounds in the JCPDS data file.

3.3.4 Fourier Transform Infra-Red Spectroscopy (FTIR)

FTIR spectroscopy was used to observe characteristic bands of various species on the surface of supports impregnated with platinum. A total of 32 scans were taken in the range between 400 and 4000 cm^{-1} for each sample with a resolution of 4 cm^{-1}. A background scan is taken before every analysis.

3.3.5 CO Chemisorption

The number of active sites on the surface of the catalysts was determined by CO chemisorption analysis using an ASAP 2020 C unit. The sample (ca. 100 mg) was degassed with helium (He) at 350 °C for 30 mins. The sample was held at 350 °C under flowing hydrogen for 12 hours at atmospheric conditions. Followed by evacuation of the sample with He for ca. 165 mins at 125 °C. CO chemisorption was performed at 35 °C.

3.3.6 NH_3 Temperature programmed desorption (NH_3-TPD)

The temperature-programmed desorption (TPD) of ammonia was used as an alternative method to determine the metal surface area using Micromeritics Autochem II. After the sample (ca.150 mg) was degassed for one hour with helium at a flow rate of 20 mL_n/min at 500 °C, 5%NH_3/He at a flow rate of 20 mL_n/min was passed over the sample at 120 °C. The remaining gaseous physisorbed ammonia was removed at 120 °C using helium at a 20 mLn/min flow rate for 1 hour. Subsequently, the sample temperature was increased linearly (heating rate: 10 °C/min) to 700 °C. At that temperature, it was kept for 3 hours. The composition of the effluent was monitored by a thermal conductivity detector (TCD). It should be noted that a cold trap (using liquid nitrogen) was employed to condense any desorbing H_2O from the sample. This was to prevent any effects of the desorbing H_2O on the NH_3-TPD profile of each sample.

3.3.7 X-ray photoelectron spectroscopy (XPS)

Semi in-situ XPS analysis of Pt-Bi/TiO_2(rutile) sample was performed at the SXS (soft X-ray spectroscopy) beamline D08A at the Brazilian Synchrotron Light Laboratory (LNLS), Campinas, Brazil, with excitation energy of 1922.6 eV using a PHOIBOS 150

electron analyzer. Before the oxidation treatment, the XPS survey scan and a scan in the region of interest of the sample were obtained. Subsequently, the sample was treated with air (10 mL_n/min) at 350 ºC in the preparation chamber for 3 hours. After the oxidation treatment, the sample was transferred to the analysis chamber. Again, high-resolution spectra were recorded using 40 eV pass energy and 0.1 eV energy step with survey scans of the samples obtained prior and post oxidation treatment between 1100 - 4 eV binding energy range. The Pt (4d and 4f) and Bi (4d) binding energy were analysed.

The binding energy in all the spectra was calibrated to the O 1s and Ti 2p photoemission peak of the oxide support at 462 eV and 532 eV, respectively. Linear-type background subtraction was applied to the photoemission lines, which were fitted using a combined Gaussian-Lorentzian line shape (CasaXPS). The Pt (4d, 4f) and Bi (4d) spectra were fitted to two components (metallic and coordinated metal) based on the binding energy values.

3.3.8 Enthalpy of immersion

The hydrophobicity/hydrophilicity of the support materials was determined by measuring the enthalpies of immersion at 25 °C using a Precision Solution Calorimeter (TA instruments). The instrument was electrically calibrated against a known power input to determine the specific heat capacity of the calorimetric system. The solution calorimeter was chemically calibrated using the dissolution of KCl (NBS1655) as a test reaction at 298.15 K.[157]

A brittle glass ampoule loaded with dry oxide support of known weight was sealed using silicon rubber and molten beeswax. The sealed ampoule was inserted into the stirrer and the reaction vessel, which was filled with 100 mL of H_2O liquid using a pipette. Enthalpy of immersion measurement was initiated by breaking the glass ampoule once thermal equilibrium was achieved.

3.3.9 Capillary rise experiment

The hydrophobicity/hydrophilicity of the support materials was further probed by measuring the contact angle between the support and water. The common method to measure the contact angles, in this case, is to conduct capillary rise experiments where the sample is suspended below a balance. The dry metal oxide powder is placed in a powder holder. Small holes in the bottom covered with filter paper are immersed into the testing liquid. The amount of liquid absorbed into the powder bed is measured against time. Figure 3.1 shows the absorption of liquid of powder sample to determine the capillary constant and contact angle using the Washburn method.

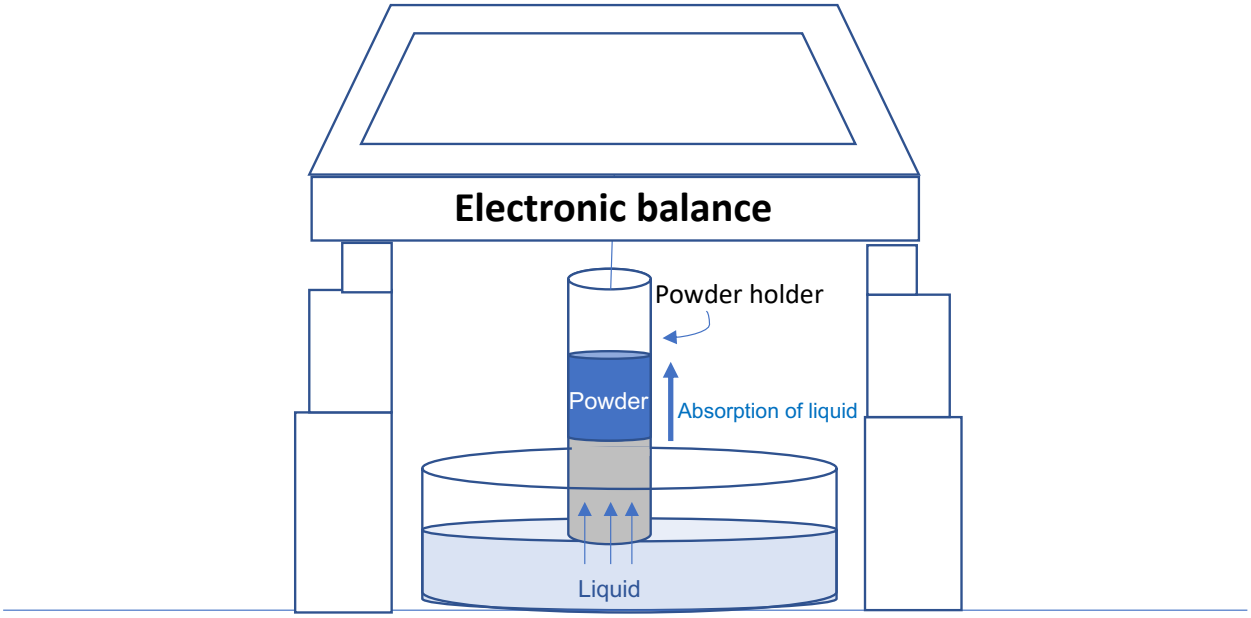

Figure 3.1: Schematic representation of liquid absorption of the metal oxide support material to determine contact angle using capillary rise.

The capillary constant was determined before determining the contact angle measurements of the oxide support material with H_2O. The capillary constant can be determined by dipping the sample into a complete wetting liquid, n-hexane. Thus, the H_2O contact angle of each oxide is derived from the average capillary constant of each oxide material using the Washburn method, refer to appendix A-3.1. Figure 3.2 show the measurement set up for capillary constant and contact angle using the Washburn method.

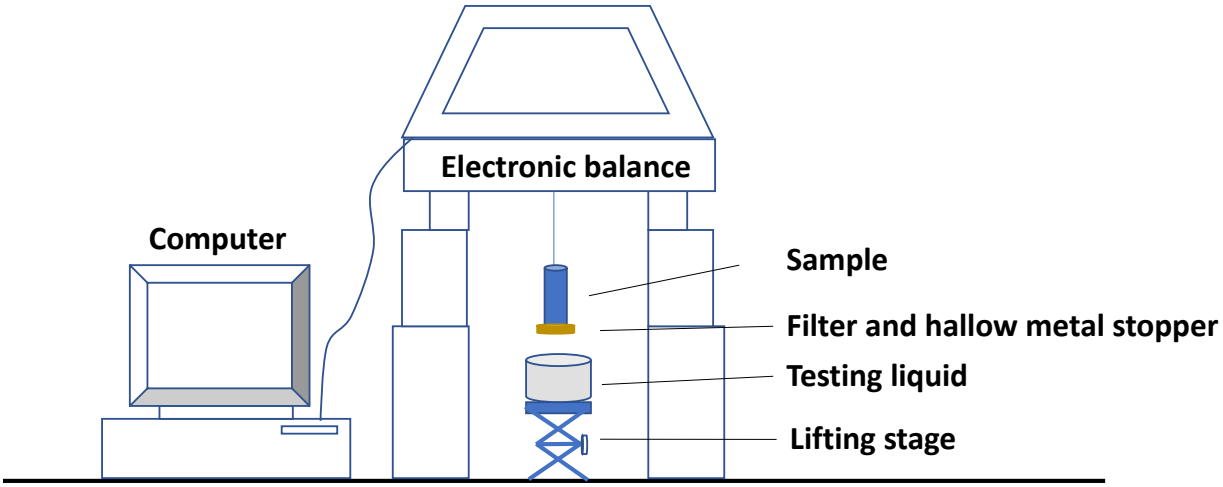

Figure 3.2: Wash-burn method contact angle and capillary rise measurement set up.

3.3.8. DFT CALCULATIONS

Periodic DFT calculations were performed to predict the effect of H_2O on O_2 adsorption on a p(3x3) Pt(111) surface slab. using the *Vienna Ab Initio* Simulation Package (VASP).[158,159] A generalized gradient approximation exchange-correlation functional with the Perdew, Burke and Ernzerhof (PBE) functional,[160] was used with the projector augmented wave (PAW) method.[161] Spin polarization was considered in all calculations. A set with a 400 eV kinetic energy cut-off was used. All relaxed atoms were optimized by minimizing the Hellman-Feynman forces to below 0.02 eV/Å. The energy was converged within 10^{-5} eV/unit cells in the self-consistency loop. The description of the electronic structure optimization was based on the Methfessel-Paxton scheme[162] with a smearing width of 0.1 eV for adsorbed states, while Gaussian smearing with a smearing width of 0.01 eV was used for gas-phase O_2 molecules. In both cases, adsorbed states and O_2 gas, the total energies were extrapolated to 0 K. The climbing image nudged elastic band (CI-NEB) method[163] was used together with the fast-inertial relaxation engine (FIRE)[164] to determine the transition states for the diffusion of atomic oxygen.

3.4. CATALYST TESTING

The performance of the synthesized platinum-based catalysts was evaluated for selective oxidation reactions in a semi-batch reactor system.

3.4.1 Reactor set-up

The liquid-phase oxidation reactions were carried out in a 250 mL autoclave reactor equipped with a magnetic stirrer, gas inlet stream, dip tube, and liquid condenser. The pressure of the synthetic air stream is reduced to ca. 5 bar, and its flow rate is controlled using a mass flow controller. The gas is sparged under the impeller through the liquid. The gas passes through a condenser operating at -7 °C, to remove the condensable vapours from the effluent. The pressure in the system was monitored using a pressure indicator mounted after the condenser. The gas flow rate was checked using a bubble foam meter.

The temperature in the reactor was maintained using an external heating element with a thermo-element measuring the temperature in the liquid. Samples of the liquid could be taken using the dip tube.

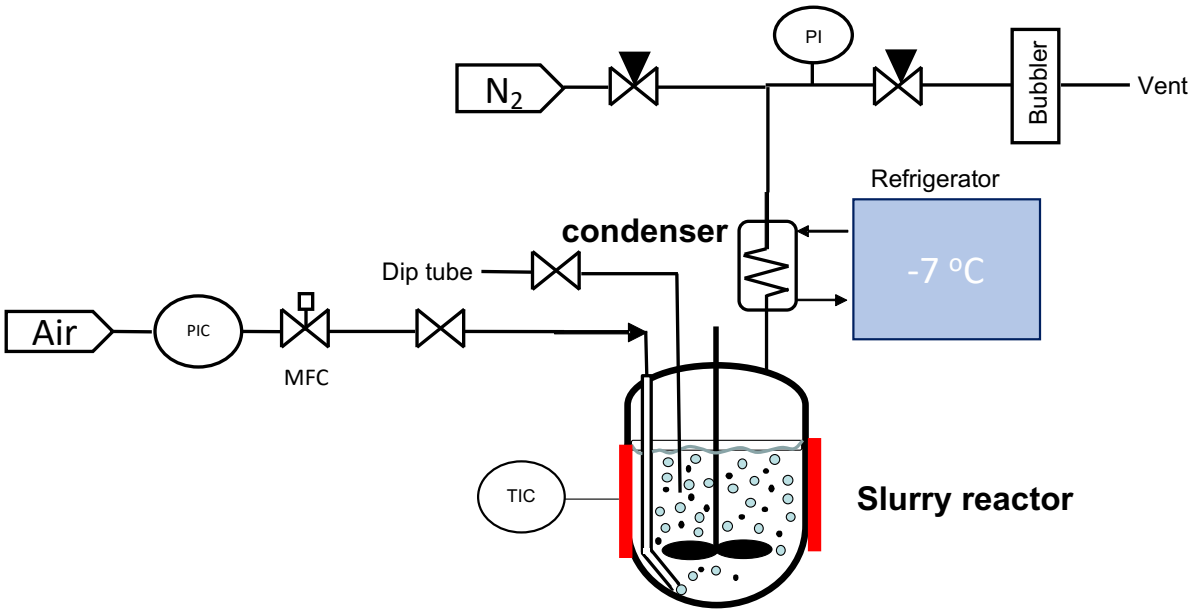

Figure 3.3: Semi-batch reactor schematic for the alcohol oxidation reaction. PIC: flow control valves; TIC: temperature controller, MFC: Mass Flow Controller, PI: Pressure Indicator and TI: Temperature Indicator.

3.4.2 Reaction procedure

The batch reactor (250 mL autoclave) is filled with a total of 70 mL of liquid with varying compositions for the different oxidation reactions. Different organic substrates were used, i.e., benzyl alcohol and cyclohexyl methanol, for oxidation reactions.

Benzyl alcohol oxidation was tested using various solvent systems, which include water, n-heptane and/or m-xylene in various proportions. Cyclohexyl methanol oxidation was also tested using water as a solvent system. A catalyst (0.5 g) is then added to the liquid mixture. The autoclave is closed and reactor tightened, ensuring that the reactor is not leaking using N_2 for pressure testing and stirred at 850 rpm. The reactor system is heated to the desired temperature at 10 ºC/min in nitrogen at atmospheric pressure. The N_2 valve was then closed, and the reactor was degassed. It was pressurized using air at a flow rate of 100 mL_n/min after the reactor attained the required reaction temperature.

After reaching a pressure of 5 bar, the outlet valve was opened, ensuring a constant flow of air out of the reactor. The catalyst was tested for 5 hours. The starting time of the reaction for some reactions is difficult to define, especially for reactions occurring at elevated temperatures and/or pressures. For this study, airflow (as an oxidant) into the reactor at the desired temperature marks the reaction's starting time (time zero).

Experiments using H_2O_2 as an oxidant were also carried out in a 250 mL autoclave batch reactor. A total liquid composition of 90 mol-% H_2O_2 in benzyl alcohol was used for alcohol oxidation with a total liquid volume of 74 mL. A catalyst (0.5 g) was then added to the liquid mixture. The autoclave is tightly closed and heated to 90 ºC at 10 ºC/min without any gas flow. Heating of the reactor to 90 ºC marked time zero for these experiments.

A blank experiment showed no conversion of benzyl alcohol/cyclohexyl methanol in the absence of Pt-based catalyst, confirming that benzyl alcohol/cyclohexyl methanol does not undergo autoxidation and all the support material is inactive under these conditions.

3.4.3 Sampling

Sampling was conducted hourly through the dip tube for the first 5 hours for all alcohol oxidation runs. Sampling was performed while stirring due to the biphasic nature of the reaction liquid (organic and aqueous liquid phases). It should be noted that during sampling, some catalysts may have also been sampled with the liquid reaction medium (ca. 0.1 mL of liquid). As such, sampling was only done hourly for 5 hours to minimize the loss of catalyst from the reactor.

The withdrawn liquid may consist of an organic and an aqueous phase. A known amount of methanol or acetone was added to homogenize the liquid sample and act as an external standard. However, the absolute determination of conversion and selectivity was not possible at the time-resolved measurement since the amount of the aqueous and organic phases withdrawn from the reactor may vary.

3.5. PRODUCT ANALYSIS

Various methodologies were employed to elucidate and monitor the extent and the selectivity of the oxidation reaction of organic substrates.

3.5.1. Gas chromatography using GC-FID

A GC (Varian 3400) fitted with a flame ionization detector (FID) was used to analyze the organic compounds in the samples. Helium was used as a carrier gas. The operating conditions and the gases detected in the column are given in Table 3.1.

Table 3.1: Conditions for gas-chromatographic analysis conditions

	Conditions
Compounds analysed	Liquid organic compounds
Column	Capillary column, stationary phase: VF-1ms, length: 15 m, inner diameter: 0.25 mm, film thickness: 0.25 µm
Column Temperature (^{0}C)	40 ˚C, 0.2 min isothermal 30 ˚C/min to 80 ˚C, 0.2 mins isothermal 30 ˚C/min to 120 ˚C 0.2 isothermal
Mode	Splitless
Carrier gas	He
Detector Temperature (°C)	200
Injector Temperature (°C)	200
Inlet Pressure (psi)	28.5

The FID response is carbon-specific and will allow for the determination of the compounds by the carbon numbers. Carboxyl and carbonyl groups, however, will give a different response, as the carbon-oxygen bond does not break during the cracking reactions within the flame. Single carbon-oxygen bonds result in a lower response. For this reason, mass-specific theoretical response factors were applied to account for these differences. The factor is calculated using the following equation:

$$f_i = \frac{N_C}{N_{C-C}+0.55 \cdot N_{C-O}+0 \cdot N_{C=O}} \qquad 3.3$$

Where f_i is the theoretical response factor (see Table A-3.1 in the Appendix), N_C is the carbon number of the compound, $N_{C\text{-}C}$ is the number of carbon atoms not bonded to an oxygen atom, and $N_{C\text{-}O}$ is the number of carbon atoms with a single bond to an oxygen atom. To determine the number of moles of each compound present in the samples, the following equation was used:

$$n_i = \frac{f_{methanol}}{f_{C,i} \cdot N_{C,i}} \cdot \frac{A_i}{A_{methanol}} \cdot n_{methanol} \qquad 3.4$$

Where n_i, N_i, f_i, and A_i are the number of moles, carbon number, response factor and peak area, respectively, for compound i, whereas the subscript 'methanol' refers to the internal standard methanol. It should be noted that upon adding methanol as the internal standard, the solution was homogenous, i.e., single phase.

3.5.2. Gas chromatography using GCxGC -MS

A 2-dimensional GC, GCxGC (LEGO PEGASUS 4D GCxGC TOFMS) fitted with a mass-specific detector (MS) was used to analyse samples. Helium was used as a carrier gas. The operating conditions are given in Table 3.2.

3.6. DATA EVALUATION

The sample readings taken were used to calculate the substrate conversion (X_i):

$$X_i = \left(1\text{-}\frac{f_i \cdot A_i}{\sum_j f_j \cdot A_j}\right) \cdot 100\% \qquad 3.5$$

The selectivity of a reaction to the product *j* is defined as the amount of product formed relative to the amount of reactant converted. In this study, the selectivity of the product obtained was determined as:

$$S_j = \frac{f_j \cdot A_j}{\sum_{k \neq i} f_k \cdot A_k} \cdot 100\% \qquad 3.6$$

The rate of reaction was determined from the mole balance around the semi-batch reactor with

$$r_i = \frac{dN_i}{dt} \qquad 3.7$$

and thus, the rate of reaction can be determined from the slope of the conversion as a function of reaction time

$$-r_i = N_{i,0} \cdot \frac{dX_i}{dt} \qquad 3.8$$

The turnover frequency (TOF) and platinum-time yield (PTY) were determined according to equations 3.9 and 3.10, respectively.

$$TOF = \frac{r_i}{(Pt\ dispersion)} \qquad 3.9$$

$$PTY = \frac{r_i}{m_{cat} \cdot \frac{loading_{Pt}}{M_{r,Pt}}} \qquad 3.10$$

Table 3.2: Conditions for GCxGC-MS (LEGO PEGASUS 4D GCxGC TOFMS) chromatographic analysis conditions.

Parameter	**Information/Values**
Sample analysed	Liquid organic compounds
Carrier gas	He
	Settings and conditions of the injector
Injection method	Split
Split ratio	1:400
Injection temperature	250 ˚C
	Columns specifications
Primary column	Varian capillary column, stationary phase: CP-Wax 52 CB, length: 30 m, inner diameter: 250 µm, film thickness: 0.25 µm
Secondary column	Fused silica capillary column, stationary phase: RTX-5, length: 1.39 m, inner diameter: 180 µm, film thickness: 0.2 µm
	Setting and conditions used during the GC×GC analysis
Detector	Time of flight mass spectrometer (TOF-MS)
Total flowrate	1.4 ml/min
Detector temperature	225 ˚C
Modulator offset	+35 ˚C
Modulation period	6 seconds
Hot pulse	1.5 seconds
Cold pulse	1.5 seconds
Primary oven	40 ˚C, 0.2 min isothermal 30 ˚C/min to 80 ˚C, 0.2 mins isothermal 30 ˚C/min to 120 ˚C 0.2 isothermal
Secondary oven	75 ˚C, 0.2 min isothermal 30 ˚C/min to 115 ˚C, 0.2 mins isothermal 30 ˚C/min to 155 ˚C 0.2 isothermal
Total analysis time	11 mins

CHAPTER 4:

The influence of water on benzyl alcohol oxidation over Pt/TiO_2(P25) catalyst

OVERVIEW

Water has been observed to promote alcohol oxidation over gold, platinum and palladium-based catalysts.[31,32] This opens up the possibility of synthesizing high-value organic compounds synthesis (through heterogeneous catalyzed alcohol oxidation) using a more environmentally benign methodology. Water is an easily accessible solvent, and its use for industrial processes, such as alcohol oxidation, may promote green chemistry. However, the effect of H_2O on alcohol liquid oxidation is not well understood, especially considering that it may form two immiscible phases with the substrate. Here, the effect of water on benzyl alcohol oxidation has been explored.

4.1 BENZYL ALCOHOL + WATER SYSTEM

Liquid-phase oxidation of organic substrates typically results in the co-formation of water. This may lead to phase separation in the reaction mixture, i.e., the formation of an organic and an aqueous phase, depending on the miscibility of the organic substrate and water and on the amount of water formed in the reaction. Hence, heterogeneously catalysed oxidations of organic substrates using air as an oxidant may involve up to four different phases, viz. a gas phase (air), a solid phase (catalyst), a liquid organic phase and an aqueous phase. It is, thus, of interest to gain a thorough insight into the phase composition at equilibrium in this type of reaction, in particular when water is present in the reaction mixture.

4.1.1. PHASE SEPARATION IN THE LIQUID-PHASE - THERMODYNAMIC MODELLING

The liquid-liquid equilibrium (LLE) of the system benzyl alcohol + benzaldehyde + water has been determined experimentally at temperatures between 303 and 343 K by Wang et al.,[165] The reported data were re-fitted to the non-random two liquid (NRTL) model using ASPEN® since the reported parameters did not seem to describe the reported data well. The data were fitted to:

$$x_i^{aqueous} \cdot \gamma_i^{aqueous} = x_i^{organic} \cdot \gamma_i^{organic} \qquad 4.1$$

with the activity coefficients given by

$$\ln(\gamma_i) = \frac{\sum_{j=1}^{3} \tau_{ji} \cdot G_{ji} \cdot x_j}{\sum_{k=1}^{3} G_{ki} \cdot x_k} + \sum_{j=1}^{3} \frac{G_{ij} \cdot x_j}{\sum_{k=1}^{3} G_{kj} \cdot x_k} \cdot \left(\tau_{ij} - \frac{\sum_{m=1}^{3} \tau_{mj} \cdot G_{mj} \cdot x_m}{\sum_{k=1}^{3} G_{kj} \cdot x_k} \right) \qquad 4.2$$

with $$\tau_{ij} = e^{-a_{ij} + \frac{b_{ij}}{T}} \qquad 4.3$$

$$G_{ij} = e^{-\alpha_{ij} \cdot \tau_{ij}} \qquad 4.4$$

where T is the absolute temperature (K), and a_{ij} and b_{ij} are the binary interaction parameters in the NRTL model. The data were regressed with all non-randomness parameters, α_{ij}, set at 0.2 and the energy parameters searched in the range of [–1000, 1000]. The regressed NRTL binary parameters, a_{ij} and b_{ij}, for the system benzyl alcohol (1) + benzaldehyde (2) + water (3) are shown in Table 4.1.

Table 4.1: Optimized binary interaction parameters for the NRTL model for benzyl alcohol (1) + benzaldehyde (2) + water (3) system obtained by regressing data obtained at 303.15 to 343.15K under atmospheric pressure by Wang et al.,[165,166]

ij	**α_{ij}**	**a_{ij}**	**a_{ji}**	**b_{ij}, K**	**b_{ji}, K**
12	0.2	6.37	-4.69	-173.48	1720.59
13	0.2	-3.32	6.75	735.16	-267.37
23	0.2	1.64	0.26	264.57	-548.07

Figure 4.1 shows the liquid-phase diagram for the system benzyl alcohol (BA) + benzaldehyde + water at 363 K. Benzyl alcohol and the primary oxidation product, benzaldehyde, are completely miscible at 363 K. However, neither the reactant nor the product is completely miscible with water. Phase segregation can be expected in the oxidation of benzyl alcohol using air at 363 K starting from pure benzyl alcohol at a conversion of benzyl alcohol of more than 60-70% of all produced water remains in the liquid phase. Conversely, the oxidation of benzyl alcohol using air as the oxidant will take place in a single liquid phase if the conversion is less than ca. 60%. It can be further noted

that the addition of water to benzyl alcohol may result in the formation of a reaction system containing two liquid phases if the water content is more than 55 mol-% and less than 99.5 mol-%.

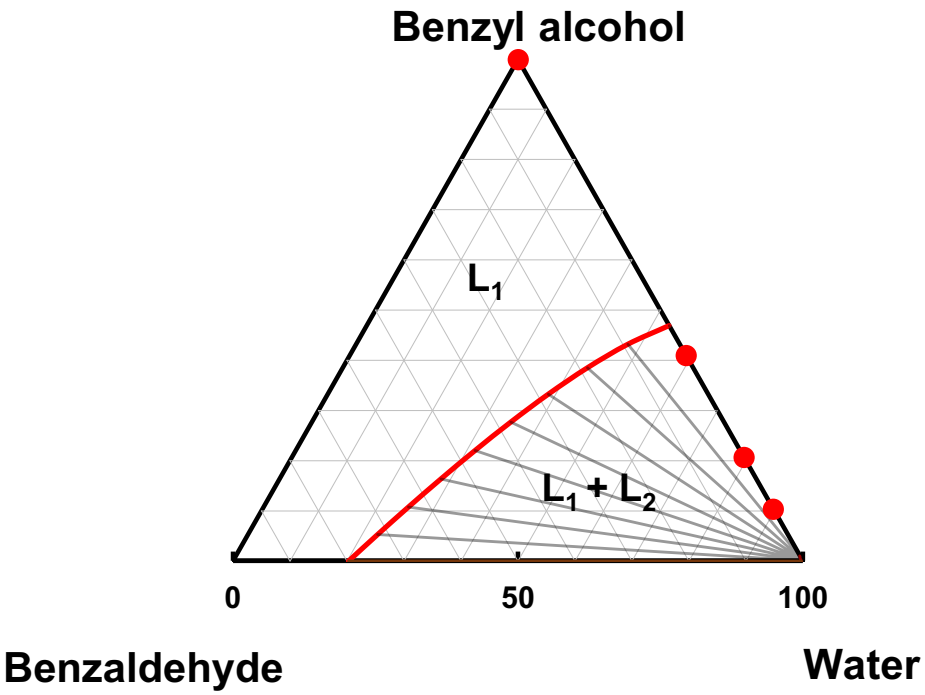

Figure 4.1: Liquid-Liquid Equilibrium (LLE) in the ternary system benzyl alcohol + benzaldehyde + water at 363.15 K and 501.125 kPa as estimated using NRTL model (parameters given in Table 4.1; concentration given in mole-%. Dots indicate the composition of the liquid mixtures investigated for benzyl alcohol oxidation in this study.

Evidently, the use of water as a solvent in an organic reaction mixture may result in the presence of two different liquid phases. Vigorous agitation may disperse the aqueous phase throughout the organic phase or vice versa. Figure 4.2 illustrates the emulsion of water and benzyl alcohol at various compositions (reported in mole percent of H_2O in the system) after the intensive stirring of the mixture. With increasing water content, the number of droplets decreases, implying the formation of an oil-in-water

emulsion rather than a water-in-oil emulsion (the latter would have increased the number of droplets with increasing water content).

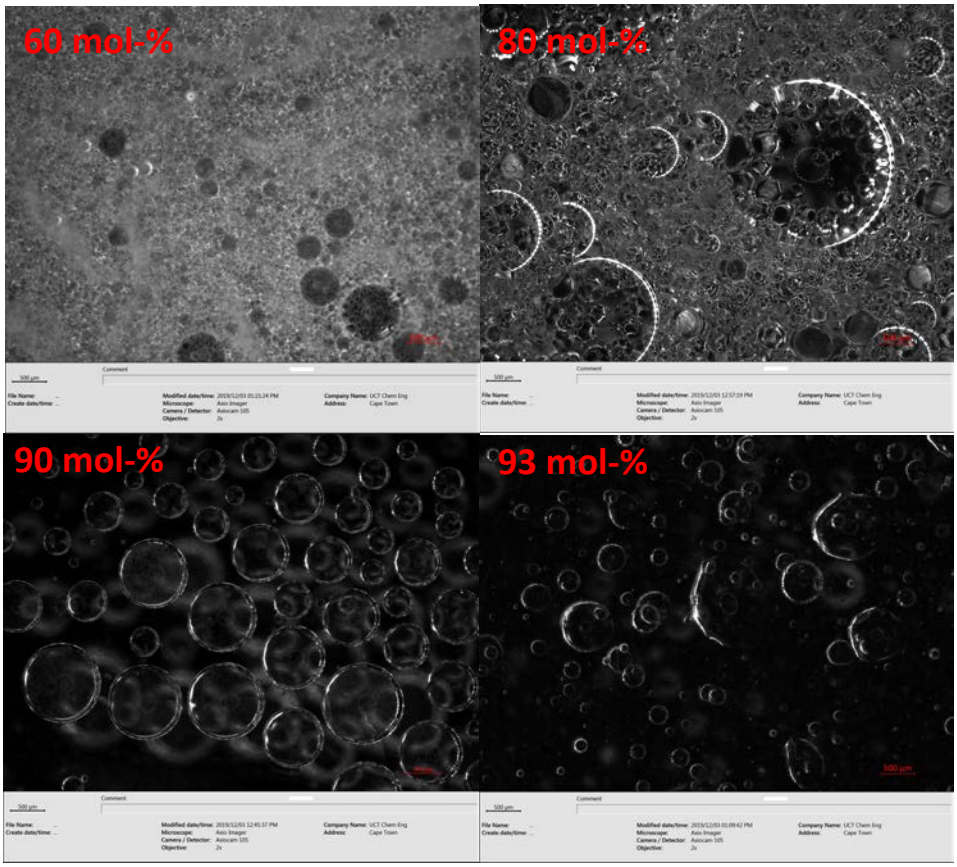

Figure 4.2: Water/benzyl alcohol emulsions with 60 mol-% water (top-left), 80 mol-% water (top-right), 90 mol-% water (bottom-right) and 93 mol-% water (bottom-right).

In a two-phase liquid system, the catalyst may be associated preferentially with one of the liquid phases or randomly distributed over the two phases. Hence, the hydrophobicity of the catalyst, Pt/TiO_2(P25), was investigated for each liquid composition. Approximately 0.05 g of Pt/TiO_2(P25) catalyst was suspended in 5 mL of a water/benzyl alcohol emulsion with various ratios of water to benzyl alcohol. The suspension was sonicated and viewed under a microscope. The recorded images (see Figure. 4.3) indicate that the catalyst is mainly associated with the organic phase rather than the aqueous phase or the interface between the organic and the aqueous phase. This

observation is consistent with the hydrophobic nature of the TiO_2(P25) support, as suggested by the measured contact angle of 89.5° of TiO_2(P25) in H_2O (see Chapter 6).

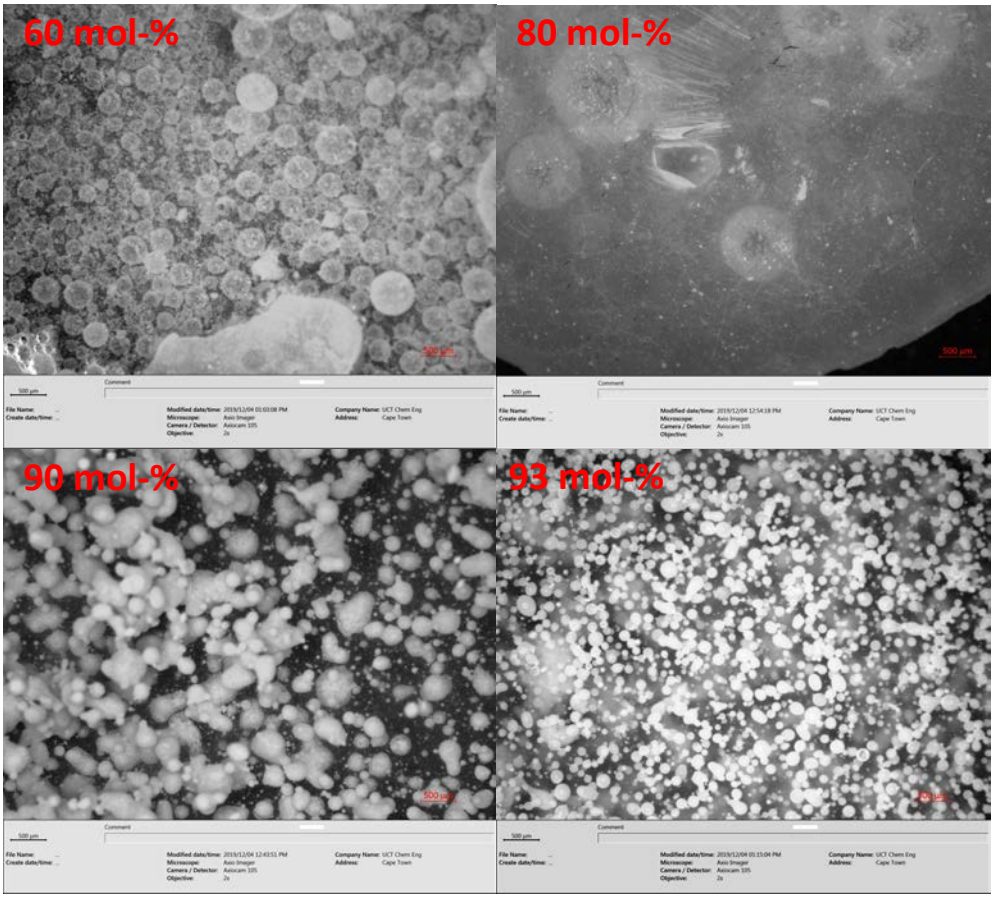

Figure 4.3: Sonicated water/benzyl alcohol emulsions containing Pt/TiO_2(P25) (0.01 g/mL) containing 60 mol-% water (top-left), 80 mol-% water (top-right), 90 mol-% water (bottom-right) and 93 mol-% water (bottom-right).

4.2 BENZYL ALCOHOL OXIDATION

Benzyl alcohol oxidation in the liquid phase using air as an oxidant was used as a model reaction to systematically probe the effect and the role of water in selective oxidations of organic substrates over Pt/TiO_2. The benzyl alcohol oxidation was performed in a semi-batch reactor at 90°C using synthetic air as the oxidant (total pressure = 5 bar) using 0.5 g of a 3.9 wt.-% Pt/TiO_2(P25). The platinum particles had an average size of 4.6 ± 0.8 nm (see Appendix B-4.1). CO and O_2 chemisorption and

dispersion analysis of Pt/TiO_2(P25) is outlined in Appendix B-4.2. Blank experiments (in the absence of a catalyst) showed no substantial benzyl alcohol conversion indicating that the benzyl alcohol does not undergo auto-oxidation under these conditions. Moreover, the support material, TiO_2(P25), was shown to be inactive for the liquid-phase oxidation of benzyl alcohol as well. Substantial conversion of benzyl alcohol was only obtained in the presence of Pt/TiO_2(P25) catalyst.

4.2.1. THE CATALYTIC PERFORMANCE IN WATER + BENZYL ALCOHOL MIXTURES

The influence of the addition and amount of H_2O on the aerobic benzyl alcohol oxidation was studied over Pt/TiO_2(P25) catalyst at 90 °C at 5 bar in a semi-batch reactor. The total liquid volume was kept constant at 70 mL, but the initial water content in the overall liquid was varied between 0 mol-% water and 90 mol-% water, cf. Table 4.2. Hence, the initial number of moles of benzyl alcohol in the mixture was changed as well. As such, it should be noted that (due to changing benzyl alcohol:catalyst ratio) the catalytic activity is monitored in terms of the number of moles of benzyl alcohol converted with time on stream.

Table 4.2: Various liquid compositions mixtures containing benzyl alcohol (BA) + water

H_2O (vol-%)	BA (vol-%)	H_2O (mmol)	BA (mmol)	Total (mmol)	H_2O (mol-%)	BA (mol-%)
0.0	70.0	0.0	647.3	676.4	0.0	100.0
14.0	56.0	776.9	517.8	1317.9	58.9	41.1
28.0	42.0	1553.8	388.4	1959.4	79.3	20.7
42.0	28.0	2330.7	258.9	2600.9	89.6	10.4

4.2.1.1. CATALYTIC ACTIVITY

Figure 4.4 shows the effect of H_2O at various H_2O-benzyl alcohol liquid compositions over Pt/TiO_2(P25) catalyst as a function of time. The number of moles of benzyl alcohol converted in a solvent-free system (absence of H_2O as a solvent, denoted as 0 mol-% H_2O in benzyl alcohol) after a reaction time of 5 hours was *ca*. 3.61 mmol.

The first observation is that upon the addition of H_2O solvent into the system, the number of moles of benzyl alcohol converted increased drastically from 3.61 mmol to 99.1 mmol for the liquid composition at 90 mol-%H_2O in benzyl alcohol after 5 hours. Evidently, the presence of H_2O enhances the catalytic activity of Pt/TiO_2(P25) in benzyl alcohol oxidation. However, it should be noted that the number of moles of benzyl alcohol converted per unit time is constant for all liquid compositions containing H_2O as a solvent, i.e., 90 mol-%, 80 mol-% and 60 mol-% H_2O in the benzyl alcohol system. Due to varying initial moles of benzyl alcohol with changing BA/H_2O liquid composition while keeping catalyst loaded in the reactor constant (thus changing benzyl alcohol:catalyst ratio), the number of moles of benzyl alcohol converted per is expected to be comparable for all BA/H_2O liquid compositions.

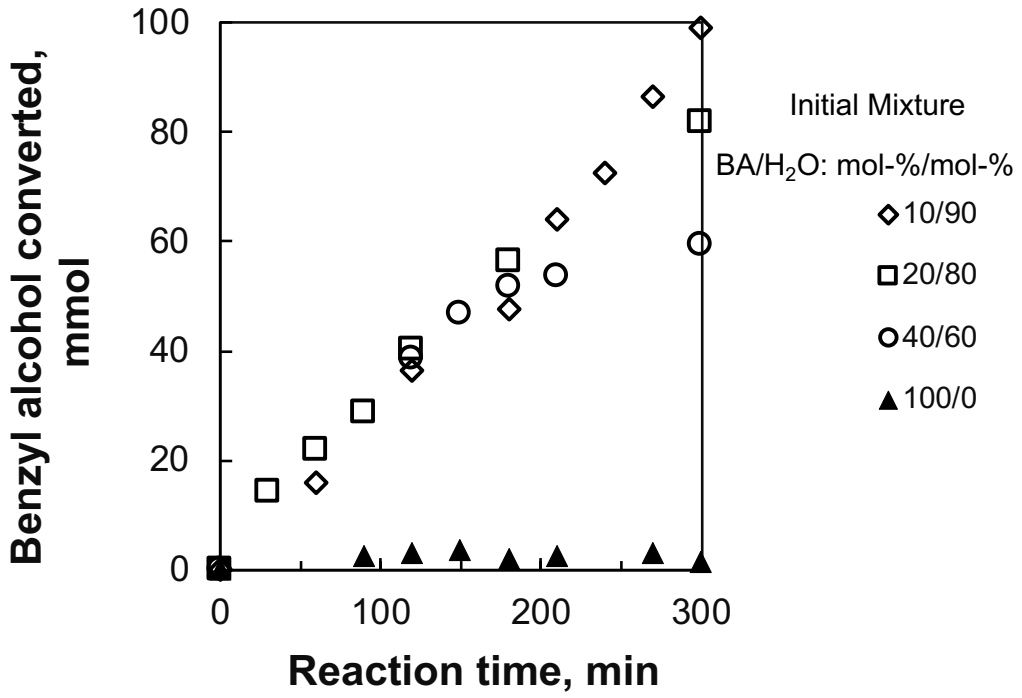

Figure 4.4: Number of moles of benzyl alcohol converted over 3.9 wt.-% Pt/TiO_2(P25) as a function of reaction time in reaction mixtures initially containing benzyl alcohol (BA) and water. Reaction conditions: V_{Liquid} = 70 mL, 0.5 g catalyst, 90°C, p_{total} = 5 bar, V_{air} = 100 mL_n/min.

A slight decrease in the slope of the number of moles of benzyl alcohol converted as a function of reaction time is observed for liquid compositions 80 and 60 mol-% H_2O in benzyl alcohol after 3 hours. This may be attributed to catalyst deactivation due to strongly adsorbing carbonaceous species formed during oxidation.[167]

It is obvious that the catalytic activity for benzyl alcohol oxidation is enhanced upon the addition of H_2O as a solvent in the initial reaction system, at constant total volume. The initial rate of reaction for the consumption of benzyl alcohol was evaluated from the slope of the conversion as a function of time, taking into consideration the initial number of moles of benzyl alcohol in the mixture. With only benzyl alcohol in the reaction mixture, i.e., without water as a solvent, the initial rate was ca. 0.05 mmol/g/min. This corresponds to a turnover frequency of 26.7 ± 6.0 hr^{-1} when taking into consideration the Pt loading (3.9 wt.-%) and a platinum dispersion of *ca*. 24% (based on the average particle size of 4.6 nm).

The rate of reaction increased significantly upon the addition of water into the system (see Figure 4.5) irrespective of the H_2O/benzyl alcohol ratio in the initial mixture, but the difference in reaction rate obtained upon decreasing the benzyl alcohol content in the mixture from 40% to 10% is negligible. The average rate of benzyl alcohol oxidation in the presence of two liquid-phases is ca. 0.60 ± 0.02 mmol/g_{Pt}/min (see Figure. 4.5), which corresponds to a turnover frequency of 677.4 ± 23 hr^{-1}. As such, the reaction rate is seemly independent of the amount of water added to the initial reaction mixture if the reaction is performed in a biphasic liquid system.

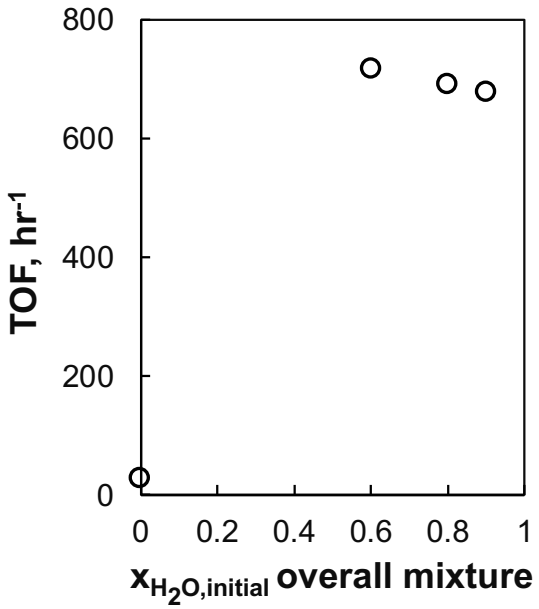

Figure 4.5: Turnover frequency in the benzyl alcohol oxidation over 3.9 wt.-% Pt/TiO_2(P25) as a function of the mole fraction of initial water in benzyl alcohol and water mixture. Reaction conditions: V_{Liquid} = 70 mL, 0.5 g catalyst, 90°C, p_{total} = 5 bar, V_{air} = 100 mL_n/min.

The reaction mixture will split into two separate liquid phases, viz. an organic phase and an aqueous phase, if the initial mixture contains between 55 mol-% and 98 mol-% water (see Figure. 4.1). Varying the water content in the initial reaction mixture between 80 mol-% and 90 mol-% changed the relative amount of the liquid phases initially present, but not the composition of these phases. The invariance of the initial rate of consumption of benzyl alcohol upon adding water to the initial reaction mixture implies that the relative amount of the two phases present within the measured range does not affect the rate of reaction.

4.2.2. THE CATALYTIC PERFORMANCE IN WATER + m-XYLENE + BENZYL ALCOHOL MIXTURES

The experiments with the benzyl alcohol + water mixtures showed clearly that the presence of water strongly enhances the rate of reaction. These experiments were performed at an essentially constant fugacity of water and a constant mole fraction of water in the organic phase. The remarkable influence of the water content in the initial

reaction mixture on the activity of Pt/TiO_2(P25) on the benzyl alcohol oxidation was investigated further using m-xylene as a high boiling point co-solvent while keeping the initial moles of the benzyl alcohol substrate in the overall mixture constant.

The phase behaviour of the system benzyl alcohol + water + m-xylene has not been determined experimentally yet but is expected to be similar to the phase behaviour of the system benzyl alcohol + water + toluene as measured by Wang et al.,[166] in the temperature range between 303 and 343 K. In order to gain insight in the LLE at the temperatures used in this study, the LLE of the system benzyl alcohol + water + m-xylene was modelled using activity coefficients as predicted by UNIFAC as implemented in ASPEN® (see Figure. 4.6). The obtained phase diagram was compared with the phase diagram obtained for the system benzyl alcohol + water + toluene extrapolated to the required reaction temperature using the non-random two liquid (NRTL) model (see Appendix B-4.3 for benzyl alcohol + water + toluene ternary phase diagram). Benzyl alcohol and m-xylene are fully miscible but adding some water to a benzyl alcohol + m-xylene mixture results in phase splitting. It should be noted that the region in which the benzyl alcohol + water + m-xylene are completely miscible is reduced in comparison to the system benzyl alcohol + water + toluene. This may be attributed to an overestimation of the immiscibility region by UNIFAC.[166] It should be noted that the equilibrium criteria for LLE require uniformity of temperature, pressure and the fugacity of each species throughout both liquid phases.[168] Therefore, for mixtures within the two-phase region, the fugacity of water in the organic phase remains virtually constant, although the mole fraction of water in the organic phase changes.

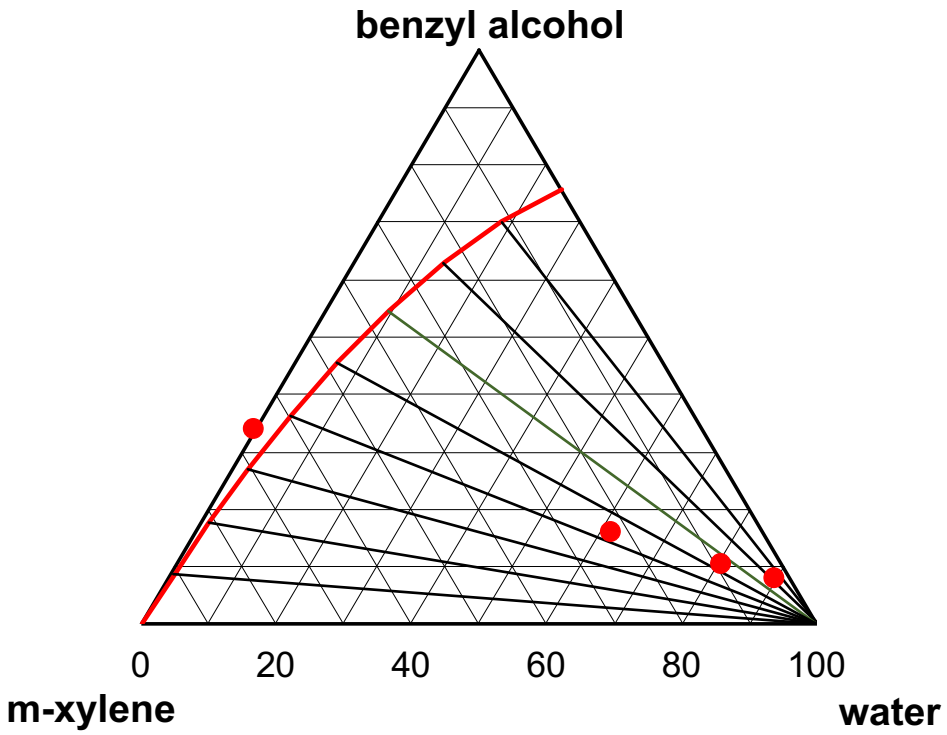

Figure 4.6: Ternary phase diagram of the liquid-phase in the system benzyl alcohol + water + m-xylene at 90 °C with tie-lines as predicted using UNIFAC (data points indicate the initial reaction mixtures for the benzyl alcohol oxidation using m-xylene as a co-solvent used in this study).

The initial reaction mixture containing benzyl alcohol + water + m-xylene readily splits into two phases (when some water is present in the mixture). The water content in the organic phase decreases upon increasing the mole fraction of m-xylene in the initial mixture.

4.2.2.1. CATALYTIC ACTIVITY

Figure 4.7 shows the number of moles of benzyl alcohol converted as a function of reaction time for the reaction mixtures containing benzyl alcohol + water + m-xylene. It should be noted that the initial amount of benzyl alcohol fixed at 0.202 mol and the total liquid volume fixed at 70 mL, *cf*. Table 4.3.

Table 4.3: Various liquid compositions mixtures containing benzyl alcohol + water + m-xylene at constant initial mole of benzyl alcohol.

Volume in mL			Moles			Total Moles	Mole-% H_2O	Mole-% Xylene	Mole-% Benzyl alcohol
H_2O	Xylene	BA	H_2O	Xylene	BA				
0	49	21	0.000	0.397	0.202	0.599	0.0	66.3	33.7
14	35	21	0.778	0.284	0.202	1.263	61.6	22.4	16.0
28	21	21	1.556	0.170	0.202	1.928	80.7	8.8	10.5
42	7	21	2.333	0.057	0.202	2.592	90.0	2.2	7.8

The amount of benzyl alcohol converted after a reaction time of 5 hours for the system with m-xylene as the only solvent in the initial reaction mixture was ca. 2.97 mmol. Having an initial reaction mixture containing m-xylene and water in a molar ratio of 90:10, 79:21 and 59:41 resulted in a number of moles of benzyl alcohol converted of 21.5 mmol, 14.5 mmol and 11.9 mmol after 5 hours, respectively.

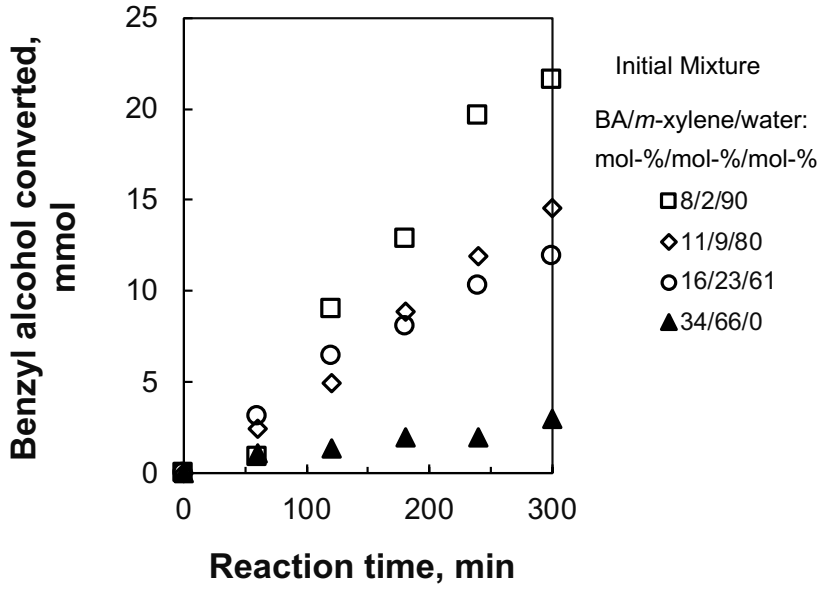

Figure 4.7: Moles of benzyl alcohol converted as a function of reaction time in the benzyl alcohol oxidation over Pt/TiO_2(P25) with initial mixtures containing

water and m-xylene as solvents and constant initial moles of benzyl alcohol (BA). Reaction conditions: V_{Liquid} = 70 mL, $n_{BA,0}$ = 0.202 mol, 0.5 g catalyst, 90 °C, p_{total} = 5 bar, V_{air} = 100 mL_n/min.

The measured turnover frequency (TOF) in the absence of H_2O, i.e., an initial mixture containing 34 mol-% benzyl alcohol and 66 mol-% m-xylene, corresponds to 23.1 ± 1.6 hr^{-1}. Interestingly, this turnover frequency obtained from 34 mol-% benzyl alcohol and 66 mol-% m-xylene system is statistically comparable to the obtained turnover frequency from solvent-free benzyl alcohol oxidation of 26.7 ± 6.0 hr^{-1} despite the varying initial moles of benzyl alcohol in the reaction mixture.

Upon the addition of H_2O to the reaction mixture at constant initial moles of benzyl alcohol and total liquid volume, TOF increases with increasing H_2O content in the initial mixture, as shown in Figure 4.8. However, in the presence of m-xylene as a co-solvent in the initial reaction mixture, TOF was lower compared to the system with H_2O as the only solvent: the turnover frequency decreased from ca. 677.4 ± 23 hr^{-1} in a system containing only benzyl alcohol and water (see Figure. 4.5) to 232.4 hr^{-1} in a system also containing some m-xylene (the highest rate). The results of the addition of m-xylene as a co-solvent in the benzyl alcohol and H_2O system in this section clearly show that the TOF of benzyl alcohol oxidation is strongly dependent on the number of moles of H_2O on the system (see Figure. 4.8). The increase in the TOF of the reaction with increasing H_2O content in the system cannot be attributed to the change in the fugacity of water, seeing that the fugacity of water is virtually constant in all systems containing two liquid phases (since the mole fraction of water in the aqueous phase is close to one). The change in the TOF may, however, be linked to the change in the mole fraction of water in the organic phase.

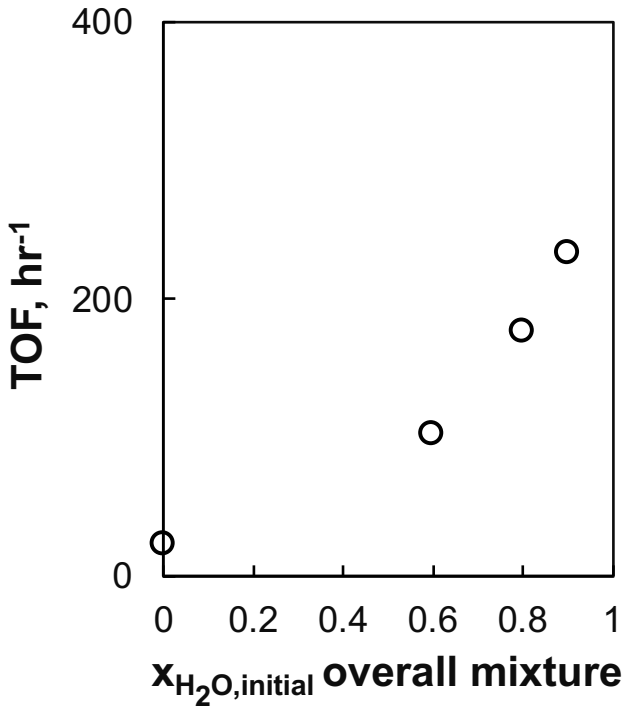

Figure 4.8: Turnover frequency in the benzyl alcohol oxidation over 3.9 wt.-% Pt/TiO_2(P25) as a function of the initial mole fraction of water in the overall mixture containing 0.202 mol of benzyl alcohol, and m-xylene and water in various amounts. Reaction conditions: V_{Liquid} = 70 mL, 0.5 g catalyst, 90 °C, p_{total} = 5 bar, V_{air} = 100 mL_n/min.

4.2.3. THE CATALYTIC PERFORMANCE IN N-HEPTANE + BENZYL ALCOHOL MIXTURE

m-Xylene is an aromatic molecule that may compete with benzyl alcohol for adsorption on the catalytically active surface. This may result in a reduction in the turnover frequency in benzyl alcohol oxidation. The oxidation of benzyl alcohol was performed in a benzyl alcohol + n-heptane liquid mixture also to avoid interference by competitive adsorption. In order to determine the effect of competitive adsorption, benzyl alcohol oxidation was performed using m-xylene and n-heptane as a solvent system. The latter is thought to have minimal interaction with the catalyst surface due to its paraffinic nature.

The LLE of the system benzyl alcohol + water + n-heptane was modelled using UNIFAC as implemented in ASPEN® (see Figure. 4.9). Benzyl alcohol and n-heptane are

fully miscible, however as expected, due to the low dielectric constant of n-heptane, the system readily splits into two phases when some water is present in the mixture. Benzyl alcohol oxidation reaction in a binary system containing 90 mol-% n-heptane in 10 mol-% benzyl alcohol will yield a bi-phasic liquid as the reaction proceeds yielding benzaldehyde and water (as indicated by the arrow in Figure 4.9). This is due to the formation of H_2O as a co-product of benzaldehyde in benzyl alcohol oxidation in oxygen, which may change the dynamics of the reaction due to the splitting of the liquid phase.

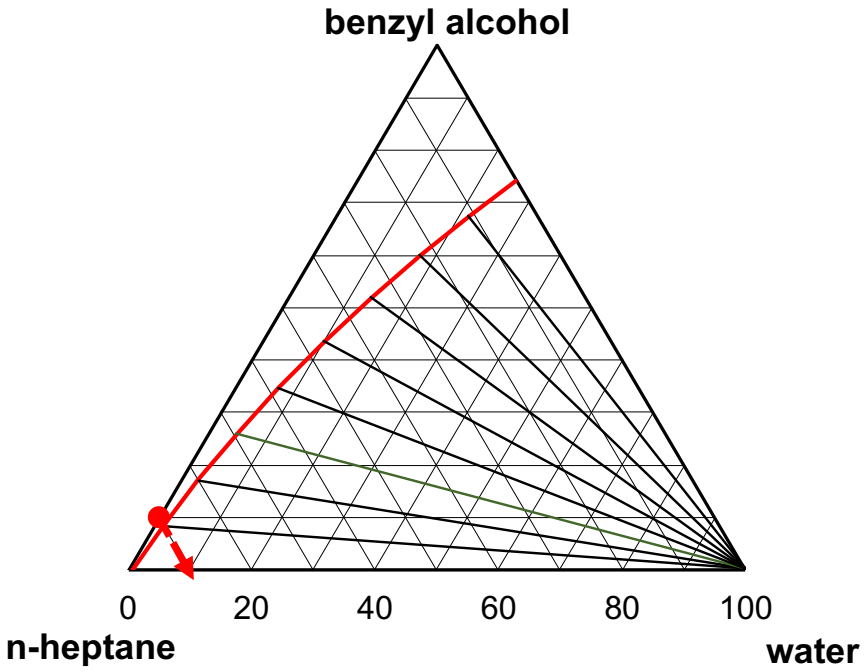

Figure 4.9: Ternary phase diagram of the liquid-phase in the system benzyl alcohol + water + n-heptane at 90°C with tie-lines (data point indicates the initial reaction mixture for the benzyl alcohol oxidation using n-heptane, with an arrow highlighting the change in the liquid-phase as the reaction proceeds at constant n-heptane moles).

4.2.3.1. CATALYTIC ACTIVITY USING n-HEPTANE OR M-XYLENE AS REACTION SOLVENTS

The initial reaction mixture was changed from the mole fraction of the benzyl alcohol in the initial reaction mixture from 34 mol-% benzyl alcohol (in 66 mol-% m-xylene)

to 10 mol-% benzyl alcohol (in 90 mol-% n-heptane) while keeping the initial total liquid volume constant at 70 mL. The obtained number of moles of benzyl alcohol converted after a reaction time of 5 hours is 2.97 mmol and 1.68 mmol for benzyl alcohol + m-xylene system and benzyl alcohol + n-heptane system, respectively (see Figure. 4.10).

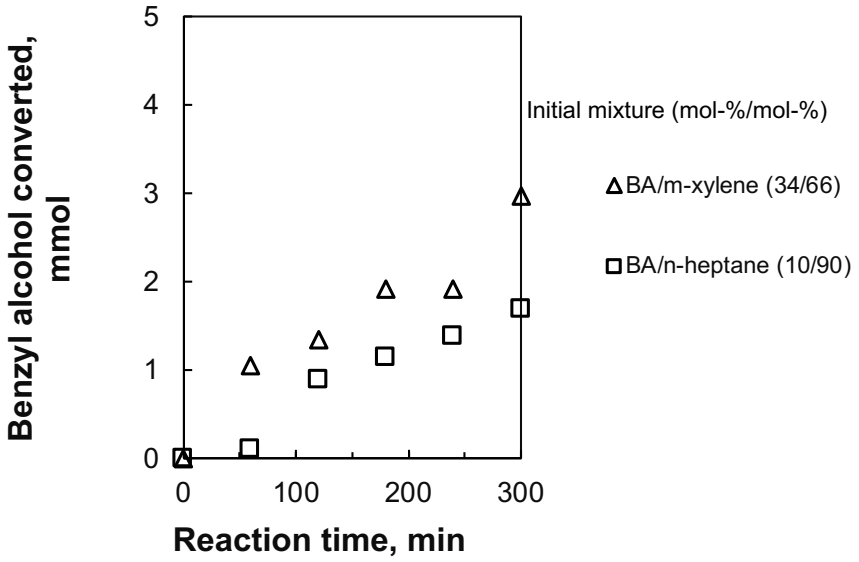

Figure 4.10: Moles of benzyl alcohol converted in reaction systems containing 34 mol-% m-xylene or 90 mol-% n-heptane solvent with the balance of benzyl alcohol (BA) as a function of reaction time. Reaction conditions: 0.5 g catalyst, 90°C, $P_{total,\ air}$ = 5 bar, V_{total} = 70 mL, V_{air} = 100 mL_n/min.

The TOF of benzyl alcohol oxidation in the presence of organic solvents are 20 ± 2 hr^{-1} and 23.1 ±1.6 hr^{-1} for the reaction mixtures initially containing 90 mol-% n-heptane and 66 mol-% m-xylene in benzyl alcohol liquid compositions, respectively. This indicates that the turnover frequency, 20 ± 2 hr^{-1} obtained from benzyl alcohol + n-heptane system, is statistically comparable to that obtained in pure benzyl alcohol (27 ± 6 hr^{-1}) and 66 mol-% m-xylene in 34 mol-% benzyl alcohol (23.1 ± 1.6 hr^{-1}). This suggests that the rate of benzyl alcohol conversion is virtually independent of the initial concentration of benzyl alcohol in the starting mixture. Importantly, the invariance of TOF for benzyl alcohol oxidation may also indicate that m-xylene does not adsorb competitively with benzyl alcohol during the reaction.

4.3. THE EFFECT OF MOLECULAR OXYGEN SOLUBILITY IN A SOLVENT SYSTEM

There is a very slight variation in the number of moles of benzyl alcohol converted per unit time in solvent-free (benzyl alcohol) and other solvent systems employed (H_2O, m-xylene and n-heptane) for benzyl alcohol oxidation at 90 °C and 5 bar in the air as shown in Figure 4.11. n-Heptane, which is the most apolar solvent in the series, showed the lowest number of moles of benzyl alcohol converted per unit time (0.338 mmol/hr). See Figure 4.11-A. The most polar solvent, H_2O, exhibited the highest number of moles of benzyl alcohol per unit time (with 19.82 mmol/hr of benzyl alcohol converted), see Figure 4.11-B.

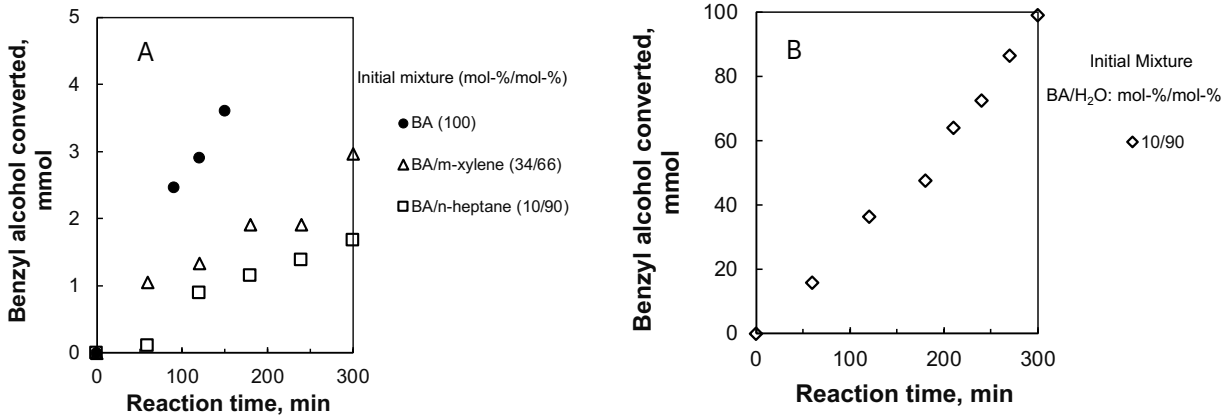

Figure 4.11: Moles of benzyl alcohol converted in reaction systems containing **A**: 34 mol-% m-xylene or 90 mol-% n-heptane solvent and **B** 90 mol-% H_2O with the balance of benzyl alcohol (BA) as a function of reaction time. Reaction conditions: 0.5 g catalyst, 90°C, $P_{total,\ air}$ = 5 bar, V_{total} = 70 mL, V_{air} = 100 mL_n/min.

The solvent in the oxidation reaction is a crucial parameter to consider since it may affect the solubility of the O_2 oxidant. This may affect the rate of the selective oxidation of benzyl alcohol if gas-liquid mass transfer limits the benzyl alcohol oxidation (otherwise, the liquid-phase and the gas phase will be close to equilibrium, and the rate of reaction will be influenced by the partial pressure of oxygen).

The solubility of oxygen has been measured in water,[169] n-hexane,[170] and toluene[171] (see, Figure. 4.12). The solubility can be expressed in terms of the Henry coefficient

$$x_{O_2}^{solvent} = H \cdot p_{O_2} \qquad 4.5$$

A higher value of the Henry coefficient implies a higher solubility of oxygen in the solvent. The solubility as given by the Henry coefficient is 83 times higher in n-hexane as a solvent compared to water as a solvent and 45 times higher in toluene as a solvent in comparison to water as a solvent.

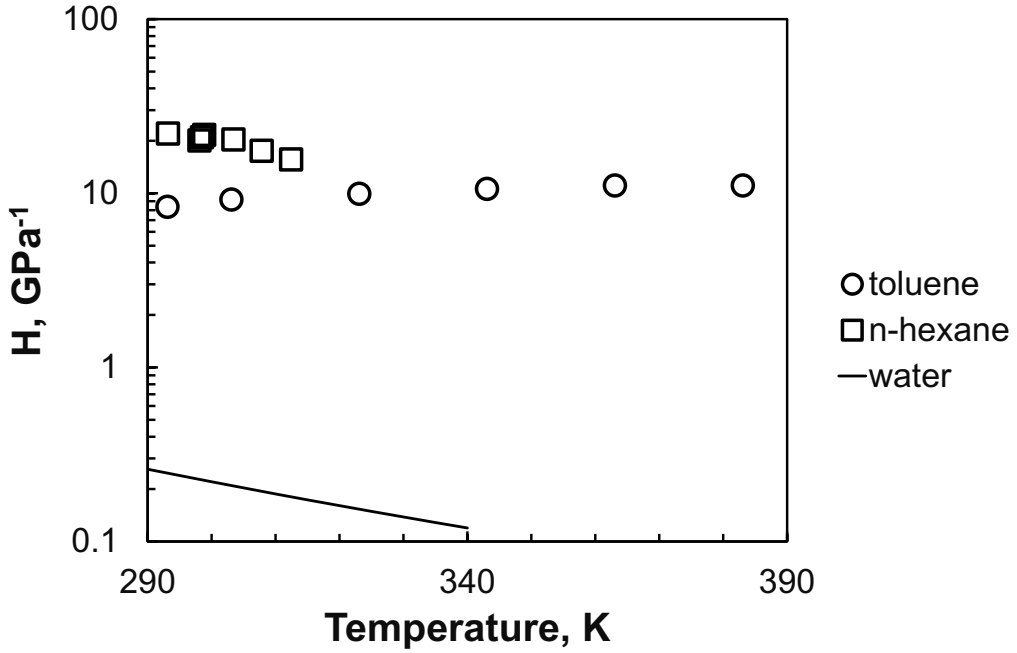

Figure 4.12: Henry's constant for oxygen solubility in various solvents over a range of temperatures.[169–171]

A similar trend to Henry's constant for oxygen solubility in toluene, n-hexane and water, is observed in oxygen solubility in xylene, n-heptane and water over a range of temperatures predicted by Peng-Robinson state of equation (PR-EOS) as implemented in ASPEN®, see Figure 4.12. At 90 °C (reaction temperature for benzyl alcohol oxidation in this study), the oxygen solubility decreases in the following trend: xylene > benzyl

alcohol > n-heptane > water. As clearly shown in Figures 4.12 and 4.13, the oxygen solubility in water is much less than in the organic solvents (up to a factor of more than 100).

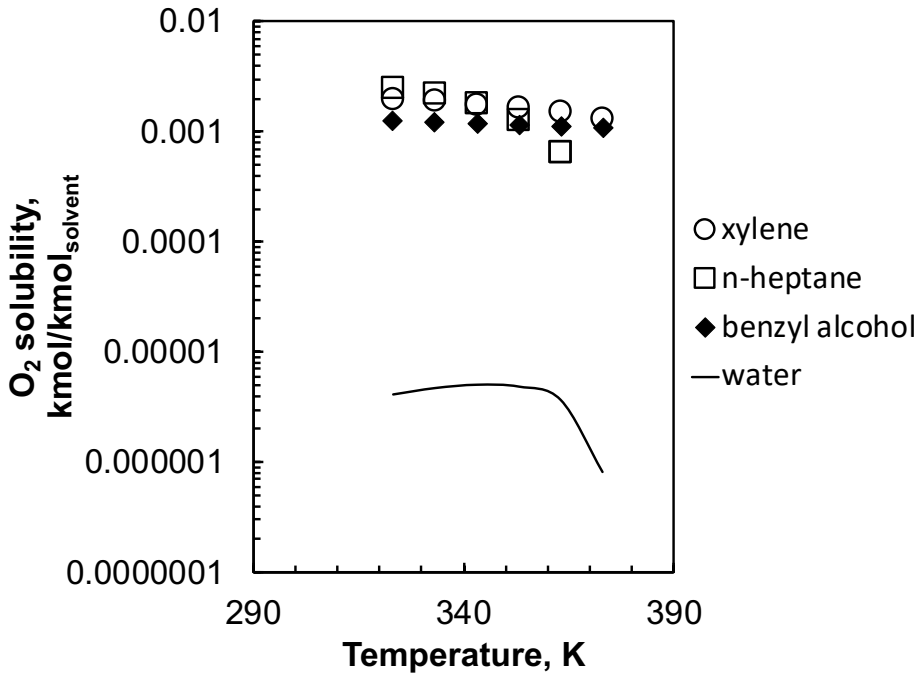

Figure 4.13: Oxygen solubility trend in various organic liquids over a range of temperature predicted by Peng-Robinson state of equation (PR-EOS).

As shown previously, the number of moles of benzyl alcohol converted per unit time in H_2O is much greater than that obtained from other organic liquid systems in the series, despite the much lower oxygen solubility. It should be noted that the solubility of oxygen in the solvent will only play a role if oxygen adsorbed on the catalytically active phase is not in (or close to) equilibrium with oxygen in the gas phase, i.e., when the adsorption of oxygen or the mass transfer of oxygen (either from the liquid-phase to the catalyst or from the gas phase to the liquid-phase) controls the rate of the reaction. The high rate of reaction in the presence of water may indicate that the solubility of oxygen in the solvent does not affect the rate of reaction and that surface oxygen is in (or close to) equilibrium with oxygen in the gas phase.

4.4. PRODUCT SELECTIVITY

For consecutive reactions, such as benzyl alcohol oxidation, the product selectivity can be strongly dependent on the conversion levels. The product selectivity was evaluated for the liquid oxidation of benzyl alcohol as a function of conversion.

Solvent-free benzyl alcohol oxidation yielded a high benzaldehyde selectivity at a very low benzyl alcohol conversion level. In the presence of H_2O as the sole solvent, a high benzaldehyde selectivity was also obtained despite high benzyl alcohol conversion after 5 hours in the stream (see Figure 4.14). Relatively low benzaldehyde selectivity was obtained in liquid systems with organic solvents (i.e., benzyl alcohol + m-xylene and benzyl alcohol + n-heptane) even at low benzyl alcohol conversion levels. Seemingly, the presence of H_2O does not only enhance the activity but also inhibits the further oxidation yielding benzoic acid.

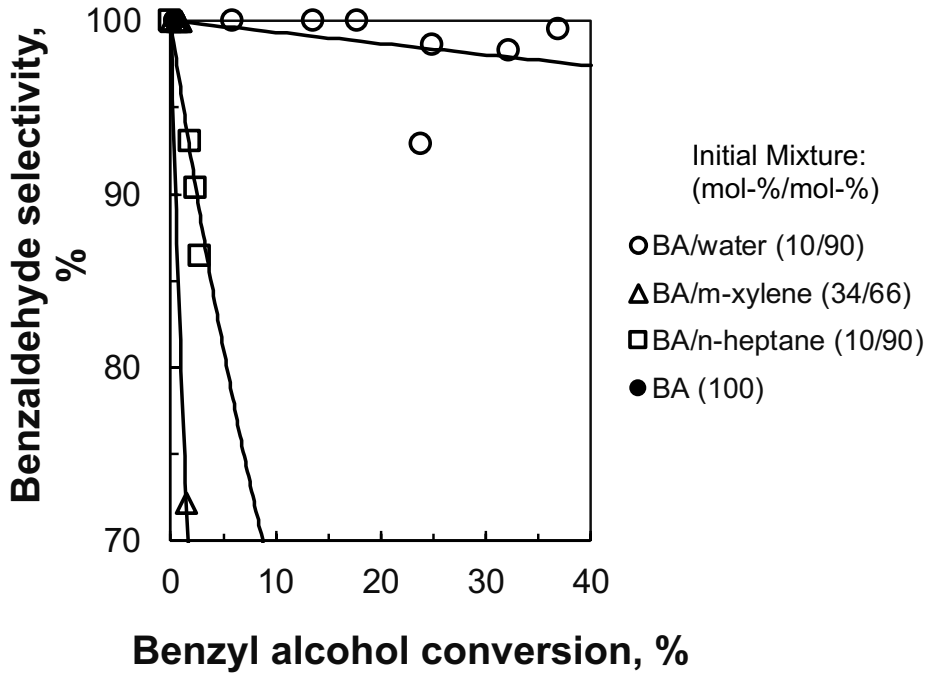

Figure 4.14: Benzaldehyde selectivity of various initial reaction mixtures (100 mol-% BA; 90 mol-% n-heptane in 10 mol-% BA; 34 mol-% m-xylene in 66 mol-% BA; 90 mol-% H_2O in 10 mol-% BA) with respect to moles of benzyl alcohol converted.

The selectivity differed quite a bit for the system benzyl alcohol and H_2O if the reaction was stopped after 5 hours. The reaction mixture was allowed to stand overnight (ca. 16 hours) to cool until room temperature without air/O_2 flow under stirring. The reaction product recovered from systems initially containing more than 60 mol-% water (and the balance benzyl alcohol) contained a liquid phase and a solid product (see Figure. 4.15). The solvent-free liquid system (100 mol-% benzyl alcohol) produced a liquid product only, which is not surprising, seeing the low conversion obtained even after a reaction time of 5 hours. The biphasic products (solid and liquid products) obtained from liquid composition greater than 60 mol-% were isolated as faint yellow crystal and clear liquid.

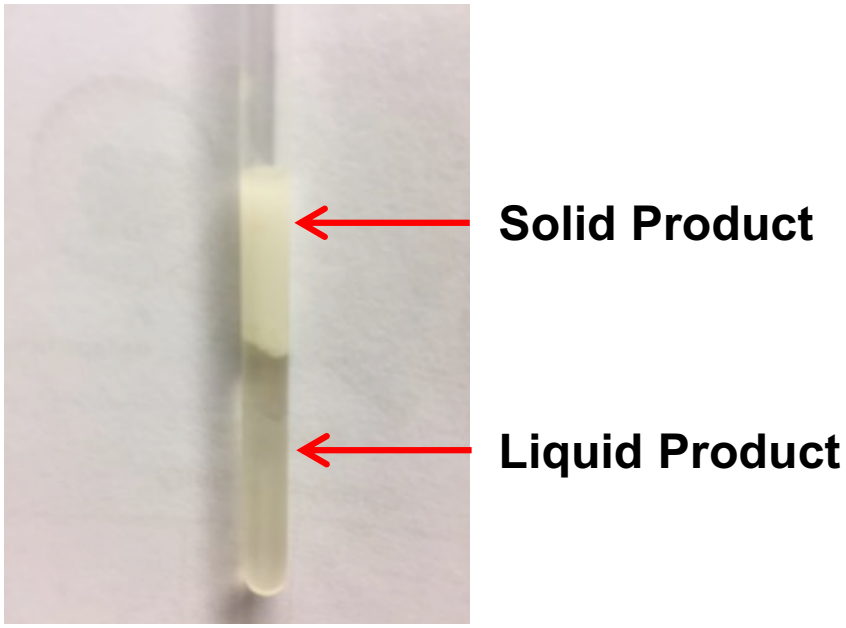

Figure 4.15: Bi-phasic product mixture obtained from benzyl alcohol oxidation over Pt/TiO_2(P25) with a reaction mixture initially containing 80 mol-% H_2O and 20 mol-% benzyl alcohol.

The liquid-phase was analysed using proton nuclear magnetic resonance spectroscopy (^{1}H NMR) in deuterated chloroform at 400Hz (see Figure. 4.16). The spectrum showed a singlet in the aldehyde region (ca. δ = 10.06 ppm) integrating for one proton. This was assigned to the proton of the aldehyde moiety. The multiplicity of the observed proton is expected to be a singlet as the neighbouring carbon is a carbonyl

carbon. The chemical shifts for benzyl ring are in the expected regions corresponding to those reported in the literature.[172] A doublet, at 8 ppm region corresponding to the hydrogens *ortho* to the aldehyde group, is also detected. Since they are the closest to aldehyde, these hydrogens should be deshielded the most and show a peak toward the end of the benzene region. In this region, a doublet of doublets is seen at ca. 7.5 ppm corresponding to hydrogens *meta* to the aldehyde. These protons are more shielded compared to protons in the *ortho* position. The doublet of doublets coupling arises from the *ortho* and para hydrogens, as they are in a different electronic environment. Finally, a triplet is seen ca. 7 ppm corresponding to the hydrogen para to the aldehyde. At this position, the hydrogens are more shielded and resonate ca. 7 ppm. The multiplicity of these hydrogens arises from the neighbouring proton in the *meta* position. Furthermore, the spectrum showed a singlet at *ca*. δ = 2.20 ppm, integrating for one proton assigned to the benzyl alcohol substrate's hydroxyl proton (H8). This suggests that the liquid phase obtained is a mixture of benzyl alcohol and benzaldehyde, as expected.

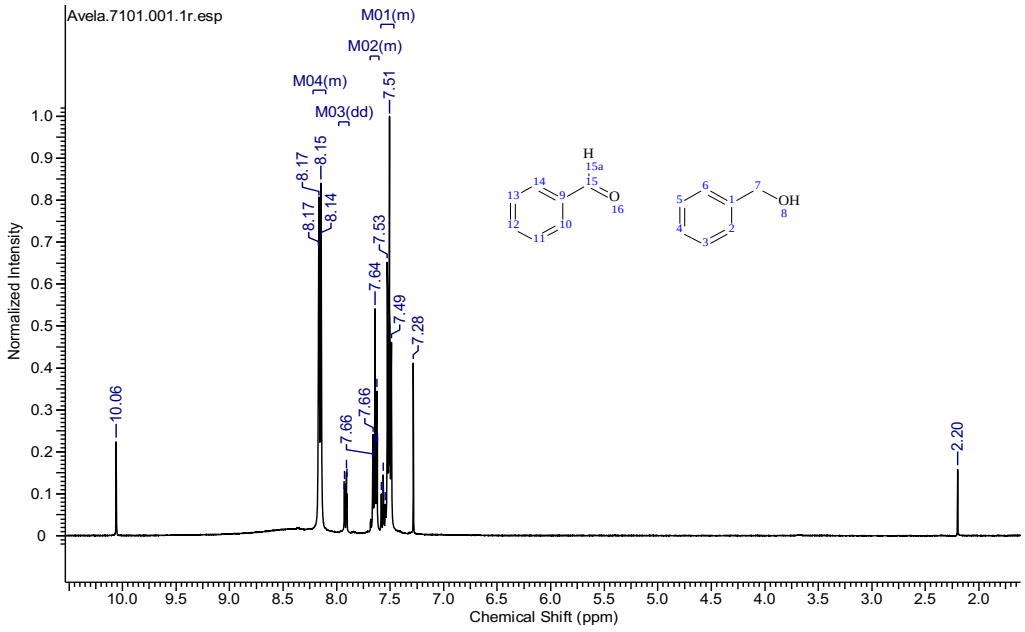

Figure 4.16: Proton nuclear magnetic resonance (^{1}H NMR) of the liquid-phase product obtained from oxidation of benzyl alcohol for the reaction mixture initially containing 80 mol-% water and 20 mol-% benzyl alcohol.

The solid phase product was analysed by determining its melting point using a hot-stage microscope. The solid product showed melting with an on-set temperature occurring at ca. 120 °C with bulk melting at 123 °C, see Figure 4.17. In literature, the melting point for benzoic acid is reported to be 122.4 °C.[173] This may suggest that the solid material observed as a product of benzyl alcohol oxidation is benzoic acid. It should be noted that in the case where benzaldehyde is desired as the product, and the formation of benzoic acid is regarded as over-oxidation since it may be formed from the consecutive oxidation of benzaldehyde.

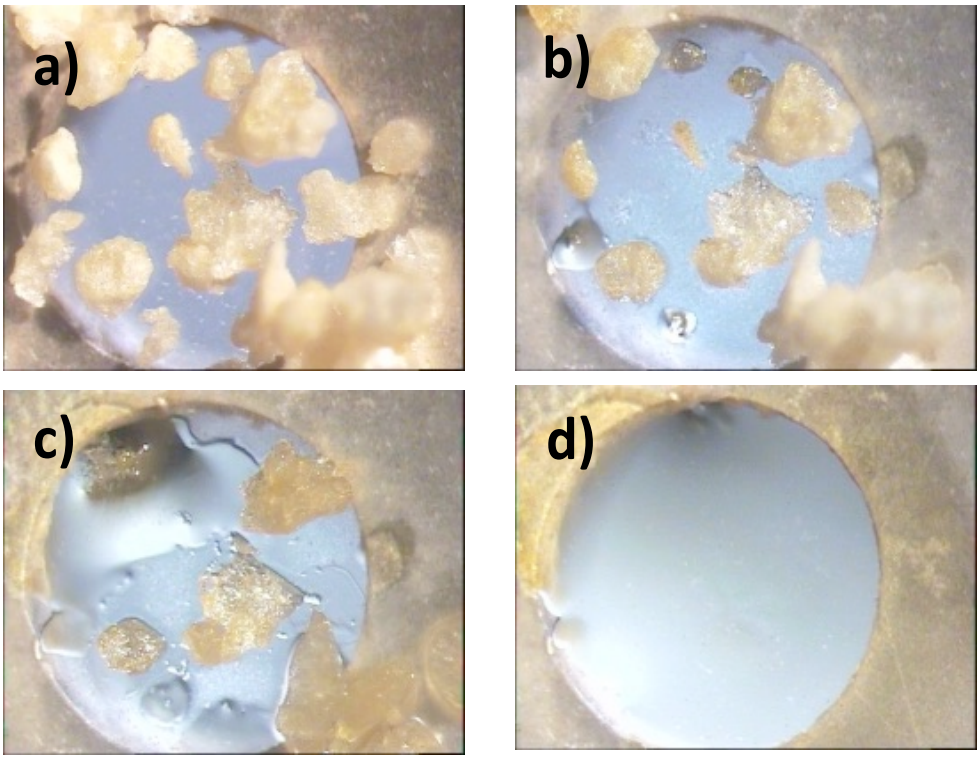

Figure 4.17: Melting point determination of the solid product obtained from oxidation of benzyl alcohol in a mixture initially containing 90 mol-% water and 10 mol-% benzyl alcohol system using a hot-stage microscope (HSM). Highlighting phases present at: **a)** 23 °C, **b)** 120 °C, **c)** 123 °C and **d)** 126 °C.

Products mixture recovered from all other liquid compositions (100 mol-% BA, 60 mol-% H_2O in BA, 80 mol-% in BA and 90 mol-% H_2O in BA) after cooling for ca. 16 hours

were analyzed using GCxGC coupled with mass spectroscopy for product identification. In the case of biphasic products, the solid and liquid products were mixed in methanol resulting in the formation of a single phase. The obtained GC-GC traces are shown in Figure 4.18. The obtained fragmentations confirmed that the liquid and solid products obtained are benzyl aldehyde and benzoic acid, respectively. Benzaldehyde and benzoic acid are thus the only observed products in all the benzyl alcohol oxidation experiments reported here.

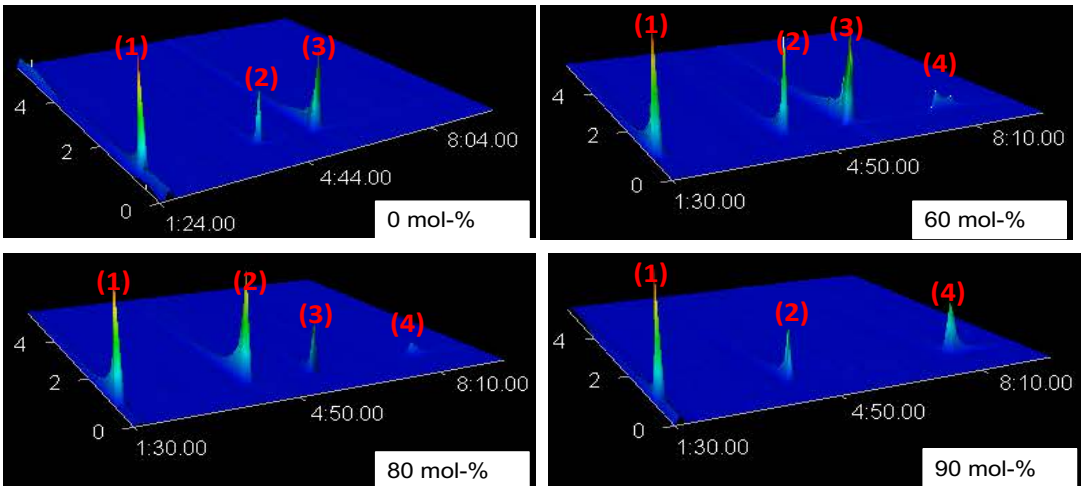

Figure 4.18: GCxGC trace of the products in the benzyl alcohol oxidation in reaction mixtures initially containing pure benzyl alcohol (top-left), 60 mol-% water and 40 mol-% benzyl alcohol (top right), 80 mol-% water and 20 mol-% benzyl alcohol (bottom left) and 90 mol-% water and 10 mol-% benzyl alcohol (bottom right). **(1)** *Methanol,* **(2)** *Benzyl aldehyde,* **(3)** *Benzyl alcohol and* **(4)** *Benzoic acid*. Reaction conditions: 0.5 g 3.9 wt.-% Pt/TiO_2(P25) catalyst after cooling for 16 hours.

Quantitative analysis suggests that the obtained benzaldehyde selectivity in the liquid initially containing pure benzyl alcohol (0 mol-% water) was larger than 99 %. Increasing the water content in the initial reaction mixture to 60 mol-% water, 80 mol-% water and 90 mol-% water resulted in the selectivity for benzaldehyde after cooling down the reactor dropping to 83 %, 8 % and <1 %, respectively. Benzaldehyde and benzoic acid were the only products obtained. While benzaldehyde selectivity diminishes with

increasing water content, the benzoic acid selectivity increases from <1 %, 7 %, 92 % to >99 % upon increasing the water content in the initial reaction mixture from 0 mol-%, 60 mol-%, 80 mol-% to 90 mol-%, respectively.

4.5. PROBING THE *IN-SITU* EVOLUTION OF HYDROPEROXYL SPECIES

The addition of water enhances the rate of benzyl alcohol oxidation over Pt/TiO_2(P25). The precise promotional role of water on benzyl alcohol oxidation is not fully established. Using DFT analysis, Yang et al.[32] showed that water facilitates the O_2 dissociation over Au(111), yielding surface hydroperoxyl species (OOH*). These *in-situ* formed OOH* species may also act as an oxidant in benzyl alcohol oxidation. However, hydroperoxyl species (OOH*) on Pt(111) has previously been shown to be unstable relative to gas-phase O_2 and gas-phase water,[34], and thus the existence of these species is doubtful over Pt systems.

4.5.1. ADDITION OF A HYDROPEROXYL SCAVENGER

The presence of OOH-intermediates was probed in this study by adding oxygen-centred radical scavengers to the reaction mixture (i.e., 0.091 mol hydroquinone, independent of the reaction mixture). Hydroquinone is thought to react with the *in-situ* formed hydroperoxyl species yielding *p*-benzoquinone as the oxidation product. Thus, the addition of hydroquinone may reduce benzyl alcohol conversion since hydroquinone is known to have a strong affinity for OOH.[174] However, the addition of hydroquinone may also lower activity through strong adsorption on the catalyst surface (catalyst poisoning).

Transformation of hydroquinone to *p*-benzoquinone in the presence of hydroperoxyl species (OOH*) may provide strong evidence of the *in-situ* formation of hydroperoxyl species on the platinum surface. Hence, various systems were investigated for benzyl alcohol oxidation, i.e., benzyl alcohol (**BA**), benzyl alcohol + hydroquinone (**BA/HQ**), benzyl alcohol + hydroquinone + water (**BA/HQ/water**) and benzyl alcohol-water system (**BA/water**). The **BA/water** system showed the highest number of moles of benzyl alcohol converted per unit time (as measured for benzyl alcohol oxidation activity) ca. 19.82 mmol/ (99.1 mmol after 5 hours), refer to section 4.2.1.1. A dramatic decrease

in the number of moles of benzyl alcohol converted per unit time is observed upon the introduction of hydroquinone, i.e., **BA/HQ/water** system, from 19.82 mmol/hr to 1.18 mmo/hr (5.92 mmol after 5 hours on stream), see Figure 4.19. This might indicate that hydroquinone in **BA/HQ/water** system reacts with *in-situ* formed hydroperoxyl species, thereby reducing the number of moles of benzyl alcohol converted per unit time. This should, however, be validated by the formation of the oxidation product, *p*-benzoquinone. However, this product could not be detected in the liquid product (after homogenizing with methanol) using either GC-FID or GCxGC-MS. Hence, it cannot be conclusively stated that the decrease in the benzyl alcohol conversion is due to a reduction in the availability of surface hydroperoxyl species. The disappearance of hydroquinone and the lack of the oxidation product *p*-benzoquinone may indicate that either or both compounds adsorb strongly on the catalytically active surface.

The **BA/HQ** systems also exhibited the lowest number of moles of benzyl alcohol converted per unit time of 0.2 mmol/hr (1 mmol after 5 hours). The further decrease in benzyl alcohol conversion in **BA/HQ** system may suggest that hydroquinone and/or the possible oxidation product *p*-benzoquinone are strongly adsorbed on the catalytically active surface, thus reducing the activity.

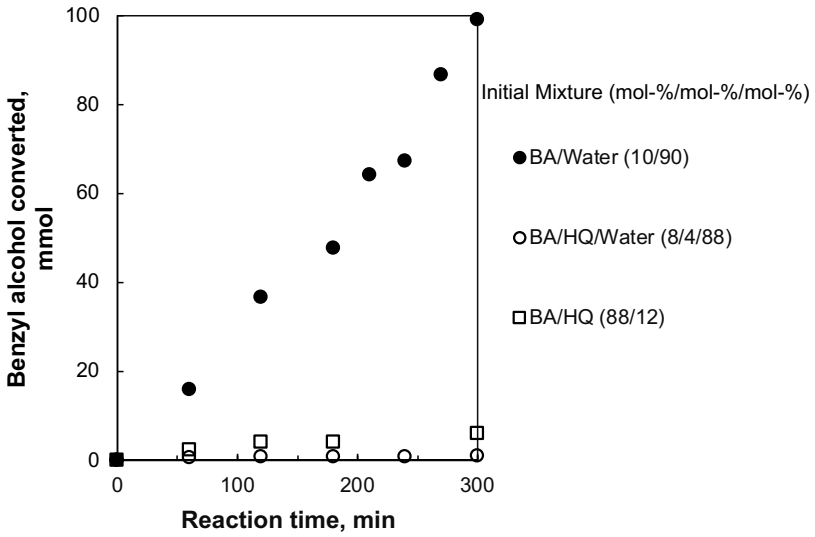

Figure 4.19: Number of moles of benzyl alcohol converted as a function of reaction time with 0.676 mol of benzyl alcohol and 0.091 mol hydroquinone, **BA/HQ**;

0.202 mol of benzyl alcohol in 0.091 mol hydroquinone and 2.33 mol of H_2O, **BA/HQ/water**; and 0.202 mol of benzyl alcohol in 2.33 mol of H_2O, **BA/water** over 0.5 g Pt/TiO_2 (P25) catalyst at 90 °C and $P_{total,\ air}$ = 5 bar. V_{liquid}= 70 mL and V_{air} = 100 mL_n/min.

4.5.2. OXYGEN DISSOCIATION IN THE PRESENCE OF WATER OVER PT(111) SURFACE: *DFT STUDY*

DFT calculations were used to explore the role of water on the dissociation of oxygen and the distribution of oxygen-containing species on Pt(111) further. It is known that OOH* species are not stable on Pt(111) relative to gas-phase O_2 and gas-phase H_2O.[34] However, water co-adsorbed with O_2 may affect the O_2 activation over Pt(111).

The dissociation behaviour of O_2 in the presence of H_2O has been investigated on a clean p(3x3)-Pt(111) surface with O_2(g) and H_2O(g) as reference states. For comparison, the dissociation of O_2 has also been investigated over a p(3x3)-Pt(111) surface in the absence of water.

4.5.2.1. O_2 ADSORPTION ON PT(111)

The optimized structures of species involved in the O_2 dissociation over Pt(111) surface in the absence of water are shown in Figure 4.20. Molecularly adsorbed oxygen prefers to be adsorbed over an *fcc* site on Pt(111). Upon adsorption, the O−O bond length in molecularly adsorbed O_2 adsorbed on Pt(111) is substantially elongated from 1.234 Å for O_2 in the gas phase to 1.396 Å. The bond length of molecularly adsorbed O_2 on Pt(111) agrees well with the experimental value of 1.40 Å for *peroxo* states.[175] The elongation of the O-O is indicative of the O_2 dissociation (bond breakage). It has been shown that the superoxo species (O_2^-) is localized at bridge sites, while the peroxo species (O_2^{2-}) are positioned at *fcc* hollow sites.[176] Thus, molecular O_2 adsorbs on Pt(111) in its initial state as something like a peroxo precursor.[176] The adsorption energy for the adsorption of molecularly adsorbed O_2 was determined to be -0.64 eV relative to gas-phase O_2 and the bare Pt(111) surface, which is in good agreement with previously reported values.[35]

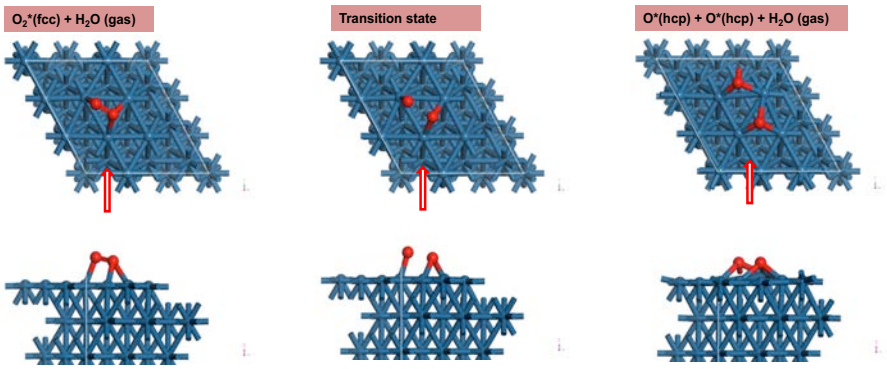

Figure 4.20: Dissociation of O_2* to O* on p(3x3)-Pt(111) using DFT (Functional: PAW-PBE; $E_{cut\text{-}off}$: 400 eV; smearing: 1st order Methfessel-Paxton with σ = 0.02 eV).

Initial state: $d_{O^*–O^*}$ = 1.396 Å; $d_{O^*–Pt,\ (O2\ atop)}$= 2.028 Å; $d_{O^*–Pt,\ (O_2\ bridge)}$= 2.224 Å and 2.182 Å.

Transition state: $d_{O^*–Pt,\ (O\ atop)}$= 2.031 Å; $d_{O^*–Pt,\ (O^*\ bridge)}$= 2.022 Å and 2.224 Å.

Final state: $d_{O^*–Pt,\ (^*O)}$ = 2.04 Å and 2.042 Å.

The Pt-O bond length was measured to be $d_{O^*–Pt,\ (O_2\ atop)}$= 2.028 Å; $d_{O^*–Pt,\ (O_2\ bridge)}$= 2.224 Å and 2.182 Å in the initial state. The transition state in the dissociation of molecularly adsorbed O_2 on Pt(111) was obtained with one oxygen almost in the atop position with a Pt-O distance of 1.944 Å and the other oxygen on a long-bridge site with Pt-O distances of 2.041 Å and 2.048 Å. The O-O bond length is now substantially elongated to 2.007 Å. The energy of the transition state is 0.43 eV higher in energy than that of molecularly adsorbed O_2 on Pt(111). In the final state, the atomic oxygen prefers to adsorb on the *hcp* site. This is in agreement with previously reported site preference.[35] The obtained Pt-O bond length in this state was measured to be 2.04 Å and 2.042 Å.

4.5.2.2. CO-ADSORPTION OF O_2 AND H_2O ON PT(111)

The effect of co-adsorption of O_2 and H_2O on O_2 dissociation is estimated by bringing the reactants (H_2O and O_2) in proximity as seen in the initial state (see Figure 4.21). In the initial state, the O_2 still prefers the *fcc* site. At the same time, the co-adsorbed H_2O adsorbs preferably on the atop site on Pt(111), through the oxygen atom. The O-O bond length of adsorbed molecular O_2 is in the presence of co-adsorbed H_2O 1.436 Å (cf.

1.396 Å in the absence of co-adsorbed water). It suggests that co-adsorption of H_2O and O_2 weakens the O-O bond in the initial state, and that oxygen will have a structure similar to a peroxo-species.[32] The shortest distance between O in adsorbed molecular oxygen and H in water is only 1.709 Å indicating a possible interaction between molecularly adsorbed oxygen and adsorbed water over the interlinking H-atom.

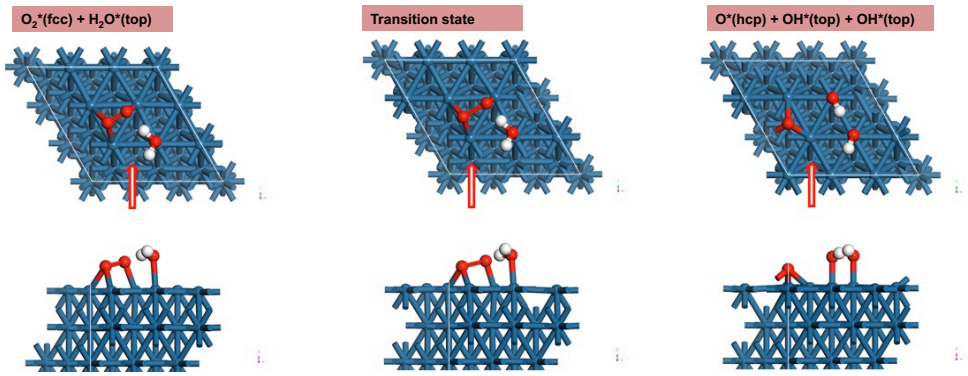

Figure 4.21: Dissociation of adsorbed molecular oxygen in the presence of water on p(3x3)-Pt(111)

Initial state: $d_{O^*-O^*}$ = 1.436 Å, d_{H-O^*H} = 1.01 Å and 0.978 Å; $d_{O^*-Pt,\ (H_2O)}$ = 2.253 Å; $d_{O^*-Pt,\ (O_2\ atop)}$= 2.053 Å $d_{O^*-Pt\ (O_2\ bridge)}$= 2.161 Å and 2.196 Å

Transition state: $d_{O^*-O^*}$ = 1.791 Å, d_{H-O^*H} = 1.055 Å; $d_{O^*-Pt,\ (H_2O)}$ = 2.182 Å; $d_{O^*-Pt,\ (O_2\ atop)}$= 1.944 Å; $d_{O^*-Pt,\ (O_2\ bridge)}$= 2.048 Å and 2.041 Å

Final state: d_{O^*-H} = 1.001 Å and 0.979 Å; $d_{O^*-Pt,\ (^*OH)}$ = 2.01 Å and 1.964 Å; $d_{O^*-Pt,\ (O)}$= 2.06 Å, 2.042 Å and 2.053 Å

The interaction energy of co-adsorbed water and molecular oxygen was calculated from the following expression:

$$E_{interaction} = E_{slab+i+j} + E_{slab} - E_{slab+i} - E_{slab+j} \qquad 4.5$$

Where $E_{slab+i+j}$ is the energy of the co-adsorbed species on the Pt(111) surface, E_{slab}, is the energy of the clean slab, E_{slab+i} and E_{slab+j} is the energy of the individual species i and j adsorbed on Pt(111). A negative value for the interaction energy ($E_{interaction}$ <0) denotes an attractive interaction, and a positive value for the interaction energy

($E_{interaction}$ >0) implies a repulsive interaction. The calculated interaction energy between O_2* and H_2O* on Pt(111) surface was -0.23 eV indicating an attractive interaction. This suggests that the presence of water stabilizes the adsorption of molecular O_2, possibly through HO-H···O-O interaction.

In the transition state for the dissociation of adsorbed, molecular oxygen in the proximity of co-adsorbed water a further elongation of the O-O bond in adsorbed molecular O_2 is observed to 1.791 Å (cf. Table 4.4). It should, however, be noted that the elongation is less than the one observed in the absence of co-adsorbed water. It can be further noted that the shortest distance between O in adsorbed, molecular O_2 and H in adsorbed water is further reduced to 1.505 Å. This implies that the transitions state seems to be an HO-H···O-O complex. The energy of the transition state 0.18 eV is higher than the energy of the initial state of co-adsorbed water and molecular O_2.

Table 4.4: Energetics excluding zero-point energy (ZPE) and geometry of the adsorption of O_2 on p(3x3)-Pt(111)

	E^{ads} (eV)	**Bond lengths**			**Ref**
		O - O (Å)	**O - H (Å)**	**Pt-O (Å)**	
O_2 (*gas*)		1.234			
H_2O *(top)*	-0.22			2.253	
O_2 (*fcc*)_dry	-0.64[1]	1.396			1.40[176–178]
O_2 (*fcc*)_near_H_2O (*is*)	-1.02[2]	1.436	1.01 & 0.978 (1.709[3])	2.053 (top), 2.161(bridge) 2.196 (bridge)	
H_2O *(ts) _ (top)*				2.182	
O_2 (*ts*)_dry	-0.21[1]	2.007			2.05[176]
O_2 (*ts*)_near_H_2O	-0.94[2]	1.791	1.505[3]	1.944 (top), 2.048(bridge) 2.041 (bridge)	
OH *(fs)_(top)*			1.001 & 0.979	2.01	
O (*fs)_*(*hcp*)	-0.94[4]	1.791	1.505[3]	2.06, 2.02 & 2.05	

[1] $E_i^{ads} = E_{i+Pt(111)}^{ads} - E_{i(g)} - E_{Pt(111)}$; [2] $E_i^{ads} = E_{i+Pt(111)+H_2O}^{ads} - E_{i(g)} - E_{Pt(111)+H_2O}$; [3] shortest distance between O in molecularly adsorbed O_2 and H in adsorbed H_2O; [4] Calculated adsorption energy with respect to ½O_2.

The final state formed upon dissociation of the HO-H···O-O complex consists of atomic oxygen in an *hcp* site and two hydroxyl species each in an atop site. The Pt-O bond length of the resulting O and OH species were measured to be 2.06, 2.02 and 2.05 Å for the O *hcp* site and 2.01 Å for the adsorbed OH in the atop site. The OH bond lengths were also measured to be 1.001 and 0.979 Å.

Figure 4.22 shows the energy diagram for the dissociation of adsorbed molecular O_2 on Pt(111) in the presence and absence of water. For comparison, the energetics for the reaction in the absence of water is also given for p(2x2)-Pt(111), as reported by Madala.[34] At a coverage of θ_{O_2}= 1/4 ML, the activation barrier for dissociating adsorbed molecular O_2 on Pt(111) is 0.61 eV (*ca*. 60 kJ/mol). Decreasing the surface coverage to θ_{O_2} = 1/9 ML results in decreased activation barrier for the dissociation of adsorbed molecular O_2 on Pt(111) to 0.41 eV (ca. 40 kJ/mol). The activation barrier for the dissociation of molecular oxygen in the presence of water on Pt(111) is reduced to only 0.18 eV (ca. 17 kJ/mol). This indicates that co-adsorption of H_2O affects the activation of O_2. This may indicate that water accelerates the benzyl alcohol oxidation rate by facilitating the dissociation of molecular oxygen over Pt-based catalyst.

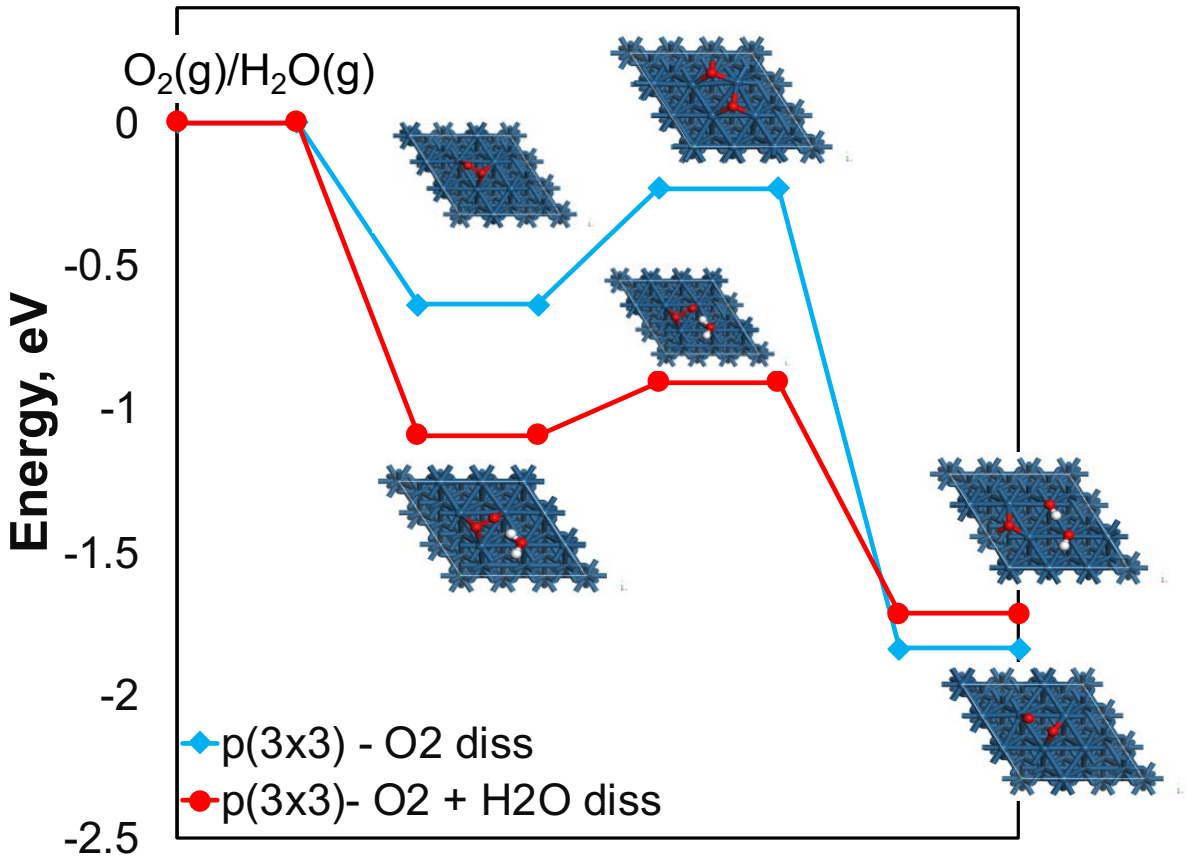

Figure 4.22: Energy profile for the formation of O*, *OH from adsorbed O_2 without (blue and with (red) the involvement of H_2O on Pt(111) surface.

4.6. DISCUSSION

The liquid-phase aerobic benzyl alcohol oxidation over Pt/TiO_2(P25) catalyst is accelerated by the presence of H_2O despite the biphasic nature of the liquid phase of the reaction mixture. The amount of water in the initial mixture, and thus changing the initial moles of the benzyl alcohol substrate as well, does not change the average turnover frequency of benzyl alcohol consumption of 677.4 ± 23 hr^{-1} for systems where two liquid-phases co-exist. This is ascribed to the fact that in such a system, neither the fugacity of H_2O nor the fugacity of benzyl alcohol change (although the fraction of each liquid-phase changes; it should be noted that the concentration of water in the organic phase is constant).

Importantly, the reaction rate seems to be almost independent of the concentration of benzyl alcohol in xylene, n-heptane solvent and solvent-free (pure benzyl alcohol) series. This implies that a change in the concentration of benzyl alcohol cannot account for the change in the rate of reaction for benzyl alcohol, m-xylene/benzyl alcohol and n-heptane/benzyl alcohol system.

The precise role of water in benzyl alcohol oxidation remains ambiguous. The fugacity of water should control the rate of the process if water adsorbed on the surface is in equilibrium with water in the fluid phase for each tested reaction mixtures. However, keeping the initial moles of benzyl alcohol substrate constant while varying moles of H_2O by introducing m-xylene as a co-solvent showed that increasing moles of H_2O solvent enhanced the rate of benzyl alcohol consumption even though the H_2O fugacity is constant. This indicates that the water fugacity does not control the rate of benzyl alcohol oxidation. It may be argued that water on the surface (or near the surface) is not in equilibrium with the water in the bulk fluid phase. The catalyst is hydrophobic (due to the hydrophobic nature of TiO_2(P25) support used in the study) and thus preferentially present in the organic phase. Hence, it may be suggested that the amount of water in the organic phase may influence the reaction rate.

A reasonable correlation is obtained between the turnover frequency and the estimated mole fraction of water in the organic phase (see Figure 4.23) despite inaccuracies in the determination of the composition of the organic phase as a consequence of the use of the UNIFAC model to describe the system benzyl alcohol + m-xylene + water, as shown in Figure 4.23.

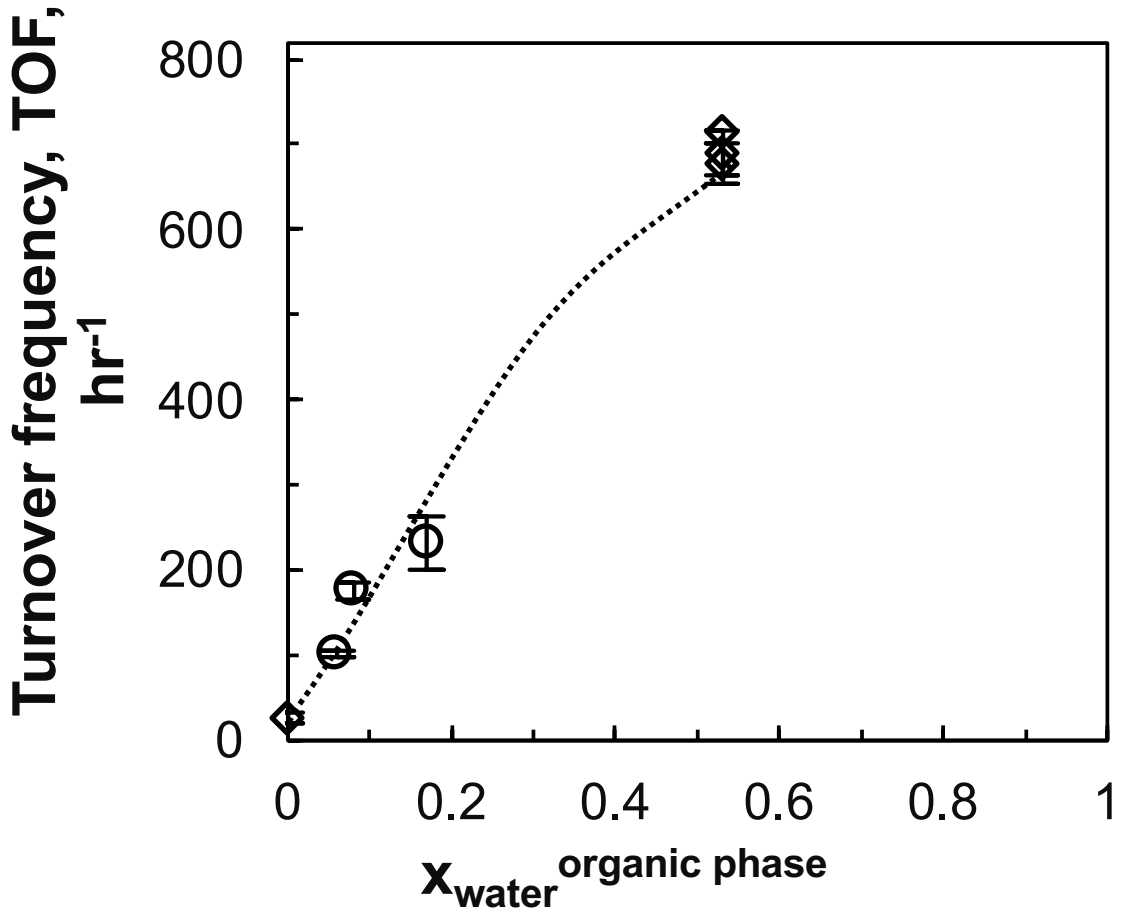

Figure 4.23: Turnover frequency in the benzyl alcohol oxidation as a function of the concentration in the organic phase estimated using NRTL-model fitted to experimental data (◊) and UNIFAC (O).

Clearly, the TOF for benzyl alcohol oxidation is enhanced by increasing the mole fraction of water in the organic phase. Remembering that the liquid system is biphasic in nature (organic and aqueous phase). The formation of organic droplets in water could lead to micelles with the hydrophobic tail of the alcohol in the organic solvent (m-xylene in this case) and the hydrophilic O–H head in the water.[179] Therefore, the presence of H_2O in the organic phase may also induce H-transfer reactions that may facilitate alcohol oxidation. According to Griffins et al.[180] H_2O can act as a weak base facilitating the abstraction of the hydrogen atom from the hydroxyl moiety of the alcohol substrate resulting in the formation of an alkoxide intermediate. Alternatively, water adsorption may

yield surface hydroxyl groups, which may be essential in alcohol oxidation, as they may be involved in other H-transfer reactions.[32] One of the proposed oxidation reaction mechanisms proceeds through a classical oxidative dehydrogenation of the adsorbed alcohol on the metal surface.[25] This leads to the formation of hydrogen adsorbed on the metal surface, which ultimately reacts with adsorbed oxygen and desorbs as water. In this study, DFT-calculations showed that the optimized co-adsorption configuration of H_2O and O_2 lowered the activation barrier for the dissociation of molecular oxygen through the formation of $HOH\cdots O_2$ intermediate which dissociates to form two moles of surface OH* per mole of atomic O*. The formed surface OH and O species on Pt moiety of the catalyst may also facilitate the activation of the O-H bond of benzyl alcohol substrate during oxidation reaction[28], yielding surface alkoxide species. Zope et al. [32] also stated that the presence of surface-bound hydroxide intermediates can facilitate O-H bond activation of the alcohol substrate (which is the initial step of alcohol oxidation) via proton transfer over Au/TiO_2 in the presence of H_2O. The promotional effects of H_2O on the alcohol oxidation over Au(111) has been linked to the *in-situ* formation of surface OOH species.[32] However, these species are not stable on Pt(111).[34]

Besides the H_2O involvement in the activation of alcohol substrate (benzyl alcohol), DFT-calculations in the current study showed that the optimized co-adsorption configuration of H_2O and O_2 has lowered the adsorption energy of O_2 from -0.64 eV to -1.02 eV and activation energy upon H_2O co-adsorption. This suggests that in the presence of H_2O, the adsorption of O_2 is more stable on the Pt surface.

Dissociation of molecular oxygen to atomic oxygen is crucial for the oxidation reaction. Therefore, lowered activation energy for the dissociation of O_2 in the presence of H_2O suggests that H_2O promotes dissociation of O_2 to atomic surface oxygen. This may suggest that the concentration of atomic oxygen on the surface in the presence of H_2O is relatively higher than on a dry surface. Atomic surface oxygen is a key constituent in the oxidation reaction. Thus high concentration of atomic oxygen promotes benzyl alcohol oxidation during the reaction.

4.5.2. EFFECT OF H_2O ON PRODUCT SELECTIVITY

Benzaldehyde is an obtained product with high selectivity even at high H_2O concentrations after 5 hours on stream. Weston et al.,[179] and Yang et al.,[33] observed that increasing H_2O initial concentration for benzyl alcohol oxidation enhances further oxidation of benzaldehyde intermediate, resulting in a decline in benzaldehyde selectivity. Further oxidation of benzaldehyde is typically observed by the formation of a benzoic acid product. In this study, benzoic acid is only observed during or after cooling the reaction mixture (cooling duration of ca. 16 hours) for all the liquid compositions containing H_2O. It is believed that after the reaction was terminated after running for 5 hours (in which it the reaction was terminated and cooled down after for ca.16 hours) there was some oxygen still in the fluid phase which continued interacting with the catalyst surface and reacting with benzaldehyde intermediate and/or benzyl alcohol. Hence, the observed further oxidation of the benzaldehyde intermediate.

4.7. CONCLUSION

This body of work has demonstrated that the addition of liquid H_2O in liquid-phase aerobic benzyl alcohol oxidation significantly enhances the reaction rate over Pt/TiO_2(P25) despite reducing the oxygen solubility in the liquid phases. This may indicate that oxygen on the surface is in equilibrium with oxygen in the gas phase. The phase involved splitting the liquid-phase upon adding water, resulting in the formation of a water-rich phase and an organic phase containing water. The water-rich phase contains more than 99 mol-% water (and thus a constant water fugacity). It is thus suggested that the reaction rate is not controlled by the fugacity of H_2O. Nevertheless, the rate of reaction increased upon increasing the amount of water in the initial benzyl alcohol/m-xylene/water mixture, which may indicate that the reaction is affected by the concentration of water in the organic phase, where the heterogeneously catalysed reaction takes place

It is believed that H_2O has a two-fold role in benzyl alcohol oxidation which result in an enhanced catalytic performance over Pt/TiO_2(P25): H_2O in the organic phase is thought to facilitate the H-transfer reactions, thus facilitating the benzyl alcohol activation. Secondly, the presence of H_2O facilitates the activation of molecular oxygen by forming surface hydroxyl species and atomic oxygen, as the energy barrier for the dissociation O_2

is reduced from 0.41 eV to 0.18 eV for dissociation of adsorbed O_2 in the absence and presence of H_2O, respectively. Overall, the reduced activation energy, in conjunction with the formation of hydroxyl species on the catalyst surface, may enhance catalytic activity. However, the role of water may not only be limited to the activation of molecular oxygen and H transfer reactions.

Benzoic acid is only obtained during the cooling process of the reaction mixture for all the liquid compositions containing water and benzyl alcohol only. This is attributed to dissolved residual oxygen that may further react or recrystallise during the cooling of the reaction mixture.

CHAPTER 5:

Pt-Ni alloy as a catalyst for alcohol oxidation

OVERVIEW

The adsorption properties of the reactants and products on the surface of the catalytically active material play a pivotal role in heterogeneously catalyzed reactions and thus also in the benzyl alcohol oxidation. Alloying Pt with Ni (forming Pt-skin alloy) may offer chemisorption properties that may influence (diminish/promote) the known effects of H_2O when using O_2 as an oxidant in benzyl alcohol oxidation.

Here, nano-sized particles with the nominal composition Pt, Pt_3Ni and PtNi have been synthesized and supported on TiO_2 (rutile phase) with a platinum loading of *ca*. 1 wt.-%. The mixed-metal catalyst systems are investigated for their role in alcohol oxidation. The effect of the Pt-Ni alloy is further investigated using H_2O_2 as an oxidant for benzyl alcohol oxidation rather than O_2. This is to probe the influence of the surface OH group (derived from H_2O_2 dissociation) on benzyl alcohol oxidation, as suggested in Chapter 4.

5.1. RESULTS

5.1.1. CHARACTERIZATION OF SYNTHESIZED NANO-SIZED MATERIALS

Nano-sized platinum-nickel alloys were synthesized using a reductive method with $Mo(CO)_6$ as the reducing agent (see Chapter 3) to obtain nano-sized materials with a nominal composition Pt_3Ni and PtNi.

X-ray diffraction analysis was used to show the formation of an alloy. Alloy formation is typically indicated by a shift of the diffraction lines relative to the pure unalloyed material. Furthermore, the samples' phase and average crystallite size can be determined from the most intense, resolved diffraction line. Figure 5.1 shows the XRD patterns of the materials with the nominal composition Pt_3Ni and PtNi. The XRD pattern of the nano-sized platinum synthesized using a similar procedure was used for comparison to identify any structural difference that arose upon alloying Pt with Ni. The XRD-pattern of nano-sized platinum shows diffraction lines at 2θ = 46.9°, 54.3°, 80.2°, 98.2° and 104.7°, which corresponds to the diffraction planes of metallic *fcc*-Pt indexed as (111), (200), (220), (311) and (222), respectively. The measured diffraction lines correspond to a lattice parameter of 3.919 ± 0.014 Å; the lattice parameter for bulk platinum, 3.9242 Å,[181] is within the error margin of the determined lattice parameter of the nano-sized platinum.

The XRD pattern of the sample with the nominal composition Pt_3Ni exhibited the same diffraction lines as the sample with Pt composition, albeit at slightly higher diffraction angles, viz. 48.4°, 56.4°, 83.6°, 102.6° and 109.4°. A similar XRD pattern for Pt_3Ni alloy is obtained by Lima et al.[182]. These diffraction lines can be matched to *fcc* structure (111), (200), (220), (311), and (222) diffraction planes, respectively. This suggests a decrease in *d*-spacing of the lattice upon incorporating the smaller nickel atom in the platinum structure, which indicates alloy formation. The obtained lattice parameter 3.791 ± 0.008Å is lower than the reported 3.841 Å by Lucas et al.,[183] for single crystal Pt_3Ni.

The XRD pattern of the material with a nominal composition PtNi showed a rather similar diffraction pattern to the pattern obtained of the material with the nominal

composition Pt_3Ni with a slight shoulder preceding from the main diffraction lines. This indicates the presence of pure Pt and Pt-Ni alloy within the sample. No additional diffraction lines correspond to metallic phase and/or oxide/hydroxides peaks of the alloying species (Ni). However, the formation of an amorphous material cannot be discarded. The diffraction lines in the XRD sample with the nominal composition PtNi pattern also corresponds to an *fcc* structure with the diffraction lines at the same position as in the XRD pattern of the sample with the nominal composition Pt_3Ni. It should be further noted that the diffraction lines are broadened significantly (see Figure 5.1). This might indicate inhomogeneous strained incorporation of the Ni component within the Pt crystal structure. The XRD pattern of PtNi alloyed material characterized by broad diffraction peaks is similar to the XRD pattern of Pt_3Ni alloy obtained by Zhang et al.[184]

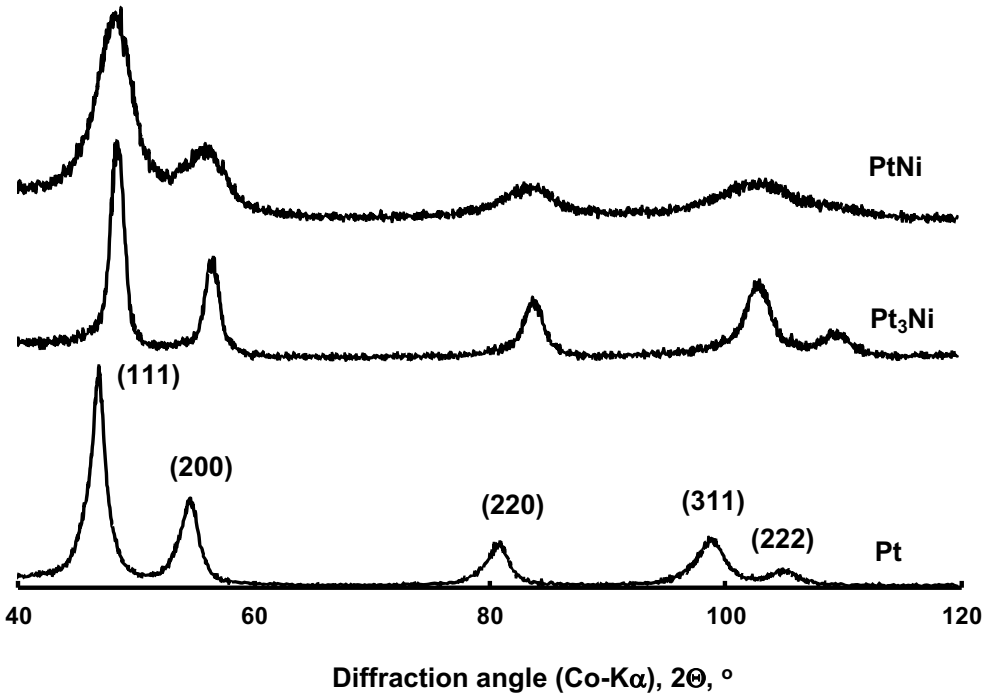

Figure 5.1: X-ray diffraction pattern of unsupported samples with the nominal composition Pt, Pt_3Ni and PtNi.

Using Vegard's law, the element composition of the Pt/Ni alloys might be estimated according to equation 5.1, using the measured lattice parameter of Pt, Pt_3Ni and PtNi (a_{Pt}, a_{Pt_3Ni}, and a_{PtNi}) of 3.916 ± 0.014 Å, 3.791 ± 0.008 Å and 3.785 ± 0.016 Å, respectively.

$$a_{Pt-Ni} = (1 - x_{Ni}) \cdot a_{Pt} + x_{Ni} \cdot a_{Ni} \qquad 5.1$$

Where *a* is the lattice parameter and *x* is the mole fraction of the components in the alloy. Thus, the mole fraction of nickel in the main, visible phase in the X-ray diffraction pattern was estimated at ca. 30 % and 31 % for the samples with a nominal composition of Pt_3Ni and PtNi, respectively assuming the validity of Vegard's law. This means that the main phase in the sample with the nominal composition Pt_3Ni, which nominally contains 25% nickel, is enriched in nickel, possibly due to the enhanced rate of nickel incorporation compared to platinum using the applied method. Similarly, the main phase in the sample with the nominal composition PtNi contains almost the same amount of nickel as the same phase with the nominal composition Pt_3Ni. This might be related to a retardation of the incorporation of more nickel in the structure.

The average size of *fcc*-crystals in the samples with the nominal composition Pt, Pt_3Ni and PtNi, was determined from the broadening of the (111) and (200) reflection for all the samples (using Scherrer's equation), obtaining an average crystallite size of 7.2 nm, 8.2 nm, and 5.4 nm, respectively.

The morphology of materials with the nominal composition Pt, Pt_3Ni and PtNi, was further analyzed using a transmission electron microscope (TEM). Illustrated in Figure 5.2 are the bright-field TEM micrographs of Pt, Pt_3Ni and PtNi. The samples contained mainly spherical nano-sized particles without any noticeable particle agglomeration. The average particle size and the variance were determined by fitting the observed particle size distribution to a log-normal distribution. The obtained average sizes of the nano-sized Pt, Pt_3Ni and PtNi, particles with the standard deviations were 4.2 ± 0.6 nm, 6.3 ± 0.6 nm, and 4.1 ± 0.7 nm, respectively.

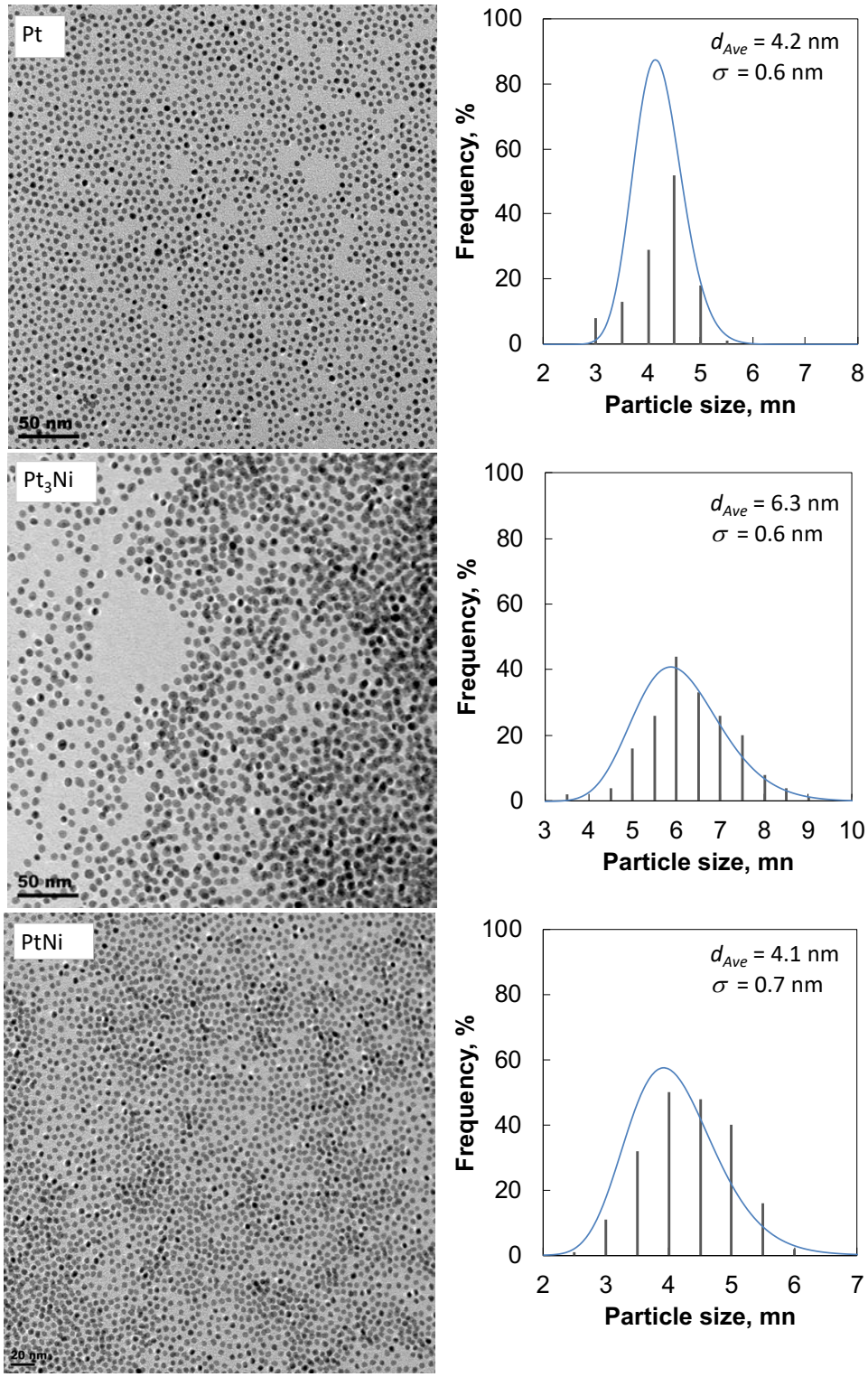

Figure 5.2: Bright-field TEM micrographs of the unsupported samples with a nominal composition of Pt, Pt_3Ni and PtNi and the log-normal distribution of the particle size (*N = 200 nanoparticles*).

Table 5.1 summarizes the average size of the synthesized nanoparticles as determined by TEM and XRD analysis. The observed difference in average particle size obtained from TEM and XRD analysis could arise from the overlapping of diffraction peaks of the XRD patterns of the analyzed samples.

Table 5.1: Morphological properties of the different of platinum-based catalyst as determined by TEM and XRD analysis.

Sample	d_{TEM} nm[1]	d_{XRD} nm[2]	lattice parameter, Å
Pt	4.2 ± 0.6	7.2	3.916± 0.014
Pt_3Ni	6.3 ± 0.6	8.2	3.791 ± 0.008
PtNi	4.1 ± 0.7	5.4	3.785 ± 0.016

Notably, as determined by XRD analysis, the average crystallite size in each sample is larger than the average particle size obtained from TEM analysis. This may be because the detection limit of XRD is biased towards larger nanoparticles.

5.1.2. CHARACTERIZATION OF SYNTHESIZED NANO-SIZED MATERIALS SUPPORTED ON TiO_2(RUTILE)

The synthesized nanoparticles with the nominal composition Pt, Pt_3Ni and PtNi, were re-dispersed in n-hexane and immobilized on TiO_2 (rutile phase; Sigma Aldrich; average nano-crystallite size *ca*. 29 nm) via colloidal deposition. The resulting catalyst samples were dried at 120 °C and annealed at 350 °C under N_2 to yield *ca*. 1 wt.-% of platinum in the nano-sized materials supported on rutile. According to XRD analysis, the

[1] Average particle size measured from TEM analysis
[2] Average crystallite size and lattice parameter of the phase belonging to the main diffraction lines attributed to *fcc*-Pt and *fcc*-Pt alloy, respectively

deposition of these materials on TiO_2(rutile) did not seem to alter the structure of the titania support (see Appendix C-5.1).

The composition and the active metal loading of the catalyst were verified using *ICP-OES* analysis (see Table 5.2; STEM-EDX mapping of Pt-Ni sample is found in Appendix C-5.2). Molybdenum, which could have originated from the reducing agent $Mo(CO)_6$ used in the synthesis, was not detected by STEM-EDX in any synthesized nano-sized particles (see Appendix C-5.2). The samples containing the alloys supported on rutile do contain ca. 1 wt.-% of platinum. Still, the sample Pt/TiO_2(rutile) contained only 0.78 wt.-% platinum.

Table 5.2: Elemental analysis and textural properties of the different platinum-based catalyst as determined by *ICP-OES* and TEM analysis.

Sample	**Composition** (wt. -%)[3]		**Ni/(Ni+Pt)** (mol/mol)	$\mathbf{d_{active\ metal}}$, (nm)[4]
	Pt	**Ni**		
Pt/TiO_2	0.78	-	0	4.2 ± 0.8
Pt_3Ni/TiO_2	0.91	0.16	0.36	11.8 ± 1.4
$PtNi/TiO_2$	0.96	0.79	0.73	12.3 ± 1.2

The elemental analysis of the sample with a nominal composition of Pt_3Ni is enriched in nickel (as was already deduced from the position of the diffraction lines and applying Vegard's law). It is thus concluded that the applied method[185] results in enhanced incorporation of nickel. The enhanced reduction of nickel compared to platinum can also be observed with the sample with a nominal composition of PtNi. However, nickel is not incorporated into a crystalline structure, nor could amorphous nickel be detected using TEM.

[3] Determined by ICP-OES analysis
[4] Average particle size determined using TEM analysis

5.1.2.1. MORPHOLOGY

A transmission electron microscope (TEM) was used to determine the morphology of the synthesized nanomaterials supported on TiO_2(rutile), their size distribution and the average particle size in all the samples (see Figure 5.3). The average particle size of the sample containing only Pt on TiO_2(rutile) was determined to be 4.2 ± 0.8 nm, which is similar to the average size obtained for the unsupported Pt-nanoparticles (4.6 ± 0.6 nm), implying that the colloidal deposition technique did not alter the particle size distribution.

The materials with a nominal composition of Pt_3Ni and PtNi supported on TiO_2(rutile) resulted in significantly larger average particle sizes (11.8 ± 1.4 nm and 12.3 ± 1.2 nm, respectively) than that of the unsupported samples. TEM analysis of the unsupported sample with the nominal composition of Pt_3Ni only showed the presence of spherical crystallites with an average crystallite size of 6.3 ±0.7 nm. This may be a consequence of bias in detecting nanoparticles on the supporting material (aggravated by the low metal loading). Alternatively, it might indicate that these samples sintered during the drying and calcination step of synthesising these supported materials, although the mechanism by which these particles sintered remains obscure, as the pure platinum particles supported on TiO_2(rutile) did not show any evidence of sintering.

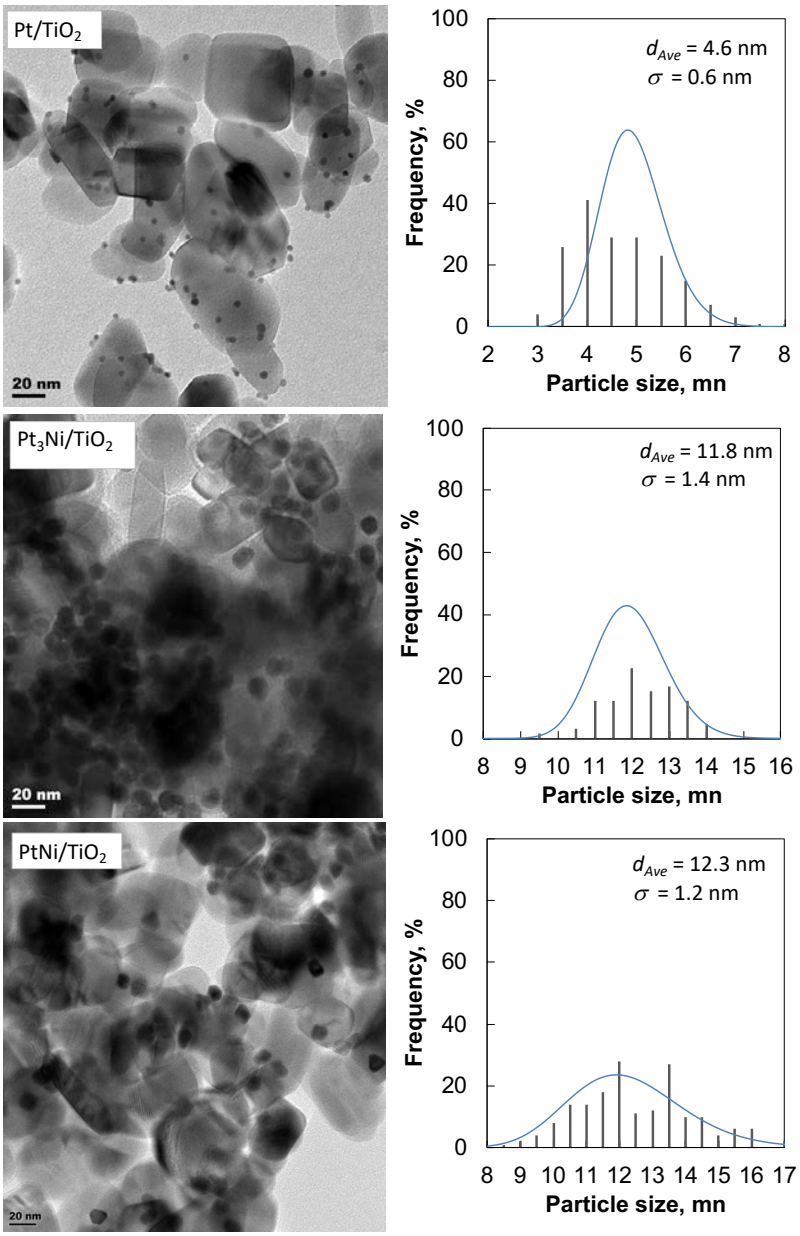

Figure 5.3: Bright-field TEM micrographs of materials with the nominal composition Pt, Pt_3Ni and PtNii supported on TiO_2(rutile) and the log-normal distribution of the nano-sized particles (*N = 200 nanoparticles*).

5.2. RESULTS

The influence of alloying platinum with nickel on the catalytic performance in the aerobic oxidation of benzyl alcohol was evaluated over Pt_3Ni/TiO_2(rutile) and $PtNi/TiO_2$(rutile). The catalytic performance over the Pt/TiO_2(rutile) catalyst is used as a

basis for comparison. Blank experiments were conducted, and no significant benzyl alcohol conversion was observed in the absence of the catalyst or even with only TiO_2(rutile). This indicates that the aerobic oxidation of benzyl alcohol requires metallic sites, such as platinum, to proceed. Hence, the benzyl alcohol conversion activity reported here is neither attributed to autoxidation of the substrate nor catalyzed by the support, TiO_2(rutile), on its own. This series of catalysts has some minor variations in active metal loading and size distribution, which must be considered when investigating the effect of alloying platinum with nickel on the aerobic benzyl alcohol oxidation.

5.2.1. SELECTIVE OXIDATION OF BENZYL ALCOHOL: EFFECT OF THE CATALYST COMPOSITION

The liquid-phase benzyl alcohol oxidation was performed in a semi-batch reactor operating at 90°C, 5 bar using air (flow rate of 100 mL_n/min(NTP)). A total of 0.5 g of the catalyst was added to the reaction mixture in the autoclave (total volume of the liquid phase of 70 mL). The liquid phase initially consisted of 2.33 mol H_2O, 0.0574 mol m-xylene and 0.202 mol benzyl alcohol. The reaction was allowed to run for 5 hours. The catalyst activity is reported in terms of benzyl alcohol conversion since the initial moles of benzyl alcohol in the system added are comparable for all catalyst evaluations. The reaction rate is reported as the number of moles of benzyl alcohol converted per mole of platinum in the catalyst loaded in the reactor (0.5 g of catalyst) per hour since the number of surface Pt atoms was not determined. This rate is defined as the platinum-time yield (referred to as PTY hereafter).

The conversion of benzyl alcohol decreases when alloying platinum with nickel (see Figure 5.4), despite the higher platinum loading. Monometallic Pt/TiO_2(rutile) catalyst was the most active for the oxidation of benzyl alcohol under these conditions, resulting in a conversion of 7.2% after 5 hours. The platinum-nickel sample with the nominal composition Pt_3Ni supported on TiO_2(rutile) exhibited the lowest conversion of 1.2 mol-% after a reaction time of 5 hours. The conversion-time profile obtained with the platinum-nickel sample with the nominal composition PtNi is rather unusual with high initial activity (same conversion as Pt/TiO_2(rutile) after 1 hour), but a strong deactivation resulting in no further reaction after 1 hour on stream.

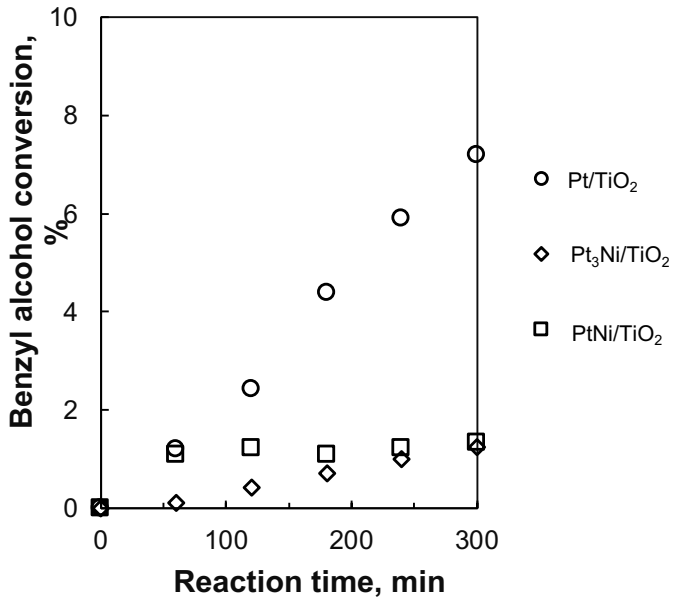

Figure 5.4: Benzyl alcohol oxidation as a function of reaction time over platinum-nickel alloys supported on TiO_2(rutile) at 90 °C. Reaction conditions: 0.202 mol of benzyl alcohol in 2.33 mol of H_2O and 0.0574 mol of xylene, as solvent mixture, 0.5 g catalyst, $P_{total,\ air}$ = 5 bar at F_{Air} = 100 mL_n/min(NTP).

Table 5.3 summarizes the catalytic performance of Pt/TiO_2(rutile), Pt_3Ni/TiO_2(rutile) and PtNi/TiO_2(rutile). The platinum-time yield (PTY) of benzyl alcohol consumption over Pt/TiO_2(rutile) was determined to be 148.8 ± 3.7 hr^{-1}. This can be re-calculated as a turnover frequency of 540 ± 13 hr^{-1} assuming a mean platinum particle size of 4.6 nm and dispersion of platinum given by $D(\%) = \frac{112}{d_{Pt}(nm)}$. The higher turnover frequency obtained with this material in comparison to the impregnated Pt/TiO_2(P25) (232.4 ± 31.1 hr^{-1}) may be related to the difference in the support structure (see Chapter 6).

Alloying platinum with nickel resulted in a strong reduction in the platinum-time yield over the material with the nominal composition of Pt_3Ni to 20.9 ± 0.9 hr^{-1}. The initial platinum-time-yield (after a reaction time of 1 hour) over the material with a nominal composition PtNi is similar to the platinum time yield obtained over Pt/TiO_2(rutile), but measured over the full 5 hours reaction time, the corresponding PTY for benzyl alcohol

oxidation reduced to 27.5 ± 5 hr^{-1} (with the corresponding high standard deviation due to deactivation). Incorporating the nickel as a second metal to Pt for benzyl alcohol oxidation does not result in an enhanced benzyl alcohol conversion when using O_2 as an oxidant.

The oxidation of benzyl alcohol over Pt/TiO_2(rutile) at 90°C after a reaction time of 5 hours was selective towards the formation of benzaldehyde with selectivity above 99 %, despite a relatively large variation in conversion levels. The oxidation of benzyl alcohol over Pt_3Ni/TiO_2 was less selective, and selectivity towards benzaldehyde of *ca*. 97 % after 5 hours on stream was obtained (the remainder was benzoic acid). The lowest benzaldehyde selectivity of ca. 49% was obtained over $PtNi/TiO_2$, and the benzoic acid selectivity is almost 51%. This may suggest that secondary oxidation, i.e., further oxidation of benzaldehyde intermediate, is favoured over the catalyst with a nominal composition of Pt-Ni possibly related to the presence of an amorphous nickel in the sample.

Table 5.3: Benzyl alcohol conversion over nickel-platinum-based catalysts supported on TiO_2 (rutile phase) at 90°C after 5 hours on stream.[5]

Catalyst sample	**Benzyl alcohol conversion,** (%)	**Platinum-time-yield** (hr^{-1})	**Benzaldehyde selectivity** (%)
Pt	7.2	148.8 ± 3.7	>99
Pt_3Ni/TiO_2	1.2	20.9 ± 0.9	97
$PtNi/TiO_2$	1.3	27.5 ± 5.0	49

5.3. KINETIC OUTLOOK: EFFECT OF TEMPERATURE

The bimetallic catalyst samples with the nominal composition Pt/TiO_2 and Pt_3Ni/TiO_2 were also tested for benzyl alcohol oxidation at 120 °C (see Figure 5.5).

[5] **Reaction conditions**: initial composition of the liquid mixture: 0.202 mol of benzyl alcohol in 2.33 mol of H_2O and 0.0574 mol of xylene, 0.5 g catalyst, $P_{total,\ air}$ = 5 bar, T = 90 °C, V_{liquid} = 70 mL, V_{air} = 100 mL_n/min.

Pt/TiO_2 catalyst showed benzyl alcohol conversion of ca. 12 % while benzyl alcohol conversion of ca. 1.8 % was obtained over Pt_3Ni/TiO_2 catalyst. The corresponding platinum-time yield (PTY) obtained over Pt/TiO_2, and Pt_3Ni/TiO_2 was 183.6 ± 22.6 hr^{-1} and 32.2 ± 1.7 hr^{-1}, respectively. The platinum-time yield (PTY) for benzyl alcohol oxidation increased upon increasing temperature from 90 °C to 120 °C, albeit rather moderately. The activation energy for the benzyl alcohol oxidation over Pt/TiO_2(rutile) was estimated to be 20 kJ/mol. Low activation energy could arise in a reaction, which is strongly inhibited by-products/reactants not directly involved in the rate-determining step. The estimated activation energy for the benzyl alcohol oxidation over the catalyst with the nominal composition Pt_3Ni/TiO_2 was even less dependent on the temperature, and activation energy of only 9 kJ/mol was determined. This may imply that either the activation energy of the rate-determining step is lowered or that the adsorption energy of the products/reactants is not directly or indirectly involved in the rate-determining step increased. Moreover, low activation energy often associated with mass transfer limitations (either gas-liquid mass transfer limitation or liquid-solid mass). If the reaction system was mass-transfer controlled, the measured rates in all the systems would be comparable and limited by the oxygen transfer rate. The oxygen transfer rate between the gas and the liquid phase and between the liquid and the solid phase may be estimated from reported values of mass transfer values/correlations, see Appendix C-5.3.

Pt/TiO_2 showed benzaldehyde selectivity of >99 % in the benzyl alcohol oxidation at the slightly elevated temperature of 120 °C, relatively independent of the benzyl alcohol conversion levels of ca. 12%. This implies that even going to a conversion level of ca 15% Benzaldehyde selectivity over Pt_3Ni/TiO_2 also remains high (99%) when operating at 120 °C. A significant increase in the extent of secondary oxidation to benzoic acid was thus not observed.

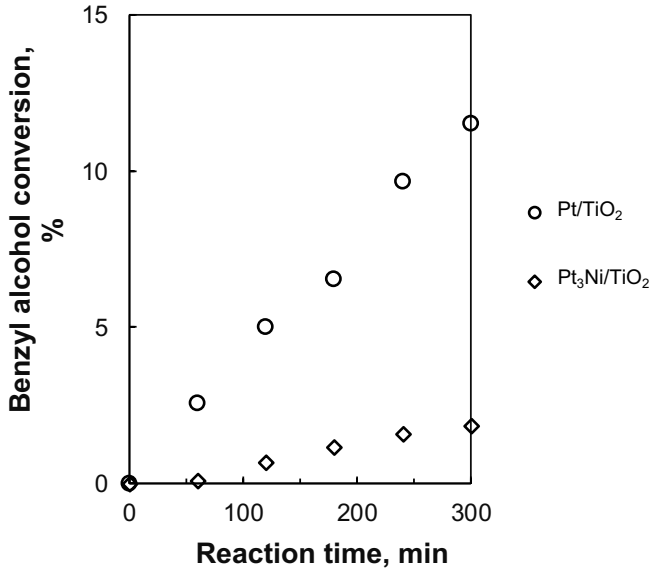

Figure 5.5: Comparison of the conversion in the benzyl alcohol oxidation over the materials with a nominal composition of Pt and Pt_3Ni supported on TiO_2(rutile) at 120 ºC using air as an oxidant at $P_{Total,\ air}$ = 5 bar.

5.4. PROBING THE ROLE OF THE OXIDANT IN THE SELECTIVE OXIDATION OF BENZYL ALCOHOL OVER PLATINUM-NICKEL BASED CATALYST

Alloying Pt with Ni, resulting in Pt-skin and Ni subsurface alloy,[186] may affect the electronic properties of the alloy constituents and, thus, the strength of adsorption of various adsorbates. Hence, the effect of Ni in a platinum-nickel alloy on benzyl alcohol oxidation was explored by comparing H_2O_2 and O_2 as oxidants.

Figure 5.6 shows benzyl alcohol conversion at 90 °C over Pt/TiO_2 and Pt_3Ni/TiO_2 using different oxidants, H_2O_2 and O_2. The use of O_2 as an oxidant in the benzyl alcohol oxidation over Pt_3Ni/TiO_2 yielded, as shown above, a rather low benzyl alcohol conversion of ca. 1.2 %, which is equivalent to a PTY of 20.9 ± 0.9 hr^{-1}. Substituting oxygen oxidant with H_2O_2 (as 90 mol-% of 30% H_2O_2-solution and 10 mol-% benzyl alcohol liquid composition) resulted in a significant enhancement of benzyl alcohol conversion over Pt_3Ni/TiO_2 to ca. 16 mol-% after a reaction time of 3 hours corresponding to platinum time yield (PTY) of 506.6 ± 37 hr^{-1}. The benzyl alcohol conversion over Pt/TiO_2 in the presence of H_2O_2 as the oxidant is slightly higher than the conversion obtained with O_2 as the

oxidation (obtaining 5.7% and 4.4% for H_2O_2 and O_2 oxidants after 3 hours on stream, respectively). Hence, the platinum time yield over Pt/TiO_2(rutile) was 120.6 ± 6.4 hr^{-1} in the presence of O_2 and 186.1 ± 15.1hr^{-1} in the presence of H_2O_2 oxidant.

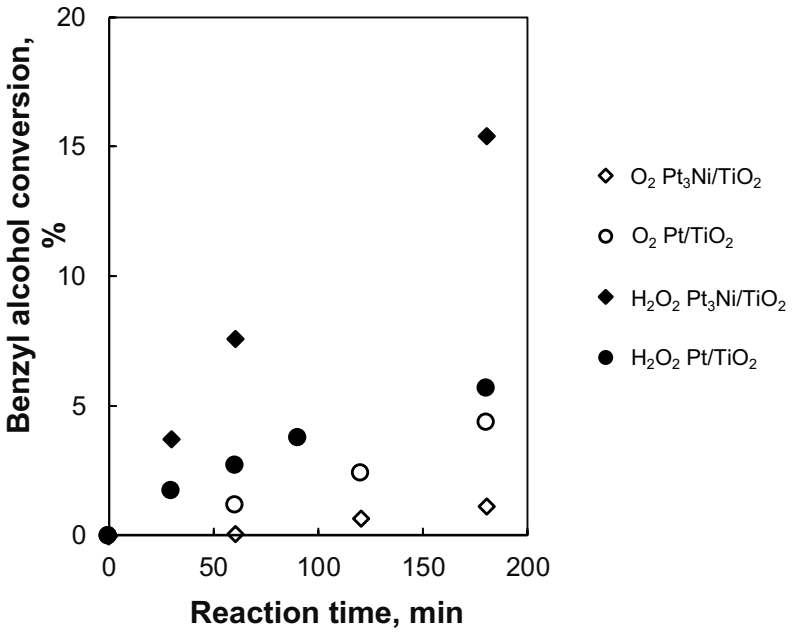

Figure 5.6: Benzyl alcohol oxidation for 3 hours of the reaction over Pt/TiO_2 and Pt_3Ni/TiO_2 catalyst at 90°C in the presence of H_2O_2 and O_2 as oxidants.

The benzaldehyde selectivity remained at >99% in the benzyl alcohol oxidation over Pt/TiO_2 and Pt_3Ni/TiO_2 catalyst when H_2O_2 was an oxidant at a reaction temperature of 90 °C. Neither the change in the oxidant nor the presence of Ni seems to affect the product selectivity despite the differences in the benzyl alcohol conversion.

5.5. DISCUSSION

Alloying may change the adsorptive properties of the catalyst surface and, thus, the prevalence of various surface species. Hammer and Nørskov[187] argued that the interactions between adsorbates and transition metal surfaces include the entire d-band and the characteristics of the surface metal d-bands. Hence, the weighted centre of the d-band plays a significant role in defining surface reactivity. There should, thus, be a correlation between chemisorption energies and the average energy of the d-state on the

surface atoms to which the adsorbate binds. The d-band centre on the surface Pt-atoms of Pt-skin $Pt_3Ni(111)$ alloy is shifted downwards by 0.30[176] - 0.36[139,188] eV relative to the d-band position of surface atoms in Pt(111). A lowering of the d-band centre will result in the weakening of the adsorption.[176] This can be explained based on the induced charge polarization between surface (Pt-skin) and subsurface (Ni) layers in the alloy. The difference in the electronegativity between Pt and Ni in the Pt-skin alloys results in an electron transfer from the subsurface to the surface metal atoms affecting the metal adsorbate bonding. This results in a higher partial density of state (PDOS) for *s,* d_{xz}, d_{yz}, d_{xy}, and d_z^2 of Pt(111) and Pt-Ni(111), which alters the chemical bonding behaviour of Pt upon alloyed with Ni. The downshift of the d-band centre of the surface Pt layer on $Pt_3Ni(111)$ would result in a reduced contribution of surface d-bands near the Fermi level, particularly d_{xz} and d_{yz} states.[139] Hence, chemisorption of molecular and atomic oxygen on Pt_3Ni (Pt-skin and Ni subsurface) alloys is thus characterized by a weaker oxygen-metal bond compared to oxygen adsorption on pure Pt. The weaker chemisorption of O_2 on the $Pt_3Ni(111)$ surface also results in a lower electron density on O_2 in comparison to the adsorption of O_2 on Pt(111) even though the surface Pt atoms of $Pt_3Ni(111)$ having more electrons.

Similarly, the chemisorption of atomic oxygen becomes weaker upon shifting the d-band centre downwards.[146] Due to the scaling relationship, the chemisorption of OH is expected to be weaker on Pt-skin $Pt_3Ni(111)$ than on Pt(111). However, the oxygen atom in OH is has a higher electron density than atomic O, due to electron transfer from H to O in OH.[189] Hence, the adsorption energy of OH changes less than the adsorption energy of atomic oxygen upon shifting the d-band centre downwards when changing from Pt(111) to Pt-skin on $Pt_3Ni(111)$.

The weaker adsorption of molecular oxygen, atomic oxygen and surface hydroxyl species on Pt-skin on $Pt_3Ni(111)$ may result in lower surface coverage of these species. Furthermore, the activation energy barrier associated with the dissociation of O_2 over Pt-skin $Pt_3Ni(111)$ is higher (0.63 eV) than over Pt(111) (0.83 eV).[190] Hence, the dissociation of molecularly adsorbed O_2 in the absence of co-adsorbed water is more facile over Pt(111) than over Pt-skin $Pt_3Ni(111)$ alloy surface.

The presence of co-adsorbed water on Pt(111) resulted in a reduced activation barrier for the dissociation of adsorbed molecular oxygen. The downshift in the d-band centre will cause a reduction in the adsorption energy of water as well.[191] This may result in a reduction in the amount of water on the surface, thus lowering the rate of O_2 dissociation over Pt-skin $Pt_3Ni(111)$ even further. A lowering of the rate of dissociation of molecular oxygen over Pt_3Ni in comparison to the dissociation over Pt(111) in addition to the reduced coverage of O_2, O, OH due to the weakening in the chemisorption may be linked to the observed reduction in catalytic activity in the aerobic oxidation of benzyl alcohol over Pt_3Ni/TiO_2(rutile) in comparison to the oxidation over Pt/TiO_2(rutile).

The oxidation of benzyl alcohol over Pt_3Ni/TiO_2(rutile) is accelerated when H2O2 is the oxidant. Hydrogen peroxide can be activated over Pt(111), resulting in its dissociation[190] via O-O bond cleavage in H_2O_2, yielding two surface OH species. Duang and Wang[190] reported an activation energy of 0.26 eV for this reaction, i.e. a slightly higher activation energy than the activation energy for the dissociation of molecular oxygen over Pt(111) in the presence of water, which also results in the formation of surface hydroxyl species in addition to atomic oxygen. The mechanism for the dissociation of H_2O_2 over Pt-skin $Pt_3Ni(111)$ alloy surface is proposed[190] to be similar to that over Pt(111), but the dissociation of adsorbed H_2O_2 over Pt-skin $Pt_3Ni(111)$ alloy surface proceeds with a significantly lower activation barrier of only *ca*. 0.08 eV. This would result in a much more facile formation of surface OH-groups on $Pt_3Ni(111)$ in comparison to their formation on Pt(111), where they can be formed either from H_2O_2 or from co-adsorbing H_2O and O_2. This may be linked to the enhanced benzyl alcohol oxidation over Pt_3Ni/TiO_2 catalyst when using H_2O_2 as an oxidant.

5.6. CONCLUSION

The catalytic studies revealed that the catalytic performance of the Pt/TiO_2 catalyst in benzyl alcohol oxidation with O_2 as an oxidant is drastically decreased upon alloying Pt with Ni (Pt_3Ni/TiO_2 and $PtNi/TiO_2$), even after increasing reaction temperature (from 90°C to 120°C). However, substituting the oxidant O_2 with H_2O_2 yielded a significant enhancement in the benzyl alcohol conversion at 90°C. The effect of alloying Pt with Ni

on benzyl alcohol oxidation reaction is, thus, thought to be due to the change in electronic properties of Pt upon alloying with Ni, to from Pt-skin alloy (Pt_3Ni). As such, the low benzyl alcohol conversion over Pt-Ni/TiO_2 catalysts is attributed to weaker adsorption of molecular and atomic oxygen, surface hydroxyl species and adsorbed water on Pt-skin Pt_3Ni alloy in comparison to on Pt(111), due to the expected downward shift of the d-band centre of surface platinum atoms when alloying the subsurface with nickel. However, using H_2O_2 as an oxidant, which dissociates into surface OH species, yields an enhanced benzyl alcohol conversion compared to the system that uses O_2 as an oxidant. This difference is most likely ascribed to the difference in the activation energy induced by the difference in the adsorption strength of the reactants and products in that particular elementary reaction step over Pt_3Ni/TiO_2.

Similar to Pt_3Ni/TiO_2 catalyst, the $PtNi/TiO_2$ catalyst also showed low catalytic activity. However, the main difference is that $PtNi/TiO_2$ catalyst resulted in an overoxidation to form benzoic acid with a selectivity level of *ca*. 49%. In contrast, the other catalysts yielded with high selectivity benzaldehyde. This might be related to the presence of an amorphous nickel in the sample.

CHAPTER 6:

Influence of the oxidic support material on benzyl alcohol oxidation

OVERVIEW

Metal oxides are often used as supports to finely disperse the catalytically active metal nanoparticles. The surface of metal oxide may have different forms of defects and/or environments (kinks, steps, terraces and/or vacancy sites), which may play a defining role in the overall catalytic phenomenon.

Here, reducible and irreducible metal oxides are employed as support material to dispersed Pt nanoparticles in the range of 2.5- 4.6 nm for benzyl alcohol oxidation catalysts. The influence of reducible (TiO_2(P25), CeO_2, MoO_3 and γ-Fe_2O_3) and irreducible metal oxides (γ-Al_2O_3) supported Pt catalyst is investigated for benzyl alcohol oxidation reaction in the presence of H_2O as a solvent.

6.1. RESULTS

Using different metal oxides as support material for the catalytically active metal in the liquid-phase oxidation of alcohols may affect the overall catalytic performance.[11] This may be caused by differences in the resulting metal dispersion. The interaction of the support with the liquid phase, i.e. its hydrophobicity, and its reducibility may play a role in the catalytic performance. Here, the catalytic performance of platinum supported on TiO_2(P25), γ-Al_2O_3, CeO_2, MoO_3 and Fe_2O_3 in benzyl alcohol oxidation is explored. The BET surface of the support materials was determined to be TiO_2(P25): 48.4 ± 0.2 m²/g, γ-Al_2O_3: 140.5 ± 0.7 m²/g, CeO_2 1.7 ± 0.0 m²/g, MoO_3: 3.0 ± 0.1 m²/g, and γ-Fe_2O_3 (maghemite):16.2 ± 0.1 m²/g, respectively.

6.1.1. Wetting behaviour: Water/oxide support interactions at the interface

Water has been shown to accelerate benzyl alcohol oxidation (see Chapter4). Appreciation of the interfacial properties of water and the oxide support material may provide an added dimension to the reaction dynamics of alcohol oxidation. Furthermore, understanding how the water at the interface interacts with the reactants at the extended hydrophobic surface may provide insights into reaction mechanisms at water/ surface interfaces. The hydrophobicity/hydrophilicity of the support material may thus affect this reaction.

The contact angle of solid material on a specific liquid can provide information about the hydrophobicity of the solid material. Thus, the contact angle, $\theta_{c,\ H_2O}$ (derived from the capillary constant) between the support, γ-Al_2O_3, γ-Fe_2O_3, CeO_2, MoO_3 and TiO_2(P25), and H_2O was measured using the Washburn method.[192]

The capillary constant and the contact angle of water with the oxidic support materials, TiO_2(P25), γ-Al_2O_3, CeO_2, MoO_3 and γ-Fe_2O_3, are given in Table 6.1. Most of the contact angles were between 50° and 65°, except for TiO_2(P25), for which a contact angle of 89.5° was determined. The measured $\theta_{c,\ H_2O}$ for TiO_2 is in agreement with that measured $\theta_{c,\ H_2O}$ for TiO_2 film (86.9°) measured by Kong et al.[193] While the measured $\theta_{c,}$

$_{H_2O}$ for Al_2O_3 measured by Cieśliński and Kryger[194] was between 91.5° -99.9°. DFT study by Fronzi et al.,[195] showed that CeO_2(111) surface is the most hydrophobic with $\theta_{c,\ H_2O}$ = 112.53° and CeO_2(100) surface measuring a $\theta_{c,\ H_2O}$ of 93.91°. However, the CeO_2(110) surface was the most hydrophilic with $\theta_{c,\ H_2O}$ = 64.09°. The latter measured is in agreement with the $\theta_{c,\ H_2O}$ of CeO_2 measured in this current study. The difference between the obtained $\theta_{c,\ H_2O}$ in this study and that reported in the literature may be due to the difference in material particle size, the porosity of the oxide support material employed and $\theta_{c,\ H_2O}$ measuring methods used.

The obtained $\theta_{c,\ H_2O}$ indicates that all these support materials, except for TiO_2(P25), have an adequate wettability since their contact angle is substantially less than 90°. TiO_2(P25) material is rather hydrophobic compared to the other oxide support materials in the series. It can be classified as almost non-wettable since the contact angle is close to 90°.

Immersion calorimetry was employed to complement contact angle measurements and to provide a thermodynamic dimension to solid-liquid interactions.[196] Immersion calorimetry is an established technique to quantify the interaction of, *e.g*. solid material with a specific liquid. The enthalpy of immersion, ΔH_{imm}, is defined as the heat change arising from the interaction of the solid-liquid interface when a solid surface is immersed in a liquid.[196] The solid-liquid interactions can be classified as physical or chemical interactions. The physical interaction is typically characterized by a negligible change in the enthalpy upon immersion. The heat of immersion, ΔH_{imm}, depends on the chemical nature of the surface of the solid material and immersion liquid. In a polar liquid, the enthalpy of immersion increases with the polarity of chemical functions on the surface of the solid. For example, using water as the immersion liquid, the enthalpy of immersion may also include the change in enthalpy due to the (partial) hydroxylation of the surface of the oxides.[197] It should be noted that samples were not preheated before the measurements, however all samples were stored in a desiccator for 24 hours before

measurements. More information on the heat of immersion of the samples is outlined in Appendix D-6.1.

The heat of immersion originates from the interaction of the surface of the solid with the liquid. Hence, the heat of immersion scales with the surface area of the material and should be normalized concerning its surface area. The normalized enthalpy of immersion of TiO_2(P25), γ-Al_2O_3, CeO_2, MoO_3, and γ-Fe_2O_3 in water was thus -0.096 J/m^2, -0.106 J/m^2, -2.875 J/m^2, 58.9 J/m^2 and -0.198 J/m^2, respectively. The enthalpy of immersion of MoO_3 is rather large. Molybdenum oxide is slightly soluble in water (solubility at 18 °C: 1.066 g/L)[198] and the heat of immersion of MoO_3 in water (176.6 J/g) comes close to the heat of dissolution of MoO_3 (328.4 J/g – estimated based on the temperature dependency of the solubility of MoO_3[169]). This may imply that a significant part of the sample dissolved during the determination of the heat of immersion.

Table 6.1: The characterization of the employed oxide support materials in terms of BET-surface area, contact angle with water (and the associated capillary constant), and the immersion enthalpy (both per unit mass and per unit surface area).

Oxide support	**BET surface,** m²/g	**capillary constant, c,** *x10^{-5}* cm^{-3}	**Contact angle,** °	$\Delta H_{imm, water}$ J/g	$\Delta H_{imm., water}$ J/m^2
TiO_2(P25)	48.4 ± 0.2	2.14	89.5	-4.6	-0.096
γ–Al_2O_3	140.5 ± 0.7	2.35	61.6	-14.9	-0.106
CeO_2	1.7 ± 0.03	0.79	52.3	-4.9	-2.875
MoO_3	3.0 ± 0.13	1.06	56.7	176.7[a]	58.9[a]
γ–Fe_2O_3	16.2 ± 0.081	1.81	65.3	-3.2	-0.198

[a] Dissolution of MoO_3 during determination of heat of immersion likely

The heterogeneously catalyzed, aerobic oxidation of benzyl alcohol in water containing medium may be a four-phase system with two liquid, an aqueous, and an organic phase (see Chapter 4). The catalyst may be preferentially located in one of the liquid phases depending on its hydrophilic or hydrophobic nature. Hence, the catalyst distribution in a liquid mixture containing 7 mol-% benzyl alcohol and 93 mol-% water was

studied (see Figure 6.1). Platinum supported on the most hydrophobic TiO_2(P25) oxide support is preferentially located in the organic phase or at the interface between the aqueous and organic phase since the aqueous phase is clear in colour with white emulsion (which is the organic phase). The catalysts comprising platinum and the relatively hydrophilic materials γ-Al_2O_3, CeO_2, and MoO_3- are distributed over both liquid phases. Notably, consistent with the reported heat of dissolution for MoO_3 (*vida supra*), MoO_3 support seems to be associated with the aqueous liquid phase also. Platinum supported on γ-Fe_2O_3 seems to be on the interface of the aqueous/organic phase of the liquid system. The distribution of the catalyst in the liquid phases may mimic the catalyst distribution during benzyl alcohol oxidation.

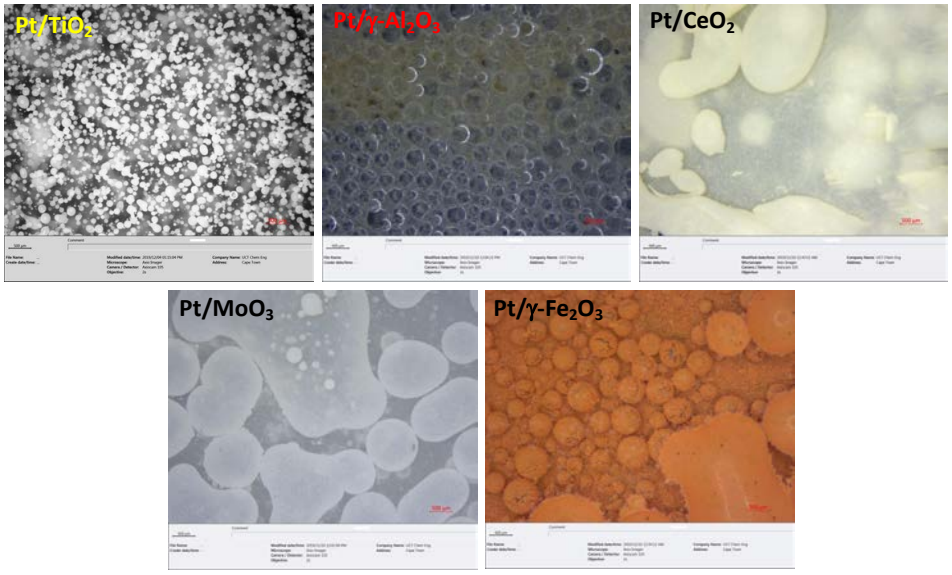

Figure 6.1: Micrographs of a platinum-based catalyst supported on various oxides suspended in an emulsion containing 93 mol-%H_2O and 7 mol-% benzyl alcohol.

6.1.2. CATALYST SURFACE MORPHOLOGY

The oxide support materials were impregnated with platinic acid yielding a 4 wt.-% Pt/TiO_2 (P25), Pt/γ-Al_2O_3, Pt/CeO_2, Pt/MoO_3 and Pt/γ-Fe_2O_3 (maghemite) using slurry impregnation. The target loading of 4 wt.-% was generally achieved (see Table 6.2). However, the experimentally determined Pt loading in Pt/CeO_2 catalyst is much lower

than expected. The low surface of CeO_2 may have resulted in poor contact with some platinum remaining behind in the crucible rather than on the support.

After calcining the catalysts at 350 °C in a static oven, the surface morphology of the synthesized supported platinum samples was viewed using a transmission electron microscope (TEM). The samples, Pt/TiO_2 (P25), Pt/MoO_3 and $Pt/\gamma\text{-}Fe_2O_3$ (maghemite), consisted of relatively small platinum particles homogeneously distributed throughout the support material surface with no visible particle agglomeration. The average particle size was determined to be 4.6 ± 0.8 nm, 3.1 ± 0.6 nm and 2.5 ± 0.5 nm for Pt/TiO_2, Pt/MoO_3 and $Pt/\gamma\text{-}Fe_2O_3$ samples, respectively, as illustrated in Figure 6.2.

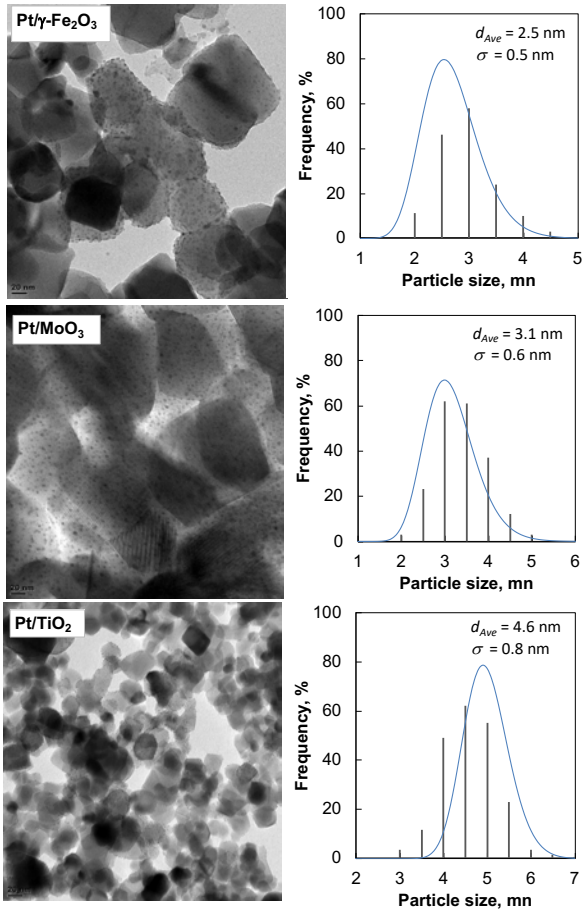

Figure 6.2: TEM-images and the average size (histogram) of platinum nano-sized particles supported on TiO_2, MoO_3 and $\gamma\text{-}Fe_2O_3$ catalyst samples, fitted in percentage probability density function (curve) (*N=200 nanoparticles*).

Poor contrast between the metallic platinum particles and the support material for Pt/γ-Al_2O_3 and Pt/CeO_2, as shown in Figure 6.3, indicates the necessity for a more detailed analysis such as chemisorption to obtain the average particle size of platinum in these samples.

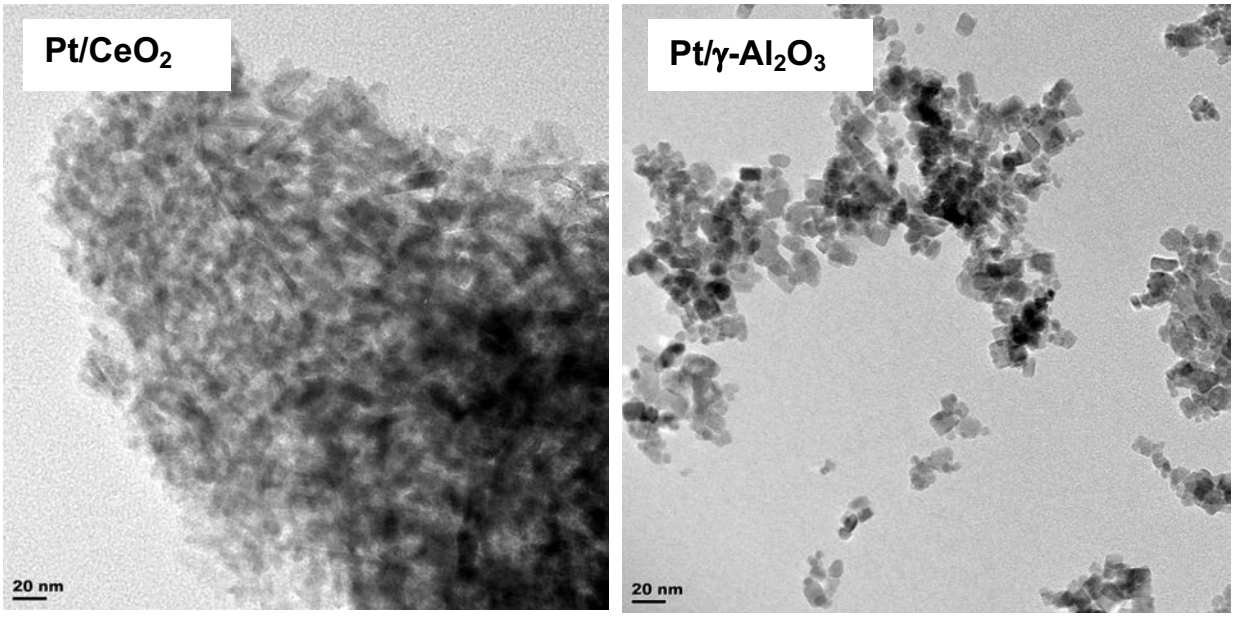

Figure 6.3: TEM-images of Pt/CeO_2 and Pt/γ-Al_2O_3 catalyst samples.

Notably, XRD analysis confirmed no phase change or alloy formation between the support material and Pt noble metal after catalyst calcination treatment (see XRD patterns of all the samples in Appendix D-6.3).

O_2 chemisorption was used to determine the metal surface area and thus the metal dispersion since these materials are used in oxidation catalysis. The average crystallite size of platinum in Pt/TiO_2(P25), Pt/γ-Al_2O_3, Pt/CeO_2, Pt/MoO_3, and Pt/γ-Fe_2O_3 (maghemite) catalyst samples according to O_2 chemisorption was determined to be 3.8 nm, 2.6 nm, 4.3 nm, 3.6 nm and 3.3 nm, respectively (see Table 6.2 for a summary). These values can reasonably well be correlated with the average particle size obtained from the evaluation of the TEM images (where possible). This corresponds to a metal dispersion in Pt/TiO_2(P25), Pt/γ-Al_2O_3, Pt/CeO_2, Pt/MoO_3 and Pt/γ-Fe_2O_3 catalyst of 29.9%, 42.3%, 28.6%, 36.1% and 44.8%, respectively.

Table 6.2: Platinum loading (determined using ICP-OES), average platinum particle size (either determined from TEM-images using ImageJ® or O_2-chemisorption) and dispersion (obtained from $D(\%) = \frac{112}{d_{Pt}}$).

Sample	**Pt loading**, wt.-%	**$d_{Pt,\ TEM}$**, nm	**$d_{Pt,\ chem}$**, nm	**D[a]**, %
Pt/TiO_2(P25)	3.9	4.6 ± 0.8	3.8	29.9
Pt/γ-Al_2O_3	4.5	-	2.6	42.3
Pt/CeO_2	1.7	-	4.3	28.6
Pt/MoO_3	3.7	3.1 ± 0.6	3.6	36.1
Pt/ γ-Fe_2O_3	4.0	2.5 ± 0.5	3.3	44.8

[a]based on an amount to form a monolayer, assuming Pt:O=2:1

6.1.3. TEMPERATURE PROGRAMMED DESORPTION OF AMMONIA (NH_3-TPD)

Ammonia TPD is typically used to characterize the acidity of materials. However, ammonia may also adsorb on metals, such as platinum. As such, the ammonia adsorption characterized by NH_3-TPD (fitted with a thermal conductivity detector, TCD) can thus be used to characterize support acidity as well as metal dispersion.[199] The peak position may indicate the strength of adsorption. At the same time, the amount desorbed is indicative of the number of adsorption sites. Typically, ammonia desorbing from acidic solids at relatively low temperatures (100-210 °C) is ascribed to the presence of a weak acid site.[200] On the other hand, ammonia desorbing from solid acids at a medium (210- 500 °C) and high temperatures (≥ 500 °C) are typically ascribed to the presence of medium and strong acid sites, respectively.[200] In the case of the pure metal oxides, the number of acid sites corresponding to the amount of ammonia desorbed can be reported in terms of the number of moles of NH_3 desorbed per unit surface area of the pure oxide. This should give insight into the density of acid sites.

NH_3-TPD profiles of the metal oxide support materials are shown in Figure 6.4. TiO_2(P25) consists of the rutile and anatase phases. The NH_3-TPD profiles obtained with TiO_2(P25) can be deconvoluted into the anatase and rutile phases (see Appendix D-6.4). The TiO_2(P25) sample shows a pronounced asymmetric desorption peak occurring at *ca*. 190 °C, which may be ascribed to the weak acid site present on the anatase phase. It

should be noted that the weak acid sites on the rutile phase will also contribute to the main desorption peak in the NH_3-TPD obtained with TiO_2(P25). The medium acid sites on the rutile phase are hidden in the tail of the main desorption peak in the NH_3-TPD obtained with TiO_2(P25). The density of acid sites in TiO_2(P25) is estimated to be 11.2 $\mu mol_{NH_3}/m^2_{oxide}$. This would correspond to a surface OH-density of 6.7 OH-groups per nm^2 assuming that surface hydroxyl groups are the acid sites on TiO_2(P25). This value corresponds well with the values reported for anatase and rutile.[201,202]

The NH_3-TPD spectrum obtained with γ-Al_2O_3 yielded two distinct desorption peaks at 257 °C and 567 °C, respectively, assigned to medium and strong acid sites. The number of acid sites estimated for γ-Al_2O_3, amounted to 5.9 $\mu mol_{NH_3}/m^2_{oxide}$ (i.e. total number of the acid centre of 822.2 $\mu mol_{NH_3}/g$). This corresponds to 3.5 molecules of NH_3 per nm^2 of the sample, which would correspond to a surface hydroxyl concentration of 3.5 OH-groups per nm^2.

The NH_3-TPD spectrum obtained with CeO_2 exhibits only one small desorption peak at 179 °C attributed to weak acid sites. Glorious et al.,[203] also obtained a similar NH_3-TPD profile with a CeO_2 sample that exhibited low surface area. The number of acid sites on CeO_2 was only 0.153 $\mu mol_{NH_3}/g$ (due to the low porosity of the sample). This would amount to 0.09 $\mu mol_{NH_3}/m^2_{oxide}$ or 0.05 OH-groups per nm^2. This is a rather low amount of surface hydroxyl groups. It should be noted that CeO_2 has a low surface area, and the amount of ammonia, which desorbed, was low. Error in each of the values may have affected the conclusion regarding the total number of surface hydroxyl groups

The NH_3-TPD spectrum with MoO_3 exhibited two desorption peaks at 183 °C and 602 °C ascribed to the weak and strong acid site, respectively. The total amount of ammonia desorbed from MoO_3 amounted to 10.6 $\mu mol_{NH_3}/m^2_{oxide}$ (31.8 $\mu mol_{NH_3}/g$). This corresponds to 6.4 molecules of ammonia per nm^2. The number of acid groups on a support can be determined by assuming a 1:1 ratio between the base (NH_3) and the acid site (OH) group. The obtained molecules of ammonia per surface area correspond to 6.4 molecules of hydroxyl species per nm^2. The sample showed a relatively higher number

of acid sites per gram compared to the literature.[204] This may be attributed to the difference in the specific surface area of MoO_3. Molybdenum oxide contains both strong and weak acid sites in a ratio of 1:0.47.

The NH_3-TPD spectrum obtained with γ-Fe_2O_3 showed two peaks at 178 °C and 482 °C, indicating the presence of weak and medium acid sites. The weak acid site of the sample has a shoulder peak at 285 °C, which corresponds to medium acid sites of the sample. However, the shoulder peak was also observed by Husnain et al.206 at a relatively low temperature of 197 °C. The difference in temperature peaks may be due to the different experimental conditions of the NH_3-TPD analysis.[205] The number of weak acid sites was determined to be 6.2 $\mu mol_{NH_3}/m^2$ (100.9 $\mu mol\ _{NH_3}/g_{cat}$), and the number of medium acid sites was determined to be 2.2 $\mu mol_{NH_3}/m^2$ (34.8 $\mu mol\ _{NH_3}/g_{cat}$). This corresponds to 3.7 and 1.3 NH_3 molecules per nm^2, respectively.

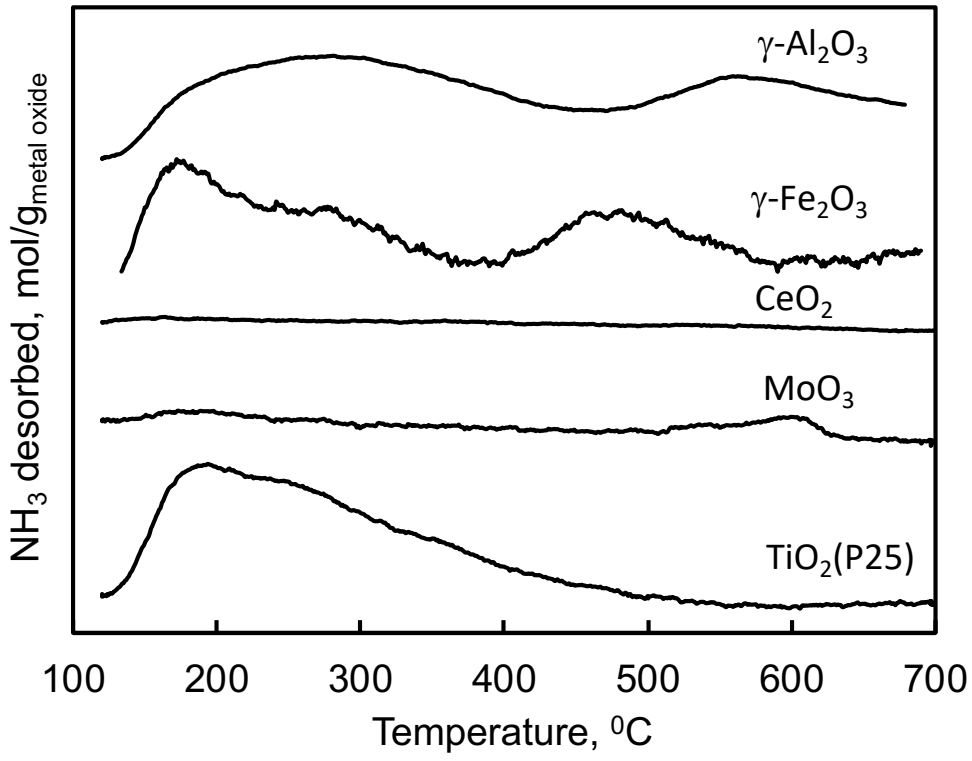

Figure 6.4: NH_3-TPD profile of various oxide support materials.

The oxide support materials in the series were impregnated with platinic acid and thermally treated, yielding metallic Pt on the support. The NH_3-TPD of the resulting catalyst samples was analyzed (see Figure 6.5). It should be noted that the presence of metallic platinum may result in the desorption of NH_3 from metallic platinum and the desorption of NH_3 from acidic sites of the support.

The NH_3-TPD spectrum obtained with Pt/TiO_2(P25) exhibited a broad single desorption peak extending to relatively high temperatures, with a maximum at ca. 238 °C. The broadness of this peak may cover the presence of multiple peaks contributed to TiO_2 anatase, TiO_2 rutile phase and metallic platinum. This may be solely ascribed to ammonia rather weakly adsorbed on the catalyst Pt/TiO_2(P25). The amount of ammonia desorbed increased slightly in the presence of platinum moiety of the catalyst from 537.5 $\mu mol_{NH_3}/g$ to 605 $\mu mol_{NH_3}/g$ (see Table 6.3). Suppose the difference can be attributed to ammonia adsorbed on metallic platinum. In that case, it implies that 0.31 mol of NH_3 desorbs per mole of platinum in the catalyst. This is in good agreement with the calculated dispersion of platinum in the catalyst (see Table 6.2) if it can be assumed that the adsorption stoichiometry of NH_3:Pt is 1:1.

The NH_3-TPD spectrum obtained with Pt/γ-Al_2O_3 also has multiple desorption peaks, with a sharp distinct peak at 284.5 °C and a broad peak at ca. 559 °C. The broad desorption peak at 559 °C is ascribed to desorption from strong acid sites on γ-Al_2O_3. Desorption at low temperature accounts for weak/medium acid sites in the γ-Al_2O_3 framework is also observed. However, the desorption of ammonia from weak and medium acid sites is overshadowed by the additional sharp peak observed in the profile of Pt/γ-Al_2O_3. As such, the sharp peak at 284.5 °C is thought to correspond to NH_3 desorbing from the Pt moiety of the catalyst. This would correspond to 0.23 mol NH_3 desorbed per mol of platinum in the catalyst (again relating reasonably to the platinum dispersion as determined by oxygen chemisorption).

The NH_3-TPD spectrum obtained with Pt/CeO_2 has a single, relatively low-intensity NH_3 desorption peak at low temperatures of ca. 187 °C, suggesting sites weakly adsorbing ammonia. The amount of NH_3 desorbed per gram of catalyst for Pt/CeO_2 is

higher than that of NH_3 desorbed per gram of catalyst for CeO_2. Ascribing the difference to NH_3 adsorbed on metallic platinum results in an amount of NH_3 desorbed relative to the amount of platinum in the catalyst of 0.33 mol_{NH3}/mol_{Pt}. This is in reasonable agreement with the dispersion determined using O_2-chemisorption, which was 28.6%, assuming dissociative adsorption of oxygen.

The NH_3-TPD obtained with the sample Pt/MoO_3 also has a single, relatively low-intensity NH_3 desorption peak, but now at slightly higher temperatures of ca. 203 °C. MoO_3 only has significant desorption at rather high temperatures, which is not observed with Pt/MoO_3. This could be observed if platinum was anchored to or covering the surface acid sites. Suppose the NH_3 desorbed at low temperature can be solely attributed to ammonia desorbing from platinum. In that case, a dispersion of platinum of 22.2% can be estimated (slightly lower than estimated using O_2-chemisorption).

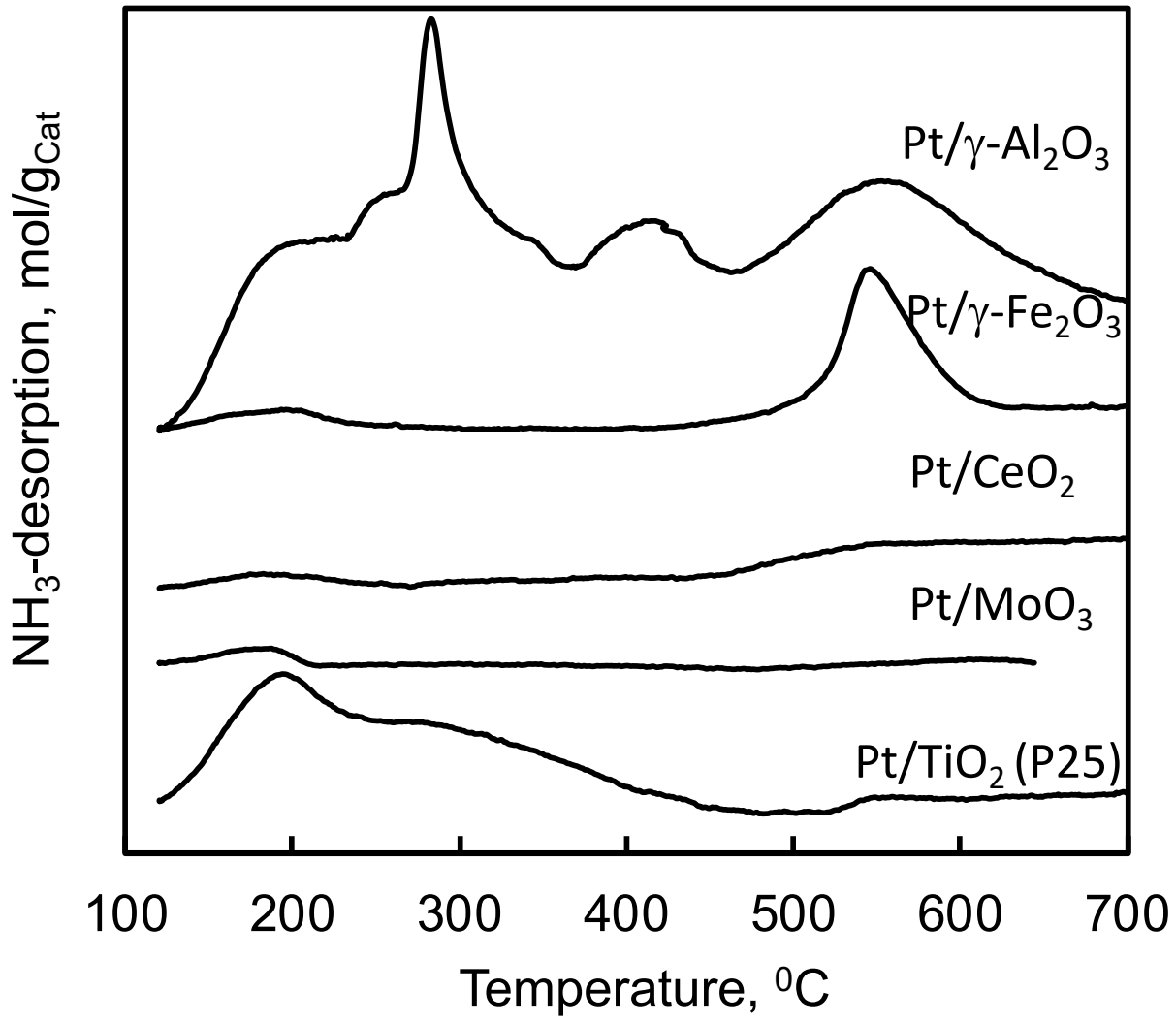

Figure 6.5: NH_3-TPD profile for platinum nanoparticles supported on various supports.

The NH_3-TPD profile obtained with Pt/γ-Fe_2O_3 catalyst sample exhibited two distinctive NH_3 desorption peaks at 200 °C and 548 °C corresponding to the weak and strong acid sites (see Table 6.3). Distinctively, upon the impregnation of γ-Fe_2O_3 with platinic acid, the β peak is more pronounced. Since γ-Fe_2O_3 is a reducible oxide sample and NH_3 can act as a reducing agent. Therefore, reduction of γ-Fe_2O_3 specifically in the presence of Pt may have occurred.

Table 6.3: Quantitative analysis of NH_3-TPD profiles of the oxide support materials and the resulting platinum catalysts.

Sample	NH_3 desorption, $\mu mol_{NH3}/g_{sample}$			T_α, °C	T_β, °C
	A_α	A_β	$A_\alpha + A_\beta$		
TiO_2(P25)	542.1	-	542.1	193	
γ-Al_2O_3	562	266.95	829	257	556
CeO_2	0.153	-	0.15	179	-
MoO_3	0.9	30.9	31.8	183	602
γ-Fe_2O_3	34.02 (34.8)[a]	20.4	89.2	179 (285)	491
Pt/TiO_2(P25)	605	-	605	239	
Pt/γ-Al_2O_3	584	298	882	258	409
Pt/CeO_2	2.9	-	291.7	182	-
Pt/MoO_3	42.15	-	42.15	191	-
Pt/γ-Fe_2O_3	36.94	215	251.9	193	548

[a] Shoulder peak

6.2. CATALYTIC PERFORMANCE OF PT-BASED CATALYST OVER THE VARIOUS SUPPORT MATERIAL

The effect of the nature of the oxidic support material on liquid-phase benzyl alcohol oxidation was probed using Pt/TiO_2(P25) and Pt/γ-Al_2O_3 as model catalysts. A semi-batch reactor was used in this study with 0.5 g of catalyst dispersed in 70 mL of benzyl alcohol operating at 90 °C and 5 bar using air as an oxidant without using a solvent. The reaction was monitored for 5 hours on stream, sampled hourly.

6.2.1. CATALYST ACTIVITY – THE ROLE OF WATER

The catalytic activity of reducible Pt/TiO_2(P25) catalyst was compared with the catalytic activity obtained over irreducible Pt/γ-Al_2O_3 catalyst using either pure benzyl alcohol or benzyl alcohol/water as a starting mixture to investigate the effects of oxidic

nature of the support material (reducible and irreducible oxide) on liquid-phase benzyl alcohol oxidation.

In the absence of water in the initial starting mixture, the benzyl alcohol conversion was 1.5% and 0.48% over Pt/TiO_2(P25) and Pt/γ-Al_2O_3, respectively, after a reaction time of 5 hours. The turnover frequency (TOF) for benzyl alcohol oxidation over Pt/TiO_2(P25) in the absence of water was 26 ± 5 $hr^{-1,}$ slightly higher than the turnover frequency obtained over Pt/γ-Al_2O_3 catalyst (TOF: 9.3 ± 3.8 hr^{-1}). Evidently, using the reducible support, Pt/TiO_2(P25), yields higher site-specific catalytic activity than using an irreducible support material, Pt/γ-Al_2O_3, at comparable reaction conditions. This indicates that the nature of the oxide support plays a role in benzyl alcohol oxidation beyond dispersing the active metal. The catalytic activity of benzyl alcohol oxidation may also depend on the nature of an oxidic support material employed.

The effect of the interaction of the catalyst with the reaction medium on TOF is also investigated using H_2O as a solvent, and a reaction medium initially containing 93 mol-% H_2O, and 7 mol-% benzyl alcohol was used. Figure 6.6 illustrates benzyl alcohol conversion obtained over Pt/TiO_2(P25) and Pt/γ-Al_2O_3, catalyst in the presence and absence of a solvent, H_2O. The obtained benzyl alcohol conversion in the presence of H_2O as a solvent after a reaction time of 5 hours was 36.2% and 6.3% over Pt/TiO_2(P25) and Pt/γ-Al_2O_3 catalyst, respectively. The corresponding TOF of benzyl alcohol consumption in the presence of water increased to *ca*. 619 ± 18 hr^{-1} and 80 ± 7 hr^{-1} over Pt/TiO_2(P25) and Pt/γ-Al_2O_3, respectively. The rate enhancement of the benzyl alcohol oxidation upon the addition of water over Pt/TiO_2 (P25) is significantly higher (26 ± 7 times higher) than over Pt/γ-Al_2O_3 (9 ± 3 times higher). As shown in Chapter 4, the initial number of moles of benzyl alcohol in the reactor did not affect the rate of benzyl alcohol consumption of Pt/TiO_2(P25), significantly influence the reaction rate. Suppose it may be assumed that it does not affect the rate of benzyl alcohol consumption over Pt/γ-Al_2O_3 either. In that case, this result must be interpreted as an indication that the support affects the absolute activity and the relative enhancement given by using water as a solvent.

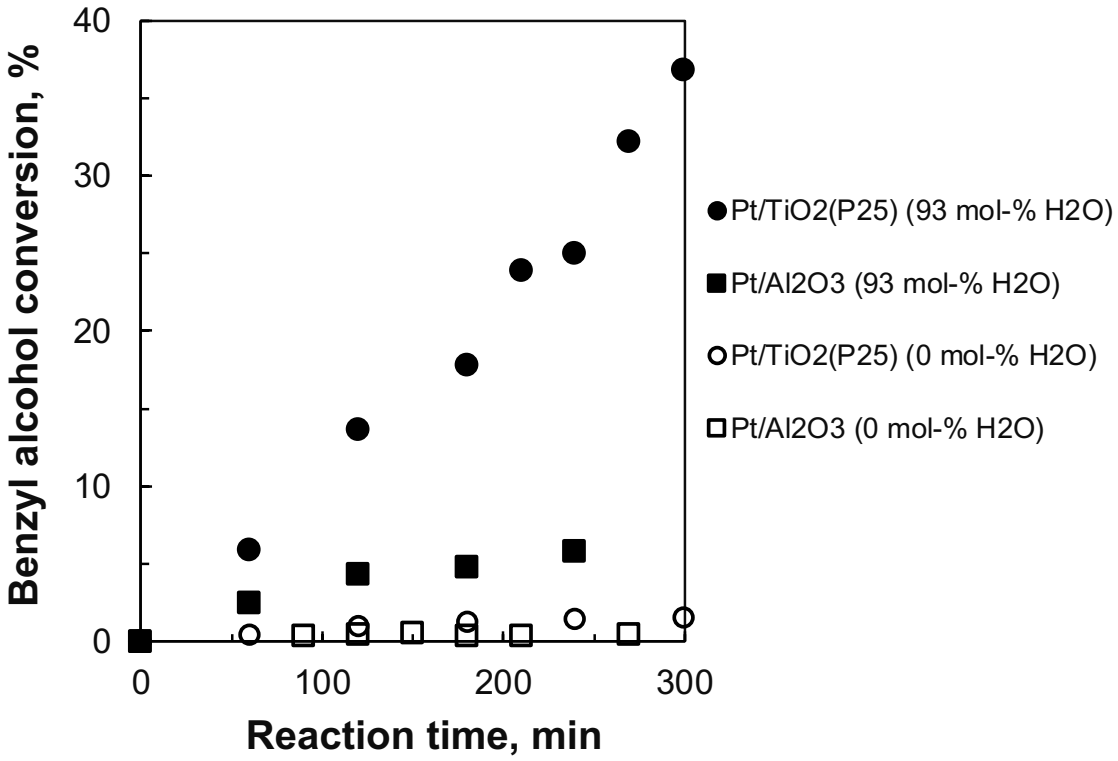

Figure 6.6: Benzyl alcohol conversion over Pt/TiO_2(P25) and Pt/γ-Al_2O_3 catalyst in the presence of water (initial reaction mixture: 93 mol-% water + 7 mol-% benzyl alcohol) and absence of water (initial reaction mixture: pure benzyl alcohol). Reaction conditions: 0.5 g catalyst, 90 °C, P_{total} = 5 bar, V_{liquid} = 70 mL, V_{air} = 100 mL_n/min.

6.2.2. CATALYST ACTIVITY – THE ROLE OF SUPPORT

The support role in benzyl alcohol oxidation using mixtures containing initially water and benzyl alcohol in a molar ratio of 9.3:0.7 was further investigated using other well-known reducible oxide support materials, such as ceria molybdenum trioxide and maghemite. Figure 6.7 shows the benzyl alcohol conversion as a function of reaction time for the various supported Pt-catalyst. Pt/TiO_2(P25), Pt/γ-Al_2O_3, Pt/CeO_2, Pt/MoO_3 and Pt/γ-Fe_2O_3 catalysts. Benzyl alcohol conversion of ca. 37%, 6% 12%, 16% and 8% was obtained over Pt/TiO_2(P25), Pt/γ-Al_2O_3, Pt/CeO_2, Pt/MoO_3 and Pt/γ-Fe_2O_3 catalysts,

respectively, after a reaction time of 5 hours using otherwise comparable reaction conditions.

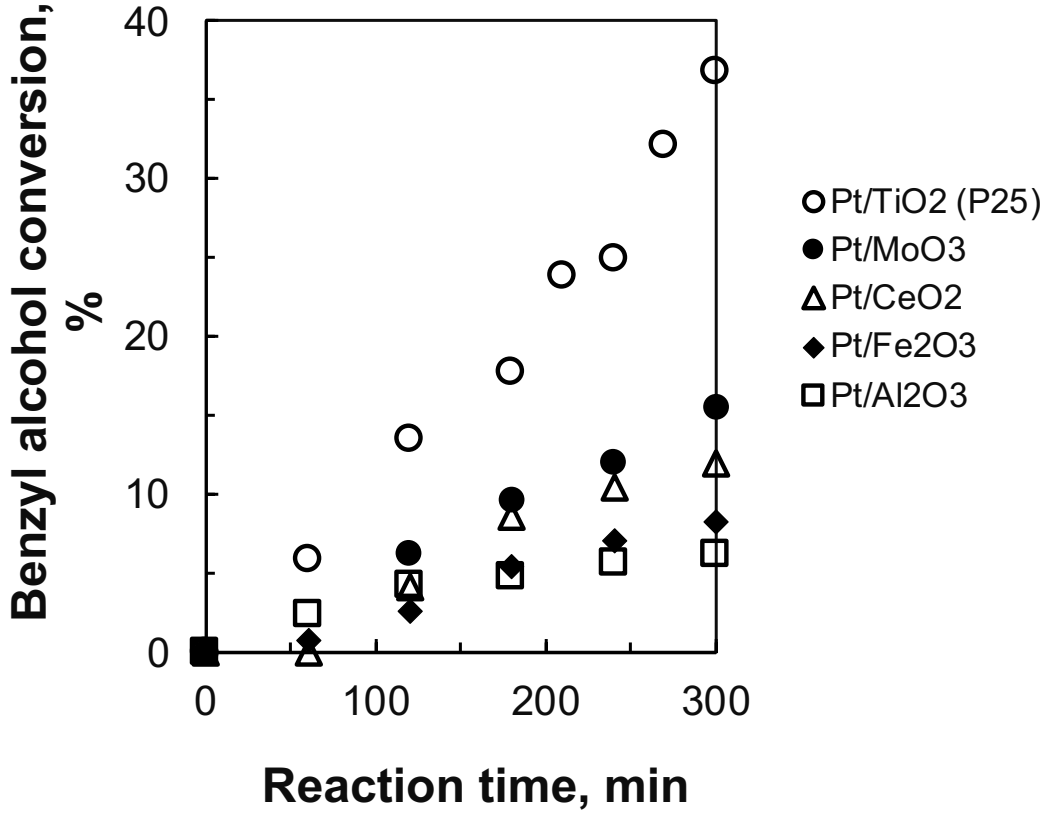

Figure 6.7: Benzyl alcohol conversion over various supported platinum catalyst. Reaction conditions: 0.5 g catalyst, 90 °C, P_{total} = 5 bar, V_{liquid} = 70 mL, V_{air} = 100 mL_n/min, initial reaction mixture 93 mol-% H_2O and 7 mol-% water.

Hereafter, the catalyst activity is reported as a rate of benzyl alcohol consumption per surface Pt-atom to account for the variation in the Pt loading and dispersion (see Table 6.2). The turnover frequency, TOF, for the benzyl alcohol consumption obtained using this initial reaction mixture (93 mol-% H_2O and 7 mol-% benzyl alcohol) is 619 ± 18 hr^{-1}, 80 ± 7 hr^{-1}, 556 ± 28 hr^{-1}, 301 ± 18hr^{-1} and 99 ± 4 hr^{-1} for Pt/TiO_2(P25), Pt/ γ-Al_2O_3, Pt/CeO_2, Pt/MoO_3 and Pt/γ-Fe_2O_3, respectively (see Table 6.4). Thus, the surface-specific catalyst activity increases in the following order: Pt/TiO_2(P25) > Pt/CeO_2 > Pt/MoO_3 >Pt/γ-Fe_2O_3 and Pt/ γ-Al_2O_3. This seems to indicate that the catalyst activity is strongly

dependent on the nature of the oxide support employed since they are investigated at comparable reaction conditions.

Table 6.4: Performance of platinum catalyst supported on various oxide support materials in the benzyl alcohol Reaction conditions: 0.5 g catalyst, 90 °C, $P_{total,\ air}$ = 5 bar, V_{total} = 70 mL at 90 °C

Catalyst Sample	**Pt loading,** (wt.-%)	**Conversion,** (%)	**TOF[a],** (hr^{-1})	**selectivity,** (%) *Benzyl aldehyde*	*Benzoic acid*
Pt/TiO_2 (P25)	3.89	36.2[b]	619 ±18	>98[b]	<2.0[b]
(0mol-% H_2O)		1.5[c]	26 ± 5	>99[c]	<1[c]
Pt/γ-Al_2O_3	4.50	6.3[b]	80 ± 7	>99[b]	<1 [b]
(0mol-% H_2O)		0.5[c]	9 ± 4	>99[c]	<1 [c]
Pt/CeO_2	1.73	12.0[b]	556 ± 28	90[b]	10 [b]
Pt/MoO_3	3.7	15.5[b]	301 ± 18	>99[b]	<1 [b]
Pt/γ-Fe_2O_3	3.86	8.3[b]	99 ± 4	94[b]	6 [b]

[a]TOF determined from the slope of the conversion as a function of reaction time and the dispersion of platinum in the catalyst

[b] initial reaction mixture: 93 mol-% water + 7 mol-% benzyl alcohol

[c] pure benzyl alcohol.

In the presence of H_2O, a higher TOF was observed over Pt nanoparticles supported on slightly reducible oxide support material (i.e., TiO_2(P25), CeO_2 and MoO_3) catalysts compared to Pt nanoparticles on a non-reducible oxide (γ-Al_2O_3). However, Pt/γ-Fe_2O_3 exhibited also a rather low TOF, indicating that the reducibility of the support material is not the only contributing factor.

It should be noted that the particles size of platinum nanoparticles in the samples may have an influence on the overall activity. However, particles size of platinum nanoparticles in the samples is increasing in the order based on O_2 chemisorption: Pt/γ-Al_2O_3 < Pt/γ-Fe_2O_3 (maghemite) <Pt/MoO_3 < Pt/TiO_2 (P25) < Pt/CeO_2. It is expected that Pt/TiO_2 (P25) and Pt/CeO_2 samples to exhibit the least catalytic activity if the average particle size was the dominating effect on catalytic activity. Yet, the catalytic activity is increasing in the order: Pt/TiO_2(P25) > Pt/CeO_2 > Pt/MoO_3 >Pt/γ-Fe_2O_3 and Pt/γ-Al_2O_3.

Therefore, the average size of the active metal is not the dominating effect on activity. Therefore, average particle size of Pt does not have effect on catalytic activity.

6.3. PRODUCT SELECTIVITY

The oxidation of benzyl alcohol is a consecutive reaction that may proceed through benzaldehyde as an intermediate yielding ultimately benzoic acid. Thus, the product distribution may change with reaction time.

High selectivity for the formation of benzaldehyde (>99 %) was obtained with both catalysts, i.e., the reducible Pt/TiO_2 and the irreducible $Pt/\gamma\text{-}Al_2O_3$, in the solvent-free liquid system (initial liquid composition of 100 mol-% benzyl alcohol). This suggests that the consecutive reaction to form benzoic acid may be suppressed due to the low concentration of benzaldehyde in the reaction mixture since the conversion levels in these systems were rather low.

The role of the support material was further probed in the benzyl alcohol oxidation using an initial reaction mixture containing water and benzyl alcohol (see Figure 6.8). It is intuitively expected that higher benzyl alcohol conversion would yield a lower selectivity for benzaldehyde. In contrast, benzoic acid selectivity would be favoured with increasing conversion. However, the support material does seem to play some role here as well. A high selectivity towards benzaldehyde of > 99 % is obtained over $Pt/\gamma\text{-}Al_2O_3$ and Pt/MoO_3 when starting with an initial reaction mixture containing 93 mol-% water and 7 mol-% benzyl alcohol. A similar, initial benzaldehyde selectivity was obtained over Pt/TiO_2(P25), albeit with some scatter. However, the selectivity seems to decrease with increasing conversion. After a reaction time of 5 hours, the selectivity towards benzaldehyde is still higher than 98% despite the relatively high conversion obtained over this catalyst. The benzaldehyde selectivity decreases more strongly as a function of the benzyl alcohol conversion when the reaction is performed using either Pt/CeO_2 and $Pt/\gamma\text{-}Fe_2O_3$ as a catalyst. This would imply that the activity for the oxidation of benzaldehyde is higher over catalysts using these support materials than the other catalysts. Furthermore, the decrease in the selectivity for benzaldehyde as a function of benzyl alcohol conversion

obtained over Pt/γ-Fe_2O_3 is slightly stronger than over Pt/CeO_2. This would imply that the activity for the oxidation of benzaldehyde over Pt/γ-Fe_2O_3 is greater than over Pt/CeO_2. However, the difference in the trend as a function of the benzyl alcohol conversion is small and may be affected by experimental error.

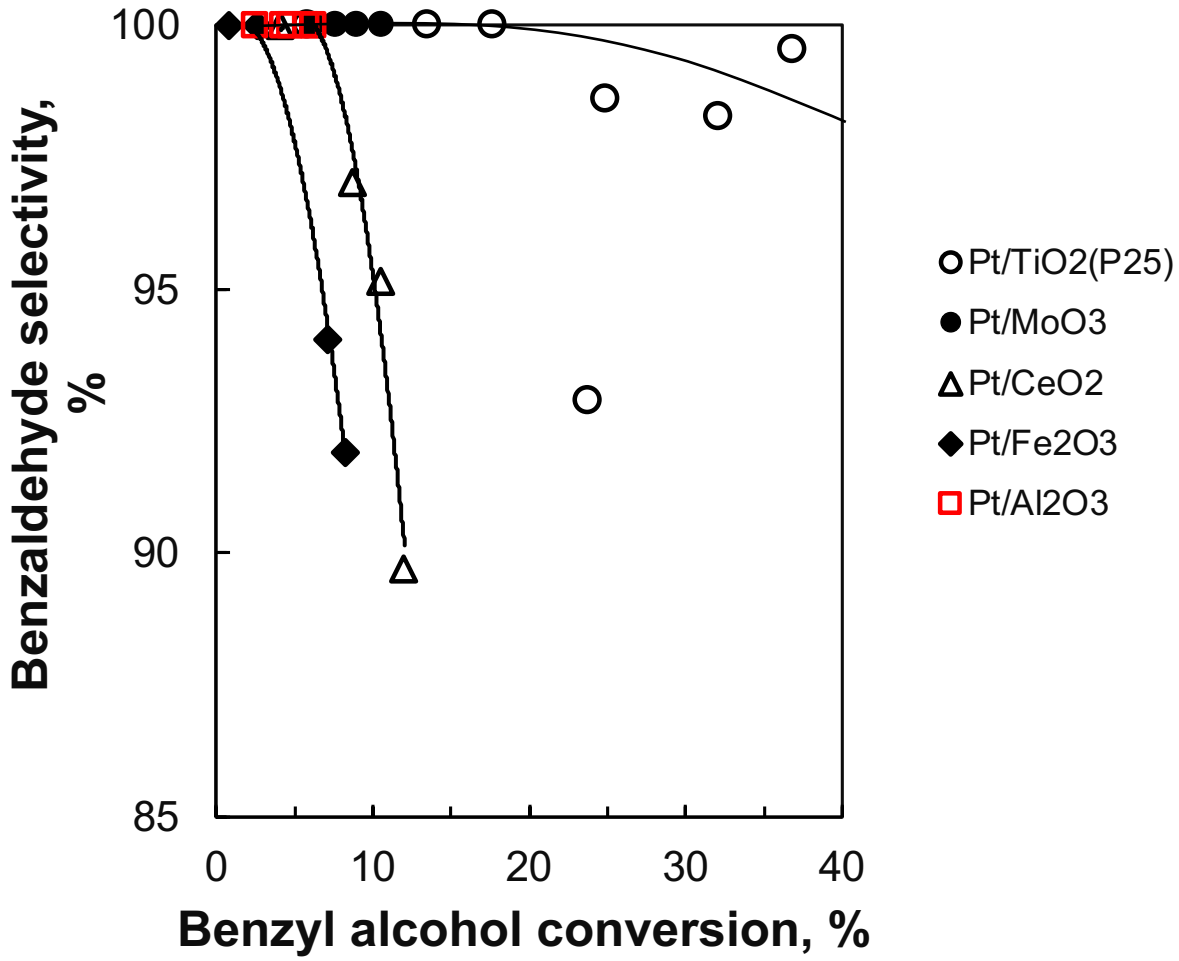

Figure 6.8: Benzyl aldehyde selectivity as a function of time on stream over various Pt-based catalyst. Reaction conditions: 0.5 g catalyst, 90 °C, P_{total} = 5 bar, V_{liquid} = 70 mL, V_{air} = 100 mL_n/min, initial reaction mixture 93 mol-% H_2O and 7 mol-% water.

6.4. DISCUSSION

Benzyl alcohol conversion over Pt-based catalyst immobilized over various metal oxide support materials shows important differences in the specific activity and some minor differences in selectivity. This implies that properties other than the use of H_2O as a solvent, as discussed in Chapter 4, affect catalytic activity and selectivity.

In a solvent-free benzyl alcohol oxidation (100 mol-% benzyl alcohol liquid composition), reducible Pt/TiO_2(P25) and irreducible Pt/γ-Al_2O_3 catalyst showed a reaction rate for benzyl alcohol oxidation of 26 ± 5 hr^{-1} and 9 ± 4 hr^{-1}, respectively. The Pt catalyst supported on reducible support (TiO_2(P25)) evidently showed higher TOF than platinum on the irreducible support material. The main difference in catalytic activity stems from the different metal oxide supports and their surface chemistry. The compositions, electronic and geometrical structures of the metal oxides may offer a very broad spectrum of properties and behaviours that can result in the difference in catalytic activity. One of those properties may include the tendency of oxides to create a surface vacancy by losing a surface oxygen atom, e.g., using it in an oxidation reaction, which may facilitate the oxidation reaction. This may be common in reducible metal oxide support, which can exchange oxygen more readily.

This characteristic feature (readily oxygen exchange) results in the formation of oxygen vacancy sites. Moreover, it may also indicate the presence of surface atomic oxygen and excess electrons redistributed on the cation empty levels, thus changing their oxidation state from M^{n+} to $M^{(n-1)+}$.[11] The alcohol oxidation over titania supported catalyst may involve surface oxygen species.[206] For instance, oxygen on the support may accept hydrogen from the alcohol yielding a surface hydroxyl species. The elimination of the formed surface hydroxyl species (as water) would create a surface vacancy.

Table 6.5 shows the reported energy to create a vacancy for the various supports used in this study. The energy to form a surface oxygen vacancy is not known for γ-Al_2O_3, but for θ-Al_2O_3, it has been reported to be 6.57 eV on the {100} facet and 6.75 eV on the {001} facet[207] and 5.71 eV on α-Al_2O_3(0001).[208] The energy required to form a vacancy on TiO_2 is much smaller, i.e. 4.37 eV on the dominant (101) surface of anatase and 3.71 eV on the (110) surface of rutile.[209] This implies that oxygen can be more easily removed

from a titania surface. In contrast, it will be difficult to create a surface oxygen vacancy on an alumina surface.

Table 6.5: Energy to form a surface oxygen vacancy (relative to ½ O_2) and the adsorption energy of water on a perfect surface and an oxygen defect site (all energies in eV).

Support	**$E_{vacancy}$**, eV	**$E_{ads,\ H_2O,\ perfect}$**, eV		**$E_{ads,\ H_2O,\ defect}$**, eV	
		Molecular	dissociated	Molecular	dissociated
TiO_2(101)- anatase	4.37[b]	-0.77[g]	-0.38[g]	-1.48[l]	-1.83[l]
θ-Al_2O_3 (100)	6.57[c]	-		-	
γ-Al_2O_3 (100)	n.a.[a]	n.a.[a]	-0.67[h]	n.a.[a]	n.a.[a]
CeO_2 (111)	2.76[d]	-0.49[i]	-0.36	-1.28[i]	-1.4[i]
MoO_3(010)	2.57[e]	-0.31[j]	n.a.[a]	-1.35[j]	-0.80[j]
γ-Fe_2O_3(111)	-1.74[f]	-0.28[k]	n.a.[a]	n.a.[a]	n.a.[a]

[a]not available, [b]Li et al.,[209] [c]Hinuma et al.,[207] [d]Mayernick et al.,[210] [e]Agarwal et al.,[211] [f]Jian et al.,[212] [g]Martinez-Casado et al.,[213] [h]Digne et al.,[214] [i]Fronzi et al.,[215] [j]Head et al.,[216] [k]Ntallis et al.,[217] [l]Tilocca [218]

The low TOF for benzyl alcohol oxidation over Pt/γ-Al_2O_3 catalyst may be due to the presence of Pt moiety in the catalyst only (and the enhancement due to the presence of water caused by the increase in the activity of platinum as outlined in Chapter 4). The obtained TOF for benzyl alcohol oxidation over reducible Pt/TiO_2(P25) is thought to be contributed by the Pt activity for oxidation reaction and oxide support influence on benzyl alcohol oxidation. It is, therefore, thought that reducible metal oxide support material facilitates benzyl alcohol oxidation according to the mechanism outlined in Figure 6.9. In the proposed mechanism, the initial step includes the benzyl alcohol substrate's adsorption through the substrate's oxygen atom over the platinum surface.

The obtained activity in the benzyl alcohol oxidation over Pt/γ-Fe_2O_3 is only slightly higher than the obtained activity in the benzyl alcohol oxidation over Pt/γ-Al_2O_3.

Maghemite is much more reducible than either alumina or even titania. The formation of a surface vacancy has been reported to be exothermic (-1.74 eV)[217] implying that a facile formation of a surface vacancy, but the filling of the vacancy is expected to be severely limited.

It is interesting to note that the activity of platinum supported on ceria and molybdenum trioxide is also lower than that of Pt/TiO_2(P25) despite a more facile formation of surface oxygen vacancies.[210,211] The adsorption energy of water in its dissociated form may be taken as a measure for the tendency of the hydrogen abstraction of adsorbed benzyl alcohol yielding a surface hydroxyl species, which upon elimination will result in a vacancy. The formation of surface hydroxyl species on the defect site is less favoured on MoO_3 (010) than on CeO_2(111), which in turn is less favoured than on anatase-TiO_2(101).

In summary, the hydrogen in the alcohol group of the substrate may interact with an oxygen atom of the support material, thus forming and metal alkoxide on the platinum surface and hydroxyl species on the surface of the support material, according to equation 6.1. Where * and ‡ represent adsorption on the platinum surface and metal oxide support material, respectively.

$$\text{Benzyl Alcohol}^* + O^{‡} \rightarrow \text{Benzalkoxide}^* + OH^{‡} \qquad 6.1$$

The oxygen atom of the formed surface hydroxyl species on the support may interact with β-hydrogen, forming benzaldehyde and H_2O product. Moreover, the active site is recovered while the oxygen vacancy site is formed upon the desorption of benzaldehyde and H_2O products, see equation 6.2.

$$\text{Benzalkoxide}^* + OH^{‡} \rightarrow \text{Benzaldehyde}^* + H_2O^{‡} \qquad 6.2$$

(and the obtained surface species may desorb)

The formed oxygen vacancy site is then recovered by the constant feed of oxygen/air oxidant used during the oxidation reaction, according to equation 6.3. It should

be noted that the dissociated oxygen may be supplied from the Pt-surface. Also, as concluded in Chapter 4, the presence of H_2O may facilitate the dissociation of molecular oxygen.

$$M^{(n-1)+} + ½\ O_2 \rightarrow M^{n+} \qquad 6.3$$

It is also possible that the formed surface hydroxyl species can recombine with other surface hydroxyl species yielding H_2O and atomic oxygen on the surface to replenish the oxygen vacant site of the metal oxide, according to equation 6.4. Water may affect the number of OH* groups on the surface, resulting in a support-specific role of water (in addition to the reasons given in Chapter 4). The hydroxylation of the oxide will thus result in partially reduced oxide support.

$$OH^* + OH^{\ddagger} \rightarrow H_2O^* + O^{\ddagger} \qquad 6.4$$

The adsorbed H_2O is then desorbed from the platinum surface, thus regenerating the active site and closing the catalytic cycle, according to equation 6.5.

$$H_2O\ * \rightarrow\ * + H_2O \qquad 6.5$$

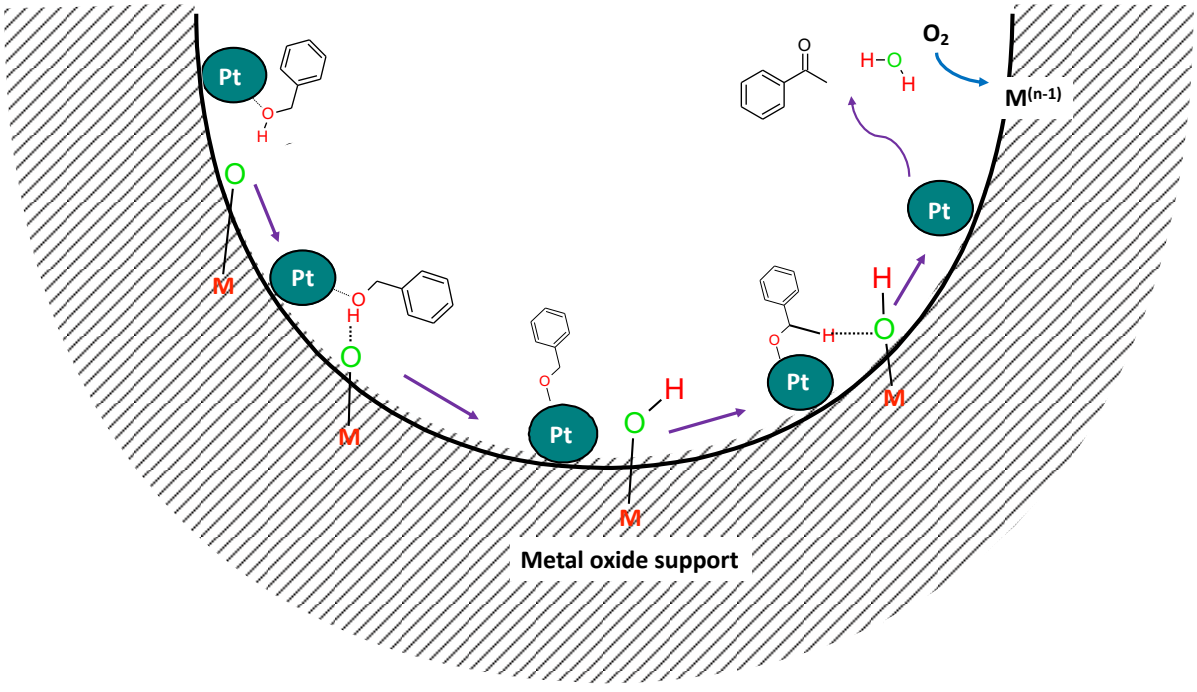

Figure 6.9: Schematic representation of the role of reducible metal oxide support material on benzyl alcohol oxidation through the formation of oxygen vacancy site, obeying Mars van Krevelen (MvK) mechanism.

6.4.1. PRODUCT SELECTIVITY

The benzyl alcohol oxidation process yields benzyl aldehyde product primarily. Benzoic acid is thought to be formed through hydration of the benzyl aldehyde intermediate followed by further oxidation, consequently forming benzoic acid.[152] A decrease in the benzyl aldehyde selectivity is thus accompanied by an increase in the benzoic acid selectivity since the formation of benzoic acid is a consecutive oxidation of benzyl aldehyde. The inhibition of benzoic acid formation is considered an essential feature in benzyl alcohol oxidation since benzoic acid is undesirable in the study but a more thermodynamically favoured product.

The oxidation of benzyl alcohol over the various supported platinum-based catalysts showed a slight variation in benzyl alcohol conversion levels; however, even at relatively high benzyl alcohol conversion, high benzaldehyde selectivity is still obtained for Pt/TiO_2, Pt/MoO_3 and $Pt/\gamma\text{-}Al_2O_3$ catalyst. Moreover, in this case, there is no well-defined correlation between benzyl alcohol conversion and benzaldehyde selectivity over different metal oxide supports. The direct influence of various oxide support on product selectivity may be determined by whether the oxide support material can form oxygen vacancy sites, which may indicate the presence of labile oxygen. Consequently, the existence of the labile oxygen (derived from the formation of oxygen vacancy sites) may promote further oxidation of the benzaldehyde intermediate, thus forming benzoic acid.

6.5. CONCLUSION

The principal purpose of the oxide support material is to disperse and immobilize the active metal of the catalyst, thereby improving the mechanical and thermal stability of

the catalyst. However, in liquid-phase oxidation, the oxidic support material does play a role beyond just dispersing the active metal. Reducibility of the metal oxide support material has an influence on alcohol oxidation. The activity obtained from irreducible Pt/γ-Al_2O_3 may be attributed solely to metallic platinum. On the other hand, the γ-Fe_2O_3 is a very reducible support material. However, the surface oxygen defects will not regenerate upon the removal of the hydroxyl group. The obtained activity over Pt/γ-Fe_2O_3 is, thus, similar to the activity obtained over Pt/γ-Al_2O_3 and may be ascribed mainly to the activity of metallic platinum.

The adsorption of the hydroxyl group on a defect site is in the order: MoO_3<CeO_2<TiO_2. The obtained TOF for benzyl alcohol oxidation is still maintained in this order. This may suggest that hydrogen abstraction (dehydrogenation of OH group of the benzyl alcohol substrate) by the oxygen in the surface of the support is more facile using TiO_2 as support in comparison to CeO_2, which in turn is more facile than on MoO_3. In essence, the promotional effect associated with the oxidic support material requires that the support material abstract hydrogen from the substrate, remove the generated hydroxyl species in the form of water (reducibility), and regenerate oxygen defect sites.

Chapter 7:

Investigating the role of bismuth in Pt-based catalyst for alcohol oxidation

OVERVIEW

Bismuth as a modifier in Pt or Pd catalyst systems has been extensively used in studies of the selective oxidation of alcohols.[106,131] Bi is thought to have a twofold influence on alcohol oxidation: assisting oxygen supply to Pt, removing the metal hydride from Pt and chelating effect.[17] Platinum may alloy with bismuth, and at low temperature, stable Bi_2Pt and BiPt phases have been reported.[219] Here, nano-sized particles with the nominal composition Pt-Bi have been synthesized and supported on TiO_2 (rutile phase) with a total metal loading of ca. 1 wt.-%. The ability of Bi to regulate oxidation of the Pt metal is probed using “semi in-situ” XPS analysis. Furthermore, the nature of the substrate is investigated by comparing similar alcohols, viz. benzyl alcohol and cyclohexyl methanol, on the role of bismuth on alcohol oxidation.

7.1. CHARACTERIZATION OF SYNTHESIZED NANO-SIZED MATERIALS

7.1.1. XRD-ANALYSIS

The platinum-bismuth system was synthesized using the reductive method with $Mo(CO)_6$ as a reducing agent (see Chapter 3). The XRD-pattern of the sample with the nominal composition Pt-Bi shows the presence of two distinctly different phases, with sharp diffraction lines at 2θ = 27.8°, 33.7°, 47.7°, 48.9°, 60.8°, 70.9°, 81.5° and 90.7° and broad diffraction lines at 2θ = 46.9°, 54.3°, 80.2°, 98.2° and 104.7° (see Figure 7.1).

A pure Bi sample was synthesized using the identical method used to synthesise the Pt-Bi sample but omitting the addition of platinic acid to the reaction mixture to elucidate the phase represented by sharp diffraction lines. The XRD pattern of this sample showed sharp diffraction lines with strong intensity at 2θ = 26.4°, 31.7°, 44.4°, 46.4°, 52.2°, 53.3°, 57.5°, 66.4°, 70.5°, 73.7°, 76.6° and 84.5°and a much broader diffraction line at 2θ = 38.9°. Similar diffraction peaks are observed by Ahila et al.,[220] for a bismuth film, which crystallizes in the rhombohedral system. The diffraction lines were indexed as the diffraction planes (003), (012), (104), (110), (015), (006), (202), (024), (107), (116), and (018) of the metallic rhombohedral bismuth, respectively. Hence, the sharp diffraction lines can be attributed to metallic Bi. The lattice parameters for metallic Bi were determined as $a = b$ = 4.505 Å, c = 11.794 Å with $\alpha = \beta = 90^o$ and $\gamma = 120^o$ (quite close to the reported lattice parameter of metallic Bi.[221,222] The broader diffraction lines at 2θ = 38.9°could be indexed as α-Bi_2O_3(121) with the more intense line belonging to α-Bi_2O_3(120) (expected at 2θ = 31.7° phase overlapping with the diffraction line belonging to Bi(012).

The sharp diffraction lines observed in the XRD-diffraction pattern of the synthesized Pt-Bi sample show similarity to those observed in the XRD-diffraction pattern of metallic Bi. Thus, the diffraction lines occurring at 2θ =27.8°, 33.7°, 47.7°, 48.9°, 60.8°, 65.8^o, 70.9°, 81.5° and 90.7° are indexed to diffraction to (hkl) equal (003), (012), (104), (110), (015), (006), (202), (107) and (116), respectively. The sharp diffraction lines obtained with the Pt-Bi sample are, however, shifted significantly towards higher values

of 2θ compared to the ones obtained with the pure Bi sample. The lattice parameters for this triclinic phase were determined as $a = b = 4.306$ Å, $c = 10.895$ Å with $\alpha = \beta = 90^{o}$ and $\gamma = 120^{o}$. The contraction in the lattice parameter is probably attributed to the alloying of the bismuth phase with platinum (the atomic radius of Pt, 175 pm, is smaller than the atomic radius of Bi, 230 pm, and thus a contraction of the lattice parameter is expected). The average nano-crystallite size of pure Bi and Pt-Bi samples was determined from the broadening of the (012) reflection measured from the sharp diffraction line at 2θ = 31.7° and 33.7° of the XRD pattern of the corresponding samples. It was 48.4 nm and 49.8 nm, respectively.

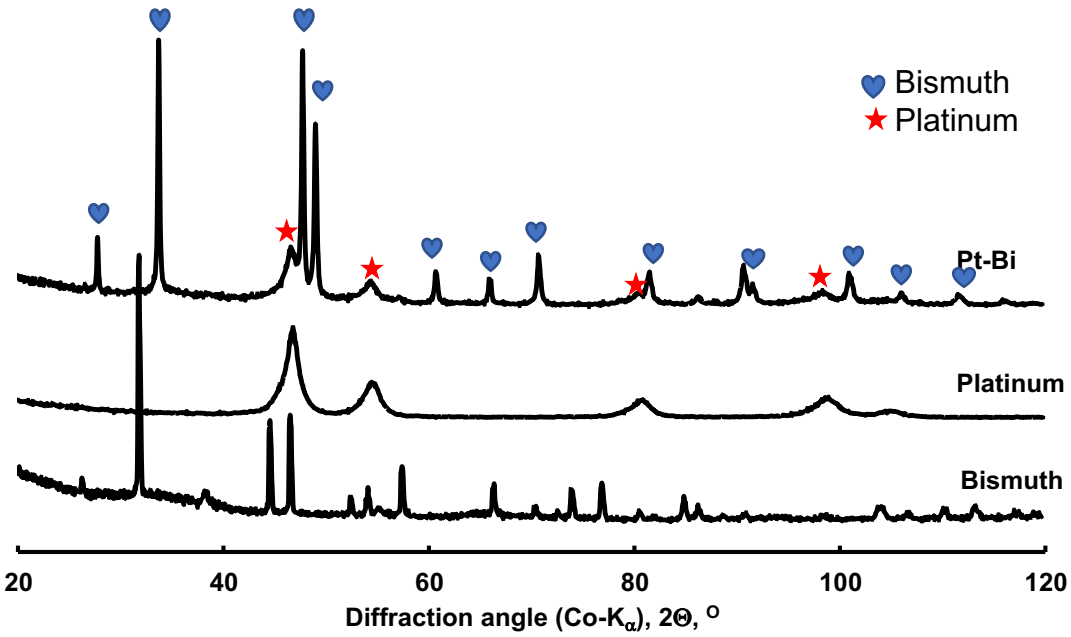

Figure 7.1: X-ray diffraction pattern of the synthesized unsupported bismuth, platinum and Pt-Bi samples.

It can be noted further that the intensity of the diffraction lines in the XRD-pattern of the alloyed, triclinic Bi-Pt phase differs significantly from that those of the pure Bi-sample (see Table 7.1). In particular, the lines attributed to (hkl) of (003), (104) and (110) are more intense upon the addition of platinum. The difference in intensity may result from

preferential crystal growth[222] with diffraction at planes in the growth direction becoming more intense. Hence, the difference in the relative peak intensity may be a consequence of a different particle shape

Table 7.1: Diffraction line positions and their relative intensity for the triclinic bismuth phase for pure bismuth and platinum-bismuth system.

(hkl)	**Pure Bi**		**Bi-Pt**	
	2Θ[1], °	**I**	**2Θ[1], °**	I
003	26.4	7	27.8	23
012	31.7	100	33.8	100
104	44.4	39	47.8	87
110	46.4	43	49.1	64
015	52.2	10	60.6	13
006	53.3	11	65.8	11
202	57.5	21	70.5	21
024	66.4	14	81.6	13
107	70.5	5	90.5	13
116	73.7	13	101	13
018	76.6	15		

[1]: diffraction angle using Co-Kα radiation (λ = 1.7891Å)

The broad diffraction lines present in the XRD-diffractogram of the sample Pt-Bi correspond exactly to the diffraction lines of *fcc*-Pt. The crystallite size of the Pt moiety in the Pt-Bi sample was determined to be 5.2 nm from the broad diffraction line at 2θ = 54.3° (the (220) reflection plane is used to determine the average crystallite size of the Pt moiety instead of (111) due to peak overlap, which would result in an inaccurate crystallite size determination; see Table 7.2).

Table 7.2: Morphological properties of the different of platinum-based catalyst as determined by *TEM* and *XRD* analysis.

Sample	$d_{average,\ XRD}$, nm		$d_{Pt,average,\ TEM}$, nm	Lattice parameter fcc-Pt, Å
	Pt-phase	Bi-phase		
Pt	7.2	-	4.2 ±0.6	3.919 ± 0.014
Pt-Bi	5.2	49.8	4.8 ±1.8	3.916

7.1.2. TEM-IMAGING

The morphology of materials with the nominal composition Pt and Pt-Bi was analyzed using a transmission electron microscope (TEM). Table 7.2 summarizes the morphological properties of the synthesized nanoparticles analyzed using TEM and XRD techniques.

Illustrated in Figure 7.2 is the bright-field TEM micrographs of Pt exhibited primarily spherical nano-sized particle shape without any noticeable particle agglomeration. The average particle size and the variance were determined by fitting the observed particle size distribution to a log-normal distribution. The obtained average size of the nano-sized Pt particles with the standard deviations was 4.2 ± 0.6 nm.

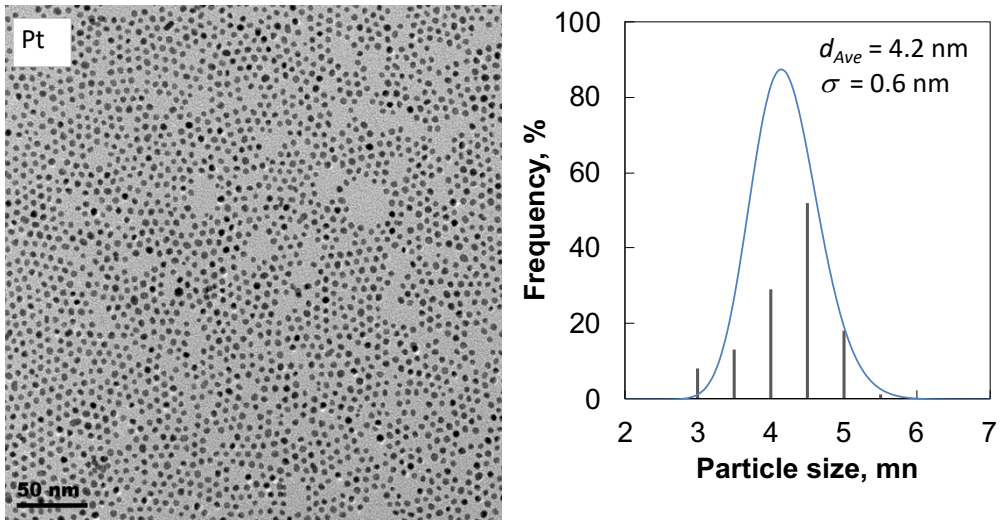

Figure 7.2: Bright-field TEM micrograph of Pt sample and the log-normal distribution of the nanoparticles (*N = 200 nanoparticles*).

The TEM analysis of the sample with the nominal composition Pt-Bi showed a mixture of different shapes of nano-sized materials, *viz*. nano-sheets and nanoparticles (*see* Figure. 7.3). The TEM micrographs of pure bismuth and pure platinum nanomaterials synthesized similarly as the Pt-Bi sample (*see* Chapter 3) are included to further differentiate between bismuth and platinum morphology from the Pt-Bi sample. The pure bismuth sample shows the presence of nano-sheets material. In contrast, the pure platinum sample is comprised of nano-sized particles. Clearly, the nano-sheets in the Pt-Bi sample corresponds to the bismuth-rich phase in the sample. At the same time, the observed nanoparticles may be attributed to Pt-rich nanoparticles. The average particle size of the nanoparticles in the Pt-Bi sample was determined to be 4.8 nm ± 1.8 nm (relatively small sample size was used to determine the average particle size, due to poor contrast between the nanoparticles and the nano-sheets, which may have affected the standard deviation to the average particle size). The average size of the nano-sheets could not be determined using TEM due to the poor definition and overlap of these sheets. The measured particle size of Pt in the Pt-Bi sample obtained from XRD is consistent with the average nano-particle size obtained from TEM analysis.

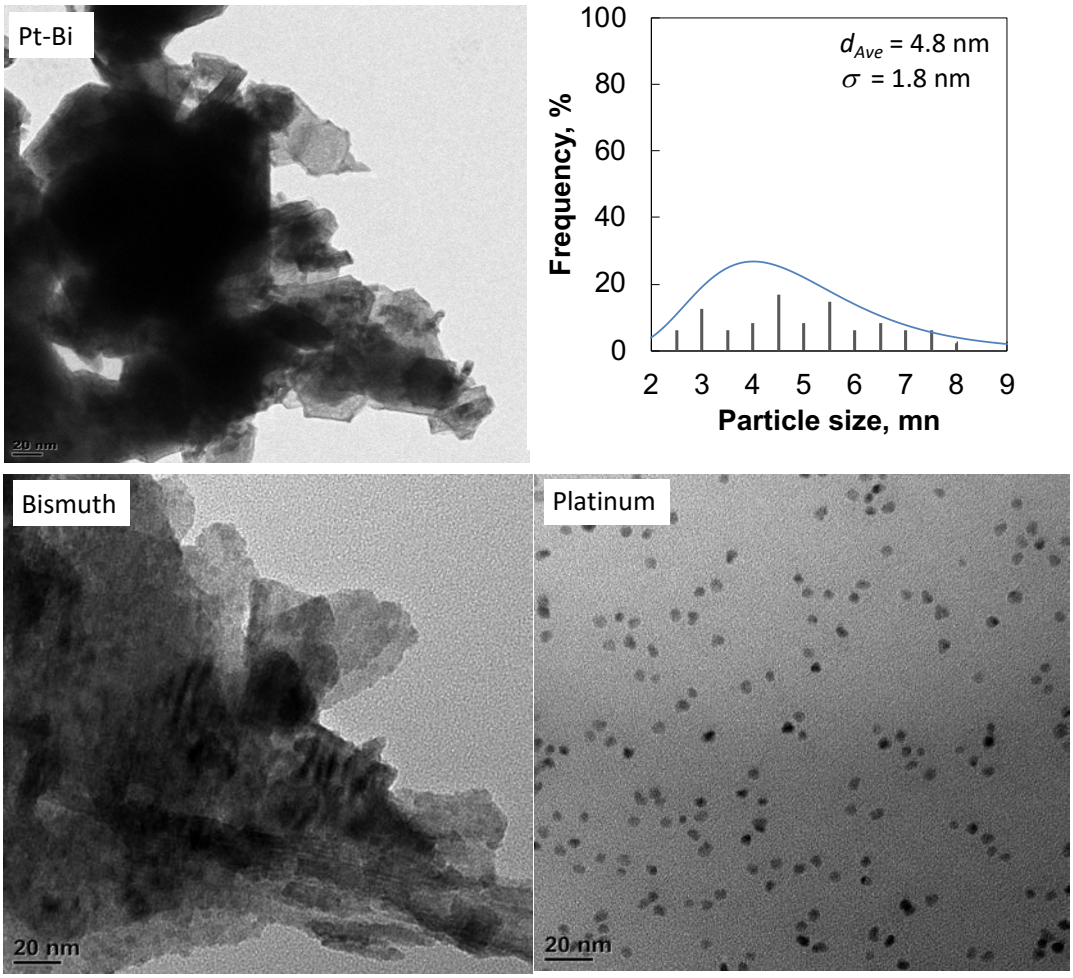

Figure 7.3: Bright-field TEM micrograph of the sample with the nominal composition of Pt-Bi (top), bismuth and platinum and the average particle size (histogram), fitted with percentage probability density function of the average size of the nanoparticles (curve) attached to the nanosheets (*N = 70 nanoparticles*).

7.2. CHARACTERIZATION OF SYNTHESIZED NANO-SIZED MATERIALS SUPPORTED ON TiO_2

The synthesized nanoparticles with the nominal composition Pt-Bi were re-dispersed in n-hexane and immobilized on TiO_2 (rutile phase; Sigma Aldrich; average nano-crystallite size ca. 29 nm) via colloidal deposition. The resulting catalyst samples were dried at 120 °C and calcined at 350 °C under N_2 to yield ca. 1 wt.-% of the nano-sized material on rutile. According to XRD analysis, the deposition of these materials on TiO_2(rutile) did not seem to alter the structure of the support (see Appendix E-7.1).

7.2.1. ELEMENTAL ANALYSIS

The composition and the active metal loading of the catalyst were verified using *ICP-OES* and *STEM-EDX* analysis (see Appendix E-7.2). The content of the sample concerning the secondary metal Bi, relative to the platinum and support (TiO_2 – rutile phase) in the samples and textural properties are shown in Table 7.3. The sample with a nominal composition of Pt-Bi/TiO_2 is enriched in Pt (molar ratio of Pt:Bi = 4.1 : 1), which can be taken as an indication that platinum is preferentially reduced in the synthesis mixture. Molybdenum, which could have originated from the reducing agent $Mo(CO)_6$ used in the synthesis, was not detected by *STEM-EDX* in any of the nano-sized particles synthesized.

Table 7.3: Elemental analysis and textural properties of the different platinum-based catalyst as determined by *ICP-OES* and TEM analysis.

Sample	**Composition** (wt -%)[6]		**Bi/(Bi+Pt)** (mol/mol)	**d_{Pt},** (nm)[7]
	Pt	**Bi**		
Pt/TiO_2	0.78	-	0	4.2 ± 0.8
Pt-Bi/TiO_2	0.96	0.25	0.21	9.1 ± 0.9

7.2.2. MORPHOLOGY

Transmission electron microscopy (TEM) was used to ascertain the morphology of the nanomaterials supported on TiO_2(rutile), their size distribution and the average particle size in all the samples (see Figure 7.4). The average particle size of the sample containing only Pt on TiO_2(rutile) using TEM was determined to be 4.2 ± 0.8 nm, which is similar to the average size obtained using TEM for the unsupported Pt-nanoparticles (4.6 ± 0.6 nm), implying that the colloidal deposition technique did not alter the particle size distribution.

[6] Determined by ICP-OES analysis
[7] Average particle size determined using TEM analysis

The nanosheets, which were observed in the unsupported material with the nominal composition Pt-Bi, can also be observed in the TEM-image of the supported materials (see Figure 7.4). Furthermore, well defined, spherical nanoparticles can be seen with an average particle size of 9.1 ± 0.9 nm. These nanoparticles are significantly larger than the nanoparticles in the unsupported material, implying that some sintering may have occurred during the drying and calcination step of the synthesis of these materials. The nanosheets' average size and size distribution could not be measured from the TEM images of the unsupported and supported samples.

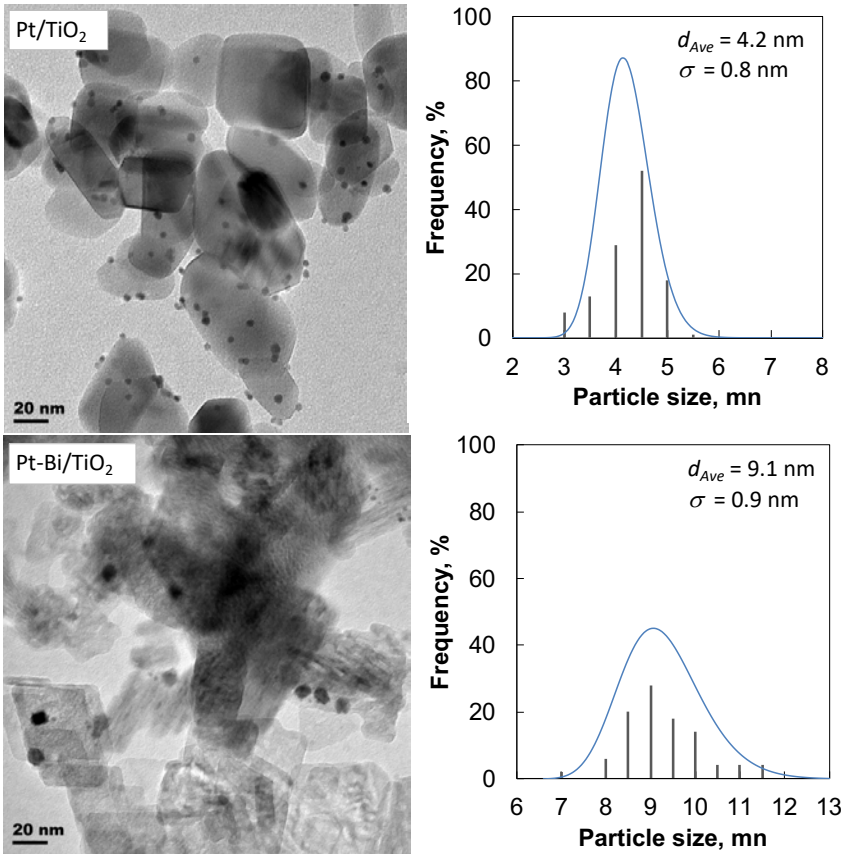

Figure 7.4: Bright-field TEM micrographs of materials with the nominal composition Pt and Pt-Bi supported on TiO_2(rutile) and the log-normal distribution of the nano-sized particles (*N = 200 nanoparticles*).

7.3. X-RAY PHOTOELECTRON SPECTROSCOPY (XPS) ANALYSIS OF PT-BI/TIO_2

Bismuth as a promoter in Pt-based catalysts is thought to assist the oxygen transfer to the noble metal Pt, which can be correlated to the oxidation state of the noble metal and the Bi promoter.[106,131] Hence, the changes in the oxidation state of platinum and bismuth in the Pt-Bi/TiO_2 catalyst sample exposed to oxidative conditions were evaluated. Specifically, this is intended to investigate the oxidation state of Bi and whether the presence of Bi impedes oxidation of Pt moiety through the formation of Pt-O species on/near the surface.

The sample was analyzed using "semi *in-situ*" conditions, *i.e.* the sample was exposed to oxygen for oxidation treatment in the pre-treatment chamber of the XPS spectrometer at 350°C before being transferred to the measurement chamber under vacuum without any exposure to the ambient atmosphere. Thus, the Pt-Bi/TiO_2 sample was treated using "semi *in-situ*" conditions under oxidative conditions at 350 °C, and the structural changes of the catalyst, especially in terms of the oxidation states of platinum and bismuth was monitored. Before oxidation treatment of the sample, a survey and characteristic region (Ti, O, Pt and Bi regions) scans were obtained. The Ti 2p and O 1s were used as references (see Appendix E-7.3).

Before the oxidation of the sample, the Pt 4f region shows two peaks (see Figure 7.5). Each peak can be deconvoluted into two peaks indicating the presence of two types of Pt species. Therefore, the XPS curve was fitted with four peaks centred at 71.2 eV, 72.5 eV, 74.2 eV and 76.1 eV. The first doublet (71.2 and 74.2 eV) has a spin-orbital split energy difference of 3.00 eV, which is characteristic of metallic platinum (Pt^0).[223] The presence of a second doublet at slightly higher energy indicate the presence of platinum in a higher valence state, e.g. PtO_x. The relative amount of Pt^0 to $Pt^{\delta+}$ before oxidation is 47:53.

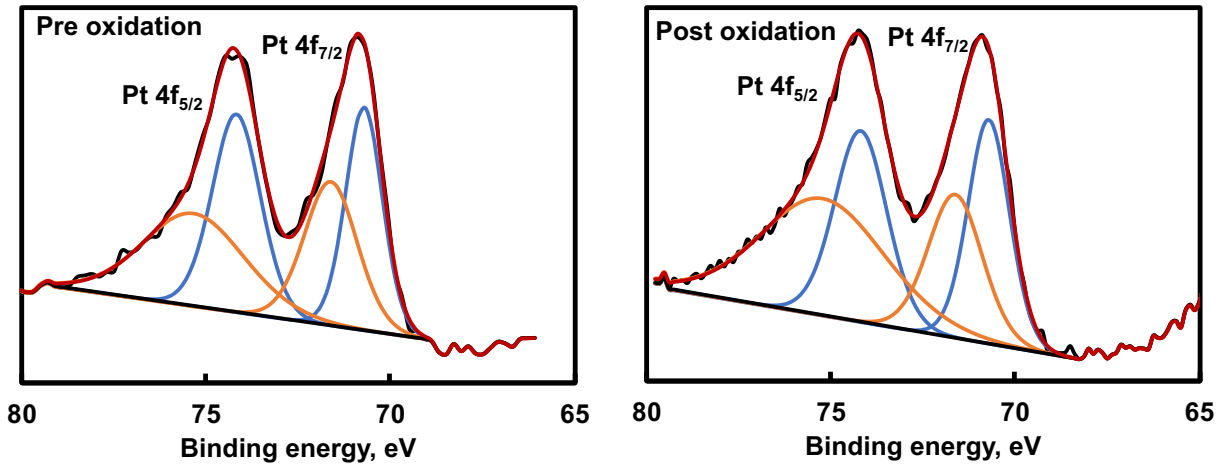

Figure 7.5: XPS spectra of the sample with the nominal composition Pt-Bi supported on TiO_2(rutile) in the Pt 4f region before (left) and after oxidation at 350 °C (right).

After the treatment under oxidative conditions at 350°C, the Pt 4f region of the spectrum for the sample is again described by two Gaussian doublets, one located at 71.2 eV (Pt $4f_{7/2}$) and 74.2 eV (Pt $4f_{5/2}$), characteristic for metallic Pt[60,223] and another strong doublet at 72.5 and 76.1 eV which can be assigned to $Pt^{\delta+}$ species.[223] The relative ratio of Pt^0 to $Pt^{\delta+}$ was determined from the Pt 4f doublets determined to be 49:51. There is thus no significant difference in the relative ratio of Pt^0 to Pt^{δ} before and post the oxidation treatment. This indicates that semi *in-situ* oxidation treatment has had a negligible influence on the valance status of Pt component in the sample with the nominal composition Pt-Bi supported on TiO_2(rutile).

The most intense absorption peaks for bismuth are identified by the Bi 4f peak typically occurring in the range 156-175 eV. The XPS spectrum of the sample before oxidation treatment shows a doublet in this region at 156.9 eV and 162.3 eV. The spin-orbital spitting for Bi in this sample was determined to be 5.4 eV, which indicates the presence of Bi^0 species.[223] After exposing this material to oxidative conditions at 350 °C, the Bi 4f binding energy shifted to higher binding energies. Each peak could be convoluted with two Gaussian peaks (see Figure 7.6). Therefore, the Bi 4f part of the XPS spectrum

post oxidation treatment was fitted with four peaks centred at 156.9 eV, 157.8 eV, 162.3 eV and 166.8 eV. The peaks at 156.9 eV and 162.3 eV represent Bi^0 $4f_{7/2}$ and $4f_{5/2}$, respectively,[224], while the fitted peaks at 157.8 eV and 166.8 eV indicate Bi^{2+} $4f_{7/2}$ and $4f_{5/2}$ existence in the sample.[223]

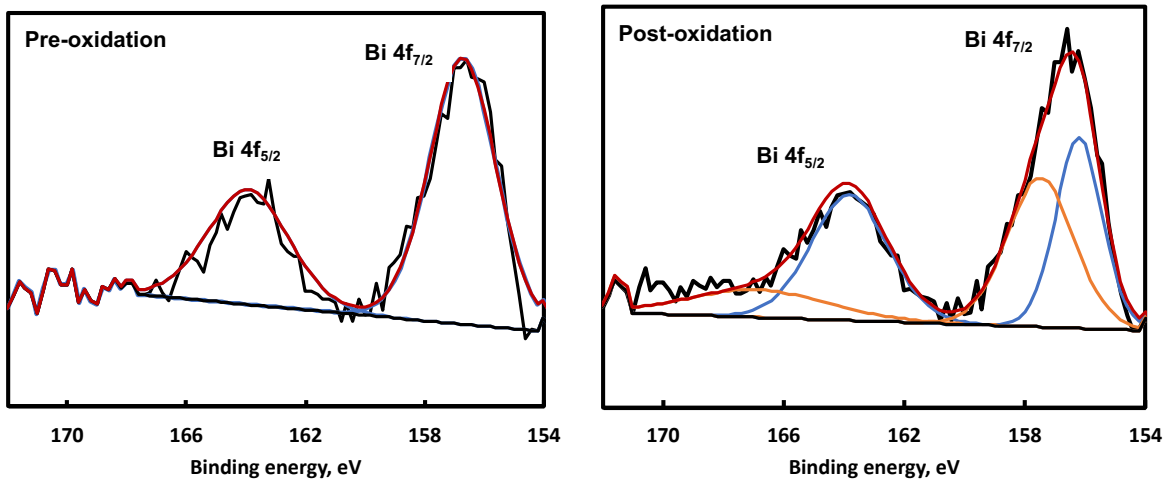

Figure 7.6: Bismuth 4f XPS spectra of 1 wt-% Pt-Bi/TiO_2 catalyst pre- and post-oxidation treatment at 350 °C.

Based on the $Pt^0/Pt^{\delta+}$ peak ratio prior and post oxidation treatment of the sample, it is evident that oxidation treatment of the sample does not affect the Pt coordination significantly. The oxidation treatment of the sample resulted in the formation of ionic Bi species, likely bismuth oxide (Bi^{2+} or BiO), which was not observed before oxidation treatment. This suggests that the new observed peaks post oxidation is due to bismuth oxide species. Thus, the semi *in-situ* XPS analysis of the Pt-Bi/TiO_2 sample may indicate that some bismuth in this sample oxidizes. In contrast, platinum does not oxidize significantly under these conditions.

7.4. SELECTIVE OXIDATION OF ALCOHOLS OVER SYNTHESIZED NANOPARTICLES SUPPORTED ON TiO_2 RUTILE

The influence of the presence of bismuth in a Pt-catalyst on the catalytic performance was evaluated in the aerobic oxidation of aromatic (benzyl alcohol) and non-

aromatic alcohol, cyclohexyl methanol. Pt/TiO_2(rutile) catalyst is used as a basis for comparison. Blank experiments were conducted, and no significant alcohol conversion was observed in the absence of a catalyst.

7.4.1. SELECTIVE OXIDATION OF BENZYL ALCOHOL: EFFECT OF THE CATALYST COMPOSITION

The effect of bismuth added to platinum on the activity and selectivity in the liquid-phase benzyl alcohol oxidation was probed in a semi-batch reactor operating at 90 °C, 5 bar using air (flow rate of 100 mL_n/min(NTP)). A total of 0.5g of the catalyst was added to the reaction mixture in the autoclave reactor (total volume of the liquid phase of 70 mL). The liquid phase consisted initially of 2.33 mol H_2O, 0.0574 mol *m*-xylene and 0.202 mol benzyl alcohol. This results in a biphasic liquid system with an organic phase and an aqueous. The reaction was allowed to run for 5 hours. Time zero is marked as the time the oxidant (air) is passed through the reaction mixture.

Figure 7.7 illustrates benzyl alcohol conversion of both Pt/TiO_2(rutile) and Pt-Bi/TiO_2(rutile) catalyst as a function of time on stream. Table 7.4 summarizes the catalytic performance of Pt-Bi/TiO_2 in comparison to Pt/TiO_2(rutile). The material containing platinum and bismuth with a composition of Pt-Bi supported on TiO_2(rutile) results in excellent catalytic activity with a conversion of 23% compared to 7% of the monometallic catalyst, Pt/TiO_2(rutile), after a reaction time of 5 hours. It can, however, be noted that the rate of reaction slowed down after a reaction time of ca. 2 hours, which may be caused by catalyst deactivation. A similar deactivation of the Pt-Bi system with reaction time was reported by Karski and Witońska[123] for the oxidation of glucose using bismuth as a promoter, which was ascribed to the deposition of carbonaceous product on the active metal surface of the catalyst. The obtained initial platinum time yield (PTY) in the benzyl alcohol oxidation over Pt-Bi/TiO_2 was 736.2 ± 24.9 hr^{-1} after 2 hours on stream. However, the rate of benzyl alcohol conversion decreased after 2 hours on stream. An integral PTY of 505.6 ± 53.0 hr^{-1} was determined after 5 hours on stream. The corresponding platinum time yield, PTY, in the benzyl alcohol oxidation over Pt/TiO_2(rutile) was 148.8 ± 3.7 hr^{-1}).

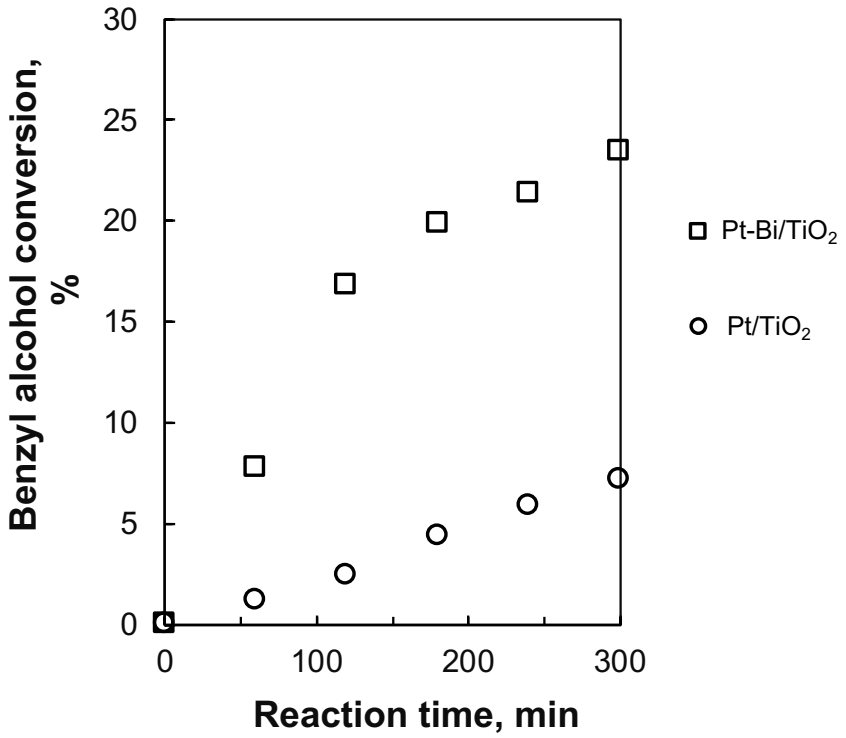

Figure 7.7: Benzyl alcohol oxidation for the first 5 hours of the reaction over Pt/TiO_2(rutile) and $Pt\text{-}Bi/TiO_2$(rutile) at 90 °C. Reaction conditions: 0.202 mol of benzyl alcohol in 2.33 mol of H_2O and 0.0574 mol of xylene, as solvent mixture, 0.5 g catalyst, P_{total} = 5 bar, V_{liquid} = 70 mL, V_{Air} = 100 mL_n/min.

The benzyl alcohol conversion over Pt/TiO_2(rutile) was also performed at 120 °C for a reaction time of 5 hours. A conversion of 12% after 5 hours on stream (see Figure 7.8) was achieved, and the corresponding platinum-time yield was 247.7 ± 4.5 hr^{-1}. This corresponds to an activation energy of 20.1 kJ/mol.

An enhanced benzyl alcohol conversion of ca. 28 % is obtained over $Pt\text{-}Bi/TiO_2$(rutile). The conversion-time plot does not seem to indicate any deactivation. A platinum-time yield of 544.3 ± 12.5 hr^{-1} was determined. The reaction rate obtained over $Pt\text{-}Bi/TiO_2$ catalyst at 120 °C is almost 2.2 times that obtained over Pt/TiO_2(rutile). Again, the promotional effects associated with the presence of Bi in the catalyst on the rate of the benzyl alcohol oxidation is evident, even at 120 °C. It should be noted that the

platinum-time yield hardly increases upon increasing temperature indicating a rather small activation energy for this reaction under the tested conditions.

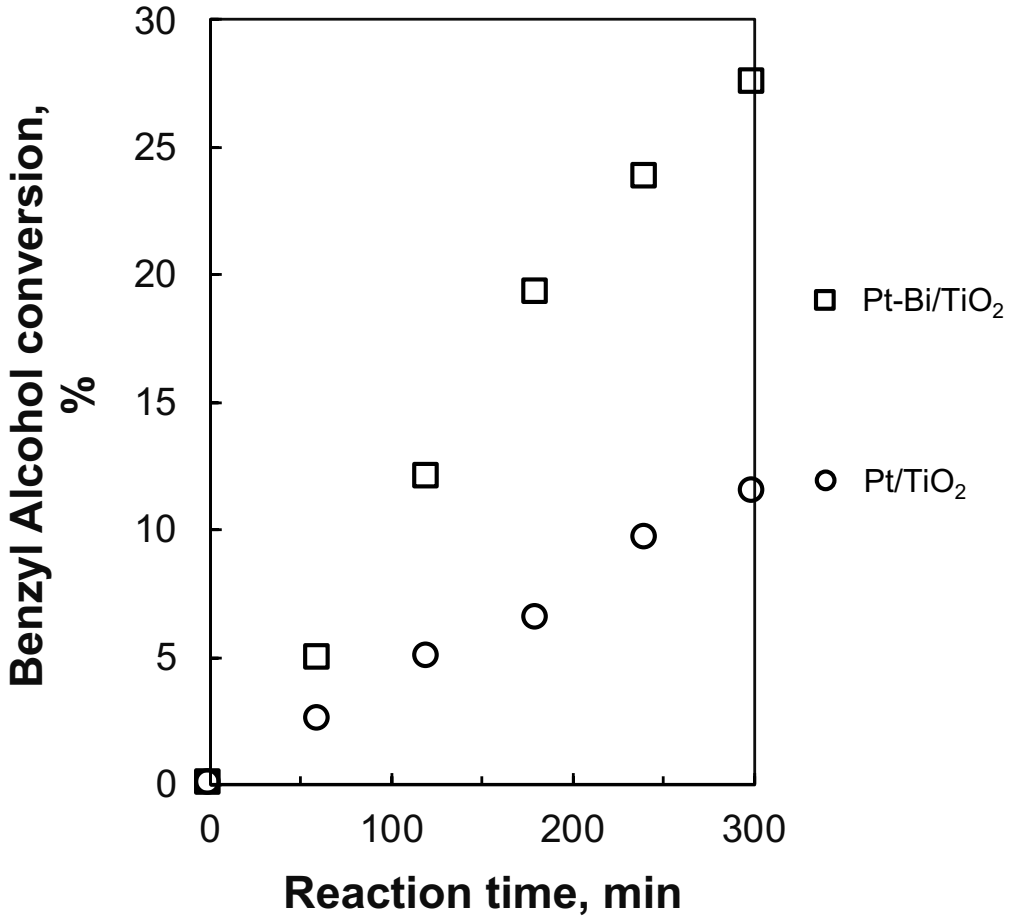

Figure 7.8: The effect of bismuth on benzyl alcohol oxidation reaction over Pt/TiO_2(rutile) and $Pt\text{-}Bi/TiO_2$(rutile) at 120 °C. Reaction conditions: 0.202 mol of benzyl alcohol in 2.33 mol of H_2O and 0.0574 mol of xylene, as solvent mixture, 0.5 g catalyst, P_{total} = 5 bar, V_{liquid} = 70 mL, V_{Air} = 100 mL_n/min(NTP).

The selectivity for the formation of benzaldehyde was obtained over both catalysts, Pt/TiO_2 and $Pt\text{-}Bi/TiO_2$, at various reaction conditions (i.e., at a reaction temperature of 90 °C and 120 °C) was larger than 99%.

7.4.2. OXIDATION OF CYCLOHEXYL METHANOL

It has also been proposed that one of the promotional effects associated with the presence of Bi on alcohol oxidation proceeds through a phenomenon called chelating effect,[17] which involves bond interaction between the alcohol substrate with Bi moiety (as a Pt-Bi alloy, Bi-metal or oxide) in the catalyst. Robinson et al.[225] showed that flat-lying conformation of benzyl alkoxide is probable over Pt(111) surface. Similar, the adsorption configuration of benzyl alcohol over polycrystalline Pt is also reported by Akinola et al.[226] This may suggest that the electronic conjugation of the aromatic alcohol substrate, benzyl alcohol, induces π bonding between the substrate and the metal surface. However, Tereshchuk et al.,[227] and Freire et al.,[228] also showed that ethanol adsorbs through the oxygen atom over Pt(111) surface. This then suggests that there are at least two adsorption conformations of benzyl alcohol over Pt-based catalyst possible. On the one hand, even though Bi has a strong affinity for oxygen compared to Pt, the adsorption of the alcohol substrate through the OH functional group over the Bi may result in an unstable bismuth hydroxide species. Frostemark et al.,[229] showed that $BiOH^{2+}$ and Bi_2OH^{5+} complexes have low stability constants of $\beta_{11}[BiOH^{2+}] = (5.6 \pm 0.1)\times 10^{-3}$ mol kg^{-1}, $\beta_{21}[Bi_2OH^{5+}] = (3.37 \pm 0.02)\times 10^{-2}$ derived from potentiometry, respectively. Therefore, it can be argued that the adsorption of benzyl alcohol over Pt-Bi/TiO_2 catalyst is such that the substrate is adsorbed through the oxygen atom on Pt while the benzyl ring interacts with Bi in Pt-Bi/TiO_2.

The promotional effects associated with the presence of Bi may then involve a preferential adsorption geometry of the substrate on the catalyst surface. It is postulated that the aromaticity of the alcohol substrate may assist the overall oxidation process through its interaction with the Bi species of the catalyst. The resultant effect of this coordination would intuitively be σ donation and π backdonation between the substrate and metal surface. The σ donation is mandatory for the binding of the substrate onto the metal. While the π bonding (which is associated with the d-orbitals of the substrate) between the substrate and the metal suggests a firm binding of the substrate. This may, then, enhance the reaction efficiency compared to the non-aromatic substrate. Therefore, to probe this promotional role of Bi, the oxidation of cyclohexyl methanol is compared with

the oxidation of benzyl alcohol. The performance over Pt/TiO_2 catalyst is used as a basis for comparison.

Cyclohexyl methanol as a substrate resulted in rather low conversions (<0.2 %) at 90 °C over both catalysts, Pt/TiO_2 and $Pt\text{-}Bi/TiO_2$. Hence, the catalytic performance obtained in the cyclohexyl methanol oxidation at 120 °C is reported here. The obtained cyclohexyl methanol conversion obtained after a reaction time of 4 hours at 120 °C over Pt/TiO_2(rutile) and $Pt\text{-}Bi/TiO_2$(rutile) was ca. 7.3 % and 7.4 % (see Figure 7.9) corresponding to a platinum-time-yield of 183.6 ± 22.6 hr^{-1} and 148.9 ± 11.9 hr^{-1}, respectively. Thus, there is no major difference in the activity for the oxidation of cyclohexyl methanol between both catalysts, despite the presence of bismuth. The morphological difference between the two catalysts may have led fortuitously to a similar platinum-time-yield. The platinum-time yield over $Pt\text{-}Bi/TiO_2$(rutile) was expected to be lower than the conversion over Pt/TiO_2(rutile) if the reaction is not affected by Bi in the sample. The average particle size of platinum nanoparticles in $Pt\text{-}Bi/TiO_2$(rutile) (9.1 ± 0.9 nm) is almost twice the average particle size of platinum nanoparticles in Pt/TiO_2(rutile) (4.2 ± 0.8 nm). Hence, the surface area of the platinum nanoparticles in the $Pt\text{-}Bi/TiO_2$(rutile) sample should only be half of the surface area of the platinum nanoparticles in Pt/TiO_2(rutile) if all platinum in $Pt\text{-}Bi/TiO_2$(rutile) is only present in platinum nanoparticles. However, some platinum in $Pt\text{-}Bi/TiO_2$(rutile) is also present in the Pt-Bi alloy. Hence, the number of surface platinum atoms on the small platinum particles in $Pt\text{-}Bi/TiO_2$(rutile) is less than half the surface area of the platinum nanoparticles in Pt/TiO_2(rutile). Hence, it is concluded that bismuth also improves the activity in the oxidation of cyclohexyl methanol.

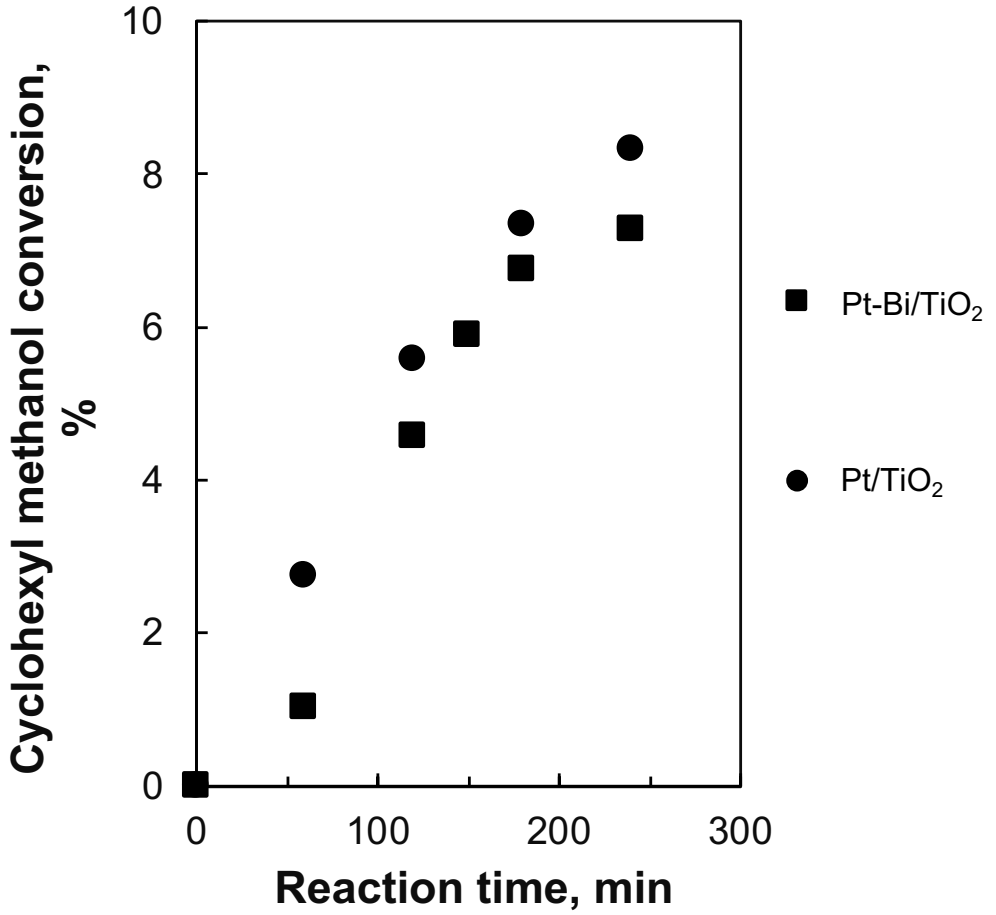

Figure 7.9: The effect of bismuth on the oxidation of cyclohexyl methanol over Pt/TiO_2(rutile) and $Pt\text{-}Bi/TiO_2$(rutile) at 120 °C. Reaction conditions: 0.202 mol of cyclohexyl methanol in 2.33 mol of H_2O and 0.0574 mol of xylene, as solvent mixture, 0.5 g catalyst, P_{total} = 5 bar, V_{liquid} = 74 mL, V_{air} = 100 mL_n/min(NTP).

Figure 7.10 illustrates the selectivity for the formation of cyclohexane carboxaldehyde in the oxidation of cyclohexyl methanol as a function of conversion. The selectivity for the aldehyde is initially high but decreased considerably for reaction times longer than 2 hours for both catalysts employed. The obtained selectivity for cyclohexane carboxaldehyde was 72 % and 78 %, over Pt/TiO_2(rutile) and $Pt\text{-}Bi/TiO_2$(rutile), respectively, after a reaction time of 4 hours at the comparable conversion of cyclohexyl methanol. This may suggest that the presence of bismuth does not influence product selectivity greatly.

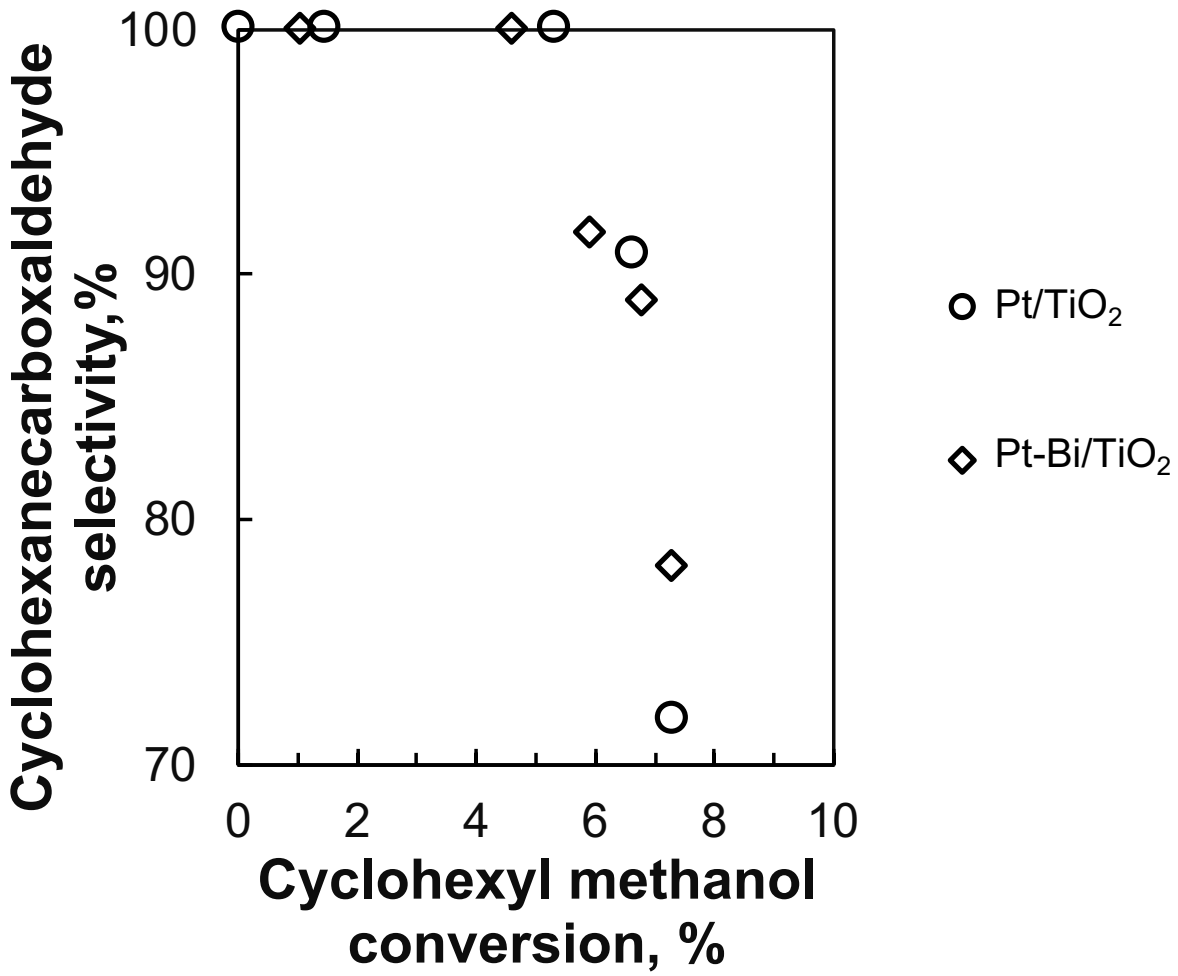

Figure 7.10: Selectivity for the formation of cyclohexane carboxaldehyde in the oxidation of cyclohexyl methanol as a function of conversion over Pt/TiO_2(rutile) and $Pt\text{-}Bi/TiO_2$(rutile) catalyst in a batch reactor with 0.5 g of the catalysts at T = 120°C, V_{liquid} = 70 mL consisting of $n_{cyclohexyl\ methanol,\ initial}$ = 0.212 mol; $n_{xylene,\ initial}$ = 0.0574 mol, $n_{H2O,\ initial}$ = 2.33 mol P_{total} = 5 bar, V_{liquid} = 74 mL, V_{air} = 100 mL_n/min.

The decrease in the selectivity towards cyclohexane carboxaldehyde is accompanied by an increase in the selectivity towards cyclohexane carboxylic acid. This suggests a consecutive reaction where a secondary oxidation reaction utilizes the cyclohexane carboxaldehyde intermediate. Thus, cyclohexane carboxylic acid is formed from the cyclohexane carboxaldehyde intermediate.

7.5. DISCUSSION

There are various roles of bismuth in alcohol oxidation that have been discussed[17,106,124,134], and there is still ongoing research to understand the promotional effects of Bi as an additive in selective oxidations. Here, bismuth is thought to have dual functionality in alcohol oxidation that ultimately enhances the catalytic activity: Assisting dissociation of oxygen, thus increasing atomic oxygen availability and promoter-substrate interaction mechanism.

7.5.1. THE PROMOTIONAL EFFECT ASSOCIATED WITH BISMUTH: EFFECT OF SUBSTRATE

The platinum-time yield in the benzyl alcohol over Pt/TiO_2 (247.7 ± 4.5 hr^{-1}) is slightly higher (35 ± 21%) than the platinum-time yield in the cyclohexyl methanol oxidation (183.6 ± 22.6 hr^{-1}; see Table 7.5). This may suggest that the oxidation mechanism between benzyl alcohol and cyclohexyl methanol over Pt/TiO_2(rutile) does not differ very much. Therefore, it is possible that both alcohol substrates are adsorbed on Pt active site through the lone pairs of the oxygen atoms of the alcohol group[230] rather than the aromatic ring of the alcohol. Some effects may be induced by the presence of the aromatic ring through electronic interaction. The adsorption of the aromatic alcohol on platinum may be stronger than the adsorption of aliphatic alcohol due to the possible electron conjugation induced by the aromaticity of the substrate. This may affect the overall reactivity.

Table 7.5: Summary of the catalyst performance over bimetallic platinum-based catalyst for selective oxidation of benzyl alcohol (after a reaction time of 5 hours) and cyclohexyl methanol (after a reaction time of 4 hours) at 120°C.

Catalyst samples	Platinum-time-yield$_{BA}$, (hr^{-1})	Platinum-time-yield$_{CycloMeOH}$, (hr^{-1})	Aldehyde selectivity	
			Benzyl aldehyde	Cyclohexane Carboxaldehyde
Pt/TiO_2	247.7 ± 4.5	183.6 ± 22.6	>99	72
$Pt\text{-}Bi/TiO_2$	544.3 ± 12.5	148.9 ±11.9	>99	78

The enhancement of the catalytic activity observed for cyclohexyl methanol oxidation over Pt-Bi/TiO_2 catalyst is not as prominent as that obtained for benzyl alcohol oxidation (although it has been argued that the observed activity for the oxidation of cyclohexyl methanol over Pt-Bi/TiO_2 is higher than expected). This difference in the influence of bismuth on catalytic activity in the cyclohexyl methanol oxidation and in the benzyl alcohol oxidation may arise from the difference in the electronic difference of the substrate-induced by the aromatic nature of the alcohol substrate. Aliphatic alcohols are typically oxidized with greater difficulty than aromatic alcohols.[231] This may be due to the induced interaction between the aromatic alcohol substrate and, e.g. bismuth in the catalyst. The interaction between the aromatic ring of the alcohol substrate and the active metal may weaken the O-H bond of the alcohol substrate, possibly through electron back-donation. On the other hand, besides the aliphatic nature of cyclohexyl methanol substrate, the steric hindrance posed by the sp^3 hybridized carbon may limit the interaction between the active metal (Pt and/or Bi), limiting interaction between the benzyl ring of the cyclohexyl methanol and surface metal.

The electron conjugation of benzyl alcohol substrate may, therefore, induce interaction with Bi species, thus influencing the bond strength of the O-H bond of the alcohol substrate allowing for facile dehydrogenation step of the oxidation of the benzyl alcohol substrate. Cyclohexyl methanol is an aliphatic substrate. As such, the interaction between Bi and cyclohexyl methanol ring is limited. Moreover, the hydrogen atoms from the sp^3 hybridized carbon atoms may pose a steric hindrance, further limiting the interaction between the Bi and the cyclohexyl methanol substrate, as demonstrated in Figure 7.10.

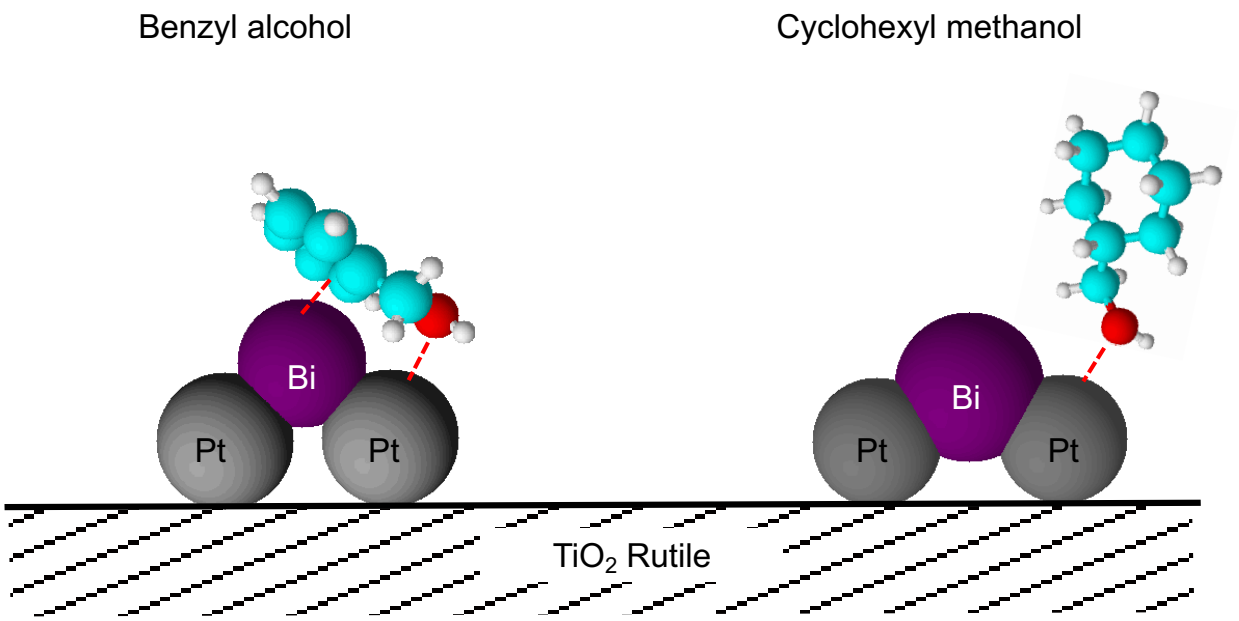

Figure 7.10: Contrasting interaction between bismuth and benzyl alcohol or cyclohexyl methanol substrate over Pt-Bi/TiO_2(rutile), highlighting the possible interaction between PtBi alloy and/or Bi species with the 6-membered ring of the alcohol substrate, while the adsorbing on Pt species through the oxygen atom.

7.5.2. ASSISTING ATOMIC OXYGEN SUPPLY TO THE PLATINUM SURFACE

The semi *in-situ* oxidation XPS analysis of the sample revealed that the Pt 4f spectrum remains unchanged post oxidation treatment at 350 °C, while some bismuth is oxidized. Zhou et al.,[124] also showed that at 75 °C Bi in Pt-Bi/CNT (CNT= carbon nanotubes) is oxidized while Pt remains in its reduced state during the electrochemical oxidation of benzyl alcohol.

One of the postulated roles of Bi in selective oxidation is regulation of the oxygen supply to the active sites avoiding rapid re-oxidation of Pt (or Pd) which strongly influences the catalytic activity.[17,64,124,125,134] Under oxidative conditions, due to its higher affinity for oxygen, bismuth may become oxidized. This proceeds through the dissociation of molecular oxygen over the Bi species. The formed atomic oxygen is thought to spillover to the metal hydride sites (on Pt surface) to form surface OH species on Pt. It is also

possible that the atomic oxygen spilled over to Pt surface may directly interact with the alcohol substrate, facilitating the dehydrogenation step, thus forming surface OH and alkoxide species on Pt surface. As the reaction proceeds to aldehyde product formation, the α-carbon is dehydrogenated and reacts with the adsorbed OH species and desorbs as an aldehyde; H_2O can desorb from the Bi-site. Bi is then thought to assist the oxidation of the alcohol adsorbed on the platinum site as illustrated in Scheme 7.1.

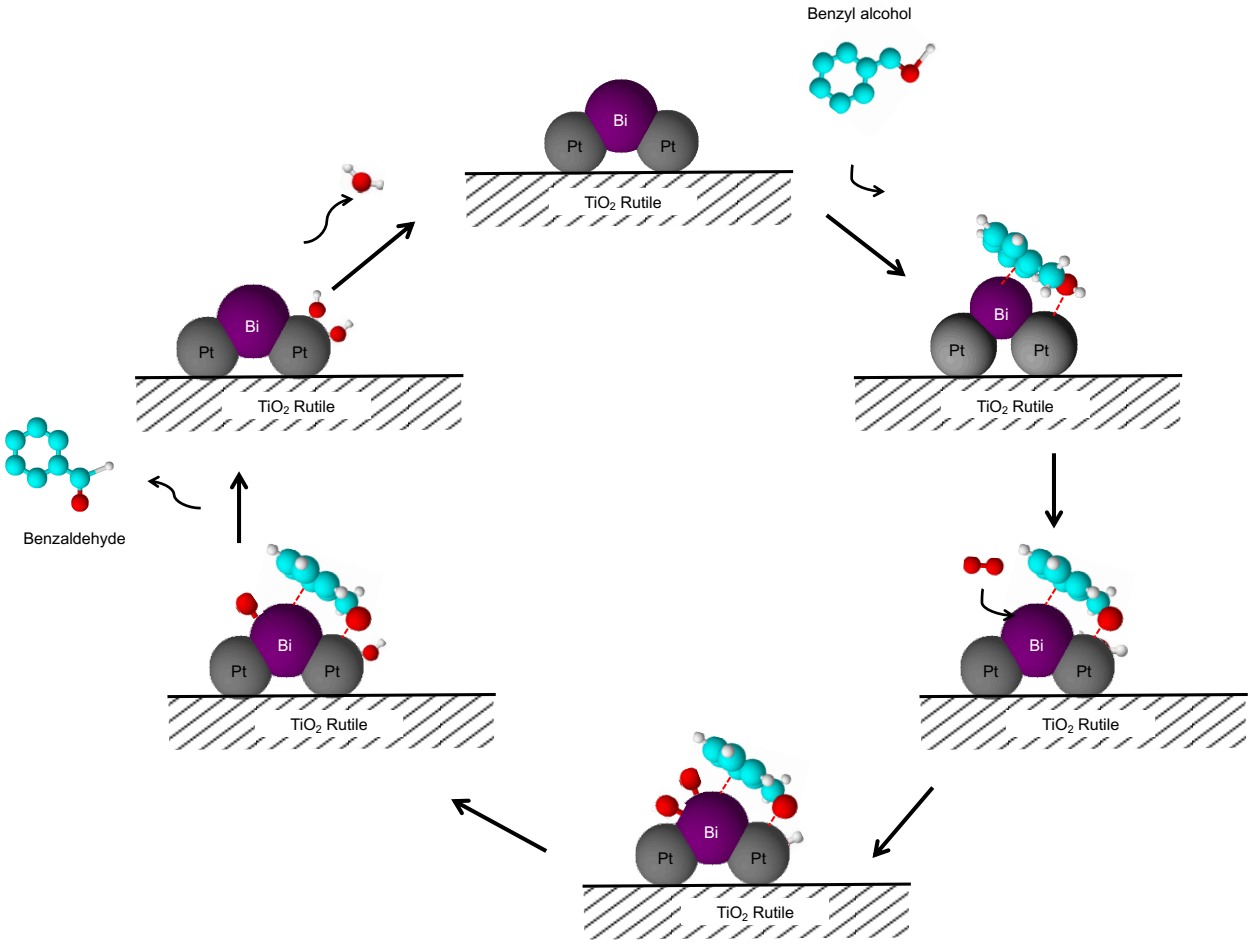

Scheme 7.1: Assisting atomic oxygen supply by bismuth in Pt-based catalyst.

7.6. CONCLUSION

Pt-Bi/TiO_2 catalyst (as a mix of Pt nanoparticles and Pt-Bi alloy with some amorphous Bi-oxide) showed superior performance in the benzyl alcohol oxidation compared to the performance over Pt/TiO_2. The promotional role associated with the

presence of Bi is thought to proceed in two mechanisms, i.e. Bi is thought to assist in molecular oxygen activation and the removal of the metal hydride from the Pt surface and Bi interaction with the alcohol substrate. For the first mechanism, semi *in-situ* XPS analysis suggests that platinum is not easily oxidized. In contrast, bismuth in the sample can be oxidized in Pt-Bi/TiO_2.

The presence of surface oxygen may be involved in the hydride abstractions in benzyl alcohol oxidation. It is thought that the removal of surface hydroxyl groups on bismuth is very facile, which may exist as bismuth hydrate. This would thus yield a facile regeneration of the active site on bismuth through the formation of H_2O.

The presence of bismuth showed a significant enhancement in the platinum-time yield in the benzyl alcohol conversion. The platinum-time yield in the cyclohexyl methanol oxidation remained constant (or even showed even a small decrease). It is, however, argued that the intrinsic activity of surface platinum in Pt-Bi/TiO_2 for the cyclohexyl methanol oxidation is higher than in Pt/TiO_2 considering the average particle size of platinum in Pt-Bi/TiO_2 (9.1 ± 0.9 nm) Pt/TiO_2 (4.2 ± 0.8 nm) in conjunction with a part of the platinum being associated with the bismuth phase. Hence, it is concluded that there is a promotional effect associated with the addition of Bi for cyclohexyl methanol oxidation as well, although not as prominent as for the benzyl alcohol oxidation. It is proposed that the additional promotional effect observed for Bi in the benzyl alcohol oxidation involves the interaction between Bi and the aromatic ring.

CHAPTER 8:

General discussion

Selective oxidation of alcohol is a non-trivial chemical transformation. An ideal environmental benign oxidation process should involve a highly active and selective heterogeneous catalyst that can drive the oxidation process at low pressures and in the absence of organic solvent. Typically, selective oxidation of alcohols involves the scission of two bonds: an O–H bond and the substrate's C–H bond.[88] The former yields an alkoxyl species on the surface of the catalyst. The resulting alkoxy species further undergoes C-H bond cleavage through β-H abstraction to form an aldehyde product/intermediate. The C-H bond cleavage step has been reported to be the rate-determining step over Pd, Au and Pt-based catalysts.[28,82,232–235] As such, achieving a highly active and selective oxidation process of alcohols involves a system that has a low activation barrier of, specifically, C-H bond cleavage. Therefore, the results obtained in this study looking at the role of water in alcohol oxidation reactions, in conjunction with the role of the support and modifiers, yield insight into the effect of these parameters on the overall reaction, and thus ultimately on how these parameters affect O-H and C-H bond cleavage during benzyl alcohol oxidation.

8.1. ACTIVATION OF MOLECULAR OXYGEN

The dissociative adsorption of molecular oxygen on the catalytically active metal yielding atomic oxygen on the surface has been suggested as the initial step in alcohol oxidations.[82] Ojifinni et al.[236] indicated that a bulk gold surface pre-covered with atomic oxygen is highly active and selective for the partial oxidation of alcohol to aldehydes, suggesting the availability of active oxidation species such as atomic oxygen is important for alcohol oxidation. The activation of O_2 over platinum has been well studied[34,35,206]: the dissociative adsorption of molecular oxygen over a platinum surface is thought to proceed via a two-step process:[34,35,177]

Adsorption of molecular oxygen: $O_2 + * \rightarrow O_2*$ 8.1

Dissociation of molecularly adsorbed oxygen: $O_2^* + * \rightarrow 2O^*$ 8.2

The overall catalytic performance in alcohol oxidation may be improved by promoting the adsorption and dissociation of oxygen on the surface of the catalytically active material.

H_2O is known to play a crucial role in a range of reactions involving molecular oxygen, such as CO oxidation, olefin epoxidation and alcohol oxidation reactions.[5,37] The main role of H_2O is thought to assist in adsorption and activation of O_2, thereby accelerating the reaction.[32,237,238] DFT calculations presented here showed that the co-adsorption of H_2O with O_2 strengthens the adsorption of molecular oxygen on Pt(111) (see Chapter 4). Shang and Liu[238] also reported a strengthening of the adsorption of molecular O_2 in the presence of H_2O (in this case, on edge sites of Au nanoparticles with an average particle size of ~4 nm), indicating that this phenomenon is not limited to just platinum. The increased strength of adsorption of molecular oxygen upon co-adsorbing H_2O implies that the surface coverage with molecular oxygen will increase upon co-adsorbing H_2O. Here, we further established that the activation barrier for O_2 dissociation over Pt(111) surface is significantly reduced from 0.41 eV (ca. 40 kJ/mol) to 0.18 eV upon co-adsorption with H_2O. A higher surface coverage with molecular oxygen in conjunction with lower activation energy for the dissociation of molecular oxygen may result in a higher rate of formation of atomic oxygen on the surface. This may increase the rate of alcohol oxidation if atomic oxygen is involved in the rate-determining step.

Besides the co-adsorption/addition of H_2O, O_2 activation may also be enhanced by adding promoters. The addition of a promoter such as Bi is postulated to promote O_2 activation by forming bismuth oxide.[14,239] Bismuth may thus act as a co-catalyst[240] assisting the activation of molecular through the formation of bismuth oxide during alcohol oxidation. Semi in-situ XPS analysis (see Chapter 7) suggested that the Bi moiety of the catalyst is more readily oxidized than platinum in Pt-Bi/TiO_2 catalyst. This is ascribed to a relatively strong oxygen affinity of Bi in comparison to Pt.[239]. This may at least partly contribute to the observed enhanced activity for the benzyl alcohol oxidation over Pt-

Bi/TiO_2 (PTY of 505.6 ± 53 hr^{-1}) in comparison to the activity over Pt/TiO_2 (PTY of 148.8 ± 3.7 hr^{-1}) at 90 °C.

Conversely, weakening oxygen adsorption via alloying may retard benzyl alcohol oxidation. The calculated platinum-time yield (PTY) for benzyl alcohol oxidation over Pt_3Ni/TiO_2 was determined to be 20.9 ± 0.9 $hr^{-1,}$ i.e., ca. 7 times slower than over Pt/TiO_2 at 90 °C (see Chapter 5). The reduced rate of reaction in the aerobic oxidation of benzyl alcohol over Pt_3Ni/TiO_2 catalyst might be linked to the reduction in the surface coverage of the kinetically important oxygen-containing species. Alloying platinum with nickel results in forming a Pt-skin alloy, thus altering the adsorption properties of Pt. The d-band centre of the surface Pt-atoms in the Pt-skin Pt_3Ni (111) alloy is shifted downwards by up to 0.36 eV relative to the d-band position of surface atoms on Pt (111).[139,188] The downshift of the d-band centre will weaken the adsorption molecular oxygen189 and the adsorption of atomic oxygen.[139] Furthermore, the activation energy barrier associated with the dissociation of O_2 over Pt-skin Pt_3Ni(111) has been reported to be higher (0.83 eV) than over Pt(111) (0.63 eV).[188] Hence, the dissociation of molecularly adsorbed O_2 in the absence of co-adsorbed water is more facile over Pt(111) than over Pt-skin Pt_3Ni(111) alloy surface. Hence, it is expected that weakening the oxygen adsorption through alloying will reduce the fraction of atomic oxygen on the surface, thus reducing the overall catalytic activity.

8.2. SURFACE OXYGEN ASSISTED ALCOHOL ACTIVATION

Atomic oxygen on the catalyst surface facilitates the activation of the adsorbed alcohol substrate[241] during oxidation reaction by forming surface alkoxyl and hydroxyl species possibly through the interaction of the adsorbed alcohol with atomic oxygen on the surface:[28,87]

$$\text{Alcohol} + * \rightarrow \text{Alcohol}* \qquad 8.3$$

$$\text{Alcohol}* + O* \rightarrow \text{Alkoxyl}* + OH* \qquad 8.4$$

The formation of the atomic oxygen on the surface of platinum (equation 8.1 and 8.2) and the elementary step described in equation 8.3 are thought to be the main reaction channel for catalytic activity observed in the absence of water (TOF of 26.7 ± 6 hr^{-1} for benzyl alcohol oxidation over Pt/TiO_2(P25)) in a solvent-free, liquid system, TOF of 20.0 ± 2 hr^{-1} in a liquid system with n-heptane and TOF of 23.1 ± 6 hr^{-1} in a liquid system with m-xylene as a solvent.

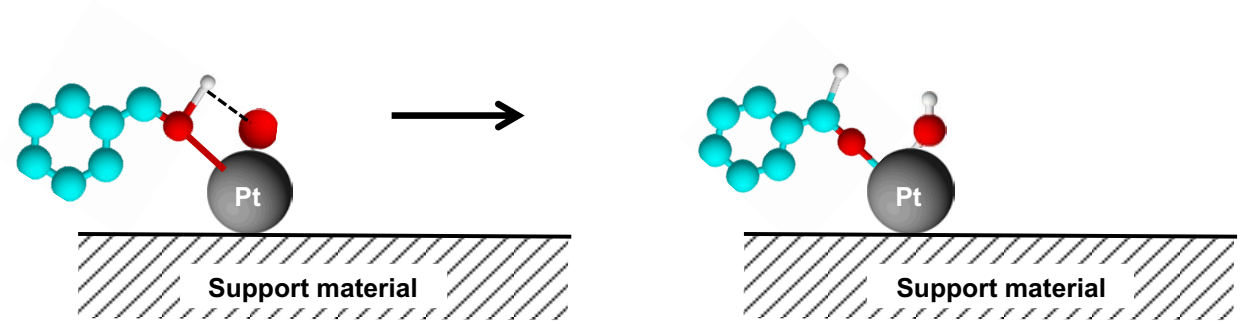

Figure 8.1: Reaction between adsorbed benzyl alcohol and adsorbed atomic oxygen on a Pt-based catalyst.

Liu et al.[82] suggested using DFT that the oxide support material (ZnO) may also be involved in the dissociation of the alcohol substrate to form an alkoxyl species on the surface of the catalyst (Pt/ZnO). Their DFT studies suggested that on an atomic oxygen pre-adsorbed Pt surface, benzyl alcohol substrate is adsorbed on the ZnO surface, forming benzyl alkoxide on the support surface and hydroxyl species on the Pt surface. Here, it is shown experimentally that the support plays an important role in the benzyl alcohol oxidation; at comparable reaction conditions, the catalytic performance of Pt/TiO_2 (reducible metal oxide support) is better (TOF = 26.7 ± 6 hr^{-1}) than the catalytic performance with $Pt/\gamma\text{-}Al_2O_3$ (irreducible metal oxide support; TOF = 9 ± 4 hr^{-1}) in a solvent-free benzyl alcohol oxidation. This suggests that, indeed, oxidic support material plays a role beyond just metal dispersion. Reducible metal oxide support materials (such as TiO_2, CeO_2 and Fe_3O_4) are characterized by their tendency to lose lattice oxygen (forming an oxygen vacancy), thus changing the surface composition of the support, from $M^{x+}O^{y}$ to $M^{(x-n)+}O^{y-n}$, specifically during oxidation reactions.[11] While irreducible metal oxide

(such as Al_2O_3 and SiO_2) do not readily lose oxygen due to the intrinsic resistance of the corresponding metal cations to change oxidation state.[11]

The identification and characterization of these oxygen vacancies on the oxide surface are not trivial. However, the observed significant difference in TOF for benzyl alcohol oxidation between the Pt/TiO_2 and $Pt/\gamma\text{-}Al_2O_3$ catalysts (in a solvent-free system – 100 mol-% benzyl alcohol) is thought to be due to the difference in reducibility of the metal oxide support material employed. It is thought that the availability of the lattice oxygen of the reducible support is directly involved in the O-H bond cleavage (activation) of the alcohol substrate. It is proposed that over a reducible metal oxide support, the lattice oxygen of the support material facilitates the OH bond cleavage of the alcohol substrate adsorbed on Pt moiety of the catalyst. Consequently, in this study, it is thought that the alkoxyl species is formed on the Pt surface while the hydroxyl is formed on the surface of the support material, as shown in Figure 8.2. The main division of opinion with Liu et al. [82] is that in the current study, it is thought that the alcohol substrate is coordinated to Pt moiety while interacting with the surface lattice oxygen of the reducible metal oxide support through the hydrogen atom of the OH functional group of the substrate. Liu et al.,[82] argue that the (ZnO) support acts as a site for benzyl alcohol adsorption. Pt facilitates the adsorption and activation of O_2, which reacts with the adsorbed benzyl alcohol. It should be noted that in the current study, the experiments were conducted in the presence of H_2O solvent. Therefore, considering the pKa value of benzyl alcohol of ca. 15.5 which is similar to that of methanol (pKa=15.4[242]) and that benzyl alcohol is a weaker acid than H_2O with a pKa value of 14.0[243], suggests that the reaction in equation 8.6 is more facile than equation 8.5.

$$\text{—Sup-O-Sup—} + \text{ROH} \rightarrow \text{—Sup-OH} + \text{RO-Sup—} \qquad 8.5$$

$$\text{—Sup-O}^{\ddagger}\text{-Sup—} + H_2O \rightarrow \text{—Sup-}^{\ddagger}\text{OH} + \text{HO-Sup—} \qquad 8.6$$

As the reaction proceeds, the surface hydroxyl species assist O-H bond cleavage by interacting with the hydrogen atom of the OH group of the substrate through hydrogen bonding, thus forming H_2O. The formed H_2O on the surface of the support desorbs, creating oxygen vacancy sites on the surface of the support. Mazumder et al.,[244]

suggested that the adsorption of benzyl alcohol onto CeO_2 moiety (reducible metal oxide material) of MnOx-CeO_2 catalyst involves the coordination of the substrate to the oxygen vacancy site of CeO_2 while the hydrogen atom of the OH group of benzyl alcohol is interaction with the surface lattice Ce atom, thus yielding cerium hydride. The formation of cerium hydride is also reported by Abad et al.[13] The metal hydride is suggested to undergo hydrolysis and desorbs as an H_2O co-product.[244] This suggests that not only the formation of surface hydroxyl species on the support material is crucial for O-H bond cleavage, but also the resulting oxygen vacancy sites are directly involved in benzyl alcohol oxidation.

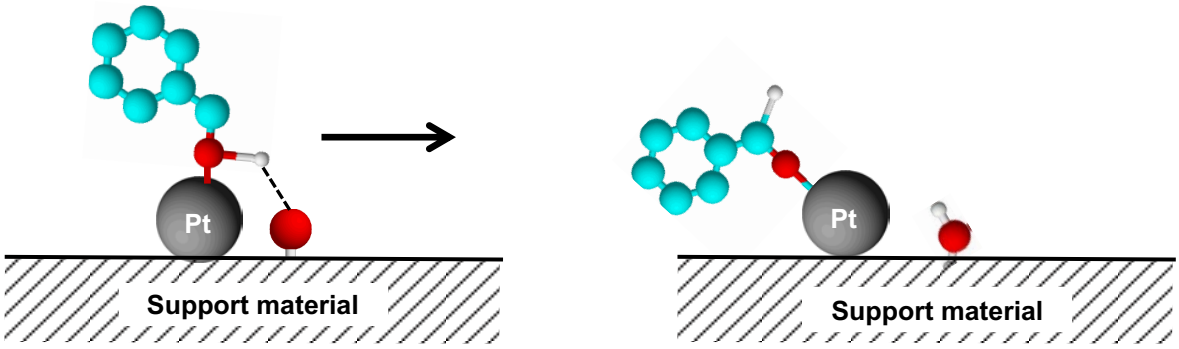

Figure 8.2: Dissociation of benzyl alcohol assisted by surface oxygen of the support material to form surface benzyl alkoxyl and hydroxyl species.

The mechanism proposed in Figure 8.2 can be extended to rationalize the promotional effect associated with the formation of bismuth oxide in Pt-Bi/TiO_2. Bismuth oxide (serving as a new site in addition to Pt and reducible TiO_2 support) may facilitate O-H bond cleavage of the alcohol substrate through coordination of the OH with bismuth oxide via $Bi_xO_y\cdots$HO(benzyl) interaction. This may yield benzyl alkoxyl and hydroxyl species on the surface of Pt and bismuth, respectively. This may be one of the reasons for the observed increase in the activity of Pt-Bi/TiO_2 (rutile phase) for the benzyl alcohol oxidation compared to the activity over Pt/TiO_2 (rutile phase).

8.3. SURFACE HYDROXYL ASSISTED ALCOHOL ACTIVATION

O-H bond cleavage of the alcohol substrate, through hydrogen transfer to atomic oxygen, was described as one of the crucial steps for benzyl alcohol activation during benzyl alcohol oxidation.[235] However, O-H bond cleavage may not only be limited to the transfer of hydrogen to atomic oxygen. The hydrogen transfer may also involve a surface hydroxyl species resulting in the formation of the corresponding alkoxide species and adsorbed water. Zope et al.[28] showed that the surface hydroxyls facilitate the OH bond cleavage in ethanol over Au(111) and Pt(111) surfaces, forming ethoxyl species. Mullen et al.[245] also stated that the presence of hydroxyls promotes partial oxidation of allylic alcohol to their corresponding aldehydes with very high aldehyde selectivity.

It was shown here that the turnover (TOF) for benzyl alcohol oxidation over Pt/TiO_2(P25) is significantly improved upon the addition of H_2O as a solvent from 26.7 ± 6.0 hr^{-1} obtained from a solvent-free liquid system to 677.4 ± 23 hr^{-1} (see Chapter 4). DFT calculations were conducted in this study to provide molecular insight into the precise role of H_2O in O_2 activation over Pt(111) surface, as well as to ultimately elucidate the observed promotional effect of H_2O in benzyl alcohol oxidation. It is highlighted, here, that the promotional effects associated with the presence of H_2O are not only limited to promoting O_2 activation by lowering the activation barrier of O_2 dissociation and adsorption energy of O_2 over Pt(111) surface, but H_2O also facilitates O_2 activation through the formation of OH species on the surface of active metal, platinum. Chibani et al.[88] also reported that co-adsorption of H_2O with O_2 over Pt(111) yields surface OH species.

Surface OH species (derived from the dissociation of O_2 in the presence of H_2O) may interact with the hydrogen atom of the OH group of the alcohol substrate. This, then, resulted in the formation of metal benzyl alkoxide species and adsorbed water. The enhancement in TOF for benzyl alcohol oxidation when performing the reaction in H_2O solvent may thus also be ascribed to the increased coverage of the surface with OH species formed from the activation of O_2 assisted by H_2O a solvent. It should be noted that the reactivity of benzyl alcohol substrate with surface oxygen (discussed in section 8.2) or hydroxyl species may operate in parallel during oxidation reactions.

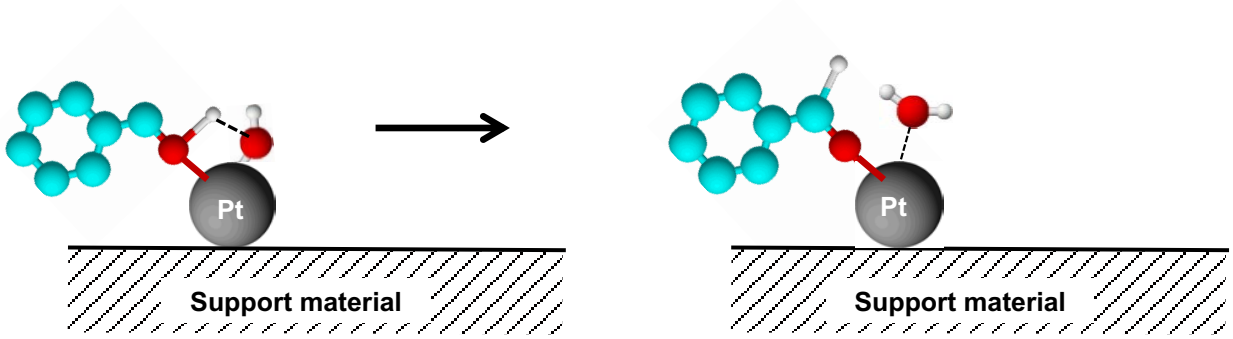

Figure 8.3: Dissociation of benzyl alcohol over surface hydroxyl species adsorbed Pt-based catalyst to form surface benzyl alkoxide and metal hydroxide species.

The importance of surface hydroxyl species was also shown by substituting molecular oxygen with H_2O_2 as the oxidant (which dissociates upon adsorption on platinum into two surface OH species[246]) in the benzyl alcohol oxidation over Pt/TiO_2(rutile) and Pt_3Ni/TiO_2(rutile) catalyst. Substituting O_2 with H_2O_2 as the oxidant resulted in an enhanced PTY for benzyl alcohol oxidation from 120.6 ± 6.4 hr^{-1} to 186.1 ± 15.1 hr^{-1} over Pt/TiO_2(rutile) and from 20.9 ± 0.9 hr^{-1} to 506.6 ± 37 hr^{-1} over Pt_3Ni/TiO_2(rutile). This suggests that the presence of surface OH species has some effect on the overall catalytic activity for alcohol oxidation over platinum. The role of surface hydroxyl species becomes much more dominant when using a catalyst, which adsorbs oxygen weaker (i.e., a platinum-nickel alloy).

It is also possible that the OH species on the support material (shown in Figure 8.3) in the vicinity of the metal interacts with the alcohol substrate adsorbed on the metal through hydrogen bonding, which may result in the formation of the metal alkoxyl species on the metal and H_2O on the oxide support, respectively. The promotional effect of H_2O was evident on irreducible support (γ-Al_2O_3) and reducible support (TiO_2(P25)). Upon the addition of H_2O, the TOF for benzyl alcohol oxidation is significantly improved from 9 ± 4 hr^{-1} to 80 ± 7 hr^{-1} over Pt/γ-Al_2O_3 and from 26 ± 5 hr^{-1} to 619 ± 18 hr^{-1} over Pt/TiO_2 catalyst. In the case of platinum supported on irreducible support, γ-Al_2O_3, the dominant mechanism could be a consequence of the role of H_2O on O_2 activation (to form surface hydroxyl as predicted by DFT calculations) on metallic platinum. It is assumed that

surface hydroxyl species on γ-Al_2O_3 do not play an important as the surface is expected to be readily saturated with hydroxyl groups.[214] While in the case of reducible support (TiO_2), water may result in the creating of surface hydroxyl species:

—Sup-O‡-Sup—+ H_2O ➔ —Sup-‡OH + HO-Sup— 8.7

Sup-‡OH + ROH* → RO* + Sup-H‡OH 8.8

Sup-H_2O → Sup + H_2O 8.9

2Sup + O_2¤ → Sup-O-Sup 8.10

With ¤,* and ‡ denoting oxygen feed, species adsorbed on Pt and component of the support material, respectively. The formed surface hydroxyl on the support (equation 8.7) may enhance the TOF for the benzyl alcohol oxidation further, e.g., through the interaction of benzyl alcohol with a hydroxyl species on the support, as illustrated in Figure 8.4 (see equation 8.6, *vida infra*). Therefore, the observed improved TOF for benzyl alcohol oxidation over Pt/TiO_2(P25) in the presence of H_2O may be contributed by the formation of surface hydroxyl on both Pt (see Figure 8.2) and on the reducible metal oxide support material (see Figure 8.4).

The improved performance of Pt-Bi/TiO_2 may also involve the interaction between adsorbed benzyl alcohol and surface hydroxyl species. Several studies suggested that surface OH species adsorb on Bi adatoms to form new active sites such as Pt-Bi-OH.[104,124] Therefore, the promotional effects associated with Bi in Pt-Bi/TiO_2 catalyst in the presence of H_2O solvent may be attributable to the formation of OH species on the Bi moiety of the catalyst, thus forming these new active sites.

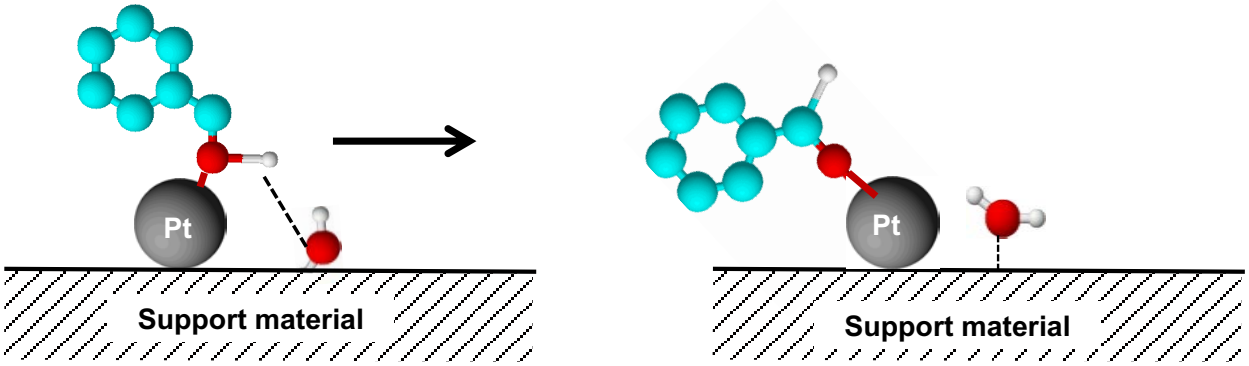

Figure 8.4: Dissociation of benzyl alcohol over lattice oxygen adsorbed of the reducible metal oxide support moiety of the catalyst to form surface benzyl alkoxyl and H_2O species.

8.4. **C-H BOND CLEAVAGE:** BENZALDEHYDE PRODUCT FORMATION

The alcohol substrate activation (through OH bond cleavage to form surface alkoxyl and hydroxyl species on the surface) is thought to be followed by the β-H abstraction to form an aldehyde product.[32,82,235] However, oxidative species (oxygen and/or hydroxyl) pre-adsorbed on the Pt surface (the active metal) has been reported to reduce the activation barrier associated with β-H abstraction (C-H bond activation) during (benzyl) alcohol oxidation, thus facilitating C-H bond cleavage to yield corresponding aldehyde product.[88,247] It is suggested that the formed oxygen/hydroxyl species on the surface of the catalyst assists hydride abstraction of alkoxyl, thus desorbing as an aldehyde product (similarly to equation 8.6, *vida supra*), as illustrated in Figure 8.5. In this mechanism, the desorption of the alkoxyl species as an aldehyde product involves Pt-$O_{alkoxyl}$ bond cleavage forming a carbonyl species while simultaneously dehydrogenating the substrate via the surface hydroxyl species (e.g., formed from the dissociation of molecular oxygen in the presence of H_2O over Pt surface) to form adsorbed H_2O as a co-product, as shown in Figure 8.5. The active sites are also regenerated, thus closing the catalytic cycle.

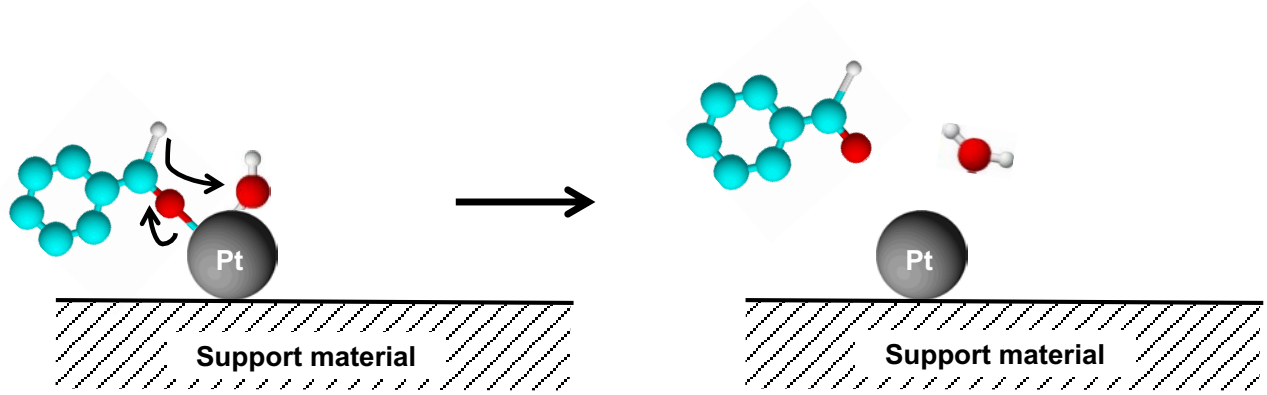

Figure 8.5: Dissociation of benzyl alcohol assisted by surface oxygen of the support material to form surface benzyl alkoxide and H_2O.

In the case of surface hydroxyl that forms on the surface of the reducible support material (described in previous sections), the formation and desorption of H_2O will occur on the support surface (as shown in equation 8.11 and 8.12), while the aldehyde product will desorb from the Pt moiety of the catalyst.

H_2O-formation on support: $\quad$ 'H' + $HO^{\ddagger}$ $\rightarrow$ $H_2O^{\ddagger}$ $\quad$ 8.11

(with 'H' β-H of the adsorbed benzyl alkoxyl species, ‡ denoting component of the support material). The formed H_2O on the surface of the support material may desorb, forming an oxygen vacancy on the surface of the metal oxide support material.

Water desorption from support: $\quad$ $H_2O^{\ddagger} \rightarrow {}^{\ddagger}$ $\quad$ 8.12

In order to be catalytic, the reaction must proceed under oxygen pressure (flow) so that O_2 can interact with the surface of the catalyst, dissociate, and eventually refill the vacancy created on the surface of the support. In this way, the original stoichiometry and composition of the catalyst are restored, closing the catalytic cycle. Therefore, the oxygen on the support can be regenerated by, e.g., dissociated oxygen spillover (refer to equation 8.13) from the active metal, Pt:

Oxygen spillover: $\quad$ $O^* + {}^{\ddagger} \rightarrow O^{\ddagger} + *$ $\quad$ 8.13

The regeneration of the oxygen vacant site on the support material is also crucial. In the catalyst series, the oxide support, γ-Fe_2O_3, is the most reducible metal oxide, yet it is the least active catalyst in the reducible support series. This has been ascribed to the fact that the formed oxygen vacancy sites are not regenerated to close the catalytic cycle, see Chapter 6, leading to the deactivation of the catalyst.

8.5. EFFECTS OF SUBSTRATE AROMATICITY

Aliphatic alcohols are typically oxidized with greater difficulty than aromatic alcohols due to the difference in aromaticity.[231] This difference may arise from the difference in the electronic difference of the substrate-induced by the aromatic nature of the alcohol substrate. In this instance, cyclohexyl methanol is less likely to be physisorbed on the metal (due to the absence of π-electrons), while the π-electrons around the benzyl ring of benzyl alcohol may interact with the catalyst surface.[247] This would increase the surface coverage with the surface alkoxyl species. As such, this may explain the difference in catalytic activity obtained over Pt/TiO_2 between benzyl alcohol oxidation ($247.7 \pm 4.5\ hr^{-1}$) and cyclohexyl methanol ($183.6 \pm 22.6\ hr^{-1}$).

Furthermore, a significant difference in PTY for cyclohexyl methanol oxidation ($148.9 \pm 9\ hr^{-1}$) and benzyl alcohol ($554 \pm 12.5\ hr^{-1}$) over $Pt\text{-}Bi/TiO_2$ catalyst is demonstrated at comparable reaction conditions. The difference in PTY for cyclohexyl methanol oxidation obtained over Pt/TiO_2 and $Pt\text{-}Bi/TiO_2$ catalyst may highlight promotional effects associated with the presence of Bi promoter. This difference in PTY may be due to the induced interaction between the aromatic alcohol substrate and, e.g., Pt and/or bismuth in the catalyst. The interaction between the aromatic ring of the alcohol substrate and the active metal may weaken the O-H bond of the alcohol substrate,[247] possibly through electron back-donation. On the other hand, besides the aliphatic nature of cyclohexyl methanol substrate, the steric hindrance posed by the sp^3 hybridized carbon may limit the interaction between the active metal (Pt and/or Bi), limiting interaction between the benzyl ring of the cyclohexyl methanol and surface metal. Though it should also be noted that the origin of the promoting role of bismuth on Pt catalyst is still under debate. One of the proposed functions of bismuth as a promoter is that bismuth

undergoes complexation with the alcohol substrate with chelating properties.[248] This has been used as an explanation for the typically observed catalytic activity improvement exhibited by bismuth promoted Pt-based catalysts.

The observed overoxidation of cyclohexyl methanol oxidation over Pt/TiO_2 and $Pt-Bi/TiO_2$ catalyst (in comparison to benzyl alcohol oxidation) may be due to the aromaticity difference between cyclohexyl methanol and benzyl alcohol. The aromaticity of the substrate is thought to be a determining factor in the sense that the aliphatic nature of cyclohexyl methanol induces charge polarization. The charge polarization makes the carbonyl carbon of the substrate susceptible to re-adsorption and nucleophilic attack of the adsorbed atomic oxygen or surface OH species. Moreover, the electron density in benzyl alcohol may induce electron repulsion between the substrate and nucleophilic oxygen and surface OH species. Due to the difference in aromaticity, this may result in overoxidation of cyclohexyl alcohol instead of benzyl alcohol.

CHAPTER 9:

Final remarks

9.1 CONCLUSION

The demand and importance of high-value chemicals, such as aldehydes, derived from the alcohol oxidation process necessitate the development of safe and environmental benign methodologies that may be sustainable and industrially relevant. Liquid-phase alcohol oxidation over heterogeneous catalyst using oxygen as an oxidant is a classic process that can be considered and suitable to meet green chemistry demands while also aiming for an enhanced overall catalytic activity.

This body of work was aimed at in-depth exploration of various factors that enhance the catalytic performance in the aerobic, liquid-phase oxidation of alcohol while promoting green chemistry. A systematic study investigating the influence and/or promotional effect of liquid water, metal oxide support materials and secondary element on alcohol oxidation has been extensively studied.

The TOF for benzyl alcohol oxidation is enhanced in the presence of H_2O solvent compared to in the presence of *m*-xylene or *n*-heptane solvent. The oxygen solubility in organic solvents, such as *m*-xylene and *n*-heptane, is approximately 100 times greater than in H_2O. As such, the observed catalytic improvements in the presence of H_2O solvent cannot be attributed to a change in the oxygen solubility. The high rate of reaction in the presence of H_2O may indicate that the solubility of oxygen in the solvent does not affect the rate of reaction and that surface oxygen is in (or close to) equilibrium with oxygen in the gas phase. DFT study concluded that the presence of H_2O promotes molecular oxygen dissociation and the presence of surface OH species. The addition of H_2O does not result in overoxidation after 5 hours on stream. However, during a cooling process (16 hours of cooling), benzoic acid is observed, indicating overoxidation.

The influence of different O_2 and H_2O_2 as the oxidant (which ultimately form atomic oxygen and hydroxyl species on the surface) was investigated in the oxidation of benzyl alcohol over Pt/TiO_2 and Pt3Ni /TiO_2 catalysts. Alloying Pt with nickel yields a diminished catalytic activity when O_2 is used as an oxidant, yielding PTY for benzyl alcohol oxidation of 20.9 ±0.9 hr^{-1} and 27.5 ±5.0 hr^{-1} over Pt_3Ni/TiO_2 and $PtNi/TiO_2$, respectively compared to activity obtained over Pt/TiO_2 catalyst (120.6 ± 6.4 hr^{-1}). This may be rationalized by a lowering of the d-band centre of the surface Pt atoms upon forming a Pt-skin material when alloying Pt with Ni. The resulting weakening of the adsorption molecular oxygen O_2 and of the adsorption of atomic oxygen together with the less facile dissociation of molecular oxygen will thus retard the O_2 activation required for benzyl alcohol oxidation. An enhanced catalytic activity is observed when O_2 oxidant is substituted with H_2O_2 oxidant over Pt_3Ni/TiO_2 catalyst. This is attributed to the increase in the surface concentration of OH from the dissociation of H_2O_2 oxidant. This highlights that the presence of surface OH groups (derived from H_2O_2 dissociation) form a crucial aspect in the overall activity of benzyl alcohol oxidation.

In a solvent-free system, reducible metal oxide support material such as TiO_2(P25) showed an enhanced TOF for benzyl alcohol oxidation (26 ± 5 hr^{-1} over Pt/TiO_2) compared to irreducible support such as γ-Al_2O_3 support (9 ± 4 hr^{-1} over Pt/ γ-Al_2O_3) at comparable reaction conditions. The observed activity over Pt/γ-Al_2O_3 is attributed to the activity of the platinum in the catalyst, the active phase. While the activity obtained from the Pt/TiO_2 catalyst is contributed by both the active metal, Pt, and oxide support. It is thought that reducible metal oxide support facilitates the oxidation of benzyl alcohol oxidation through the formation of oxygen vacancy sites.

In the presence of H_2O solvent, the TOF for benzyl alcohol oxidation is improved to 80 ± 7 hr^{-1} over Pt/γ-Al_2O_3 catalyst. This improvement in TOF is ascribed to the promotional effects associated with the presence of H_2O, i.e., surface hydroxyl species formation. A more significant increase in TOF for benzyl alcohol oxidation over Pt/TiO_2 in the presence of water is observed to be 619 ± 18 hr^{-1}, i.e., 23-times faster than in a solvent-free system. Besides the reported promotional effect of H_2O, it is further suggested that there is a collaborative promotional effect between H_2O and reducible

support material during benzyl alcohol oxidation. It is thought that water as a solvent affects the formation of hydroxyl species on both the platinum surface and the surface of the reducible metal oxide support material. The interaction between adsorbed benzyl alkoxide and surface hydroxyl and lattice oxygen species on the support opens up an additional reaction channel increasing the rate of reaction.

The role of bismuth in alcohol oxidation was investigated over Pt-Bi/TiO_2 catalyst. It is concluded that bismuth has at least a dual promotional effect on alcohol oxidation. Semi in-situ XPS analysis of Pt-Bi/TiO_2 catalyst oxidation suggest that Bi oxidizes while the oxidation of the Pt moiety of the catalyst is negligible. As such, it postulated that the presence of bismuth may act as a co-catalyst assisting O_2 activation by forming bismuth oxide. The presence of H_2O in the bismuth oxide sites are thought to form Pt-Bi-OH sites, thus facilitating substrate activation. As a consequence, this may enhance the overall activity for benzyl alcohol oxidation. Moreover, it is proposed that the additional promotional effect observed for Bi in the benzyl alcohol oxidation involves stabilization through the interaction between Bi and the aromatic ring.

Significant parallelism in the role of these system parameters (H_2O, metal oxide support and an alloyed/mixed metal) on the mechanism of alcohol activation, consequently influencing the overall activity, is described in this work. The common theme in each parameter change that yields an enhancement in catalytic activity is thought to induce coordination of the substrate while adsorbing on the Pt surface through the lone pair of the oxygen atom of the alcohol substrate and the subsequent formation of surface OH species on the catalyst (whether Pt surface, alloy surface or metal oxide support surface). These mechanistic occurrences assist in the dehydrogenation of the alcohol functional group of the substrate. Importantly, the presence of surface OH species enhances the activity (either measured using TOF or platinum-time-yield, PTY) for alcohol oxidation.

Besides evidencing these similarities in the role of these alcohol oxidation system components, some striking differences between these contributing factors propose different reaction pathways, which ultimately determines the conversion levels in each

system. This arises from the difference in reactivity behaviour of each system component. An illustrative example is the contrasting benzyl alcohol oxidation outcome between Pt-Bi/TO_2 and Pt-Ni/TiO_2 catalyst using molecular oxygen as an oxidant. Strong oxygen affinity of Bi may assist dissociation of oxygen, which consequently result in the availability of atomic oxygen on both surfaces, Pt and Bi surface. This then facilitates oxidation reaction thus, enhances benzyl alcohol conversion. While on the contrary, Pt-skin on a Pt-Ni alloy results in weak adsorption of molecular oxygen, thus limiting activation of oxygen and diminishing benzyl alcohol conversion.

It is, thus, concluded in this study that enhancement of catalytic activity is not only limited to the addition of a promoting element. Other reaction parameters that enhance green chemistry, such as H_2O and metal oxide support material, can be considered for an efficient alcohol oxidation reaction. Particularly, reaction parameters that subsequently promote the formation of surface OH species are considered to be essential for alcohol oxidation promotion.

9.2 THE NOVELTY OF THE STUDY

Although the promotional effects associated with the addition of H_2O solvent in liquid-phase benzyl alcohol oxidation have been noted in the literature, the general understanding of the precise role of H_2O in benzyl alcohol oxidation is still in its infancy. As such, this body of work extensively explored the influence of H_2O solvent in alcohol oxidation, taking into account LLE due to liquid separation (organic and aqueous liquid-phase). This thesis highlights that oxygen solubility cannot be attributed to the promotional effect of H_2O in benzyl alcohol oxidation. Rather the formation and the presence of surface hydroxyl species are highly probably for the observed enhancement in catalytic activity in the presence of H_2O.

Furthermore, very few attempts have been made to explore metal oxide support material beyond just dispersing active metal nanoparticles. The reducibility of metal oxide support is considered as an important parameter in this study, specifically suggesting that the formation of oxygen vacancy sites (from the removal of the lattice oxygen of the metal

oxide) and surface hydroxyl species may be a contributing factor for the observed difference in activity obtained over different metal oxide support materials.

9.3 FUTURE DIRECTIONS AND RECOMMENDATIONS

Following this study, the formation of the oxygen vacancy site on reducible oxide support during alcohol oxidation can be further investigated by using ^{18}O labelled oxygen feed as an oxidant. This will share some light on the transfer of oxygen atoms from the metal oxide support structure and the regeneration of these oxygen vacancies.

The adsorption and activation properties of O_2 and H_2O_2 of Pt_3Ni and/or PtNi surface can be further be investigated using DFT study, thus, its effect on alcohol oxidation. Importantly, the effect of an upward shift of the d-band centre of surface Pt atoms on oxygen adsorption and dissociation, ultimately benzyl alcohol oxidation using Pt_3Co alloy system, can be investigated.

Pt-Bi/TiO_2 catalyst showed a slight catalyst deactivation at 90 °C. As such, the cause and deactivation mechanism can be further investigated. Analysis of the spent catalyst to gain broader understanding of the deactivation mechanisms and guide reactivation protocols

References

1. Ali, M. E., Rahman, M. M. & Hamid, S. B. A. Nanoclustered Gold: A Promising Green Catalysts for the Oxidation of Alkyl Substituted Benzenes. *Adv. Mater. Res.* **925**, 38–42 (2014).

2. Parmeggiani, C., Matassini, C. & Cardona, F. A step forward towards sustainable aerobic alcohol oxidation: New and revised catalysts based on transition metals on solid supports. *Green Chem.* **19**, 2030–2050 (2017).

3. Xu, C., Zhang, C., Li, H., Zhao, X., Song, L. & Li, X. An Overview of Selective Oxidation of Alcohols: Catalysts, Oxidants and Reaction Mechanisms. *Catal. Surv. from Asia* **20**, 13–22 (2016).

4. Prati, L. & Porta, F. Oxidation of alcohols and sugars using Au/C catalysts: Part 1. Alcohols. *Appl. Catal. A Gen.* **291**, 199–203 (2005).

5. Tran, H. V., Doan, H. A., Chandler, B. D. & Grabow, L. C. Water-Assisted Oxygen Activation During Selective Oxidation Reactions oxidation reactions. *Curr. Opin. Chem. Eng.* **13**, 100–108 (2016).

6. Saavedra, J., Whittaker, T., Chen, Z., Pursell, C. J., Rioux, R. M. & Chandler, B. D. Controlling activity and selectivity using water in the Au-catalysed preferential oxidation of CO in H2. *Nat. Chem.* **8**, 584 (2016).

7. Viswanathan, V., Hansen, H. A., Rossmeisl, J. & Nørskov, J. K. Universality in oxygen reduction electrocatalysis on metal surfaces. *ACS Catal.* **2**, 1654–1660 (2012).

8. Qi, L. & Li, J. Adsorbate interactions on surface lead to a flattened Sabatier volcano plot in reduction of oxygen. *J. Catal.* **295**, 59–69 (2012).

9. Laguna, O. H., Centeno, M. A., Romero-Sarria, F. & Odriozola, J. A. Oxidation of CO over gold supported on Zn-modified ceria catalysts. *Catal. Today* **172**, 118–123 (2011).

10. Lam, E. & Luong, J. H. T. Carbon Materials as Catalyst Supports and Catalysts in the Transformation of Biomass to Fuels and Chemicals. *ACS Catal.* **4**, 3393–3410 (2014).

11. Puigdollers, A. R., Schlexer, P., Tosoni, S. & Pacchioni, G. Increasing oxide reducibility: The role of metal/oxide interfaces in the formation of oxygen vacancies. *ACS Catal.* **7**, 6493–6513 (2017).

12. Hu, Z., Zhou, G., Xu, L., Yang, J., Zhang, B. & Xiang, X. Preparation of ternary Pd/CeO 2 -nitrogen doped graphene composites as recyclable catalysts for solvent-free aerobic oxidation of benzyl alcohol. *Appl. Surf. Sci.* **471**, 852–861 (2019).

13. Abad, A., Concepción, P., Corma, A. & García, H. A collaborative effect between gold and a support induces the selective oxidation of alcohols. *Angew. Chemie - Int. Ed.* **44**, 4066–4069 (2005).

14. Ferri, D. & Baiker, A. Advances in infrared spectroscopy of catalytic solid-liquid interfaces: The case of selective alcohol oxidation. *Top. Catal.* **52**, 1323–1333 (2009).

15. Anderson, R., Griffin, K., Johnston, P. & Alsters, P. L. Selective Oxidation of Alcohols to Carbonyl Compounds and Carboxylic Acids with Platinum Group Metal Catalysts. *Adv. Synth. Catal.* **345**, 517–523 (2003).

16. Yang, L., Li, X., Chen, P. & Hou, Z. Selective oxidation of glycerol in a base-free aqueous solution: A short review. *Chinese J. Catal.* **40**, 1020–1034 (2019).

17. Ning, X., Li, Y., Yu, H., Peng, F., Wang, H. & Yang, Y. Promoting role of bismuth and antimony on Pt catalysts for the selective oxidation of glycerol to dihydroxyacetone. *J. Catal.* **335**, 95–104 (2016).

18. Che, J., Hao, M., Yi, W., Kobayashi, H., Zhou, Y., Xiao, L. & Fan, J. Selective suppression of toluene formation in solvent-free benzyl alcohol oxidation using supported Pd-Ni bimetallic nanoparticles. *Cuihua Xuebao/Chinese J. Catal.* **38**, 1870–1879 (2017).

19. Davies, P. R. On the Role of Water in Heterogeneous Catalysis : A Tribute to Professor M . Wyn Roberts. *Top. Catal.* **59**, 671–677 (2016).

20. Haruta, M. Moisture Effect on CO Oxidation over Au / TiO 2 Catalyst. *J. Catal.* **224**, 221–224 (2001).

21. Caporali, R., Chansai, S., Burch, R., Delgado, J. J., Goguet, A., Hardacre, C., Mantarosie, L. & Thompsett, D. Critical role of water in the direct oxidation of CO and hydrocarbons in diesel exhaust after treatment catalysis. *Appl. Catal. B, Environ.* **147**, 764–769 (2014).

22. Liu, S. P., Zhao, M., Sun, G. E., Gao, W. & Jiang, Q. Different effects of water molecules on CO oxidation with different reaction mechanisms. *Phys. Chem. Chem. Phys.* **20**, 8341–8348 (2018).

23. Dalai, A. K. & Davis, B. H. Fischer – Tropsch synthesis : A review of water effects

on the performances of unsupported and supported Co catalysts. *Appl. Catal. A Gen.* **348**, 1–15 (2008).

24. Tatsumi, H., Liu, F., Han, H., Carl, L. M., Sapi, A. & Somorjai, G. A. Alcohol Oxidation at Platinum − Gas and Platinum − Liquid Interfaces : The Effect of Platinum Nanoparticle Size , Water Coadsorption , and Alcohol Concentration. *J. Phys. Chem.* **121**, 7365–7371 (2017).

25. Frassoldati, A., Pinel, C. & Besson, M. Promoting effect of water for aliphatic primary and secondary alcohol oxidation over platinum catalysts in dioxane / aqueous solution media. *Catal. Today* **173**, 81–88 (2011).

26. Ribe, S. & Wipf, P. Water-accelerated organic transformations. *Chem. Commun.* 299–307 (2001).

27. Bergeld, J., Kasemo, B. & Chakarov, D. V. CO oxidation on Pt (1 1 1) promoted by coadsorbed H 2 O. *Surf. Sci.* **495**, L815–L820 (2001).

28. Zope, B. N., Hibbitts, D. D., Neurock, M. & Davis, R. J. Reactivity of the Gold/Water Interface During Selective Oxidation Catalysis. *Science (80).* **330**, 74–79 (2010).

29. Goldsmith, B. R., Hwang, T., Seritan, S., Peters, B. & Scott, S. L. Rate-Enhancing Roles of Water Molecules in Methyltrioxorhenium- Catalyzed Olefin Epoxidation by Hydrogen Peroxide. *J. Am. Chem. Soc* **137**, 9604–9616 (2015).

30. Lee, S., Molina, L. M., López, M. J., Alonso, J. A., Hammer, B., Lee, B., Seifert, S., Winans, R. E., Elam, J. W., Pellin, M. J. & Vajda, S. Selective propene epoxidation on immobilized Au(6-10) clusters: the effect of hydrogen and water on activity and selectivity. *Angew Chem Int Ed Engl* **48**, 1467–1471 (2009).

31. Uozumi, Y. & Nakao, R. Catalytic oxidation of alcohols in water under atmospheric oxygen by use of an amphiphilic resin-dispersion of a nanopalladium catalyst. *Angew. Chemie - Int. Ed.* **42**, 194–197 (2003).

32. Chang, C., Yang, X., Long, B. & Li, J. A Water-Promoted Mechanism of Alcohol Oxidation on a Au (111) Surface : Understanding the Catalytic Behavior of Bulk Gold. *ACS Catal.* **3**, 1693–1699 (2013).

33. Yang, X., Wang, X., Liang, C., Su, W., Wang, C., Feng, Z., Li, C. & Qiu, J. Aerobic oxidation of alcohols over Au/TiO2 : An insight on the promotion effect of water on the catalytic activity of Au/TiO2. *Catal. Commun.* **9**, 2278–2281 (2008).

34. Madala, T. Reaction pathways for the formation of hydrogen peroxide in fuel cells: - a DFT study. (University of Cape Town, 2013).

35. Gambu, G. T. A DFT study of the interaction of Ox with Pt nanorod edge sites : a model for the ORR activity on Pt nanoparticle edges. *University of Cape Town* (University of Cape Town, 2015).

36. Kluytmans, J., Markusse, A. & Kuster, B. Engineering aspects of the aqueous noble metal catalysed alcohol oxidation. *Catal. Today* **57**, 143–155 (2000).

37. Bongiorno, A. & Landman, U. Water-enhanced catalysis of CO oxidation on free and supported gold nanoclusters. *Phys. Rev. Lett.* **95**, (2005).

38. Sharma, R. V, Soni, K. K. & Dalai, A. K. Preparation, characterization and application of sulfated Ti-SBA-15 catalyst for oxidation of benzyl alcohol to benzaldehyde. *Catal. Commun.* **29**, 87–91 (2012).

39. Söderhjelm, E., House, M. P., Cruise, N., Holmberg, J., Bowker, M., Bovin, J. O. & Andersson, A. On the synergy effect in MoO3-Fe2(MoO 4)3 catalysts for methanol oxidation to formaldehyde. *Top. Catal.* **50**, 145–155 (2008).

40. Wachs, I. E. & Briand, L. E. In situ regeneration of metal molybdate catalyst for methanol oxidation to formaldehyde. (2000).

41. Soares, A. P. V., Farinha Portela, M., Kiennemann, A., Hilaire, L. & Millet, J. M. M. Iron molybdate catalysts for methanol to formaldehyde oxidation: Effects of Mo excess on catalytic behaviour. *Appl. Catal. A Gen.* **206**, 221–229 (2001).

42. Sohrabi, M. & Aghdasinia, H. Catalytic Oxidation of Methanol to Formaldehyde in a Continuous Fluidized-Bed Reactor. *Chem. Eng. Technol.* **26**, 69–73 (2003).

43. Yılmaz, A. H., Atalay, F. S. & Atalay, S. Catalytic Oxidation of Methanol to Formaldehyde BT - Sustainable Strategies for the Upgrading of Natural Gas: Fundamentals, Challenges, and Opportunities. in (eds. Derouane, E. G., Parmon, V., Lemos, F. & Ramôa Ribeiro, F.) 345–349 (Springer Netherlands, 2005).

44. Millar, G. J. & Collins, M. Industrial Production of Formaldehyde Using Polycrystalline Silver Catalyst. *Ind. Eng. Chem. Res.* **56**, 9247–9265 (2017).

45. Bronkema, J. L. & Bell, A. T. Mechanistic studies of methanol oxidation to formaldehyde on isolated vanadate sites supported on high surface area zirconia. *J. Phys. Chem. C* **112**, 6404–6412 (2008).

46. Dutta, D. K. Carbonylation of methanol to produce acetic acid : A versatile reaction to study. *J. Indian Soc.* **95**, 879–892 (2018).

47. Yoneda, N., Kusano, S., Yasui, M., Pujado, P. & Wilcher, S. Recent advaances in processes and catalysts for the prodcution of acetic acid. *Appl. Catal. A Gen.* **221**, 253–265 (2001).

48. Bauer, J. C.,Veith, G. M., Allard, L. F., Oyola, Y., Overbury, S. H. & Dai, S. Silica-Supported Au–CuOx Hybrid Nanocrystals as Active and Selective Catalysts for the Formation of Acetaldehyde from the Oxidation of Ethanol. *ACS Catal.* **2**, 2537–2546 (2012).

49. Redina, E. A., Greish, A., Redina, E. A., Greish, A. A., Mishin, I. V., Kapustin, G. I., Tkachenko, O. P., Kirichenko, O. A. & Kustov, L. M. Selective oxidation of ethanol to acetaldehyde over Au – Cu catalysts prepared by a redox method. *Catal. Today* **241**, 246–254 (2017).

50. Christensen, C. H., Jørgensen, B., Rass-Hansen, J., Egeblad, K., Madsen, R., Klitgaard, S. K., Hansen, S. M., Hansen, M. R., Andersen, H. C. & Riisager, A. Formation of Acetic Acid by Aqueous-Phase Oxidation of Ethanol with Air in the Presence of a Heterogeneous Gold Catalyst. *Angew. Chemie Int. Ed.* **45**, 4648–4651 (2006).

51. Takei, T., Iguchi, N. & Haruta, M. Synthesis of Acetoaldehyde, Acetic Acid, and Others by the Dehydrogenation and Oxidation of Ethanol. *Catal. Surv. from Asia* **15**, 80–88 (2011).

52. Sun, K. Q., Luo, S. W., Xu, N. & Xu, B. Q. Gold nano-size effect in Au/SiO2 for selective ethanol oxidation in aqueous solution. *Catal. Letters* **124**, 238–242 (2008).

53. Cheng, F., Dai, X., Wang, H., Jiang, S. P., Zhang, M. & Xu, C. Synergistic effect of Pd-Au bimetallic surfaces in Au-covered Pd nanowires studied for ethanol oxidation. *Electrochim. Acta* **55**, 2295–2298 (2010).

54. Jelemensky, L., Kuster, B. F. M. & Marin, G. B. Kinetic modelling of multiple steady-states for the oxidation of aqueous ethanol with oxygen on a carbon supported platinum catalyst. *Chem. Eng. Sci.* **51**, 1767–1776 (1996).

55. Mostrou, S., Nagl, A., Ranocchiari, M., Föttinger, K. & Van Bokhoven, J. A. The catalytic and radical mechanism for ethanol oxidation to acetic acid. *Chem. Commun.* **55**, 11833–11836 (2019).

56. Olivier, K. L. & Schaeffer, W. D. United States Patent Office. *ACM SIGGRAPH Computer Graphics* **28**, 131–134 (1994).

57. Ibrahim, S. Y. & Hassaballah, A. A. Production of Acetic Acid by Oxidation of Butane with Air Under High Pressure. *Pet. Sci. Technol.* **23**, 67–73 (2005).

58. Armstrong, G. P. & Millidge, A. F. United States Patent Office. *ACM SIGGRAPH Computer Graphics* **28**, 131–134 (1994).

59. Ciriminna, R., Fidalgo, A., Ilharco, L. M. & Pagliaro, M. Dihydroxyacetone: An Updated Insight into an Important Bioproduct. *ChemistryOpen* **7**, 233–236 (2018).

60. El Roz, A., Fongarland, P., Dumeignil, F. & Capron, M. Glycerol to glyceraldehyde oxidation reaction over Pt-based catalysts under base-free conditions. *Front. Chem.* **7**, 1–9 (2019).

61. Carrettin, S., McMorn, P. & Johnston, P. Oxidation of glycerol using supported Pt, Pd and Au catalysts. *Phys. Chem. Chem. Phys* **5**, 1329–1336 (2003).

62. Tongsakul, D., Nishimura, S. & Ebitani, K. Platinum / Gold Alloy Nanoparticles-Supported Hydrotalcite Catalyst for Selective Aerobic Oxidation of Polyols in Base-Free Aqueous Solution at Room Temperature. *ACS Catal.* **3**, 2199–2207 (2013).

63. Kimura, H., Tsuto, K., Wakisaka, T., Kazumi, Y. & Inaya, Y. Selective oxidation of glycerol on a platinum-bismuth catalyst. *Appl. Catal. A, Gen.* **96**, 217–228 (1993).

64. Garcia, A. C., Birdja, Y. Y., Tremiliosi-Filho, G. & Koper, M. T. M. Glycerol electro-oxidation on bismuth-modified platinum single crystals. *J. Catal.* **346**, 117–124 (2017).

65. Liu, L., Liu, Y., Li, J., Du, G. & Chen, J. Microbial production of hyaluronic acid: current state, challenges, and perspectives. *Microb. Cell Fact.* **10**, 99 (2011).

66. Chong, B. F., Blank, L. M., Mclaughlin, R. & Nielsen, L. K. Microbial hyaluronic acid production. *Appl. Microbiol. Biotechnol.* **66**, 341–351 (2005).

67. Amaniampong, P. N., Karam, A., Trinh, Q. T., Xu, K., Hirao, H., Jérôme, F. & Chatel, G. Selective and Catalyst-free Oxidation of D-Glucose to D-Glucuronic acid induced by High-Frequency Ultrasound. *Sci. Rep.* **7**, 1–8 (2017).

68. Cocchiara, J., Letizia, C. S., Lalko, J., Lapczynski, A. & Api, A. M. Fragrance material review on cinnamaldehyde. *Food Chem. Toxicol.* **43**, 867–923 (2005).

69. Lee, A. F., Gee, J. J. & Theyers, H. J. Aspects of allylic alcohol oxidation — a bimetallic heterogeneous selective oxidation catalyst. *Green Chem.* **2**, 279–282 (2000).

70. Balcha, T., Strobl, J. R., Fowler, C., Dash, P. & Scott, R. W. J. Selective Aerobic Oxidation of Crotyl Alcohol Using AuPd Core-Shell Nanoparticles. *ACS Catal.* **1**, 425–436 (2011).

71. Corma, A. & Garcia, H. Supported gold nanoparticles as catalysts for organic reactions. *Chem. Soc. Rev.* **37**, 2096–2126 (2008).

72. Liu, X., Madix, R. J. & Friend, C. M. Unraveling molecular transformations on surfaces: a critical comparison of oxidation reactions on coinage metals. *Chem. Soc. Rev.* **37**, 2243–2261 (2008).

73. Ogliaruso, M. A. & Wolfe, J. F. Comprehensive Organic Functional Group Transformations. in *Chemistry, Molecular Sciences and Chemical Engineering* (eds. Katritzky, A. R., Meth-Cohn, O. & Rees, C. W. B. T.-C. O. F. G. T.) 23–120 (Elsevier Science, 1995).

74. Wu, G., Brett, G., Cao, E., Constantinou, A., Ellis, P., Kuhn, S., Hutchings, G. J., Bethell, D. & Gavriilidis, A. Oxidation of cinnamyl alcohol using bimetallic continuous flow packed bed microreactor. *Catal. Sci. Technol.* **6**, 4749–4758 (2016).

75. Chan-Thaw, C. E., Savara, A. & Villa, A. Selective benzyl alcohol oxidation over Pd catalysts. *Catalysts* **8**, 1–21 (2018).

76. Zhu, J., Faria, J. L., Figueiredo, J. L. & Thomas, A. Reaction mechanism of aerobic oxidation of alcohols conducted on activated-carbon-supported cobalt oxide catalysts. *Chem. - A Eur. J.* **17**, 7112–7117 (2011).

77. Narayanan, S., Judith Vijaya, J., Sivasanker, S., John Kennedy, L. & Ariharan, A. Enhanced selectivity to benzaldehyde in the liquid phase oxidation of benzyl alcohol using nanocrystalline ZSM-5 zeolite catalyst. *J. Porous Mater.* **21**, 633–641 (2014).

78. Kumar, A., Kumar, V. P., Srikanth, A., Vishwanathan, V. & Chary, K. V. R. Vapor Phase Oxidation of Benzyl Alcohol over Nano Au/SBA-15 Catalysts: Effect of Preparation Methods. *Catal. Letters* **146**, 35–46 (2016).

79. Ali, M. E., Rahman, M. M. & Hamid, S. B. A. Nanoclustered Gold: A Promising Green Catalysts for the Oxidation of Alkyl Substituted Benzenes. *Adv. Mater. Res.* **925**, 38–42 (2014).

80. Waitkins, G. R. & Clark, C. W. Selenium dioxide: Preparation, properties, and use as oxidizing agent. *Chem. Rev.* **36**, 235–289 (1945).

81. Choudhary, V. R., Chaudhari, P. A. & Narkhede, V. S. Solvent-free liquid phase oxidation of benzyl alcohol to benzaldehyde by molecular oxygen using non-noble transition metal containing hydrotalcite-like solid catalysts. *Catal. Commun.* **4**, 171–175 (2003).

82. Liu, J., Zou, S., Wu, J., Kobayashi, H., Zhao, H. & Fan, J. Green catalytic oxidation of benzyl alcohol over Pt/ZnO in base - free aqueous medium at room temperature. *Chinese J. Catal.* **39**, 1081–1089 (2018).

83. Hughes, M. D., Xu, Y. J., Jenkins, P., McMorn, P., Landon, P., Enache, D. I., Carley, A. F., Attard, G. A., Hutchings, G. J., King, F., Stitt, E. H., Johnston, P., Griffin, K. & Kiely, C. J. Tunable gold catalysts for selective hydrocarbon oxidation under mild conditions. *Nature* **437**, 1132–1135 (2005).

84. Yadav, G. D. & Mewada, R. K. Chemical Engineering Research and Design Selectivity engineering in the synthesis of value added chemicals : Oxidation of 1-octanol to 1-octanal over nano-fibrous Ag – OMS-2 catalysts. *Chem. Eng. Res. Des.* **0**, 86–97 (2011).

85. Sato, T. & Komanoya, T. Selective oxidation of alcohols with molecular oxygen catalyzed by Ru / MnOx/CeO2 under mild conditions. *Catal. Commun.* **10**, 1095–1098 (2009).

86. Chern, C., Tseng, C., Hsiao, R., Wong, F. F. & Kuo, Y. Cyclopentadienyl Ruthenium (II) Complex-Mediated Oxidation of Benzylic and Allylic Alcohols to Corresponding Aldehydes. *Heteroat. Chem.* **2019**, (2019).

87. Savara, A., Chan-Thaw, C. E., Rossetti, I., Villa, A. & Prati, L. Benzyl Alcohol Oxidation on Carbon-Supported Pd Nanoparticles: Elucidating the Reaction Mechanism. *ChemCatChem* **6**, 3464–3473 (2014).

88. Chibani, S., Michel, C., Pinel, C. & Online, V. A. On the key role of hydroxyl groups in platinum-catalysed alcohol oxidation in aqueous medium. *Catal. Sci. Technol.* **3**, 339–350 (2013).

89. Abad, A., Corma, A. & Hermenegildo, G. Catalyst Parameters Determining Activity and Selectivity of Supported Gold Nanoparticles for the Aerobic Oxidation of Alcohols : The Molecular Reaction Mechanism. *Chem. A Eur. J.* **14**, 212–222 (2008).

90. Davis, S. E., Ide, M. S. & Davis, R. J. Selective oxidation of alcohols and aldehydes over supported metal nanoparticles. *Green Chem.* **15**, 17–45 (2013).

91. Smits, P. C. C., Kuster, B. F. M., van der Wiele, K. & van der Baan, H. S. The selective oxidation of aldoses and aldonic acids to 2-ketoaldonic acids with lead-modified platinum-on-carbon catalysts. *Carbohydr. Res.* **153**, 227–235 (1986).

92. Eichler, A. & Hafner, J. Molecular Precursors in the Dissociative Adsorption of O2 on Pt(111). *Phys. Rev. Lett.* **79**, 4481–4484 (1997).

93. Ford, D. C., Nilekar, A. U., Xu, Y. & Mavrikakis, M. Partial and complete reduction of O2 by hydrogen on transition metal surfaces. *Surf. Sci.* **604**, 1565–1575 (2010).

94. Li, X., Heryadi, D. & Gewirth, A. A. Electroreduction Activity of Hydrogen Peroxide on Pt and Au Electrodes. *Langmuir* **21**, 9251–9259 (2005).

95. Fratesi, G., Gava, P. & Gironcoli, S. de. Direct methane-to-methanol conversion: Insight from first-principles calculations. *J. Phys. Chem. C* **111**, 17015–17019 (2007).

96. Palkovits, R., Antonietti, M., Kuhn, P., Thomas, A. & Schüth, F. Solid catalysts for the selective low-temperature oxidation of methane to methanol. *Angew. Chem. Int. Ed. Engl.* **48**, 6909–12 (2009).

97. Besson, M. & Gallezot, P. Selective oxidation of alcohols and aldehydes on metal catalysts. *Catal. Today* **57**, 127–141 (2000).

98. Mori, K., Hara, T. & Mizugaki, T. Hydroxyapatite-supported palladium nanoclusters: a highly active heterogeneous catalyst for selective oxidation of alcohols by use of molecular oxygen. *J. Am. Chem. Soc* **126**, 10657–10666 (2004).

99. Bronnimann, C., Bodnar, Z., Hug, P., Mallat, T. & Baiker, A. Direct oxidation of L-sorbose to 2-keto-L-gulonic acid with molecular oxygen on platinum-and palladium-based catalysts. *J. Catal.* **150**, 199–211 (1994).

100. Bianchini, C. & Shen, P. Palladium-based electrocatalysts for alcohol oxidation in half cells and in direct alcohol fuel cells. *Chem. Rev.* **109**, 4183–4206 (2009).

101. Zhou, G., Gui, B., Xie, H., Yang, F., Chen, Y., Chen, S. & Zheng, X. Influence of CeO2 morphology on the catalytic oxidation of ethanol in air. *J. Ind. Eng. Chem.* **20**, 160–165 (2014).

102. Akbari, A., Hakimi, M., Hassani, H. & Vahedi, H. Oxidation of Some Alcohols to the Corresponding Carbonyl Derivatives Using the H 3 PW 12 O 40 HeteropolyAcid as Catalyst. *Int. J. ChemTech Res.* **4**, 729–732 (2012).

103. Hackett, S. & Brydson, R. High-Activity, Single-Site Mesoporous Pd/Al2O3 Catalysts for Selective Aerobic Oxidation of Allylic Alcohols. *Angew. Chem. Int. Ed.* **46**, 8593 –8596 (2007).

104. Mallat, T., Bodnar, Z., Baiker, A. & Greis, O. Preparation of promoted platinum catalysts of designed geometry and the role of promoters in the liquid-phase oxidation of 1-methoxy-2-propanol. *J. Catal.* **142**, 237–253 (1993).

105. Wu, P., Cao, Y., Zhao, L., Wang, Y., He, Z., Xing, W., Bai, P., Mintova, S. & Yan, Z. Formation of PdO on Au–Pd bimetallic catalysts and the effect on benzyl alcohol oxidation. *J. Catal.* **375**, 32–43 (2019).

106. Mondelli, C., Ferri, D., Grunwaldt, J. D., Krumeich, F., Mangold, S., Psaro, R. & Baiker, A. Combined liquid-phase ATR-IR and XAS study of the Bi-promotion in the aerobic oxidation of benzyl alcohol over Pd/Al2O3. *J. Catal.* **252**, 77–87 (2007).

107. Bond, G. C. & Thompson, D. T. Catalysis by Gold. *Catal. Rev. -Science Eng.* **41**, 319–388 (1999).

108. Prati, L. & Rossi, M. Gold on carbon as a new catalyst for selective liquid phase oxidation of diols. *J. Catal.* **176**, 552–560 (1998).

109. Bianchi, C., Porta, F., Prati, L. & Rossi, M. Selective liquid phase oxidation using gold catalysts. *Top. Catal.* **13**, 231–236 (2000).

110. Carrettin, S., McMorn, P., Johnston, P., Griffin, K. & Hutchings, G. J. Selective oxidation of glycerol to glyceric acid using a gold catalyst in aqueous sodium hydroxide. *Chem. Commun.* 696–697 (2002). doi:10.1039/B201112N

111. Roldán, A., González, S., Ricart, J. M. & Illas, F. Critical Size for O2 Dissociation by Au Nanoparticles. *ChemPhysChem* **10**, 348–351 (2009).

112. Zhang, C., Wang, T., Liu, X. & Ding, Y. Selective oxidation of glycerol to lactic acid over activated carbon supported Pt catalyst in alkaline solution. *Chinese J. Catal.* **37**, 502–509 (2016).

113. Gangwal, V. R., Schaaf, J. Van Der, Kuster, B. F. M. & Schouten, J. C. Influence of

pH on noble metal catalysed alcohol oxidation : reaction kinetics and modelling. *J. Catal.* **229**, 389–403 (2005).

114. Saliger, R., Decker, N. & Prüße, U. D-Glucose oxidation with H2O2 on an Au/Al2O3 catalyst. *Appl. Catal. B Environ.* **102**, 584–589 (2011).

115. de Wilt, H. G. J. Part I. Oxidation of Glucose to Gluconic Acid. Survey of Techniques. *Ind. Eng. Chem. Prod. Res. Dev.* **11**, 370–373 (1972).

116. de Wilt, H. G. J. & van der Baan, H. S. Part II. Oxidation of Glucose to K-Gluconate. Platinum-Catalyzed Oxidation with Oxygen in Aqueous Alkaline Solutions. *Ind. Eng. Chem. Prod. Res. Dev.* **11**, 374–378 (1972).

117. Önal, Y., Schimpf, S. & Claus, P. Structure sensitivity and kinetics of D-glucose oxidation to D-gluconic acid over carbon-supported gold catalysts. *J. Catal.* **223**, 122–133 (2004).

118. Ishida, T., Watanabe, H., Bebeko, T., Akita, T. & Haruta, M. Aerobic oxidation of glucose over gold nanoparticles deposited on cellulose. *Appl. Catal. A Gen.* **377**, 42–46 (2010).

119. Delidovich, I. V., Moroz, B. L., Taran, O. P., Gromov, N. V., Pyrjaev, P. A., Prosvirin, I. P., Bukhtiyarov, V. I. & Parmon, V. N. Aerobic selective oxidation of glucose to gluconate catalyzed by Au/Al2O3 and Au/C: Impact of the mass-transfer processes on the overall kinetics. *Chem. Eng. J.* **223**, 921–931 (2013).

120. Zhang, H. & Toshima, N. Synthesis of Au/Pt bimetallic nanoparticles with a Pt-rich shell and their high catalytic activities for aerobic glucose oxidation. *J. Colloid Interface Sci.* **394**, 166–176 (2013).

121. Hermans, S., Deffernez, A. & Devillers, M. Au-Pd/C catalysts for glyoxal and glucose selective oxidations. *Appl. Catal. A Gen.* **395**, 19–27 (2011).

122. Bujak, P., Bartczak, P. & Polanski, J. Highly efficient room-temperature oxidation of cyclohexene and d-glucose over nanogold Au/SiO2 in water. *J. Catal.* **295**, 15–21 (2012).

123. Karski, S. & Witońska, I. Bismuth as an additive modifying the selectivity of palladium catalysts. *J. Mol. Catal. A Chem.* **191**, 87–92 (2003).

124. Zhou, C., Guo, Z., Dai, Y., Jia, X., Yu, H. & Yang, Y. Promoting role of bismuth on carbon nanotube supported platinum catalysts in aqueous phase aerobic oxidation of benzyl alcohol. *"Applied Catal. B, Environ.* **181**, 118–126 (2016).

125. Fordham, P., Besson, M. & Gallezot, P. Catalytic oxidation with air of tartronic acid to mesoxalic acid on bismuth-promoted platinum. **46**, 195–199 (1997).

126. de Souza, M. B. C., Yukuhiro, V. Y., Vicente, R. A., Vilela Menegaz Teixeira Pires,

C. T. G., Bott-Neto, J. L. & Fernández, P. S. Pb- and Bi-Modified Pt Electrodes toward Glycerol Electrooxidation in Alkaline Media. Activity, Selectivity, and the Importance of the Pt Atoms Arrangement. *ACS Catal.* **10**, 2131–2137 (2020).

127. Xu, C., Zhang, L., An, Y., Wang, X., Xu, G., Chen, Y. & Dai, L. Promotional synergistic effect of Sn doping into a novel bimetallic Sn-W oxides/graphene catalyst for selective oxidation of alcohols using aqueous H2O2 without additives. *Appl. Catal. A , Gen.* **558**, 26–33 (2018).

128. Mallat, T. & Baiker, A. Oxidation of alcohols with molecular oxygen on solid catalysts. *Chem. Rev.* **104**, 3037–3058 (2004).

129. Keresszegi, C., Grunwaldt, J. D., Mallat, T. & Baiker, A. Liquid phase oxidation of alcohols with oxygen: In situ monitoring of the oxidation state of Bi-promoted Pd/al2O3. *Chem. Commun.* **9**, 2304–2305 (2003).

130. Keresszegi, C., Grunwaldt, J. D., Mallat, T. & Baiker, A. In situ EXAFS study on the oxidation state of Pd/Al2O 3 and Bi-Pd/Al2O3 during the liquid-phase oxidation of 1-phenylethanol. *J. Catal.* **222**, 268–280 (2004).

131. Mondelli, C., Grunwaldt, J., Ferri, D. & Baiker, A. Role of Bi promotion and solvent in platinum-catalyzed alcohol oxidation probed by in situ X-ray absorption and ATR-IR spectroscopy. *Phys. Chem. Chem. Phys* **12**, 5307–5315 (2010).

132. Besson, M., Flèche, G., Fuertes, P., Gallezot, P. & Lahmer, F. Oxidation of glucose and gluconate on Pt, Pt Bi, and Pt Au catalysts. *Recl. des Trav. Chim. des Pays-Bas* **115**, 217–221 (1996).

133. Zhang, W., Xiao, Z., Wang, J., Fu, W., Tan, R. & Yin, D. Selective Aerobic Oxidation of Alcohols over Gold-Palladium Alloy Catalysts Using Air at Atmospheric Pressure in Water. *ChemCatChem* **11**, 1779–1788 (2019).

134. Mounguengui-Diallo, M., Vermersch, F., Perret, N., Pinel, C. & Besson, M. Base free oxidation of 1,6-hexanediol to adipic acid over supported noble metal mono- and bimetallic catalysts. *Appl. Catal. A Gen.* **551**, 88–97 (2018).

135. Dimitratos, N., Villa, A., Wang, D., Porta, F., Su, D. & Prati, L. Pd and Pt catalysts modified by alloying with Au in the selective oxidation of alcohols. *J. Catal.* **244**, 113–121 (2006).

136. Zhang, C., Wang, T. & Ding, Y. One-step synthesis of pyruvic acid from glycerol oxidation over Pb promoted Pt/activated carbon catalysts. *Chinese J. Catal.* **38**, 928–937 (2017).

137. Tang, C., Zhang, N., Shao, Q., Huang, X. & Xiao, X. Rational design of ordered Pd-Pb nanocubes as highly active, selective and durable catalysts for solvent-free benzyl alcohol oxidation. *Nanoscale* **11**, 5145–5150 (2019).

138. Mallat, T. & Baiker, A. Liquid-phase oxidation of 1-methoxy-2-propanol with air. I. Lead and bismuth promotion and deactivation of palladium catalysts. *Appl. Catal. A, Gen.* **79**, 41–58 (1991).

139. Kim, Y. S., Jeon, S. H., Bostwick, A., Rotenberg, E., Ross, P. N., Stamenkovic, V. R., Markovic, N. M., Noh, T. W., Han, S. & Mun, B. S. Role of transition metal in fast oxidation reaction on the Pt3TM (111) (TM = Ni, Co) surfaces. *Adv. Energy Mater.* **3**, 1257–1261 (2013).

140. Iglesia, E. Design, synthesis, and use of cobalt-based Fischer-Tropsch synthesis catalysts. *Appl. Catal. A Gen.* **161**, 59–78 (1997).

141. De Beer, M., Kunene, A., Nabaho, D., Claeys, M. & Van Steen, E. Technical and economic aspects of promotion of cobalt-based Fischer-Tropsch catalysts by noble metals-a review. *J. South. African Inst. Min. Metall.* **114**, (2014).

142. Bezemer, G. L., Bitter, J. H., Kuipers, H. P. C. E., Oosterbeek, H., Holewijn, J. E., Xu, X., Kapteijn, F., van Dillen, A. J. & de Jong, K. P. Cobalt Particle Size Effects in the Fischer−Tropsch Reaction Studied with Carbon Nanofiber Supported Catalysts. *J. Am. Chem. Soc.* **128**, 3956–3964 (2006).

143. Rotan, M., Rytter, E., Einarsrud, M. & Grande, T. Solid state mechanism leading to enhanced attrition resistance of alumina based catalyst supports for Fischer – Tropsch synthesis. *J. Eur. Ceram. Soc.* **33**, 1–6 (2013).

144. Qi, B., Wang, Y., Lou, L. L., Yang, Y. & Liu, S. Solvent-free aerobic oxidation of benzyl alcohol over palladium catalysts supported on MnOx prepared using an adsorption method. *React. Kinet. Mech. Catal.* **108**, 519–529 (2013).

145. Hong, Y., Yan, X., Liao, X., Li, R., Xu, S., Xiao, L. & Fan, J. Platinum nanoparticles supported on Ca(Mg)-zeolites for efficient room-temperature alcohol oxidation under aqueous conditions. *Chem. Commun.* **50**, 9679–9682 (2014).

146. Chen, J., Zhang, Q., Wang, Y. & Wan, H. Size-Dependent Catalytic Activity of Supported Palladium Nanoparticles for Aerobic Oxidation of Alcohols. *Adv. Synth. Catal.* **350**, 453–464 (2008).

147. Zhao, G., Yang, F., Chen, Z., Liu, Q., Ji, Y., Zhang, Y., Niu, Z., Mao, J., Bao, X., Hu, P. & Li, Y. Metal/oxide interfacial effects on the selective oxidation of primary alcohols. *Nat. Commun.* **8**, 1–8 (2017).

148. Mori, S., Takubo, M., Makida, K., Yanase, T., Aoyagi, S., Maegawa, T., Monguchi, Y. & Sajiki, H. A simple and efficient oxidation of alcohols with ruthenium on carbon. *Chem. Commun.* **34**, 5159–5161 (2009).

149. Helali, Z., Jedidi, A., Syzgantseva, O. A., Calatayud, M. & Minot, C. Scaling reducibility of metal oxides. *Theor. Chem. Acc.* **136**, 100 (2017).

150. Skupien, E., Berger, R. J., Santos, V. P., Gascon, J., Makkee, M., Kreutzer, M. T., Kooyman, P. J., Moulijn, J. A. & Kapteijn, F. Inhibition of a Gold-Based Catalyst in Benzyl Alcohol Oxidation: Understanding and Remediation. *Catalysts* **4**, 89–115 (2014).

151. Villa, A., Wang, D., Dimitratos, N., Su, D., Trevisan, V. & Prati, L. Pd on carbon nanotubes for liquid phase alcohol oxidation. *Catal. Today* **150**, 8–15 (2010).

152. Donze, C., Korovchenko, P. & Gallezot, P. Aerobic selective oxidation of (hetero) aromatic primary alcohols to aldehydes or carboxylic acids over carbon supported platinum. *Appl. Catal. B Environ.* **70**, 621–629 (2007).

153. Zhang, J. & Fang, J. A general strategy for preparation of Pt 3d-transition metal (Co, Fe, Ni) nanocubes. *J. Am. Chem. Soc.* **131**, 18543–18547 (2009).

154. Zhang, J., Yang, H., Fang, J. & Zou, S. Synthesis and oxygen reduction activity of shape-controlled Pt3Ni nanopolyhedra. *Nano Lett.* **10**, 638–644 (2010).

155. Zhao, X., Di, Q., Li, M., Yang, Q., Zhang, Z., Guo, X., Fan, X., Deng, K., Chen, W., Zhang, J., Fang, J. & Quan, Z. Generalized Synthesis of Uniform Metal Nanoparticles Assisted with Tungsten Hexacarbonyl. *Chem. Mater.* **31**, 4325–4329 (2019).

156. Wu, J., Gross, A. & Yang, H. Shape and Composition-Controlled Platinum Alloy Nanocrystals Using Carbon Monoxide as Reducing Agent. *Nano Lett.* **11**, 798–802 (2011).

157. Wadsö, I. & Goldberg, R. N. Standards in isothermal microcalorimetry (IUPAC Technical Report). *Pure Appl. Chem.* **73**, 1625–1639 (2001).

158. Kresse, G. & Hafner, J. Ab initio molecular dynamics for liquid metals. *Phys. Rev. B* **47**, 558–561 (1993).

159. Kresse, G. & Furthmiiller, J. Efficiency of ab-initio total energy calculations for metals and semiconductors using a plane-wave basis set. *Comput. Mater. Sci.* **6**, 15–50 (1996).

160. Perdew, J. P., Burke, K. & Ernzerhof, M. Generalized Gradient Approximation Made Simple. *Phys. Rev. Lett.* **77**, 3865–3868 (1996).

161. Blöchl, P. E. Projector augmented-wave method. *Phys. Rev. B* **50**, 17953–17979 (1994).

162. Methfessel, M. & Paxton, A. T. High-precision Sampling for Brillouin-zone Integration in Metals. *Phys. Rev. B* **40**, 3616–3621 (1989).

163. Henkelman, G. & Jo, H. A climbing image nudged elastic band method for finding saddle points and minimum energy paths. *J. Chem. Phys.* **113**, 9901–9904 (2000).

164. Moseler, M. & Gumbsch, P. Structural Relaxation Made Simple ¨. *Phys. Rev. Lett.* **97**, 170201 (2006).

165. Wang, H., Wang, Q., Chen, C. & Xiong, Z. Liquid − Liquid Equilibria for the Ternary System Water + Benzyl Alcohol + Benzaldehyde at (303 . 2 to 343 . 2) K. *J. Chem. Eng. Data* **59**, 2805–2812 (2014).

166. Wang, H., Wang, Q., Xiong, Z. & Chen, C. Liquid − Liquid Equilibria for the Ternary System Water + Benzyl Alcohol + Methylbenzene at (303 . 2 to 343 . 2) K. *J. Chem. Eng. Data* **59**, 2045–2053 (2014).

167. Xie, J., Duan, P., Kaylor, N., Yin, K., Huang, B., Schmidt-Rohr, K. & Davis, R. J. Deactivation of supported Pt catalysts during alcohol oxidation elucidated by spectroscopic and kinetic analyses. *ACS Catal.* **7**, 6745–6756 (2017).

168. Jens. M., S., Thomas, M., Peter, R. & Aage, F. Liquid-liquid equilibrium data: Their retrieval, correlation and prediction Part II: Correlation. *Fluid Phase Equilib.* **3**, 47–382 (1979).

169. Lide, D. R. *CRC Handbook ofChemistry and Physics, Internet Version 2005*. (Boca Raton : CRC Press, ©2005, 2005).

170. Dias, A. M. A., Bonifácio, R. P., Marrucho, I. M., Pádua, A. A. H. & Costa Gomes, M. F. Solubility of oxygen in n-hexane and in n-perfluorohexane. Experimental determination and prediction by molecular simulation. *Phys. Chem. Chem. Phys.* **5**, 543–549 (2003).

171. Wu, X., Deng, Z., Yan, J., Zhang, Z., Zhang, F. & Zhang, Z. Experimental Investigation on the Solubility of Oxygen in Toluene and Acetic Acid. *Ind. Eng. Chem. Res.* **53**, 9932–9937 (2014).

172. Remaud, G., Debon, A. A., Martin, Y. L., Martin, G. G. & Martin, G. J. Authentication of Bitter Almond Oil and Cinnamon Oil: Application of the SNIF-NMR Method to Benzaldehyde. *J. Agric. Food Chem.* **45**, 4042–4048 (1997).

173. Poling, B. E., Thomson, G. H., Friend, D. G., Rowley, R. L. & Wilding, W. V. *Section 2: Physical and Chemical Data*. *Perry's Chemical Engineers' Handbook* (2007). doi:10.1036/0071511253

174. Shetti, V. N., Srinivas, D. & Ratnasamy, P. Ti-Oxo Radicals and Product Selectivity in Olefin Oxidations over Titanosilicate Molecular Sieves. *Zeitschrift für Phys. Chemie* **219**, 905–920 (2005).

175. Mittendorfer, F., Eichler, A. & Hafner, J. Molecular precursors in the dissociative adsorption of O2 on Ni(111). *Surf. Sci.* **433**, 756–760 (1999).

176. Yang, Z., Wang, J. & Yu, X. Density functional theory studies on the adsorption, diffusion and dissociation of O2 on Pt(111). *Phys. Lett. Sect. A Gen. At. Solid State*

Phys. **374**, 4713–4717 (2010).

177. Montemore, M. M., van Spronsen, M. A., Madix, R. J. & Friend, C. M. O2 Activation by Metal Surfaces: Implications for Bonding and Reactivity on Heterogeneous Catalysts. *Chem. Rev.* **118**, 2816–2862 (2018).

178. McEwen, J.-S., Bray, J. M., Wu, C. & Schneider, W. F. How low can you go? Minimum energy pathways for O2 dissociation on Pt(111). *Phys. Chem. Chem. Phys.* **14**, 16677–16685 (2012).

179. Weston, J. O., Miyamura, H., Yasukawa, T., Sutarma, D., Baker, C. A., Singh, P. K., Bravo-Sanchez, M., Sano, N., Cumpson, P. J., Ryabenkova, Y., Kobayashi, S. & Conte, M. Water as a catalytic switch in the oxidation of aryl alcohols by polymer incarcerated rhodium nanoparticles. *Catal. Sci. Technol.* **7**, 3985–3998 (2017).

180. Anderson, R., Griffin, K., Johnston, P. & Alsters, L. Selective Oxidation of Alcohols to Carbonyl Compounds and Carboxylic Acids with Platinum Group Metal Catalysts. *Adv. Synth. Catal.* **345**, 517–523 (2003).

181. Davey, W. P. Precision Measurements of the Lattice Constants of Twelve Common Metals. *Phys. Rev.* **25**, 753–761 (1925).

182. Lima, F. H. B., Salgado, J. R. C., Gonzalez, E. R. & Ticianelli, E. A. Electrocatalytic Properties of PtCo/C and PtNi/C alloys for the Oxygen Reduction Reaction in Alkaline Solution. *J. Electrochem. Soc.* **154**, A369 (2007).

183. Lucas, C. A., Cormack, M., Gallagher, M. E., Brownrigg, A., Thompson, P., Fowler, B., Gründer, Y., Roy, J., Stamenković, V. & Marković, N. M. From ultra-high vacuum to the electrochemical interface: X-ray scattering studies of model electrocatalysts. *Faraday Discuss.* **140**, 41–58 (2009).

184. Zhang, H., Zeng, Y., Cao, L., Yang, L., Fang, D., Yi, B. & Shao, Z. Enhanced electrocatalytic performance of ultrathin PtNi alloy nanowires for oxygen reduction reaction. *Front. Energy* **11**, 260–267 (2017).

185. Leteba, G. M., Mitchell, D. R. G., Levecque, P. B. J., Van Steen, E. & Lang, C. I. Topographical and compositional engineering of core-shell Ni@Pt ORR electro-catalysts. *RSC Adv.* **10**, 29268–29277 (2020).

186. Su, L., Jia, W., Li, C. M. & Lei, Y. Mechanisms for enhanced performance of platinum-based electrocatalysts in proton exchange membrane fuel cells. *ChemSusChem* **7**, 361–378 (2014).

187. Hammer, B. & Nørskov, J. K. B. T.-A. in C. Theoretical surface science and catalysis—calculations and concepts. in *Impact of Surface Science on Catalysis* **45**, 71–129 (Academic Press, 2000).

188. Stamenkovic, V. R., Fowler, B., Mun, B. S., Wang, G., Ross, P. N., Lucas, C. A. &

Markovic, N. M. Improved oxygen reduction activity on Pt3Ni(111) via increased surface site availability. *Science (80-.).* **315**, 493–497 (2007).

189. Xin, H. & Linic, S. Communications: Exceptions to the d-band model of chemisorption on metal surfaces: The dominant role of repulsion between adsorbate states and metal d-states. *J. Chem. Phys.* **132**, 221101 (2010).

190. Duan, Z. & Wang, G. A first principles study of oxygen reduction reaction on a Pt(111) surface modified by a subsurface transition metal M (M = Ni, Co, or Fe). *Phys. Chem. Chem. Phys.* **13**, 20178–20187 (2011).

191. Fischer, J. M., Mahlberg, D., Roman, T. & Groß, A. Water adsorption on bimetallic PtRu / Pt (111) surface alloys. *Proc. R. Soc. A* **472**, 20160618 (2016).

192. Galet, L., Patry, S. & Dodds, J. Determination of the wettability of powders by the Washburn capillary rise method with bed preparation by a centrifugal packing technique. *J. Colloid Interface Sci.* **346**, 470–475 (2010).

193. Kong, X., Hu, Y., Wang, X. & Pan, W. Effect of surface morphology on wettability conversion. *J. Adv. Ceram.* **5**, 284–290 (2016).

194. Cieśliński, J. T. & Krygier, K. A. Sessile droplet contact angle of water–Al2O3, water–TiO2 and water–Cu nanofluids. *Exp. Therm. Fluid Sci.* **59**, 258–263 (2014).

195. Fronzi, M., Assadi, M. H. N. & Hanaor, D. A. H. Theoretical insights into the hydrophobicity of low index CeO2 surfaces. *Appl. Surf. Sci.* **478**, 68–74 (2019).

196. Taguta, J., O'Connor, C. T. & McFadzean, B. The relationship between enthalpy of immersion and flotation response. *Colloids Surfaces A Physicochem. Eng. Asp.* **558**, 263–270 (2018).

197. Milonjic, S. K., Ruvarac, L. & Šušič, M. V. The heat of immersion of natural magnetite in aqueuous solutions. *Thermochim. Acta* **11**, 261–266 (1975).

198. Rempel, K. U., Williams-Jones, A. E. & Migdisov, A. A. The solubility of molybdenum dioxide and trioxide in HCl-bearing water vapour at 350 ° C and pressures up to 160 bars. *Geochim. Cosmochim. Acta* **72**, 3074–3083 (2008).

199. Guo, W. & Vlachos, D. G. Patched bimetallic surfaces are active catalysts for ammonia decomposition. *Nat. Commun.* **6**, 8619 (2015).

200. Govender, A., Mahomed, A. S. & Friedrich, H. B. Water: Friend or foe in catalytic hydrogenation? A case study using copper catalysts. *Catalysts* **8**, 1–12 (2018).

201. Bredow, T. & Jug, K. SINDO1 Study of Photocatalytic Formation and Reactions of OH Radicals at Anatase Particles. *J. Phys. Chem.* **99**, 285–291 (1995).

202. Parfitt, G. D. Surface chemistry of oxides. *Pure Appl. Chem.* **48**, 415–418 (1977).

203. Glorius, M., Markovits, M. A. C. & Breitkopf, C. Design of specific acid-base-properties in CeO2-ZrO2-mixed oxides via templating and Au modification. *Catalysts* **8**, 358–383 (2018).

204. Schuh, K., Kleist, W., Høj, M., Jensen, A. D., Beato, P., Patzke, G. R. & Grunwaldt, J. D. Systematic study on the influence of the morphology of α-MoO3 in the selective oxidation of propylene. *J. Solid State Chem.* **228**, 42–52 (2015).

205. Monti, D. A. M. & Baiker, A. Temperature-programmed reduction. Parametric sensitivity and estimation of kinetic parameters. *J. Catal.* **83**, 323–335 (1983).

206. Santen, R. A. Van, Tranca, I. & Hensen, E. J. M. Theory of surface chemistry and reactivity of reducible oxides. *Catal. Today* **244**, 63–84 (2015).

207. Hinuma, Y., Toyao, T., Kamachi, T., Maeno, Z., Takakusagi, S., Furukawa, S., Takigawa, I. & Shimizu, K. I. Density Functional Theory Calculations of Oxygen Vacancy Formation and Subsequent Molecular Adsorption on Oxide Surfaces. *J. Phys. Chem. C* **122**, 29435–29444 (2018).

208. Ovcharenko, R., Voloshina, E. & Sauer, J. Water adsorption and O-defect formation on Fe2O3(0001) surfaces. *Phys. Chem. Chem. Phys.* **18**, 25560–25568 (2016).

209. Li, H., Guo, Y. & Robertson, J. Calculation of TiO2 Surface and Subsurface Oxygen Vacancy by the Screened Exchange Functional. *J. Phys. Chem. C* **119**, 18160–18166 (2015).

210. Mayernick, A. D. & Janik, M. J. Methane activation and oxygen vacancy formation over CeO2 and Zr, Pd substituted CeO2 surfaces. *J. Phys. Chem. C* **112**, 14955–14964 (2008).

211. Agarwal, V. & Metiu, H. Energy of Oxygen-Vacancy Formation on Oxide Surfaces: Role of the Spatial Distribution. *J. Phys. Chem. C* **120**, 2320–2323 (2016).

212. Jian, W., Wang, S.-P., Zhang, H.-X. & Bai, F. Q. Disentangling the role of oxygen vacancies on the surface of Fe3O4 and γ-Fe2O3. *Inorg. Chem. Front.* **6**, 2660–2666 (2019).

213. Martinez-Casado, R., Mallia, G., Harrison, N. M. & Pérez, R. First-Principles Study of the Water Adsorption on Anatase(101) as a Function of the Coverage. *J. Phys. Chem. C* **122**, 20736–20744 (2018).

214. Digne, M., Sautet, P., Raybaud, P., Euzen, P. & Toulhoat, H. Use of DFT to achieve a rational understanding of acid-basic properties of γ-alumina surfaces. *J. Catal.* **226**, 54–68 (2004).

215. Fronzi, M., Piccinin, S., Delley, B., Traversa, E. & Stampfl, C. Water adsorption on the stoichiometric and reduced CeO2(111) surface: A first-principles investigation. *Phys. Chem*. Chem. Phys. **11**, 9188–9199 (2009).

216. Head, A. R., Gattinoni, C., Trotochaud, L., Yu, Y., Karslloğlu, O., Pletincx, S., Eichhorn, B. & Bluhm, H. Water (Non-)Interaction with MoO3. *J. Phys. Chem. C* **123**, 16836–16842 (2019).

217. Ntallis, N., Peyre, V., Perzynski, R., Dubois, E. & Trohidou, K. N. disentangling the role of oxygen vacancies on the surface of FeO4 and. *J. Magn. Magn. Mater.* **484**, 74–82 (2019).

218. Tilocca, A. & Selloni, A. Structure and Reactivity of Water Layers on Defect-Free and Defective Anatase TiO2(101) Surfaces. *J. Phys. Chem. B* **108**, 4743–4751 (2004).

219. Zhuravlev, N. N. & Kertes, L. Structure of Superconductors. XI Investigation of Alloys of Bismuth with Platinum, Ruthenium, Osmium and Iridium. *Sov. Phys. JETP* **5**, 1073–1078 (1957).

220. Ahila, M., Malligavathy, M., Subramanian, E. & Pathinettam Padiyan, D. Effect of anodization time on the growth of twinned pyramid crystals of bismite from polyhedral bismuth particle by facile electrolysis-based oxidation. *Part. Sci. Technol.* **36**, 655–659 (2018).

221. Zhu, H., Zhou, W. & Yarmo, J. A. The growth of bismuth on Bi2Se3 and the stability of the first bilayer. *Thin Solid Films* **660**, 343–352 (2018).

222. Hofmann, P. The surfaces of bismuth : Structural and electronic properties. *Prog. Surf. Sci.* **81**, 191–245 (2006).

223. Xiao, Y., Wang, Y. & Varma, A. Low-temperature selective oxidation of methanol over Pt-Bi bimetallic catalysts. *J. Catal.* **363**, 144–153 (2018).

224. Nie, R., Liang, D., Shen, L., Gao, J., Chen, P. & Hou, Z. Selective oxidation of glycerol with oxygen in base-free solution over MWCNTs supported PtSb alloy nanoparticles. *Appl. Catal. B Environ.* **127**, 212–220 (2012).

225. Robinson, A. M., Mark, L., Rasmussen, M. J., Hensley, J. E. & Medlin, J. W. Surface Chemistry of Aromatic Reactants on Pt- and Mo-Modified Pt Catalysts. *J. Phys. Chem. C* **120**, 26824–26833 (2016).

226. Akinola, J., Barth, I., Goldsmith, B. R. & Singh, N. Adsorption Energies of Oxygenated Aromatics and Organics on Rhodium and Platinum in Aqueous Phase. *ACS Catal.* **10**, 4929–4941 (2020).

227. Tereshchuk, P. & Da Silva, J. L. F. Ethanol and Water Adsorption on Close-Packed 3d, 4d, and 5d Transition-Metal Surfaces: A Density Functional Theory Investigation with van der Waals Correction. *J. Phys. Chem. C* **116**, 24695–24705 (2012).

228. Freire, R. L. H., Kiejna, A. & Da Silva, J. L. F. Adsorption of water and ethanol on

noble and transition-metal substrates: a density functional investigation within van der Waals corrections. *Phys. Chem. Chem. Phys.* **18**, 29526–29536 (2016).

229. Frostemark, F., Bengtsson, L. A. & Holmberg, B. Formation and structure of mono- and di-bismuth hydroxide and fluoride complexes in molten NH4NO3· 1.5H2O at 50 °C. *J. Chem. Soc. Faraday Trans.* **90**, 2401–2412 (1994).

230. Alcalá, R., Mavrikakis, M. & Dumesic, J. A. DFT studies for cleavage of C-C and C-O bonds in surface species derived from ethanol on Pt(111). *J. Catal.* **218**, 178–190 (2003).

231. Diehl, F., Barbier, J., Duprez, D., Guibard, I. & Mabilon, G. Applied Catalysis B : Environmental Catalytic oxidation of heavy hydrocarbons over Pt / Al 2 O 3 . Influence of the structure of the molecule on its reactivity. *"Applied Catal. B, Environ.* **95**, 217–227 (2010).

232. Boronat, M. & Corma, A. Molecular approaches to catalysis: Naked gold nanoparticles as quasi-molecular catalysts for green processes. *J. Catal.* **284**, 138–147 (2011).

233. Della Pina, C., Falletta, E., Prati, L. & Rossi, M. Selective oxidation using gold. *Chem. Soc. Rev.* **37**, 2077–2095 (2008).

234. Tsukuda, T., Tsunoyama, H. & Sakurai, H. Aerobic Oxidations Catalyzed by Colloidal Nanogold. *Chem. – An Asian J.* **6**, 736–748 (2011).

235. Göksu, H., Burhan, H., Mustafov, S. D. & Fatih, Ş. Oxidation of Benzyl Alcohol Compounds in the Presence of Carbon Hybrid Supported Platinum Nanoparticles (Pt @ CHs) in Oxygen Atmosphere. *Sci. Rep.* **10**, 5439–5447 (2020).

236. Ojifinni, R. A., Froemming, N. S., Gong, J., Pan, M., Kim, T. S., White, J. M., Henkelman, G. & Mullins, C. B. Water-Enhanced Low-Temperature CO Oxidation and Isotope Effects on Atomic Oxygen-Covered Au(111). *J. Am. Chem. Soc.* **130**, 6801–6812 (2008).

237. Liu, L. M., McAllister, B., Ye, H. Q. & Hu, P. Identifying an O2 Supply Pathway in CO Oxidation on Au/TiO2(110): A Density Functional Theory Study on the Intrinsic Role of Water. *J. Am. Chem. Soc.* **128**, 4017–4022 (2006).

238. Shang, C. & Liu, Z.-P. Origin and Activity of Gold Nanoparticles as Aerobic Oxidation Catalysts in Aqueous Solution. *J. Am. Chem. Soc.* **133**, 9938–9947 (2011).

239. Besson, M., Flèche, G., Fuertes, P., Gallezot, P. & Lahmer, F. Oxidation of glucose and gluconate on Pt, Pt Bi, and Pt Au catalysts. *Recl. des Trav. Chim. des Pays-Bas* **115**, 217–221 (1996).

240. Besson, M., Lahmer, F., Gallezot, P., Fuertes, P. & Flèche, G. Catalytic Oxidation

of Glucose on Bismuth-Promoted Palladium Catalysts. *J. Catal.* **152**, 116–121 (1995).

241. Karp, E. M., Silbaugh, T. L., Crowe, M. C. & Campbell, C. T. Energetics of Adsorbed Methanol and Methoxy on Pt(111) by Microcalorimetry. *J. Am. Chem. Soc.* **134**, 20388–20395 (2012).

242. Takahashi, S., Cohen, L. A., Miller, H. K. & Peake, E. G. Calculation of the pKa values of alcohols from .sigma. constants and from the carbonyl frequencies of their esters. *J. Org. Chem.* **36**, 1205–1209 (1971).

243. Silverstein, T. P. & Heller, S. T. pKa Values in the Undergraduate Curriculum: What Is the Real pKa of Water? *J. Chem. Educ.* **94**, 690–695 (2017).

244. Mazumder, T., Dandapat, S., Baidya, T., Likhar, P. R., Clark, A. H., Bera, P., Tiwari, K., Payra, S., Srinivasa Rao, B., Roy, S. & Biswas, K. Dual-Site Cooperation for High Benzyl Alcohol Oxidation Activity of MnO2 in Biphasic MnOx–CeO2 Catalyst Using Aerial O2 in the Vapor Phase. *J. Phys. Chem. C* **125**, 20831–20844 (2021).

245. Mullen, G. M., Zhang, L., Jr, J. E. & Yan, T. Control of selectivity in allylic alcohol oxidation on gold surfaces : the role of oxygen adatoms and hydroxyl species. *Phys. Chem. Chem. Phys.* **17**, 4730–4738 (2015).

246. Balbuena, P. B., Calvo, S. R., Lamas, E. J., Salazar, P. F. & Seminario, J. M. Adsorption and Dissociation of H2O2 on Pt and Pt−Alloy Clusters and Surfaces. *J. Phys. Chem. B* **110**, 17452–17459 (2006).

247. Kodchasee, J., Chanloi, C., Khemthong, P., Uapipatanakul, B., Ehara, M. & Bobuatong, K. Catalytic Oxidation of Benzyl Alcohol to Benzaldehyde on Au 8 and Au 6 Pd 2 Clusters : A DFT Study on the Reaction Mechanism. *Catalysis* **11**, 720–734 (2021).

248. Abbadi, A. & van Bekkum, H. A : Highly selective oxidation of aldonic acids to 2-keto-aldonic acids over Pt-Bi and Pt-Pb catalysts. *Appl. Catal. A Gen.* **124**, 409–417 (1995).

249. Kluytmans, J. H. J., Wachem, B. G. M. Van, Kuster, B. F. M. & Schouten, J. C. Mass transfer in sparged and stirred reactors : in uence of carbon particles and electrolyte. *Chem. Eng. Sci.* **58**, 4719–4728 (2003).

250. Tromans, D. Temperature and pressure dependent solubility of oxygen in water: a thermodynamic analysis. *Hydrometallurgy* **48**, 327–342 (1998).

251. Marsac, R., Réal, F., Banik, N. L., Pédrot, M., Pourret, O. & Vallet, V. Aqueous chemistry of Ce (IV): estimations using actinide analogues. *Dalt. Trans. R. Soc. Chem.* **46**, 13553–13561 (2017).

252. Morimoto, T., Shiomi, K. & Tanaka, H. The Heat of Immersion of Aluminum Oxide

in Water. *Bull. Chem. Soc. Jpn.* **37**, 392–395 (1964).

253. Moreno-Piraján, J. C., Giraldo, L. & Rodríguez-Estupiñán P. Calorimetry of Immersion in the Energetic Characterization of Porous Solids *Intechopen*, 13 (2016).

APPENDIX A-3.1: DETERMINING LIQUID CONTACT ANGLE OF AN OXIDE SUPPORT MATERIAL

The H_2O contact angle of each metal oxide support material is derived from the average capillary constant of each oxide material using the Washburn method, according to equation A-3.1.

$$\frac{M^2}{t} = \frac{C_w \rho^2 \gamma}{\eta} cos\theta \qquad \text{A-3.1}$$

Where *M*–is the weight of the sample

t–is the time taken for the liquid to seep into capillary.

C_w–capillary constant.

γ–is the surface tension of liquid.

η–is the viscosity of the liquid.

θ–is the contact angle of the liquid on capillary walls.

ρ – is the liquid density

Firstly, the capillary constant is determined by using a fully wetting liquid, n-hexane, with known ρ and γ. Since n-hexane is a completely wetting liquid, then cos *θ* = 1. The linear dependence of M^2 versus time (slope) is obtained from the weight of n-hexane taken up by the powder by capillarity as a function of time (see Figure A-3.1) and used to compute constant C_w.

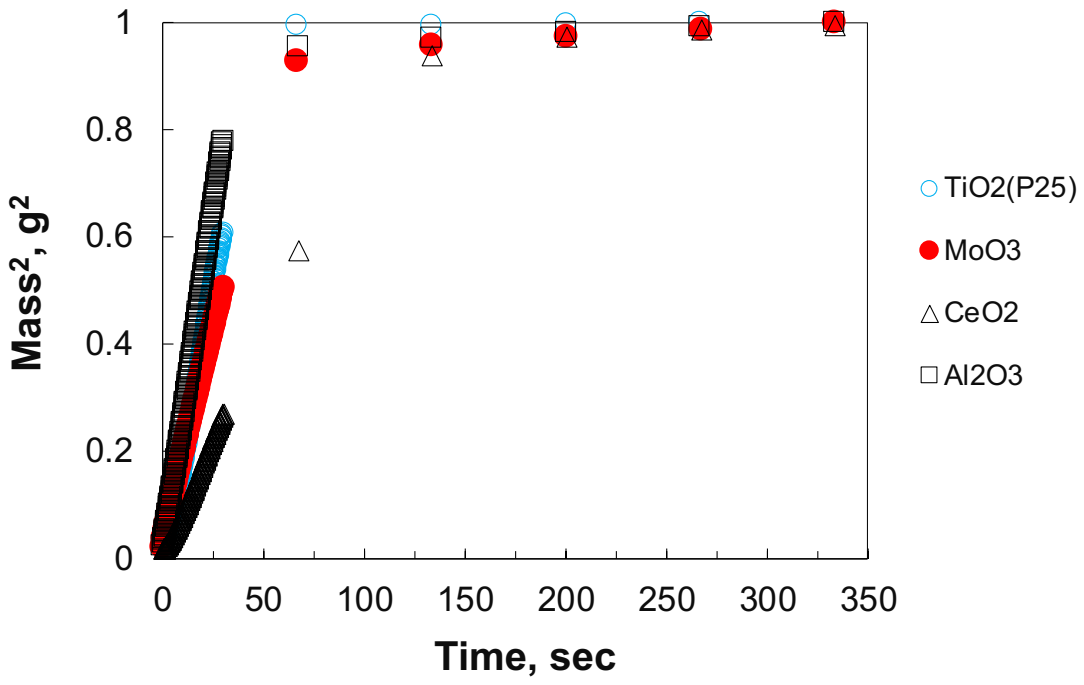

Figure A-3.1: Plot for determining capillary constant of metal oxide support material using n-hexane (non-wetting) solvent.

A second experiment was then performed using the H_2O also with known ρ and γ. In this H_2O does not fully wet the solid sample, therefore, $\cos\theta \neq 1$. Notably, for this experiment, similar powder packing was considered to achieve the same constant C_w. Again, linear dependence M^2 versus time (slope) is obtained from the weight of H_2O taken up by the powder by capillarity as a function of time (see Figure A-3.2) and used to determine the H_2O contact angle. Both experiments (determination of the capillary constant and contact angle) for all the metal oxide support materials were done in triplicates and averaged out.

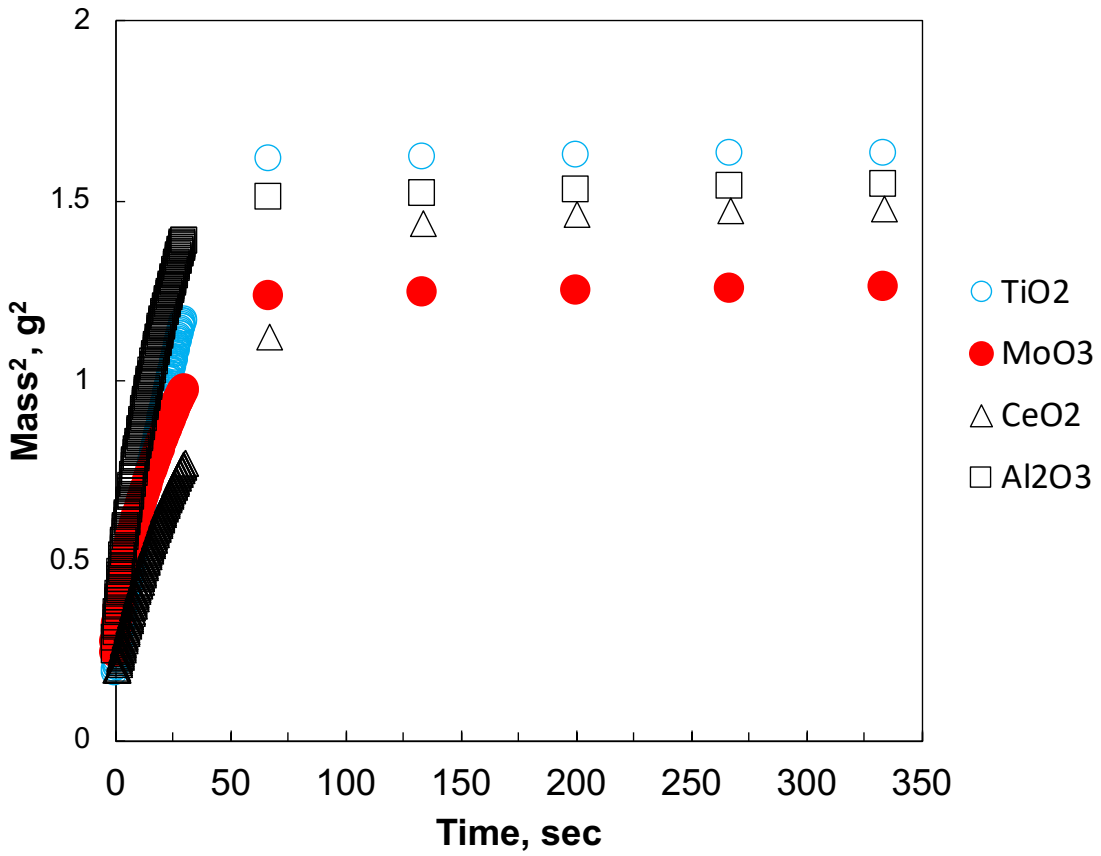

Figure A-3.2: Plot for determining contact angle of metal oxide support material using with H_2O.

Table A-3.1: Mass specific theoretical response factors

Carbon-oxygen bond	**Molecule**	**Response**	**Factor (f_i)**
None (C-C)	Bn-CH_3 (Toluene)	1	1
Single (C-O)	Bn-CH_2OH (Benzyl Alcohol)	0.55	1.07
Double (C=O)	Bn-CHOH (Benzyl Aldehyde)	0	1.17

Appendix B-4.1: Morphological analysis of Pt/TiO_2(P25)

The morphology of the nanoparticles in the catalyst sample was imaged by transmission electron microscope (TEM) using a TECHNIA 200II operating at 200kV. The particle size distribution was obtained from the cumulative particle size distribution modelled using a log-normal distribution, shown in Figure B-4.1. The average particle size of the platinum nanoparticles was determined to be 4.6 ±0.8 nm (measuring between ca. 200 nanoparticles using ImageJ®).

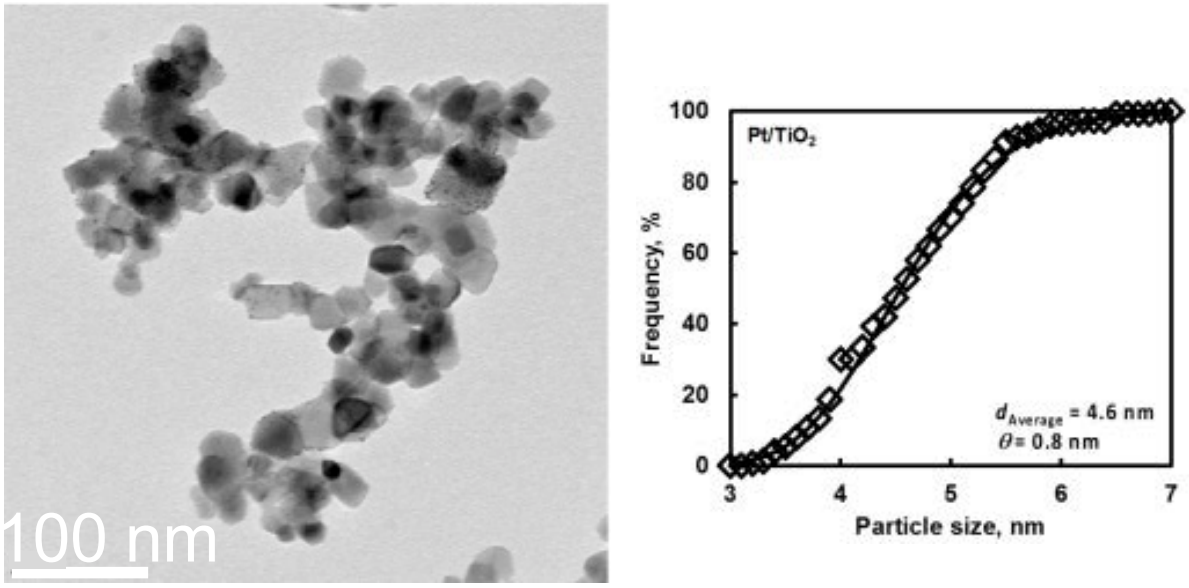

Figure B-4.1: TEM image of Pt/TiO_2(P25) and the obtained cumulative particle size distribution

APPENDIX B-4.2: OXYGEN UPTAKE

The oxygen uptake was determined by chemisorption analysis in an ASAP 2020 C unit (Micromeritics). The sample (ca. 150 mg) was evacuated at 110 °C for 30 minutes. Subsequently, the sample was treated in flowing hydrogen for 12 hours at 350-400 °C and atmospheric pressure. Followed by evacuation of the sample at the reduction temperature for 120 minutes. CO chemisorption was performed at 35 °C, and O_2-uptake was determined at 90 °C. The CO-uptake was highly reversible (see Fig. B1), and the first analysis was modelled as:

$$V_{ads,CO} = V_{ads,CO,monolayer} \cdot \frac{K_1 \cdot p_{CO}}{1 + K_1 \cdot p_{CO}} + K_3 \cdot p_{CO}$$

(the last term representing the steady increase in the uptake with increasing pressure, possibly representing CO spilling over onto the support). The oxygen uptake is

strongly irreversible. Oxygen upon adsorption on platinum may dissociate (vide verde), and the oxygen uptake was modelled accounting for the associative and dissociative adsorption of oxygen:

$$V_{ads,O_2} = V_{monolayer,O_2} \cdot \frac{K_1 \cdot p_{O_2} + 0.5 \cdot K_1^{0.5} \cdot K_2 \cdot p_{O_2}^{0.5}}{1 + K_1 \cdot p_{O_2} + K_1^{0.5} \cdot K_2 \cdot p_{O_2}^{0.5}} + K_3 \cdot p_{CO}$$

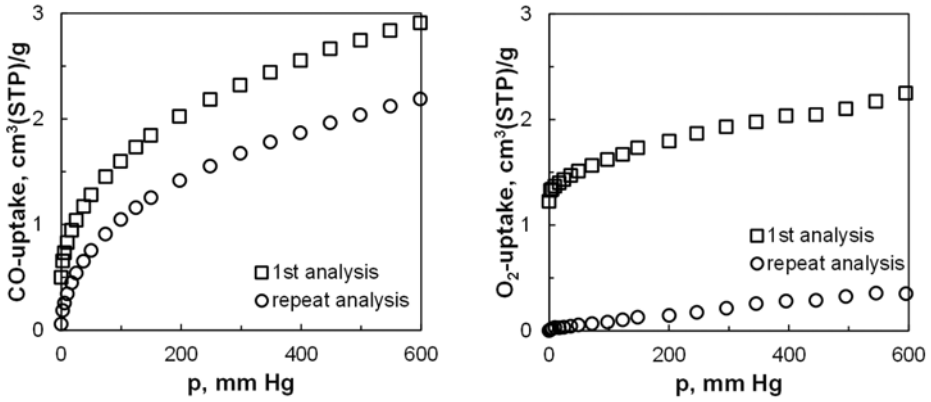

Figure B-4.2: CO-uptake at 35ºC (left) and O_2-uptake at 90ºC (right) of the reduced Pt/TiO_2 sample.

Table B1: Physico-chemical characterization of Pt/TiO_2

	CO-chemisorption [a]	**O_2-chemisorption [b]**
$V_{monolayer}$, $cm^3(STP)/g$	1.41	1.41
K_1, $(mm\ Hg)^{-1}$	0.152	105.9
K_2	-	$1.1 \cdot 10^{-4}$ [c]
K_3, $cm^3(STP)/g/mm\ Hg$	$2.78 \cdot 10^{-3}$	$1.55 \cdot 10^{-3}$
R^2 [c]	0.963	0.962
D,% [d]	33.5	33.5
$d_{chemisorption}$, nm	3.4	3.4
S_{metal}, m^2/g [e]	3.2	3.2

[a]Based on the 1st analysis; [b]Based on the difference between 1st and repeat analysis; [c] dimensionless; [d] Goodness of fit; [d] Metal dispersion; [e]assuming 12.5 Pt atoms on the surface per nm^2

The O_2 and CO-chemisorption seem to underpredict the average metal particle size in comparison to the size obtained from TEM, which would yield a metal dispersion of 24.6% based on the particle size distribution.

Appendix B-4.3: Phase diagram for benzyl alcohol + water + toluene the system using the non-random two liquid (NRTL) model.

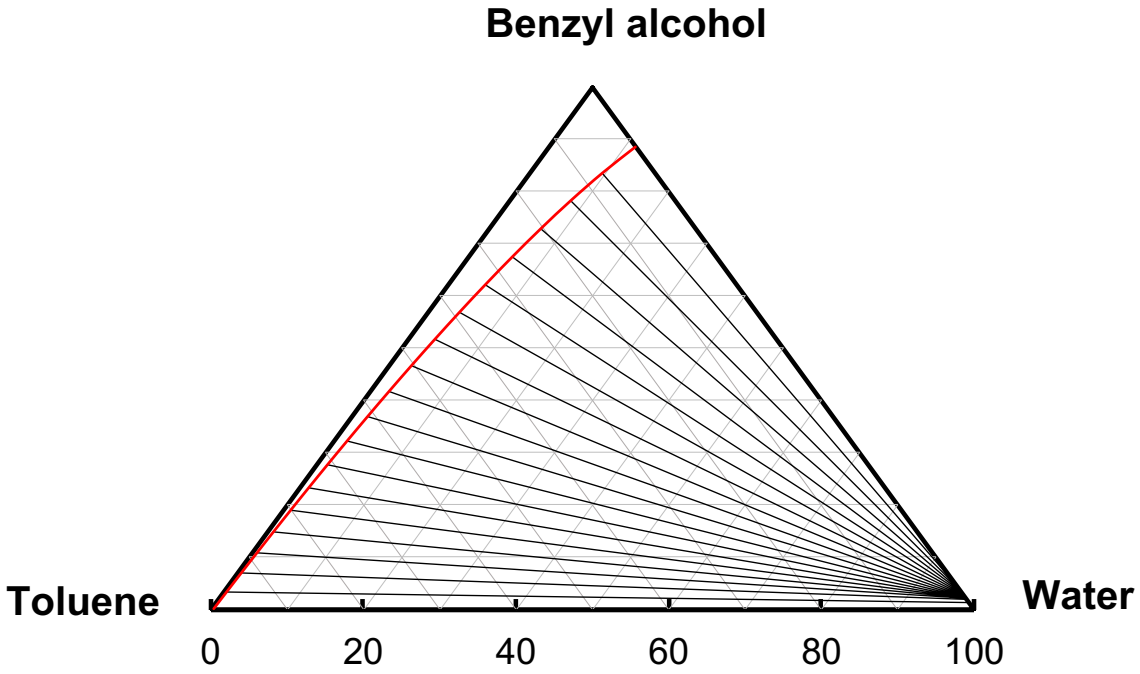

Figure B-4.3: Ternary phase diagram of the liquid-phase in the system benzyl alcohol + water + toluene at 80°C with tie-lines.

APPENDIX C-5.1: X-RAY DIFFRACTION ANALYSIS OF THE BIMETALLIC SYSTEM

X-ray diffraction characterization was performed on the platinum alloyed samples to assess the average crystallite sizes and the phase compositions, *cf*. Figure C-5.1. TiO_2 rutile phase was used as a basis for comparison. The existence of rutile in all samples was readily distinct from its diffraction peak located at 2θ = 31.9°, 42.2°, 45.8°, 48.4°, 51.7°, 64.1°, 66.9°, 74.4°, 76.1°, 82.2°, and 83.4° corresponding to (110), (101), (200), (111), (210), (211), (222), (002), (310), (301) and (311) planes.

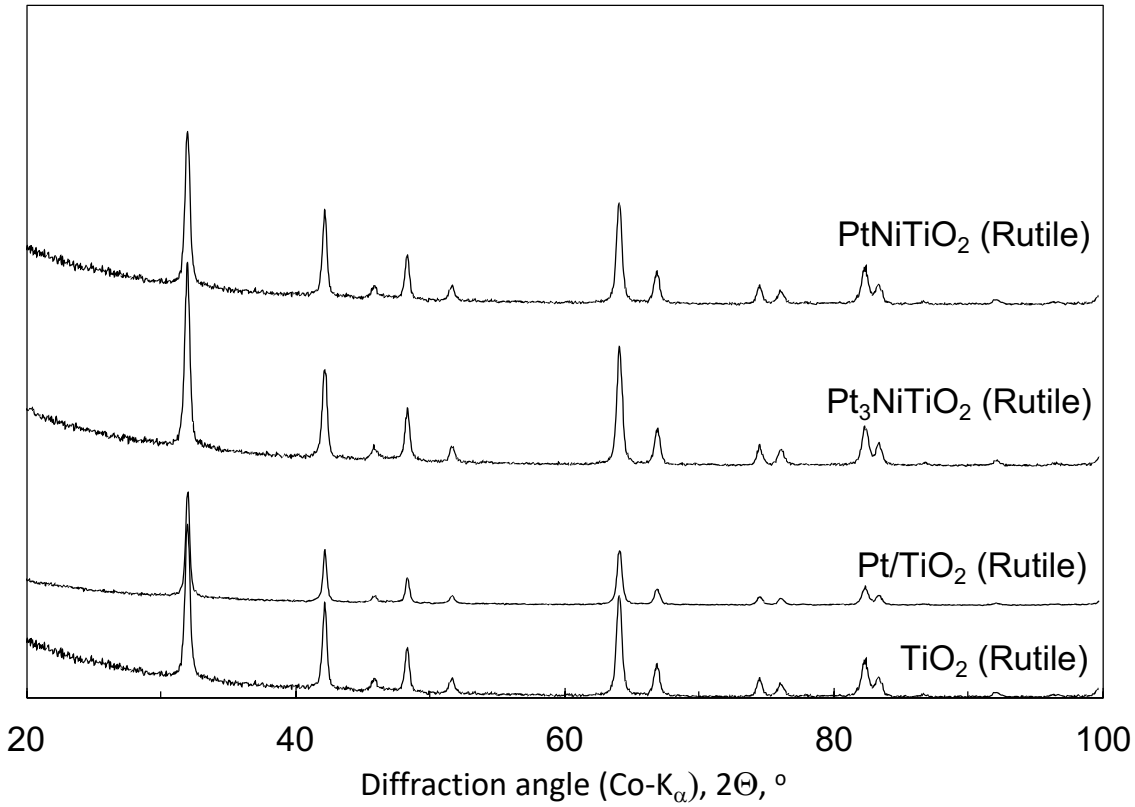

Figure C-5.1: X-ray diffraction patterns of Pt, Pt_3Ni and PtNi nanoparticles immobilized on TiO_2 (Rutile phase) supported with rutile for diffraction pattern comparison.

Due to low active metal loading, distinct diffraction peaks attributed to the active metal (platinum and/or platinum alloys) could not be detected. As such, the phase composition of the noble metal over the TiO_2 (rutile) support could not be determined.

The (200) and diffraction plane of the TiO_2 overlap with the (111) diffraction plane of the active metal. Moreover, due to the relatively smaller nano-crystal size of the active metal compared to the larger nano-crystals of the TiO_2 support, the diffraction peaks corresponding to the active metal are overshadowed by the sharp, intense peaks of the TiO_2 support. Notably, the angle of the diffraction peaks of the TiO_2 support remains unchanged. This further confirms that the active metal is neither incorporated into the lattice structure of the TiO_2 support nor forming an alloy after deposition of the active nanoparticles.

APPENDIX C-5.2: EDX ANALYSIS OF THE PT-NI BIMETALLIC SYSTEM

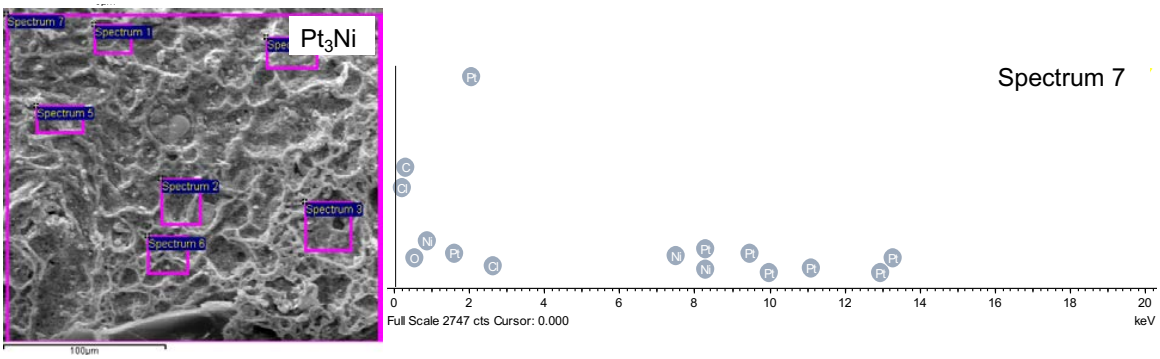

Figure C-5.2: EDX elemental mapping of Pt_3Ni/TiO_2 (rutile) catalyst samples.

APPENDIX C-5.3: LOW ACTIVATION ENERGY ASSOCIATED WITH MASS-TRANSFER LIMITATIONS -CALCULATIONS.

Low activation energy often associated with mass transfer limitations (either gas-liquid mass transfer limitation or liquid-solid mass). If the reaction system was mass-transfer limited, the measured rates in all the systems would be comparable to the mass transfer rate due to either gas-liquid mass transfer limitation or liquid-solid mass. The gas-liquid mass transfer coefficient may be estimated as 0.00053 s^{-1} for the system oxygen-water[249] (it should be noted that the presence of solid catalyst particles and benzyl alcohol in the system may increase the mass transfer coefficient). The maximum rate of oxygen transfer may thus be estimated as 0.0314 mol $O_2/s/m^3$ (thus corresponding to a maximum rate of benzyl alcohol consumption of 0.0628 mol benzyl alcohol/s/m^3 This can be

recalculated in terms of the reaction volume (70 mL), the mass of catalyst (0.5 g) and the platinum content (4wt.-%) as 1300 mmol/g_{Pt}/min, which is ca. 80 times larger than the highest measured rate. It may thus be concluded that gas-liquid mass transfer of oxygen does not control the rate of reaction

1) Assuming that the liquid-solid mass transfer can be described using Sh=2, the mass transfer coefficient can be estimated as 0.155 m/s (using a diffusivity of oxygen in water of $7.8.10^{-9}$ m^2/s, and a particle size of P25 of 0.1 μm). This implies that the solid-liquid mass transfer coefficient is 0.155 m/s. Hence, the maximum amount of oxygen transferred from the liquid to the solid is given by:

$$r = k_m \cdot a \cdot C_{O_{2,liquid}} = 0.155 \cdot \frac{6}{\rho \cdot d_P} \cdot C_{O_{2,liquid}}$$

Taking again the particle diameter as 0.1 μm, the density of the particle as 4.1 g/cm^3 and the concentration of oxygen in the liquid at 363K as $7.9 \cdot 10^{-4}$ mol O_2/L,[21] results in a maximum rate of 3.6 mol benzyl alcohol/g/s, i.e. much faster than either the benzyl alcohol oxidation (0.6 mmol/g_{Pt}/min or $4 \cdot 10^{-7}$ mol/g/s) or the gas-liquid mass transfer of oxygen (see above)

The calculations above shows that mass transfer limitations in the benzyl alcohol oxidation, which is a slow reaction, is not really important.

APPENDIX D-6.1: HEAT OF IMMERSION ANALYSIS

The heat of immersion of the CeO_2 support per unit surface area is high, -2.875 J/m^2, whic might be related to a chemical transformation in the sample. It should, however, be realized that the observed heat effect per mole of CeO_2 is rather low (ca. 840 J/mol), and thus a bulk transformation of CeO_2 to $Ce(OH)_4$ seems unlikely. However, the hydroxylation of the cerium oxide surface may have resulted in the formation of an impenetrable cerium hydroxide film.[251]

The heat of immersion of the other oxides per unit surface area is only a fraction of this value and increase in the order TiO_2(P25) > γ-Al_2O_3 > γ-Fe_2O_3. The heat of immersion per unit surface area does not correlate with the contact angle. This may imply that the determination of the heat of immersion involves more than just wetting the surface. It has been found that hydroxyl groups on the surface of oxides may form hydrogen bonds with water molecules upon immersion[252]. The heat of immersion increases with an increasing concentration of surface hydroxyl groups.[252,253] Furthermore, the interaction of liquid water with the sample may have resulted in the formation of additional hydroxyl groups, thus also affecting the heat of immersion.

APPENDIX D-6.2: ADDITIONAL XRD ANALYSIS (PT ON VARIOUS METAL OXIDE SUPPORT MATERIALS)

The XRD pattern of the samples is depicted in Figure D-6.2. Evidently, the characteristic peaks corresponding to the support materials are observed for all the samples, indicating that the original structure of the support is maintained during the catalyst preparation process. More importantly, this suggests that deposition of platinum active metal does not form an alloy with the support material, as additional diffraction peaks suggesting the presence of platinum species are distinct. Albeit, the diffraction peaks corresponding to the noble metal may be overlapping with diffraction peaks of the support.

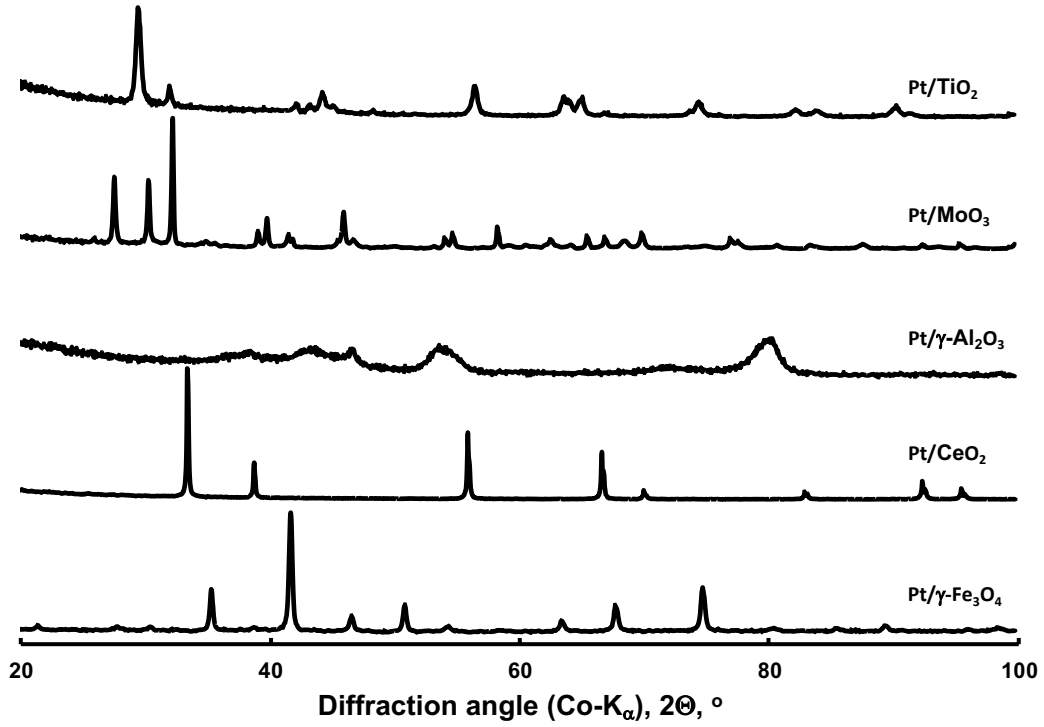

Figure D-6.2: XRD pattern of a platinum-based catalyst supported on various carriers.

Despite the low amount and/or smaller nano-sized particles of the platinum noble metal, some reflections due to the presence of platinum are visible. This is more

pronounced for Pt/TiO_2 and $Pt/\gamma–Fe_2O_3$ catalyst samples. The diffraction peak ranging from 2θ ~ 41° to 47° is distorted for Pt/TiO_2; this further suggests the presence of platinum metal. Additional diffraction peaks corresponding to *fcc*-platinum are observed at 2θ ~ 30.4°, 46.5°, 54.3° and 80.5° in $Pt/\gamma–Fe_2O_3$ sample. These are characteristic for the most intense diffraction lines of *fcc*-Pt (corresponding to (hkl) of (100), (111), (200), (220) and (311) plane, respectively). The sharp diffraction peaks corresponding to the active metal suggest a relatively bigger average crystallite size. The obtained average crystallite size of platinum metal is *ca.* 29.1nm, as determined using the Debye-Scherrer equation. Precipitation of $FeCl_3$ in the presence of NaOH forming iron oxide exhibited diffraction peaks at 2θ ~ 21.2°, 34.4°, 41.6°, 43.4°, 50.4°, 63.2°, 67.1°, 74.4°, 84.8°, 88.7°, 90.1° and 95.2° corresponding to (hkl) of (111), (220), (311), (222), (400), (422), (511), (440), (620), (533), (622) and (444) plane, respectively. These diffraction planes suggest maghemite iron(II)oxide phase. On the other hand, the Pt/Al_2O_3 sample exhibited broad diffraction peaks at 2θ ~ 44.0°, 46.2°, 53.7°, 72.1° and 79.4° corresponding to (hkl) of (311), (222), (400), (511) and (444) plane, respectively. This suggests that Al_2O_3 support exists as γ-Al_2O_3 phase.

The average crystallite size determination of a material is typically determined from the most intense and well-resolved XRD peaks. The diffraction peaks corresponding to platinum overlap with the support diffraction peaks for Pt/CeO_2 and Pt/γ-Al_2O_3 as chemisorption studies are required to obtain the average particle size making the assignment of the peak maximum a non-trivial exercise. Furthermore, an exact determination of the average crystallite size of the noble metal using the Debye-Scherrer was therefore not feasible.

APPENDIX D-6.3: NH_3-TPD ANALYSIS

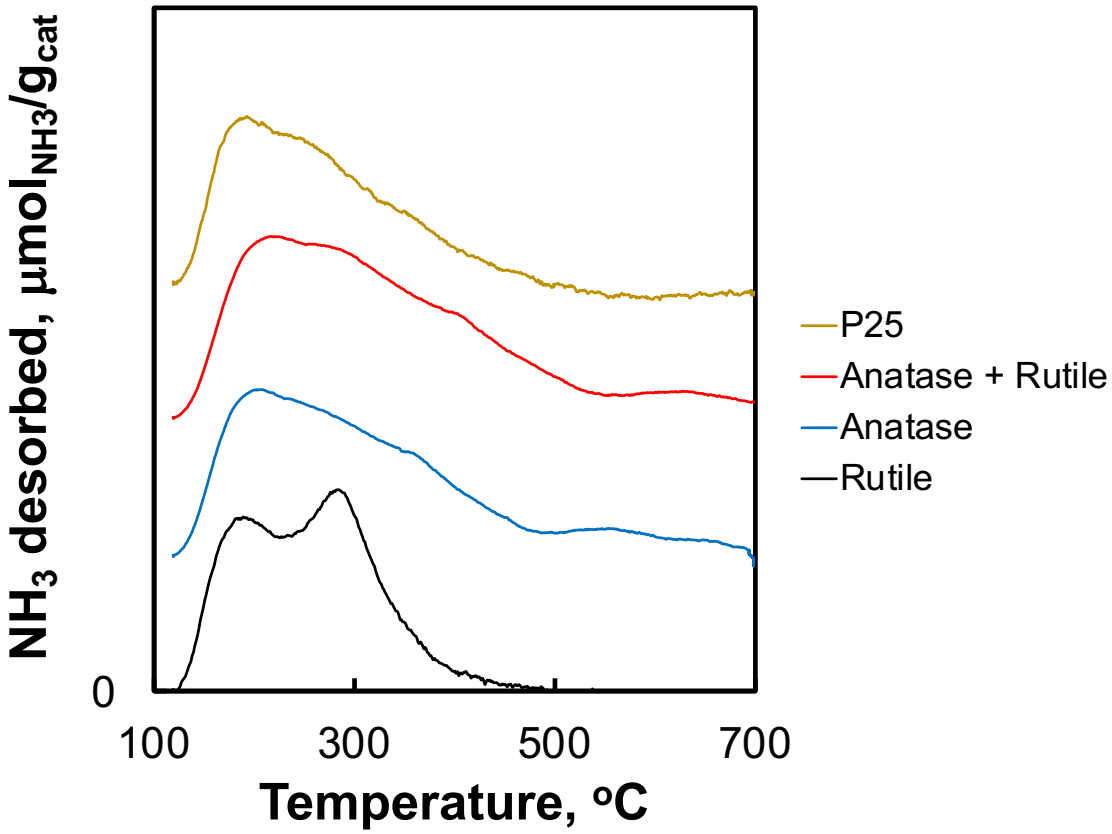

Figure D-6.3: NH_3-TPD profile of Titania phases, *i.e.*, rutile, anatase and P25.

APPENDIX E-7.1: X-RAY DIFFRACTION ANALYSIS OF PT-BI/TiO_2 CATALYST

X-ray diffraction characterization was performed on the Pt-Bi/TiO_2 sample to assess the average crystallite size and the phase compositions, *cf*. Figure E-7.1. TiO_2 rutile phase was used as a basis for comparison. The existence of rutile in the sample was readily distinct from its diffraction peak located at 2θ = 31.9°, 42.2°, 45.8°, 48.4°, 51.7°, 64.1°, 66.9°, 74.4°, 76.1°, 82.2°, and 83.4° corresponding to (110), (101), (200), (111), (210), (211), (222), (002), (310), (301) and (311) planes

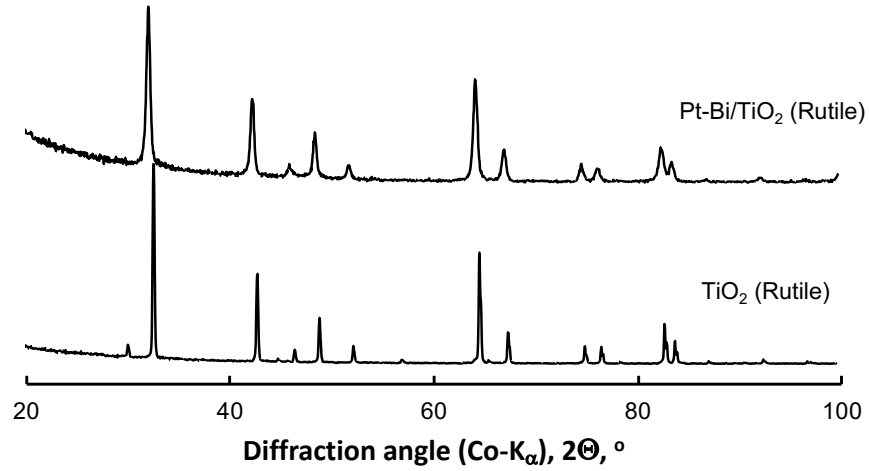

Figure E-7.1: X-ray diffraction patterns of Pt-Bi nanoparticles immobilized on TiO_2 (Rutile phase) supported with rutile for diffraction pattern comparison.

Due to low active metal loading, distinct diffraction peaks attributed to the active metal (platinum and/or platinum alloy) could not be detected. As such, the phase composition of the noble metal over the TiO_2 (rutile) support could not be determined.

Notably, the angle of the diffraction peaks of the TiO_2 support remains unchanged. This further confirms that the active metal is neither incorporated into the lattice structure of the TiO_2 support nor forming an alloy after deposition of the active nanoparticles.

APPENDIX E-7.2: EDX ANALYSIS OF THE PT-BI BIMETALLIC SYSTEM

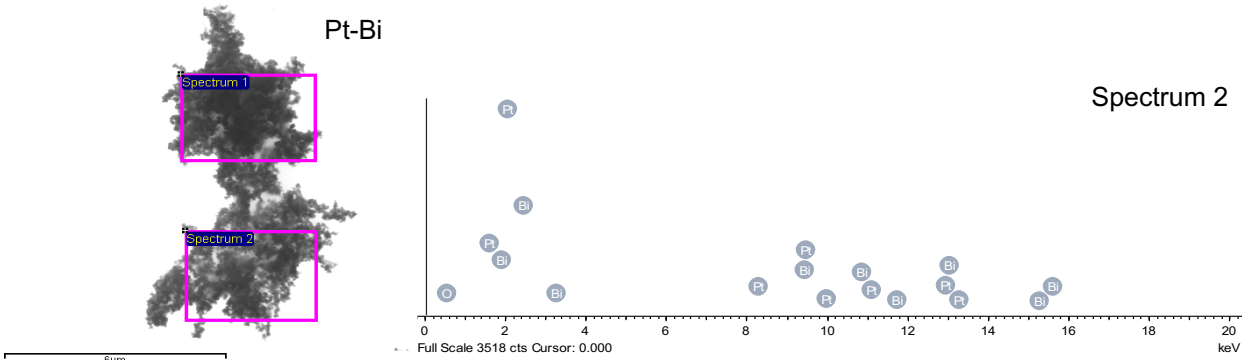

APPENDIX E-7.2: XPS ANALYSIS OF THE TiO_2

Peaks that correspond to the rutile (TiO_2) support are shown in C-6.3 exhibiting the Ti 2p and O 1s region for all the samples. Two strong symmetrical peaks around 462 eV and 468 eV are recognized as Ti $2p_{1/2}$ and Ti $2p_{3/2}$, respectively. The spin-orbital energy splitting for the Ti 2p doublet is 5.4 eV, which is diagnostic of the rutile TiO_2 support. The peaks corresponding to O 1s are located at about 530.8 eV, whose energy is equal to the O 1s electron binding energy for TiO_2. The peak is made of two peaks, identified due to the different chemical bonding of the oxygen species. Peak occurring at 530.1 eV for all samples is due to O^{2-} ion in the TiO_2 lattice. A second peak is located at a binding energy of 531.4 eV, attributed to the surface hydroxyl groups of possibly chemisorbed water molecules on the titania.

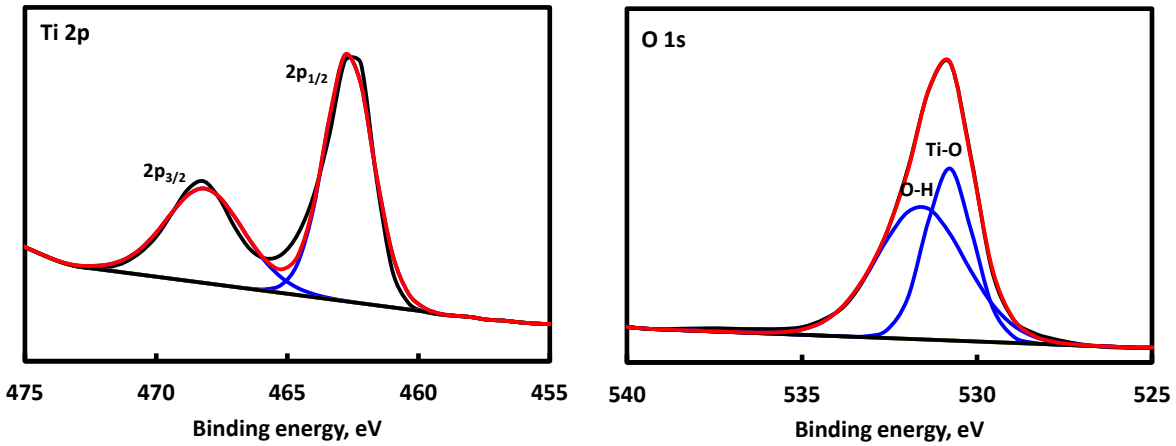

Figure E-7.1: XPS spectra of TiO_2 (rutile phase) support highlighting high resolution of Ti 2p and O 1s spectra of TiO_2 rutile phase.